

1983

# The hydraulics of the hereford inlet-and back bay system, Jan. 1983

R. J. Gabriel

G. P. Lennon

R. N. Weisman

Follow this and additional works at: <http://preserve.lehigh.edu/engr-civil-environmental-fritz-lab-reports>

---

## Recommended Citation

Gabriel, R. J.; Lennon, G. P.; and Weisman, R. N., "The hydraulics of the hereford inlet-and back bay system, Jan. 1983" (1983). *Fritz Laboratory Reports*. Paper 2271.  
<http://preserve.lehigh.edu/engr-civil-environmental-fritz-lab-reports/2271>

This Technical Report is brought to you for free and open access by the Civil and Environmental Engineering at Lehigh Preserve. It has been accepted for inclusion in Fritz Laboratory Reports by an authorized administrator of Lehigh Preserve. For more information, please contact [preserve@lehigh.edu](mailto:preserve@lehigh.edu).

Tidal Hydraulics

THE HYDRAULICS OF THE  
HEREFORD INLET-BAY SYSTEM

by

Ralph J. Gabriel

Gerard P. Lennon

Richard N. Weisman

This work has been sponsored by a  
Fleischmann Foundation grant to the Wetlands Institute

Department of Civil Engineering

Fritz Engineering Laboratory

Lehigh University

Bethlehem, Pennsylvania

January 1983

Fritz Engineering Laboratory Report No. 477.1

## ABSTRACT

An explicit, two-dimensional finite difference hydrodynamic model was applied to the Hereford Inlet-bay system and used to predict the system's hydraulic response to an applied exciting tide. Given the inputs of known exciting tides, external inflows, wind data, rainfall and evaporation rates, and channel or bay geometry (length, width, depth) and roughness, the model solves the vertically averaged continuity equation and the two-dimensional equations of motion for the unknown water height and flow per unit width in two horizontal directions at each point in the system.

A coarse grid model was run encompassing the entire study area and calibrated to yield good reproduction of observed tidal heights in the back bays and main channels. Using the output from this coarse grid model, fine grid models were run in three back bays to better define the flow fields in these locations.

The quality of the results was found to be sensitive to the ground elevations assigned to inundatable areas. Once these elevations were chosen, the model showed accurate reproduction of most tidal records. Predicted tidal heights were relatively insensitive to channel or bay depth and roughness, and to the effects of precipitation, evaporation, and wind stress. Discharge, however, was found to be very sensitive to depth, roughness, and wind stress parameters. The model is not yet calibrated to predict discharges, since no field measurements of discharges or velocities are yet available.

TABLE OF CONTENTS-

	Page
ABSTRACT	
1. INTRODUCTION	1
1.1 Background and Study Objectives	1
1.2 Tidal Inlet Stability	4
1.3 Tidal Hydraulics	6
1.4 Scope of Present Work	9
2. HYDTID MODEL FORMULATION	11
2.1 Mathematical Development	11
2.2 Boundary Conditions	13
3. MODEL IMPLEMENTATION	18
3.1 Implementation Procedure	18
3.2 Model Application	19
3.3 Presentation of the Results	33
4. DISCUSSION OF THE RESULTS	35
4.1 Coarse Grid	35
4.2 Jenkins Sound Fine Grid	49
4.3 Great Sound Fine Grid	58
4.4 Richardson and Grassy Sound Fine Grid	69
4.5 Comments	83
5. SUMMARY, CONCLUSIONS, AND RECOMMENDATIONS	84
5.1 Summary	84
5.2 Conclusions	85

	Page
5.3 Recommendations for Future Study	85
6. ACKNOWLEDGMENTS	88
7. REFERENCES	89
APPENDICES	
1. Tidal Hydrodynamic Equations	92
2. Tidal Data	100
3. Flow Pattern: Coarse Grid	102
4. Flow Pattern: Jenkins Sound	129
5. Flow Pattern: Great Sound	156
6. Flow Pattern: Grassy and Richardson Sounds	183

## LIST OF FIGURES

Figure		Page
1	Location Map of Hereford Inlet and Study Area	2
2	Variable Locations in HYDTID	12
3	Cell Flagging Scheme for Identifying Flow Boundary Conditions	16
4	Coarse Grid Model	20
5	Coarse and Fine Grid Models	21
6	Convective Flagging Scheme	23
7	Stage versus Correction Regression	29
8	Start-up Techniques	31
9	Coarse Grid	36
10	Flow Rate versus Time - Coarse Grid Model	39
11	Volume versus Time - Coarse Grid Model	40
12	Tidal Height versus Time - Old Turtle Thorofare	41
13	Tidal Height versus Time - West Wildwood Gage	42
14	Tidal Height versus Time - Nummy Island Gage	44
15	Tidal Height versus Time - Shellbed Landing Gage	45
16	Tidal Height versus Time - Great Channel Gage	46
17	Tidal Height versus Time - Great Sound Gage	47
18	Jenkins Sound Fine Grid	50
19	Flow Rate versus Time - Jenkins Sound Fine Grid	52
20	Volume versus Time - Jenkins Sound Fine Grid	53
21	Tidal Height versus Time - Jenkins Sound Fine Grid	54
22	Flow Rate versus Time - Jenkins Sound Grids	55

Figure		Page
23	Volume versus Time - Jenkins Sound Grids	56
24	Tidal Height versus Time - Jenkins Sound Gage	57
25	Great Sound Fine Grid	59
26	Flow Rate versus Time - Great Sound Fine Grid	61
27	Volume versus Time - Great Sound Fine Grid	63
28	Flow Rate versus Time - Townsend Inlet	64
29	Volume versus Time - Townsend Inlet	65
30	Flow Rate versus Time - Great Channel	66
31	Volume versus Time - Great Channel	67
32	Tidal Height versus Time - Great Sound Fine Grid	68
33	Tidal Height versus Time - Great Sound Gage	70
34	Grassy and Richardson Sound Fine Grid	71
35	Flow Rate versus Time - Grassy and Richardson Sound Fine Grid Model	73
36	Volume versus Time - Grassy and Richardson Sound Fine Grid Model	74
37	Flow Rate versus Time - Sunset Lake	75
38	Volume versus Time - Sunset Lake	76
39	Flow Rate versus Time - Nummy Island	77
40	Volume versus Time - Nummy Island	78
41	Tidal Height versus Time - Old Turtle Thorofare - Richardson and Grassy Sound Fine Grid Model	79
42	Tidal Height versus Time - West Wildwood Gage - Richardson and Grassy Sound Fine Grid Model	80
43	Tidal Height versus Time - Old Turtle Thorofare	81
44	Tidal Height versus Time - West Wildwood Gage	82

LIST OF TABLES

Table		Page
1	Tidal Gages	24
2	Fine Grid Tidal Data	26
3	Selected Tidal Heights 26 August 1978	27



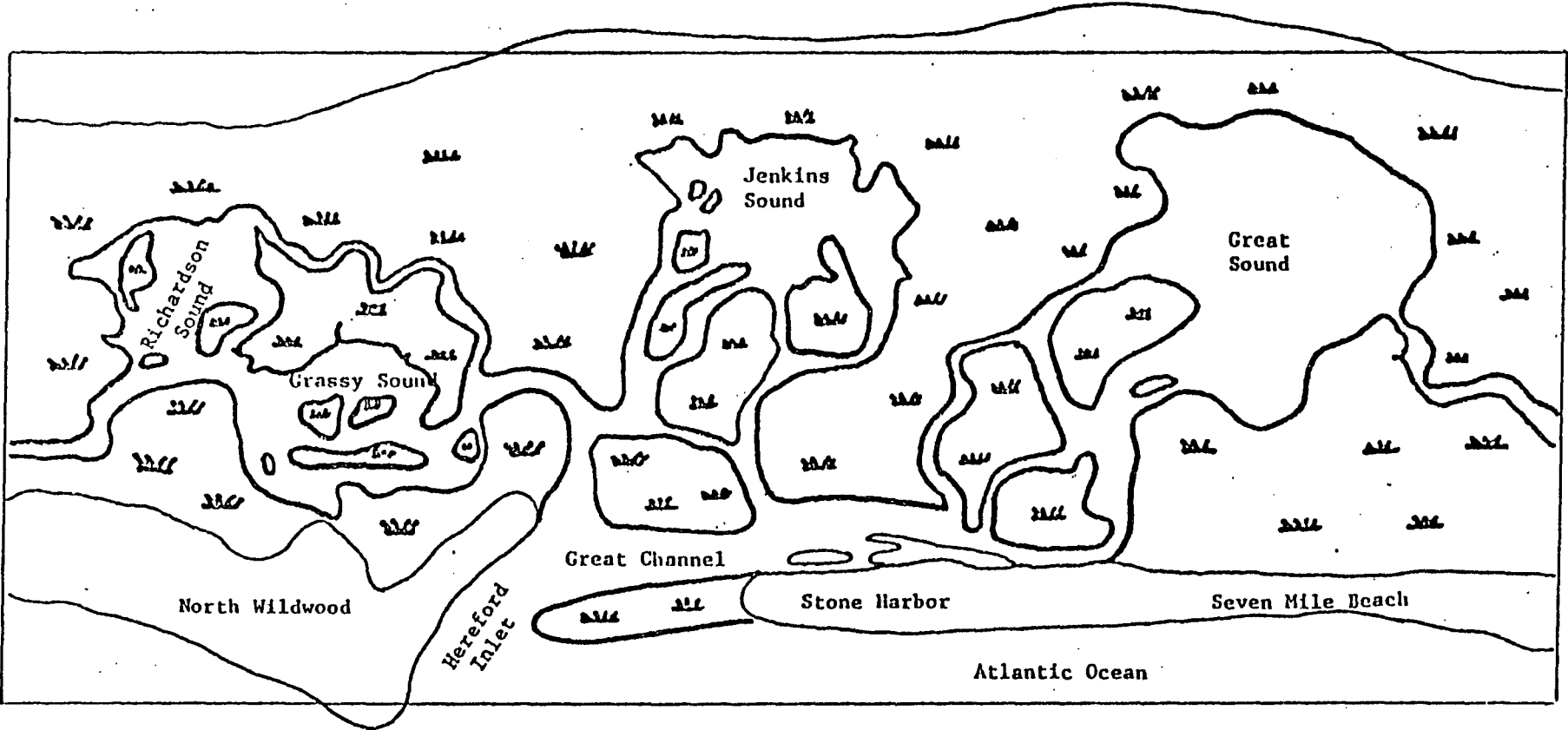
## 1. INTRODUCTION

### 1.1 Background and Study Objectives

A tidal inlet-bay system, or wetlands, is a complex environment in which man, flora, and fauna live under the continual influence of the tides. For man, the wetlands provide a major location for recreational activities such as swimming, boating, and fishing, in addition to being a homeland for many full-time residents. Man affects the plants and animals of the region directly through these activities, and indirectly through his efforts to use and control the water and tides by construction of jetties, groins, and bulkheads, and through dredging and filling operations. Any effort directed at understanding a wetlands ecosystem must include a means of describing the tidal action in that system.

The barrier islands, tidal inlets, and back bay areas along the New Jersey shore form such a wetlands, and it is the intent of this paper to focus attention on one such area: the Hereford Inlet-bay system (see Fig. 1). Hereford Inlet is located between North Wildwood, New Jersey, and Seven Mile Beach and is the principal source of tidal flow to the back bay areas lying between these barrier islands and the mainland. Some influence is also felt from Townsend Inlet to the north and Cape May Inlet to the south. The study area encompasses most of the Stone Harbor Quadrangle (USGS 7.5 minute topographic series) and parts of the adjacent Avalon and Wildwood Quadrangles.

Location Map of Hereford Inlet and Study Area



-2-

FIGURE 1

Location Map of Hereford Inlet and Study Area

The overall objective of this effort was to define the hydrodynamics of Hereford Inlet and its back bay areas resulting primarily from the astronomical tides. While the hydrodynamics can be described by physical hydraulic models, passive electrical analog models, and mathematical models, the high cost associated with constructing and operating physical models and passive electrical analog models eliminated these types of models from consideration. A mathematical model based upon the finite difference method was chosen.

Specific questions answered by this research include:

1. What is the flow field in the inlet and the bays throughout the tidal cycle?
2. What are the corresponding tidal elevations?
3. What is the tidal prism? That is, what is the volume of water entering and leaving the system through each of the inlets over a tidal cycle?

The answers to these questions provide the basis for future chemical, biological, and hydraulic modeling of the system.

Hereford Inlet, as well as most of the other inlets separating the barrier islands, constantly changes. This is evident in air photos and from past surveys. The main channel in Hereford Inlet frequently migrates from north to south across its outer sand bars. The channel normally breaks through the bars at the northern end and gradually migrates to the south, where it nearly closes before opening again to the north. This type of migration is also seen at other adjacent inlets. [Caccesse and Spies (1977)].

The more dramatic and significant changes in the inlet's configuration are frequently the result of major storms or severe wind conditions. These events can alter the inlet, even rendering it temporarily closed, resulting in changes in the back bay circulation pattern. Since it is so dynamic, Hereford Inlet is classified as nonnavigable by the U. S. Coast Guard, and its channel is dredged only on an intermittent basis (J. Selmon, personal communication). This important aspect of tidal hydrodynamics concerns inlet stability, and while it is not the focus of attention in this paper, it cannot be overlooked. A brief summary of tidal inlet stability will be presented, followed by a review of tidal inlet hydraulics.

## 1.2 Tidal Inlet Stability

A method for predicting the stability of tidal inlets was first proposed by Escoffier (1940). The theory suggested the maximum velocity in an inlet would occur at a critical, or equilibrium, cross-sectional area. If the cross-sectional area of the inlet was greater than the critical area, the inlet would be resistant, or stable, against closure. Under these conditions, any deposition of matter in the inlet would result in higher velocities which would scour away the deposited material. If the cross-sectional area of a stable inlet was increased, the velocities would be lower and deposition would result until the area decreased and the velocity increased to return to the equilibrium area.

If, on the other hand, the area was less than the critical area, the inlet would be unstable, and any deposition would cause the area to decrease even further. Likewise, if the area of an unstable inlet were to increase, the inlet should perpetuate the increase by an increase in velocity.

O'Brien (1931, 1969) presented a relationship between inlet throat cross-sectional area and the tidal prism passing through a jettied inlet under spring tide conditions. His results indicated that tidal inlet equilibrium exists when the efforts of the tidal prism to enlarge the inlet just balance the efforts of sedimentation, vegetation, and artificial fill to close it.

Jarrett (1976), using O'Brien's data and additional data published by other investigators, developed similar relations for both jettied and non-jettied inlets on the Atlantic, Pacific, and Gulf coasts. He determined no modifications to O'Brien's relations were necessary.

O'Brien and Dean (1972) brought together concepts of Keulegan (1951, 1967), O'Brien (1931, 1969), and Escoffier (1940) into a method for assessing the ability of inlets to resist closure due to sand transport and deposition. They defined a "stability index" which incorporated inlet area and flow velocity in its formulation, and represented the capability of the inlet to store and transport sand prior to closure. Czerniak (1977) presented a number of case studies which supported O'Brien and Dean's theory. A comprehensive discussion of tidal inlet stability is available in Bruun and Gerritsen (1960).

### 1.3 Tidal Hydraulics

One of the earliest attempts at describing tidal hydraulics was by Brown (1928). Brown discussed the important processes near tidal inlets and presented a technique for determining tidal hydraulics. The method assumed the inlet under study is the only one connecting the sea and an enclosed back bay. Thus, the flows in the inlet could be considered one dimensional, and transverse flows and Coriolis effects neglected. Brown further assumed the bay water surface remained horizontal throughout the tidal cycle and the bay walls were vertical, so the water surface area remained constant. He permitted inflow to the bay only through the inlet of known length and uniform cross-section. Lastly, he neglected density effects, assumed a sinusoidal sea tide and basin response, and disregarded the head due to acceleration.

With these assumptions, Brown formulated two equations: a continuity equation, which equated the inflow to the bay to the rate at which the water was stored in the bay, and an energy equation, which equated the difference in water surface elevation between the sea and the bay to the head loss in the inlet channel. He then approximated the head loss in a linear fashion and subsequently derived expressions for the mean range of tide, the maximum current velocity, and mean tidal prism. While Brown's method may be useful for determining preliminary estimates, it is too simplistic for use in obtaining detailed results.

Keulegan (1951, 1967), while following Brown's approach, retained the nonlinear nature of the energy equation and relaxed the assumption that the water level in the bay was sinusoidal. He derived a set of differential equations which related the change in water surface elevation in the inlet with respect to dimensionless time to the water surface elevations in the sea and bay, the tidal range in the sea, and a "coefficient of repletion", a parameter which incorporated the effects of inlet and bay dimensions, inlet roughness, and period and range of the tidal fluctuations of the water level in the bay. Analytic solutions of the resulting equations were found through the use of Fourier series. They were published in tabular form in his paper and can be used to predict the bay maximum amplitude, maximum inlet velocity, and bay tidal prism. While application of Keulegan's method is necessarily restricted because of the assumptions employed in its derivation, it is, nonetheless, recommended as a means of obtaining an order of magnitude estimate of these quantities [Harris and Bodine (1977), Huval and Wintergerst (1977)].

With the advent of the digital computer, more of the terms of the equations of motion neglected by Brown or Keulegan could be included. [Lamb (1932) and Dronkers (1964) provide complete development of these equations.] Van de Kreeke (1967) presented a numerical solution of the inlet-bay problem which incorporated the effects of fresh water inflow. Oliveira (1970) developed a scheme to permit variable inlet depth and variable bay surface area.

Hinwood and Wallis (1975 a and b) evaluated the state of the art in numerical modeling at that time. They presented a classification scheme for numerical models based upon the number of spatial dimensions, the reference frame used, and the degree to which the hydrodynamic processes were included. The mathematical development of each of the classifications was presented and scrutinized. In all, approximately 100 models of water and contaminant transport were reviewed and their predictive capabilities and limitations assessed.

In its General Investigation of Tidal Inlets (GITI), the U. S. Army Corps of Engineers developed and applied physical and numerical models to Masonboro Inlet, North Carolina. As part of this effort, Seelig, Harris, and Herchenroder (1977) developed a model based along the lines of Keulegan, yet general enough to be applicable to single or multiple inlets, bays, and seas. Their model was a time marching model that simultaneously solved the area-averaged momentum equation for the inlet and the continuity equation for the bay to yield inlet velocities, discharges, and resulting bay level fluctuations.

Huval and Wintergerst (1977) presented a lumped parameter approach to describe tidal hydrodynamics. Their model was more general than Keulegan's and was extended to include variable inlet and basin surface area, variable inlet channel depth, nonsinusoidal sea tides, inlet inertia effects, and bay inflows and outflows other than to the sea. Two finite difference models were also developed, one of which was used in this effort. A complete discussion of the modeling efforts at Masonboro is available in Harris and Bodine (1977).



#### 1.4 Scope of Present Work

For this project the two-dimensional, explicit finite difference model HYDTID, developed by Masch, Brandes, and Reagan (1977 a and b) for the Corps of Engineers GITI, was adapted for use on Lehigh University's CDC Cyber 170/720 computing system and used to develop the desired hydrodynamics. HYDTID was chosen in deference to other mathematical models because of the quality of its results in the Masonboro Inlet application and because of its availability.

Once calibrated, the models used in the Masonboro study yielded tidal hydrographs of substantially the same quality. HYDTID, however, was the most accurate of the numerical models in its flow estimates, and its overall results were comparable to those obtained in a distorted scale, fixed-bed physical model [Harris and Bodine (1977)]. The model was readily obtained from the Coastal Engineering Research Center, Fort Belvoir, Virginia.

HYDTID assumes that vertical accelerations are negligible, pressures are hydrostatic over the depth, and the fluid density is constant. Thus, the three-dimensional flow problem is reduced to one of two dimensions by depth averaging. Given the inputs of known exciting tides, external inflows, wind data, rainfall and evaporation rates, and channel or bay geometry (length, width, depth), and roughness, the model solves the continuity equation and the two-dimensional equations of motion for the unknowns of height and flow per unit width in two horizontal directions at each point in the system.

Initially, a coarse grid model was run encompassing the entire study area and calibrated to yield good reproduction of known tidal records in the back bays and main channels. Using the output from this coarse grid model, finer grid models were run in each of the bays to better define the flow fields in these locations. However, no flow or velocity measurements are available to verify those predicted by the models. Thus, the models are not yet calibrated to predict discharge.

Conclusions drawn from the study are:

1. The flow field cannot be accurately defined until the models are calibrated using field discharge measurements.
2. The models accurately predict tidal heights.
3. An order of magnitude estimate for the minimum flood or ebb tidal prism for Hereford Inlet is  $6 \cdot 10^8$  ft<sup>3</sup>.

Lastly, calibration of the models with field observations of tidal height and discharge is recommended for future study. This calibration must be accomplished prior to using the computed hydrodynamics as input to salinity or contaminant transport models or before attempting to assess changes in geometry on the flow field.

## 2. HYDTID MODEL FORMULATION

### 2.1 Mathematical Development

The explicit finite difference technique is used to HYDTID to solve the equations of motion and the continuity equation to obtain the hydrodynamics of a tidal system. In the finite difference scheme, a grid is placed over the region being studied and is used to represent the physical parameters being modeled. This discretization is shown in Fig. 2. In this figure it is seen that the parameters defined at the center of a cell include:  $d$ , the depth of water equal to  $h - z$ ,  $h$  being the height of the water surface and  $z$  being the bottom elevation;  $r$ , the rainfall intensity;  $e$ , the evaporation rate; and  $n$ , Manning's roughness coefficient. The parameters  $q_x$  and  $q_y$  represent the flows per unit width in the  $x$  and  $y$  directions, and are defined on the cell's right and top sides, respectively. The cell indices are represented by  $(i, j)$ .

The solution scheme begins with a given set of initial and boundary conditions and proceeds to update the initial values of  $q_x$ ,  $q_y$ , and  $h$  for the next time step. Once the values have been recomputed for every cell, time is advanced, and the entire process is repeated for the new set of boundary conditions. For the development of the finite difference forms of the basic equations, the reader is referred to Masch, Brandes, and Reagan (1977 a) and to Appendix 1.

The explicit finite difference technique cannot be applied without restriction, however, as the cell size and time step are related

# VARIABLE LOCATIONS IN HYDTID

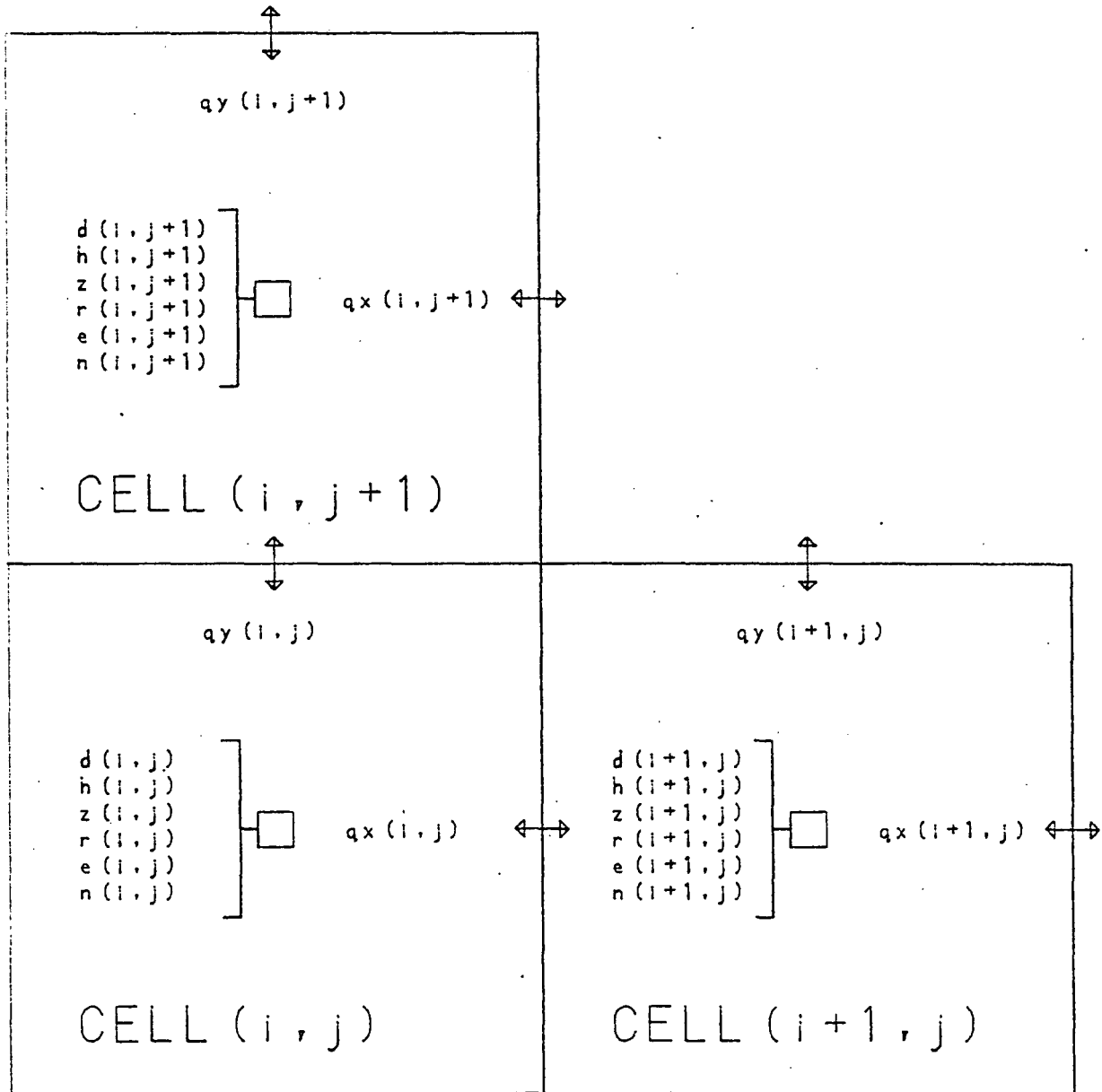


FIGURE 2  
Variable Locations in HYDTID

through the mathematical considerations of stability and convergence. Specifically, the following criteria must be satisfied in order for the scheme to work:

$$\Delta t \leq \frac{\Delta s}{\sqrt{2 g d_{\max}}} \quad (1)$$

where  $\Delta t$  = time step;  $\Delta s = \Delta x = \Delta y$  = cell or mesh size on a side;  $d_{\max}$  = maximum water depth in the model, and  $g$  = gravitational acceleration, 32.2 ft/sec/sec. Dronkers (1964) presents the theoretical development of the finite difference method as applied to tidal computations and discusses the stability and convergence criteria.

## 2.2 Boundary Conditions

The boundary conditions to be applied to the basic equations depend upon the physical situation being modeled and take on seven general forms:

1. Water-land boundaries
2. Submerged barrier boundaries
3. Overtopping barrier boundaries
4. External flow boundaries
5. Artificial offshore tidal boundaries
6. Artificial tidal storage boundaries
7. Inundation boundaries

Water-land boundaries are characterized by no flow across the boundary. Islands, jetties, and other impermeable structures are modeled this way.

The water level on both sides of a submerged barrier boundary always exceeds the barrier crest elevation. Flows across submerged reefs and sand bars can be modeled in this manner. Since the submerged barrier is essentially a submerged weir, it can also be used to control the flow through narrow channels and passes. Because its use requires determination of a discharge coefficient and barrier crest elevation, the device was not used in this effort.

Overtopping barrier boundaries model situations in which the water level on only one side of the boundary exceeds the barrier crest elevation, and, thus, are equivalent to broad crested weirs. As with the submerged barrier, a barrier crest elevation and discharge coefficient must be specified.

External flow boundaries are used to model inflows and outflows around the grid perimeter. This permits the effect of river inflows or sewage outfalls to be included.

Artificial offshore tidal boundaries describe the tidal action occurring offshore in the study area. The flow across the boundary is computed as a function of the difference in the tidal height across the boundary from the relation:

$$q = C (H - h) \quad (2)$$

where  $q$  is the flow rate per foot of width in the  $x$  or  $y$  direction,  $C$  is an admittance coefficient with the units of velocity,  $H$  is the measured tidal height in the offshore cell, and  $h$  is the tidal height in the landward cell.

Artificial tidal-storage boundaries are computationally similar to the artificial offshore tidal boundaries just described, except they lie within the mouth of the tidal system. They provide for the proper exchange of water in the back bays and channels by relating an actual or derived tidal record to the flow at that point.

Inundation boundaries permit the flooding of areas when the water level in a cell rises above the ground elevation in an adjacent cell. Computations at this type of boundary are characterized by a check of water and ground elevations in the adjacent cell to determine if flow can occur. When flow is possible, it is computed from Eqs. 14, 16 and 25 in Appendix 1. If flow is not possible, the boundary is treated as a water-land boundary.

The model uses the above boundary conditions in identifying the cell type and for determining what computations are to be performed in that cell. Cells are identified by the configurations of their top and right sides. There are 45 different cell configurations as shown in Fig. 3.

The boundary conditions not only determine what computations are to be performed in a cell, but also affect how cells interact through the convective terms of the basic equations. The model employs a convective flagging scheme which designates the appropriate calculation to be performed in each direction in each cell. The convective flagging scheme is discussed further in Section 3.

Cell Flagging Scheme For Identifying  
Flow Boundary Conditions

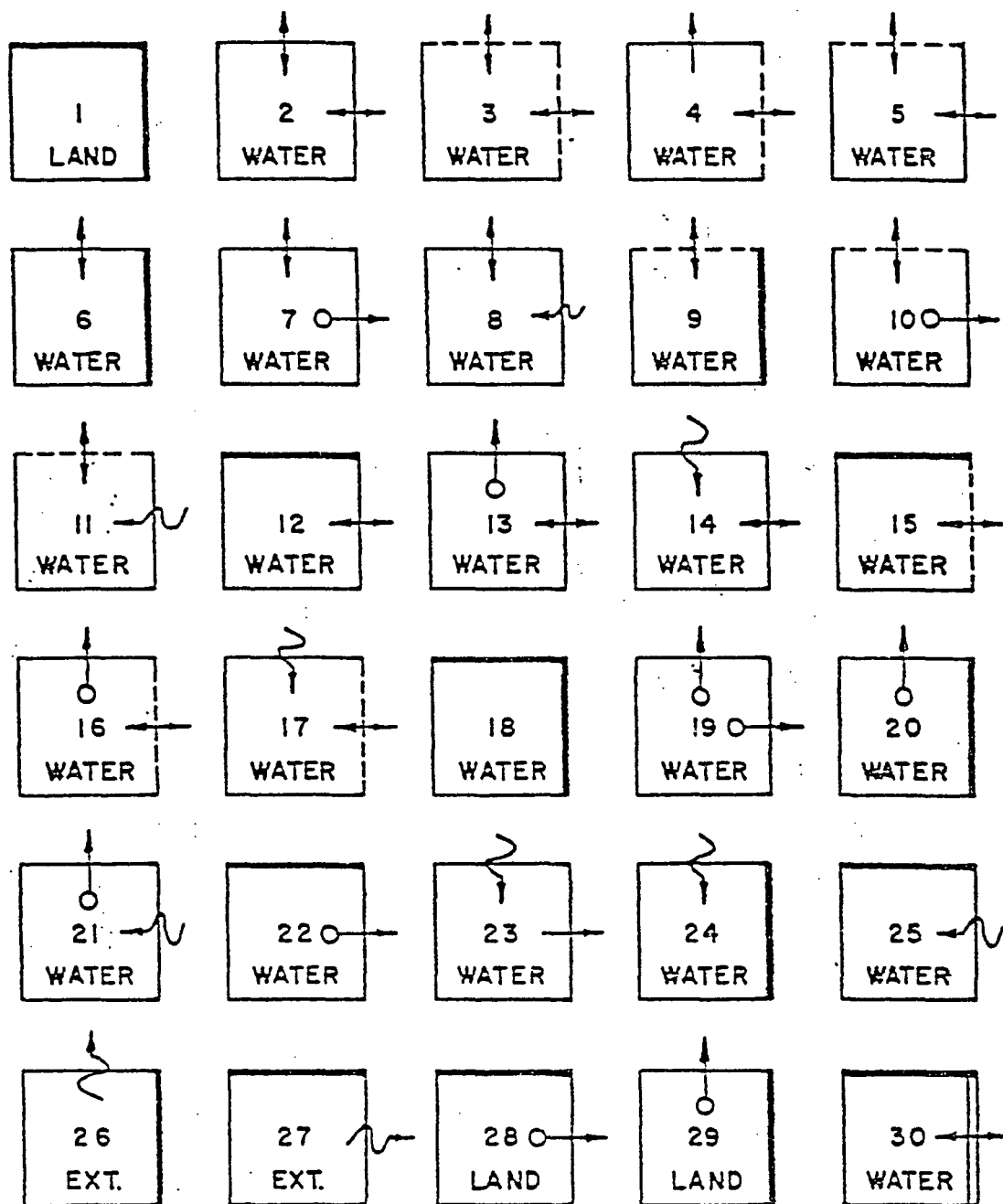


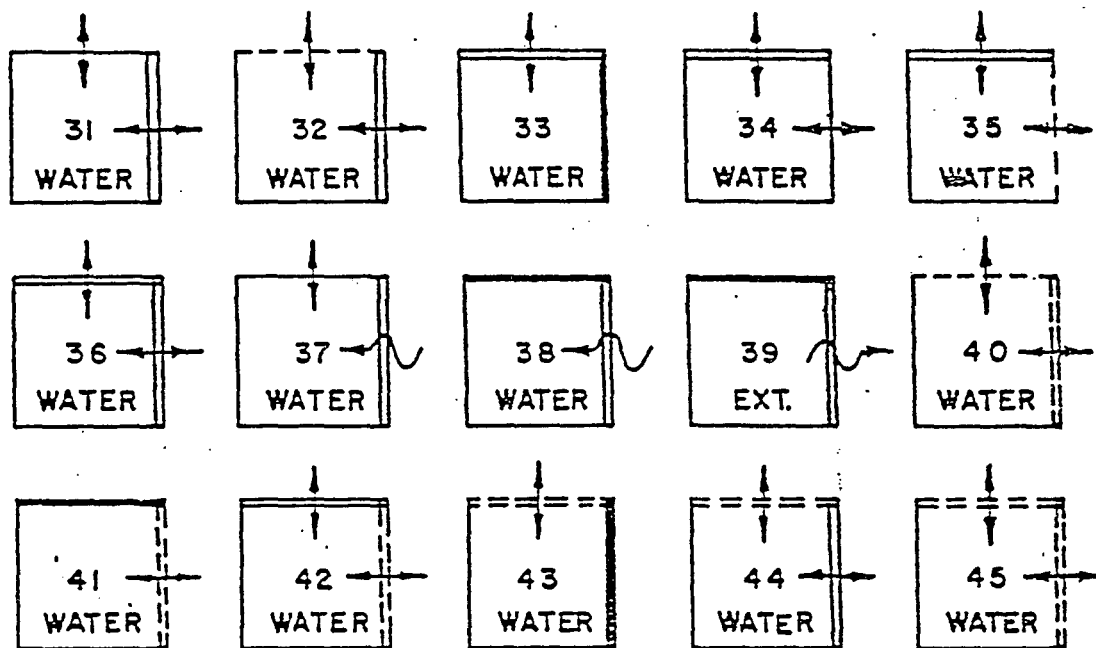
FIGURE 3

[after Masch, Brandes, and Reagan (1977a)]

Cell Flagging Scheme for Identifying Flow Boundary Conditions



Cell Flagging Scheme For Identifying  
Flow Boundary Conditions



LEGEND

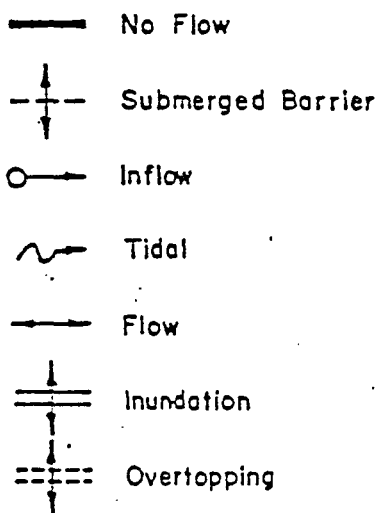


FIGURE 3, continued

[after Masch, Brandes, and Reagan (1977a)]

Cell Flagging Scheme for Identifying Flow Boundary Conditions

### 3. MODEL IMPLEMENTATION

#### 3.1 Implementation Procedure

To apply HYDTID to a given location, Masch, Brandes, and Reagan (1977 a and b) recommend the following procedure:

1. Select the grid size,  $\Delta s$ , and the time step,  $\Delta t$ .
2. Overlay a grid of  $\Delta s$  on a side over a map of the study area.
3. Determine the average bottom depth or land elevation in each resulting cell.
4. Identify each cell computation flag.
5. Assign convective acceleration flags.
6. Assign discharge coefficients and barrier crest elevations to all barriers.
7. Estimate Manning's  $n$  for each cell.
8. Collect necessary data and select the calibration period.
9. Format the data for input.
10. Operate the model for the selected calibration period.
11. Refine the output by adjusting friction values, barrier characteristics, cell elevations, and derived forcing functions.
12. Carry out operational runs with the calibrated model.

The remainder of this chapter details how this procedure was applied to this modeling effort.

### 3.2 Model Application

Selection of the grid spacing,  $\Delta s = \Delta x = \Delta y$ , depends upon available prototype data, required model resolution, available computer resources (execution time and central memory requirements), and the stability criteria of Eq. (1). Due to the size of the study area (about 50,000 ft. by 22,000 ft. or 39.5 sq. mi.), a compromise between detail and cost was reached by running four different models. A coarse grid, which encompassed the entire study area, 2000 ft. on a cell side and requiring a 60 second time step, was used to determine the overall flow pattern, while finer grids of 500 ft. on a side with 12-15 second time steps were used to better define the hydrodynamics in the back bays and sounds. The coarse grid is shown in Fig. 4 and the three fine grids overlaying the coarse grid in Fig. 5.

Bottom depths and land elevations for each cell were determined from surveys obtained from the State of New Jersey, the USGS topographic maps, navigation charts, and from site visits. When the bottom elevation was not constant throughout a cell, an average cell elevation consistent with those in adjacent cells was chosen. Elevations for the marshy areas were varied during the calibration process in an attempt to account for the water which is stored in them. It was found that adjacent inundatable areas should have their elevations set at different values. This is to preclude computational

Coarse Grid Model

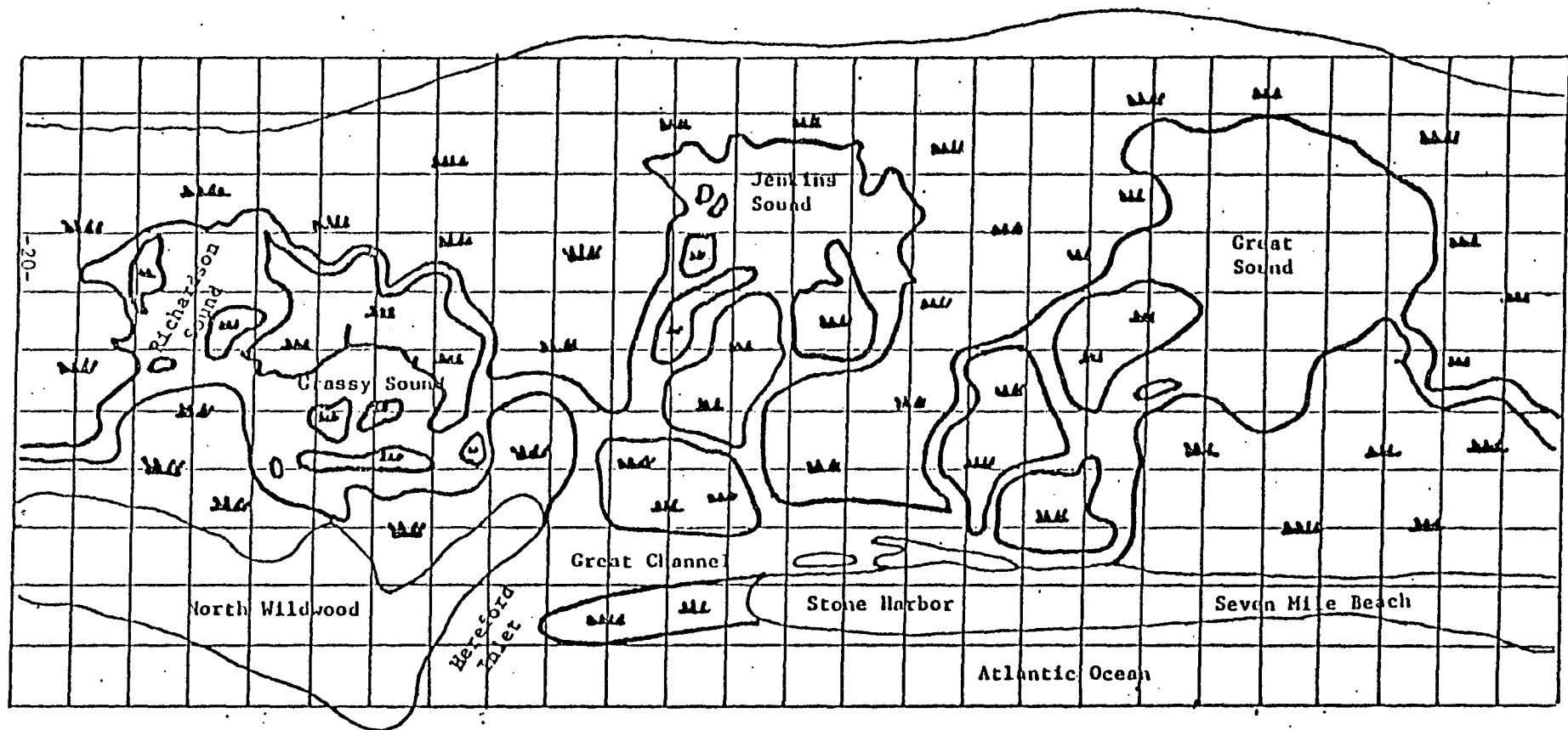


FIGURE 4

Coarse Grid Model

Coarse and Fine Grid Models

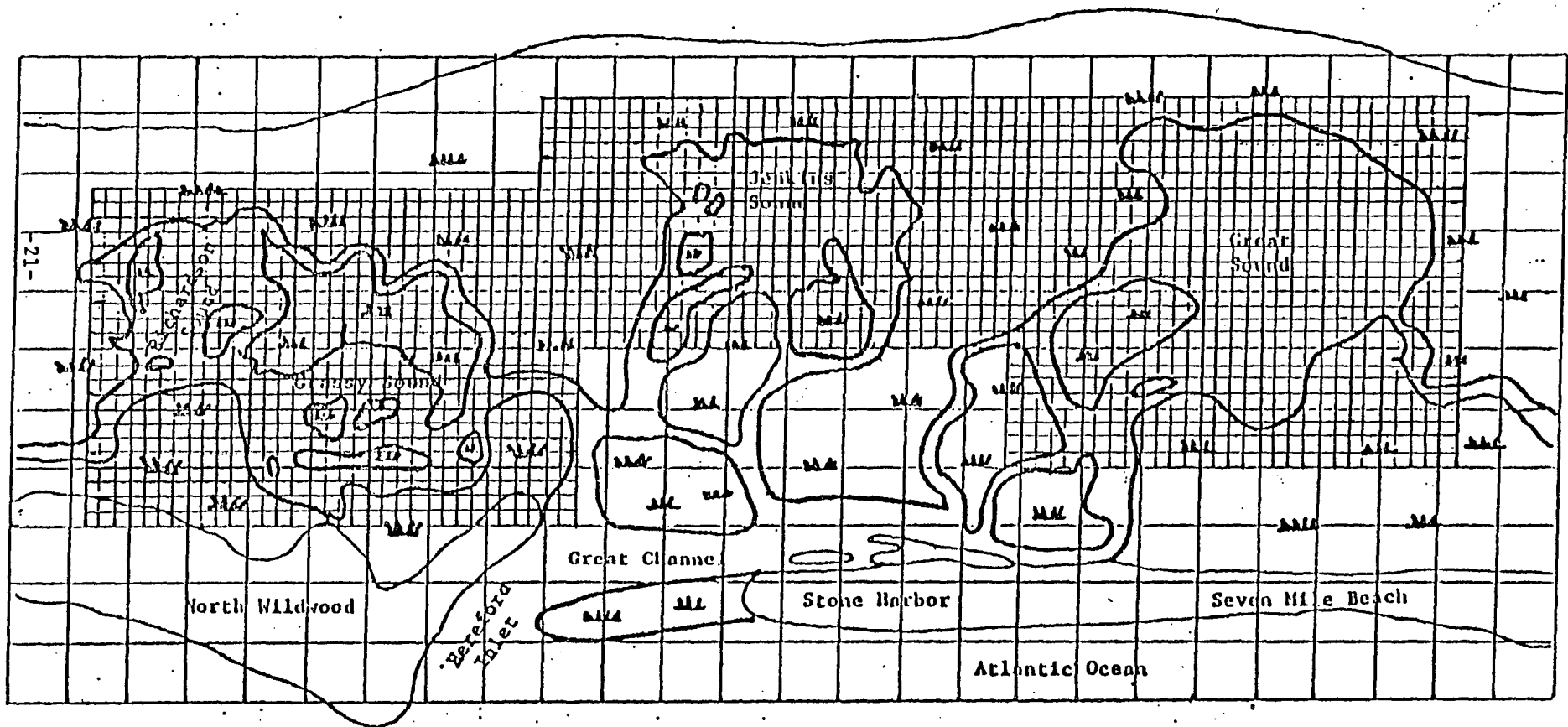


FIGURE 5

instabilities which can result when water is routed between a large number of slightly inundated areas at the same elevation. The datum for all elevations was mean low water (MLW).

Cell computation flags were determined by comparing the cell's top and right sides to those in Fig. 3. The cells in the marshy areas were encoded as inundation cells to permit filling on the flood tide and draining on the ebb tide. For computational reasons, an extra row of cells must be included along the top and right sides of each grid and are encoded as land cells. No computations are performed in these or any land cells.

Convective acceleration flags were assigned by comparing flow and no-flow sides around each cell to those in Fig. 6. To insure computational stability, it is necessary for forcing cells and inundation cells with positive elevations to be considered closed cells and assigned convective flag 22. As modified, the program automatically assigns a flag of 22 to all cells and then changes those for which a different flag is input.

As indicated previously, submerged and overtopping barriers were not employed in this study, as they introduce two more parameters, the discharge coefficient and the barrier crest elevation, which then must be determined. Should the use of these devices be desired, guidance for selecting values for these parameters can be found in Reid and Bodine (1968) and Masch, Brandes, and Reagan (1977 a and b).

# CONVECTIVE FLAGGING SCHEME










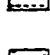
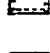
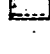
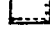

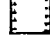
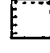
FLAG	SCHEMATIC	FLOW CONDITION			
		TOP	BOTTOM	R SIDE	L SIDE
11		FLOW	FLOW	FLOW	FLOW
12		FLOW	FLOW	NO FLOW	NO FLOW
13		FLOW	FLOW	FLOW	NO FLOW
14		FLOW	FLOW	NO FLOW	FLOW
21		NO FLOW	NO FLOW	FLOW	FLOW
22		NO FLOW	NO FLOW	NO FLOW	NO FLOW
23		NO FLOW	NO FLOW	FLOW	NO FLOW
24		NO FLOW	NO FLOW	NO FLOW	FLOW
31		FLOW	NO FLOW	FLOW	FLOW
32		FLOW	NO FLOW	NO FLOW	NO FLOW
33		FLOW	NO FLOW	FLOW	NO FLOW
34		FLOW	NO FLOW	NO FLOW	FLOW
41		NO FLOW	FLOW	FLOW	FLOW
42		NO FLOW	FLOW	NO FLOW	NO FLOW
43		NO FLOW	FLOW	FLOW	NO FLOW
44		NO FLOW	FLOW	NO FLOW	FLOW

FIGURE 6  
Convective Flagging Scheme

Estimates for Manning's  $n$  were based upon the values recommended by Chow (1964) and Escoffier (1977). The following formulas were used to compute Manning's  $n$  from the cell elevation,  $z$ :

$$z \leq 0 \quad n = 0.028 + z/1000. \quad (3)$$

$$z > 0 \quad n = 0.028 + z/200. \quad (4)$$

Tidal data were obtained from the Tidal Datums and Information Branch, Tides and Water Levels Division, National Ocean Survey (NOS), National Oceanic and Atmospheric Administration, Rockville, Maryland 20852. Records of hourly heights were obtained for the month of August, 1978, at the gages shown in Table 1.

TABLE 1  
Tidal Gages

<u>Gage Number</u>	<u>Gage Name/Location</u>
853-1680	Sandy Hook (SH)
-5375	Townsend Inlet (TI)
-5445	Great Sound (GS)
-5562	Shellbed Landing, Jenkins Sound (JS)
-5581	Stone Harbor, Great Channel (GC)
-5561	Nummy Island (NI)
-5695	Old Turtle Thorofare (OTT)
-5726	West Wildwood, Grassy Sound (WW)
-5838	Sunset Lake (SL)



For each of the records, except Great Sound and Jenkins Sound, a correction to be subtracted from each of the hourly heights to refer the data to MLW was provided by NOS. The records in these two sounds indicated that whenever those gages went below one foot staff reading, the gages stuck until the tide rose again to free them. Thus, those two records contained no low water data except on 25, 26, and 27 of August 1978, which was a neap tide period. In order to use a complete set of tidal data, one of those days, 25 August, was selected as the calibration day.

For the coarse grid, the tidal record at Sunset Lake was used to force the system from the south and the Townsend Inlet record from the north. To force the system from the ocean, the Sandy Hook record was used and modified to approximate the tide to be expected at Hereford Inlet. Tide tables (1978) provided the following relations between the Sandy Hook and Hereford Inlet tides:

Differences

<u>Time</u>		<u>Height</u>	
<u>High Water</u>	<u>Low Water</u>	<u>High Water</u>	<u>Low Water</u>
h m	h m	ft	ft
+0 02	+0 02	-0.5	0.0

These corrections indicate on the average the high and low tides occur two minutes later at Hereford Inlet than at Sandy Hook and the high water height is one-half foot lower at Hereford Inlet than at

Sandy Hook, while the low water heights are essentially the same. Since the time difference between the two stations was considered negligible, the Hereford Inlet tide was derived from the Sandy Hook by adjusting that record as follows: the recorded low water was left unchanged, the recorded high was reduced by an amount up to 0.5 ft., and all intermediate heights reduced by linear interpolation. During the calibration process, different corrections were applied, and the correction yielding the best reproduction at Nummy Island, located just inside the inlet, was accepted. This value was 0.25 ft.

For the three fine grids, the tidal heights for the forcing cells were derived from known records or from the tidal heights computed in the coarse grid, as indicated in Table 2.

TABLE 2

Fine Grid Tidal Data

<u>Fine Grid</u>	<u>Forcing Cell</u>	<u>Source</u>
Jenkins Sound	All	Coarse Grid I10J04 (computed Nummy Island)
Great Sound	I05J01	Coarse Grid I19J05
	I06J01	Coarse Grid I19J05
	I08J01	Coarse Grid I19J05
	I29J05	Townsend Inlet
Grassy-Richardson Sound	I32J05	Coarse Grid I10J04
	I01J09	Sunset Lake

In this table, IxxJyy refer to the x and y indices resulting from the discretization process of Fig. 2.

The missing records from the Great Sound and Jenkins Sound gages required an estimate be made of the correction to reference those readings to MLW. A correlation was found between the low water reading on any day and the correction to be applied to that reading to reference it to MLW. A least squares analysis of the data in Table 3 yielded a correlation coefficient of 0.9987.

TABLE 3

Selected Tidal Heights 26 August 1978

	<u>Low Water Reading</u>	<u>MLW Correction</u>
Old Turtle Thorofare	1.20	0.46
Sunset Lake	1.53	0.72
Nummy Island	1.87	1.01
Townsend Inlet	2.11	1.34
West Wildwood	3.28	2.47
Great Channel	4.07	3.39

The least squares analysis yielded the regression equation:

$$\text{MLW Correction} = 1.0 \cdot (\text{Low Water Reading}) - 0.84 \quad (5)$$

as the line of best fit and was used to determine corrections of 0.30 for Great Sound and 0.50 for Jenkins Sound. The data and the

best fit line are shown in Fig. 7. The measured and adjusted tidal data for 25 August are contained in Appendix 2.

The next step in the implementation procedure was to select the program control options and to assemble the data into the required input formats. Masch, Brandes, and Reagan (1977 a and b) detail these options and formats. While the program does permit inclusion of wind, precipitation, and evaporation effects, accurate information concerning these effects was not available, and hence, they were not included. Further, since these effects are expected to be small compared to the tidal effect, their exclusion should not cause any significant errors.

The first run for all of the grids was the "zero" test case. In this test, zero height tides were applied to the grid and used to locate any miscoded cells which produced nonzero flows and heights.

After correcting any coding errors detected by the zero test, the next run was to generate the flows and heights in each cell corresponding to the initial conditions of the calibration period. This was accomplished through the program's control options to set the initial hydrodynamics to zero or read them from tape or cards, and to save the ending hydrodynamics on file.

For the coarse grid, four start-up techniques were tested. The first technique was to set the initial hydrodynamics to zero and to apply the observed tidal heights in the forcing cells for one tidal cycle of approximately 12.4 hours. The ending hydrodynamics for each

STAGE - VS CORRECTION  
REGRESSION  
+ - RECORDED STAGE  
- - BEST FIT LINE

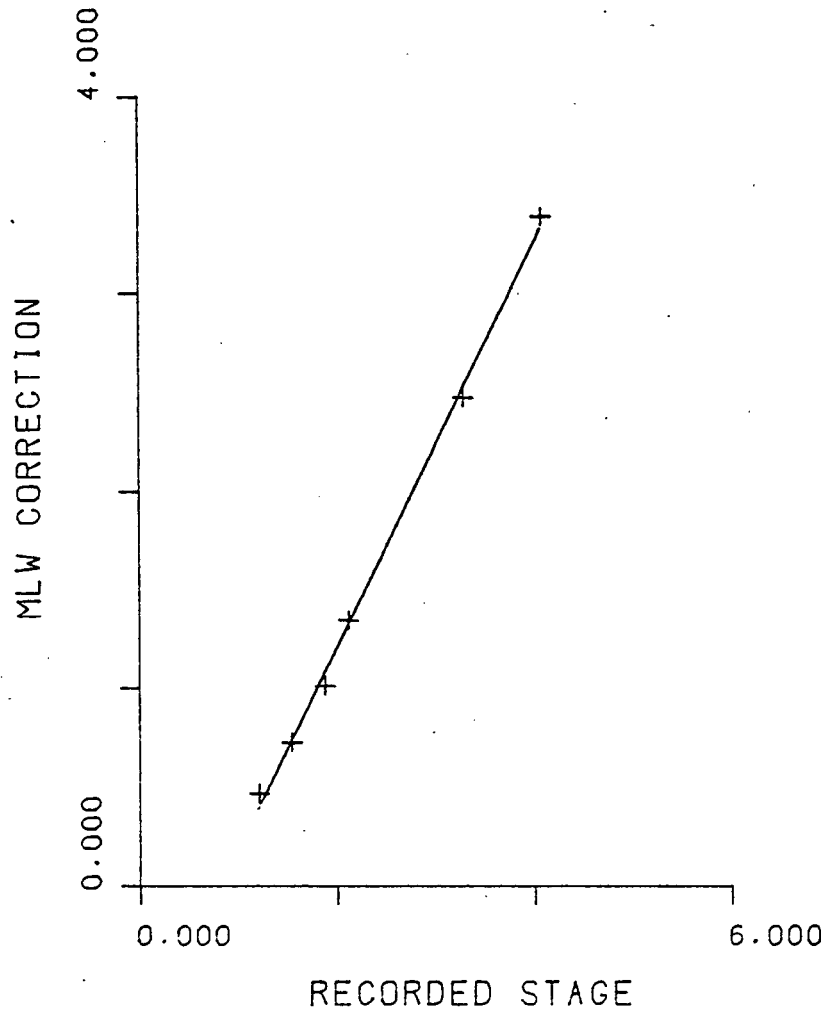


FIGURE 7

Stage versus Correction Regression

cell were then saved and used to approximate the initial conditions at the beginning of the tidal cycle. This technique is illustrated in Fig. 8a, which shows the response of a typical back bay cell to the application of an observed ocean tide in a nearby forcing cell.

This proved unsatisfactory for two reasons. First, it was found that if start-up was attempted with the initial hydrodynamics set to zero while the applied tides were much different than zero, surges would develop. These surges could result in computational instabilities and physical impossibilities, such as water levels greatly in excess of those applied. Second, upon restart, the flows and heights across the tidal boundaries did not exactly correspond to those required by Eq. (2). This resulted in the first 10-20 time steps of the restart being used to realign these flows and heights, adversely affecting the simulation for a short time period at the beginning of the restart.

The second technique also involved setting the initial hydrodynamics to zero, but applied synthetic tides which started at zero height and increased in magnitude following the observed tides until the starting heights were reached. This is illustrated in Fig. 8b. This technique eliminated the problems associated with the first technique and had an additional advantage of saving on computer resources by reducing the computation effort required to generate the initial conditions. However, since the datum chosen for the model was mean low water, the tidal height at low water in the previous tidal cycle was over a foot and a half. Using this technique,

# START-UP TECHNIQUES

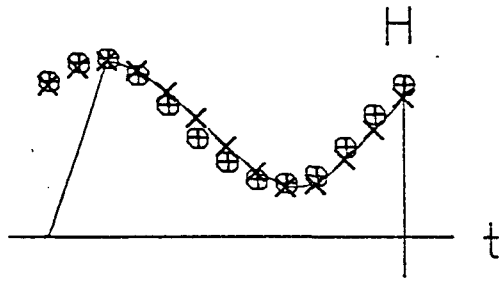


FIGURE 8a

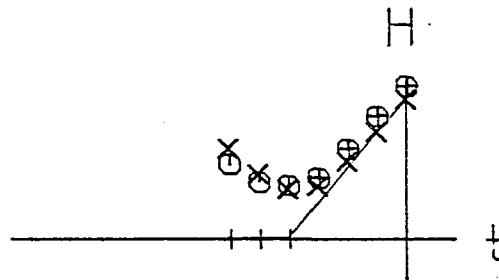


FIGURE 8b

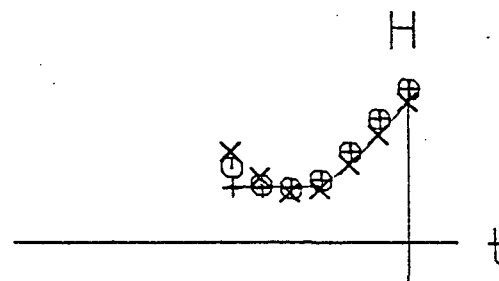


FIGURE 8c

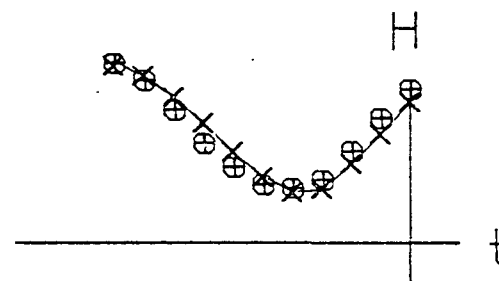


FIGURE 8d

- ⊙ - OBSERVED OCEAN TIDE
- + - APPLIED OCEAN TIDE
- × - OBSERVED BAY RESPONSE
- - COMPUTED BAY RESPONSE

substantial depth changes were required to fill the water cells to that depth before proceeding through the tidal cycle.

The third technique involved writing a separate routine to fill all water cells to the low water depth (1.69 ft. for the coarse grid) and to set the x and y flows to zero. This information was stored on file and read as the initial hydrodynamics for a run which started at this height and followed the observed records to the heights of interest (see Fig. 8c).

The last technique was similar to the third technique, except the water cells were filled to the highest value observed in the previous cycle and then permitted to drain and refill following the observed records (see Fig. 8d).

The tidal heights computed by the last three techniques were within the thousandths of a foot in any one cell, with the corresponding flows within 10%. Confident that these results were equally accurate, the third technique was adopted, since it required the least computational effort. For the fine grids, this same technique was used, with the tidal heights applied being those generated by the coarse grid during its start-up.

Given these starting conditions, calibration runs were conducted for the neap tide case and the output refined through the adjustment of the bottom friction and the elevations assigned to the inundatable areas. The Hereford Inlet tide was also modified until satisfactory reproduction of known back bay records was achieved.



These final parameter values became those adopted for future operational runs.

### 3.3 Presentation of the Results

As currently structured, the program's output includes printing hourly flows in the x and y directions and computed tidal heights for twenty predesignated cells. Line printer plotting of computed and observed heights is also available. While this information provided some understanding of the system's response, it did not provide the insight into the system's hydraulics that was desired. A picture of the flow pattern at any point in time would readily provide the desired insight.

Development of the picture concept was easily accomplished by combining the program's ability to store instantaneous hydrodynamics ( $h$ ,  $q_x$ , and  $q_y$ ) for every cell at any desired time level with a plotting routine designed to accurately display the information in pictorial form. By checking the height in the cell, the plotting routine determines whether the cell is a land cell, water cell, or inundatable area, and whether the inundatable area is wet or dry. It then plots the x flow on the right side of the cell and the y flow on the top side, each appropriately scaled to represent the magnitude of that flow. No-flow boundaries and forcing cells are indicated. A title box is included, providing the name of the grid being plotted, the date and time of the information, a key to the symbols employed, and

the scale of the flow vectors. A marker indicates the point in the tidal cycle relative to the ocean tide..

The models were run to simulate two tidal cycles (approximately 25 hours), beginning 2400 hours (midnight) 25 August 1978 and ending 0100 hours (1:00 a.m.) 27 August 1978. Instantaneous hydrodynamics were saved at ten minute intervals and later used to plot flow patterns, flow rate versus time, volume versus time, and tidal height versus time at selected locations. The ten minute time interval was selected because it provided sufficient detail without an overabundance of data being saved.

In reviewing the flow patterns it must be remembered that the models are not yet calibrated to predict flows. The flow patterns are contained in Appendices 3 through 6. These results are discussed in the next section.

#### 4. DISCUSSION OF THE RESULTS

##### 4.1 Coarse Grid

Figure 9 shows the coarse grid and its relation to the study area. The output from the grid is contained in Appendix 3. Throughout the following discussion, any reference to Hereford Inlet, Sunset Lake, or Townsend Inlet is construed to mean the forcing cells at these locations.

At the start of the simulation period the tide is rising. Sunset Lake is filling Richardson and Grassy Sounds, with some flow through to Nummy Island. Hereford Inlet is filling Jenkins Sound, with some flow up Great Channel to Great Sound. Great Sound is also being filled from Townsend Inlet.



At 0100 hours the flows are decreasing. Jenkins Sound is now being filled entirely from Sunset Lake. Little influence is being felt from Townsend Inlet.

At 0200 hours high ocean tide occurs. An unexpected flow-through condition exists, with flow in at Sunset Lake, through the system along the Intercoastal Waterway and out at Townsend Inlet. A near slack condition exists in Hereford Inlet and Jenkins Sound.

By 0300 hours the tide is falling, but the flow-through condition still exists. Richardson, Grassy, and Jenkins Sounds are draining, with about half of the water leaving the system through Hereford Inlet, the remainder flowing up Great Channel to Great Sound where it drains through Townsend Inlet.

Coarse Grid

Note: See Table 1 for abbreviations

Key:  - Tidal Gage  
 - Forcing Cell

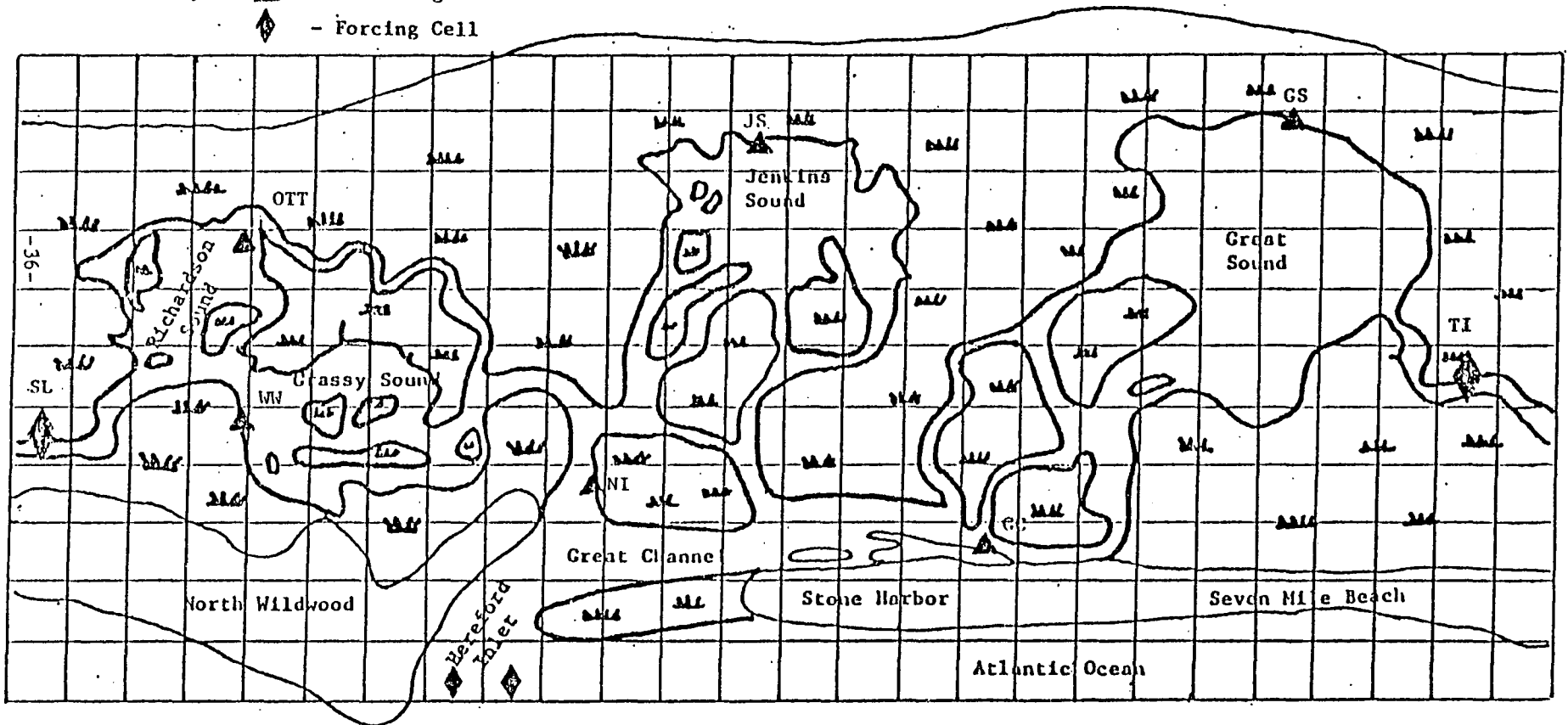


FIGURE 9  
Coarse Grid

As the tide falls, so does the influence of Sunset Lake. At 0400 hours the drainage pattern is similar to that at 0300 hours, but the flow in Great Channel is greatly diminished. There is evidence of a nodal point forming, indicating flow both up and down the channel.

Maximum ebb flow occurs through Hereford Inlet about 0500 hours. The nodal point has moved five or six cells up Great Channel, as there is little inflow from Sunset Lake and increased discharge out Townsend Inlet.

As the tide continues to fall through 0600 hours, flow is now out through Sunset Lake. Flow magnitudes continue to decrease, and at 0800 hours low water is reached. A slight flow is indicated up the Intercoastal Waterway and out Townsend Inlet, but there is little flow past Sunset Lake or Hereford Inlet. This corresponds to the slack water condition.

By 0900 hours the tide is rising. Sunset Lake is filling Richardson and Grassy Sounds. Hereford Inlet fills Jenkins Sound and Great Sound through Great Channel, while Townsend Inlet contributes a small volume to Great Sound. The flow magnitudes increase as the tide rises, reaching maximum flood flow through Hereford Inlet about 1100 hours and then decrease as high tide is approached. High tide occurs at 1400 hours, but it is not until 1500 hours that the slack water condition exists in the inlet. At this time, the flow pattern exhibits the same flow-through condition as seen at 0200 hours, and hereafter the cycle repeats itself.

The flow-through character of the system is further displayed in Fig. 10, which depicts the flow rate versus time at Hereford Inlet, Sunset Lake, and Townsend Inlet. Flow into the system is defined as positive, outflow as negative. Figure 10 indicates the flow at Hereford Inlet is generally sinusoidal, the flow at Sunset Lake is predominately in and at Townsend Inlet it is predominately out.

Integrating the flow versus time curve with the trapezoidal rule yields the volume passing the point with time. If the flow versus time curve was a true sine curve, integration over one cycle would yield zero net volume. From the total volume line in Fig. 11, it can be seen that zero net volume occurs at 1214 hours, or 11 minutes before the end of the typical 12 hour, 25 minute tidal cycle. At the end of the two cycles, however, there is a net outflow of water on the order of  $1.8 \cdot 10^8$  cubic feet. Extrapolation of the results indicate it would take an additional 50 minutes to bring the system back to zero net volume, while Hereford Inlet would take about 80 minutes before its next zero crossing.

Computed and observed tidal heights generally compared quite well. At Old Turtle Thorofare, located in Richardson Sound, computed and observed tidal heights agreed quite favorably, although the predicted values were slightly higher than observed values at low water (see Fig. 12). The same was true for the West Wildwood gage, located in Grassy Sound, as can be seen in Fig. 13.

FLOW RATE VS TIME  
COARSE GRID MODEL

- 1 - FLOW AT HEREFORD INLET
- 2 - FLOW AT SUNSET LAKE
- 3 - FLOW AT TOWNSEND INLET

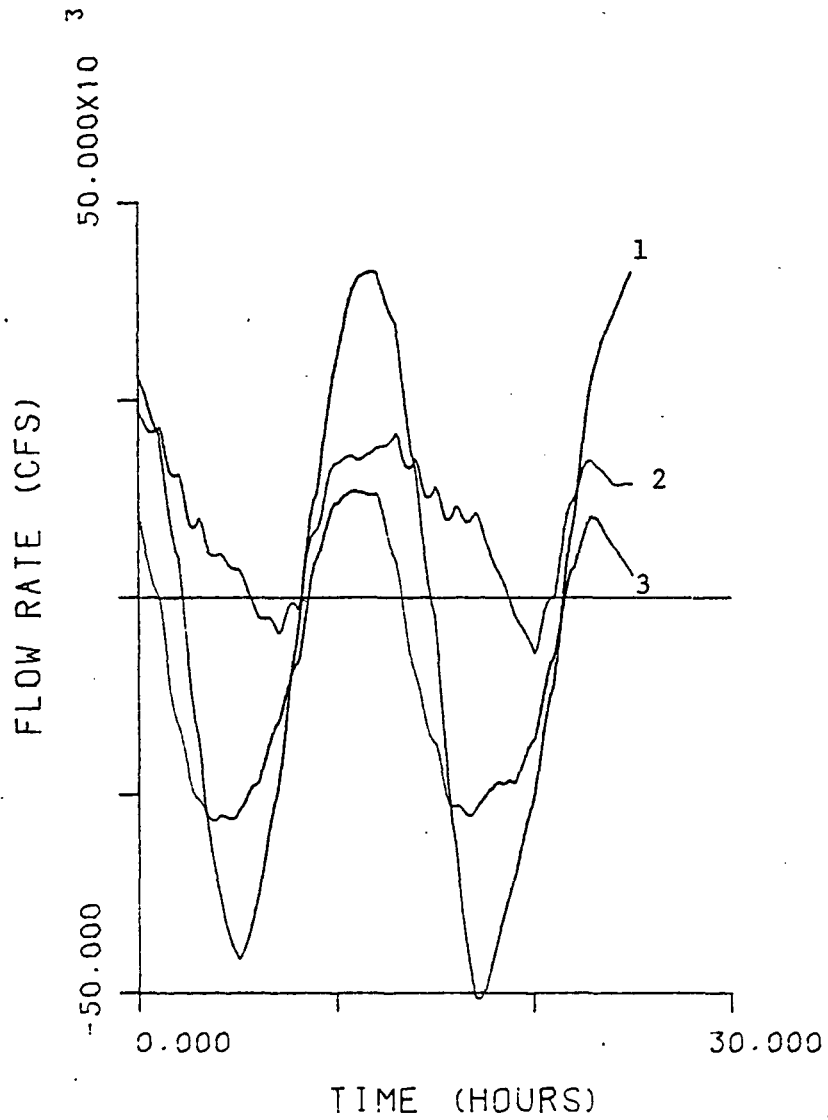


FIGURE 10

Flow Rate versus Time -- Coarse Grid Model

VOLUME VS TIME  
COARSE GRID MODEL

- 1 - VOL PAST HEREFORD INLET
- 2 - VOL PAST SUNSET LAKE
- 3 - VOL PAST TOWNSEND INLET
- 4 - TOTAL VOLUME

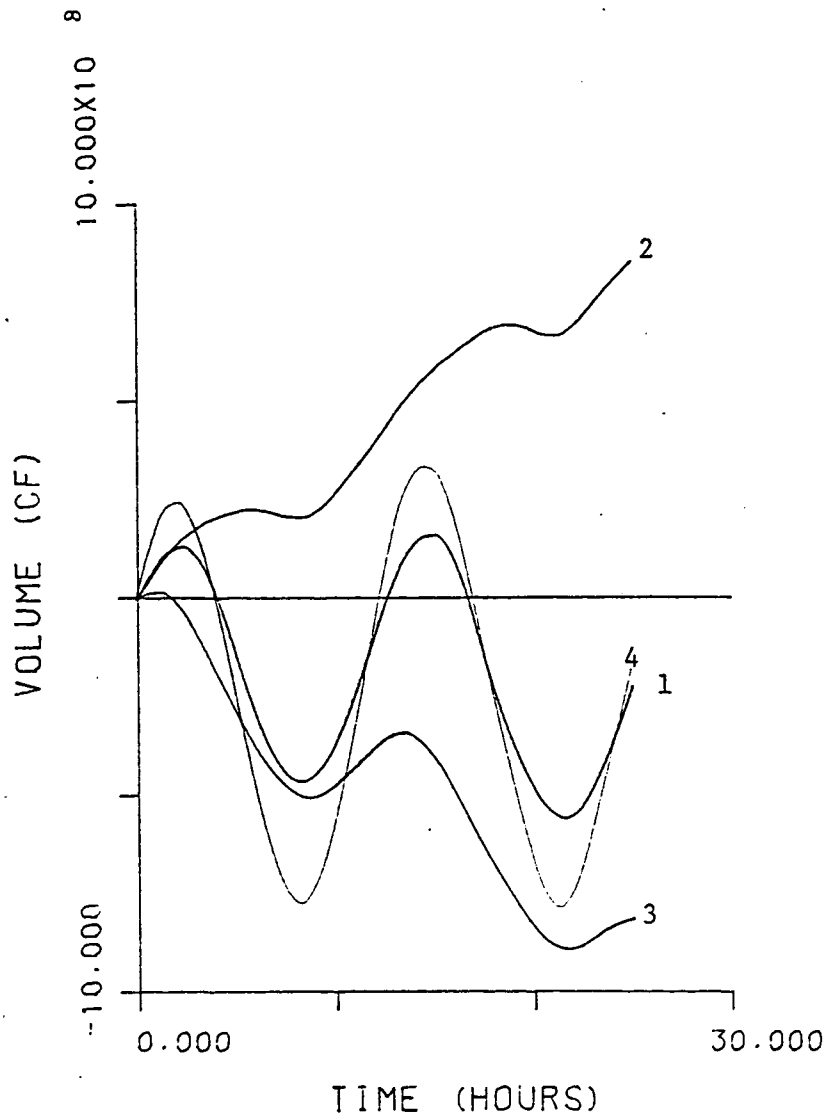


FIGURE 11

Volume versus Time - Coarse Grid Model



TIDAL HEIGHT VS TIME  
 OLD TURTLE THOROFARE  
 + - OBSERVED MLW HEIGHT  
 - - COMPUTED MLW HEIGHT

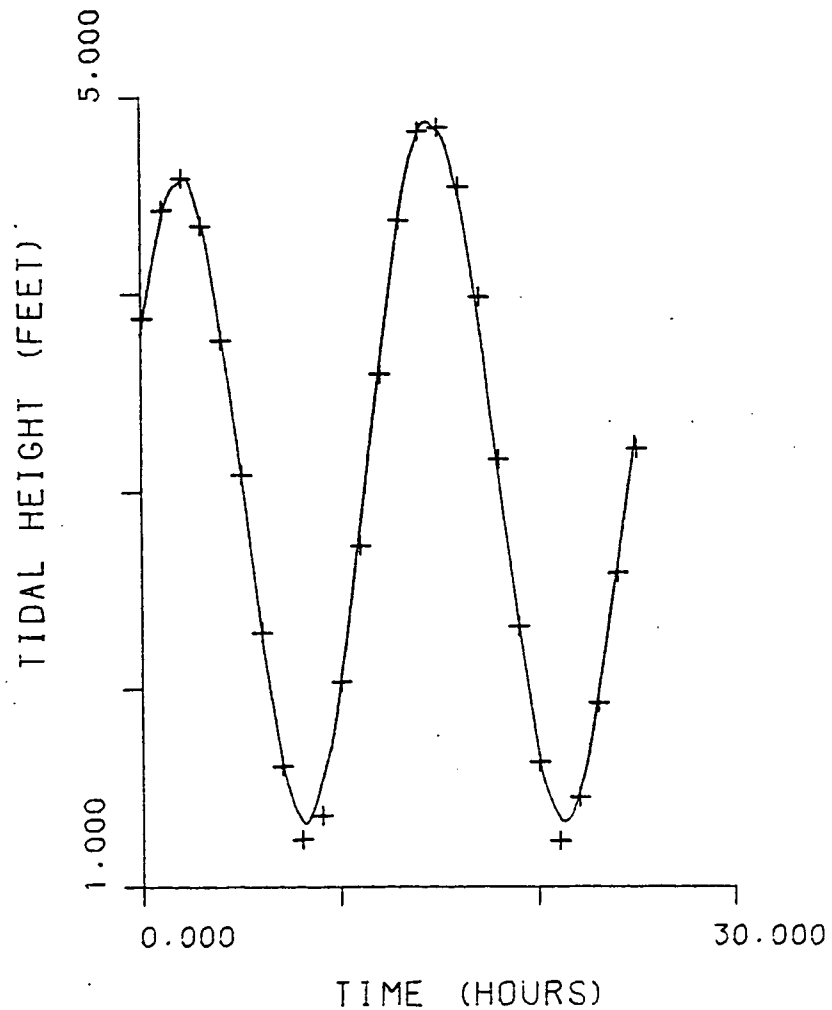


FIGURE 12

Tidal Height versus Time - Old Turtle Thorofare

TIDAL HEIGHT VS TIME  
WEST WILDWOOD GAGE  
+ - OBSERVED MLW HEIGHT  
- - COMPUTED MLW HEIGHT

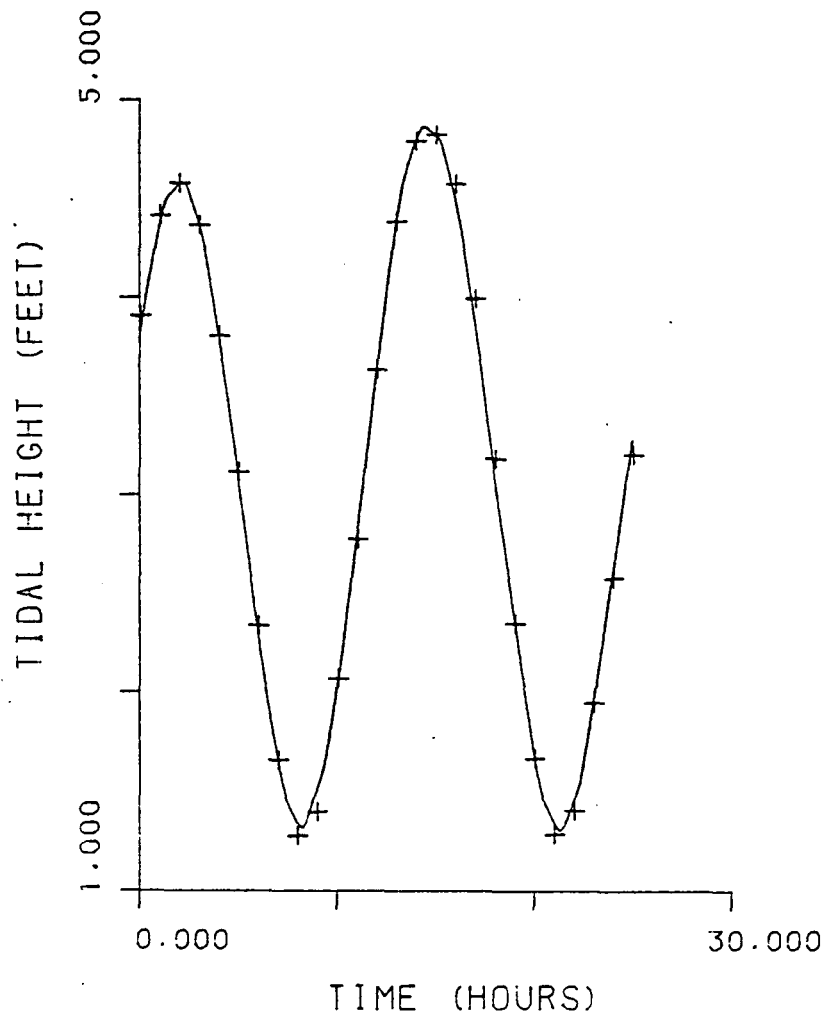


FIGURE 13

Tidal Height versus Time - West Wildwood Gage

At Nummy Island reproduction was generally accurate, although a slight phase lag was evidenced near the extremes (see Fig. 14). At the extremes the model slightly overestimated the highs and underestimated the lows. These errors are directly related to the adjustment of the Sandy Hook tide.

At Shellbed Landing, located in Jenkins Sound, reproduction was also adequate, although the same situations occurred as with Nummy Island. The observed and computed tidal heights show close agreement, lending credibility to the least squares technique used to obtain the MLW correction (see Fig. 15).

Comparison of the observed computed heights at the Stone Harbor gage, Great Channel, is presented in Fig. 16. While of lesser quality than the others, the reproduction of the observed record is still considered satisfactory.

At the last gage, Great Sound, the computed tidal heights generally lead the observed heights by about half an hour (see Fig. 17). Observed heights at Great Sound are consistent with the heights observed at other cells in that the lows are not low enough, but they also suffer in that the highs are not high enough. This may result from too much water leaving the system at Townsend Inlet, thus not permitting the tidal height to build up.

Overall, the ability of the coarse grid to reproduce observed tidal heights is good. The problems related to the computed low water heights are directly associated with the decision to leave the low

TIDAL HEIGHT VS TIME  
 NUMMY ISLAND GAGE  
 + - OBSERVED MLW HEIGHT  
 - - COMPUTED MLW HEIGHT

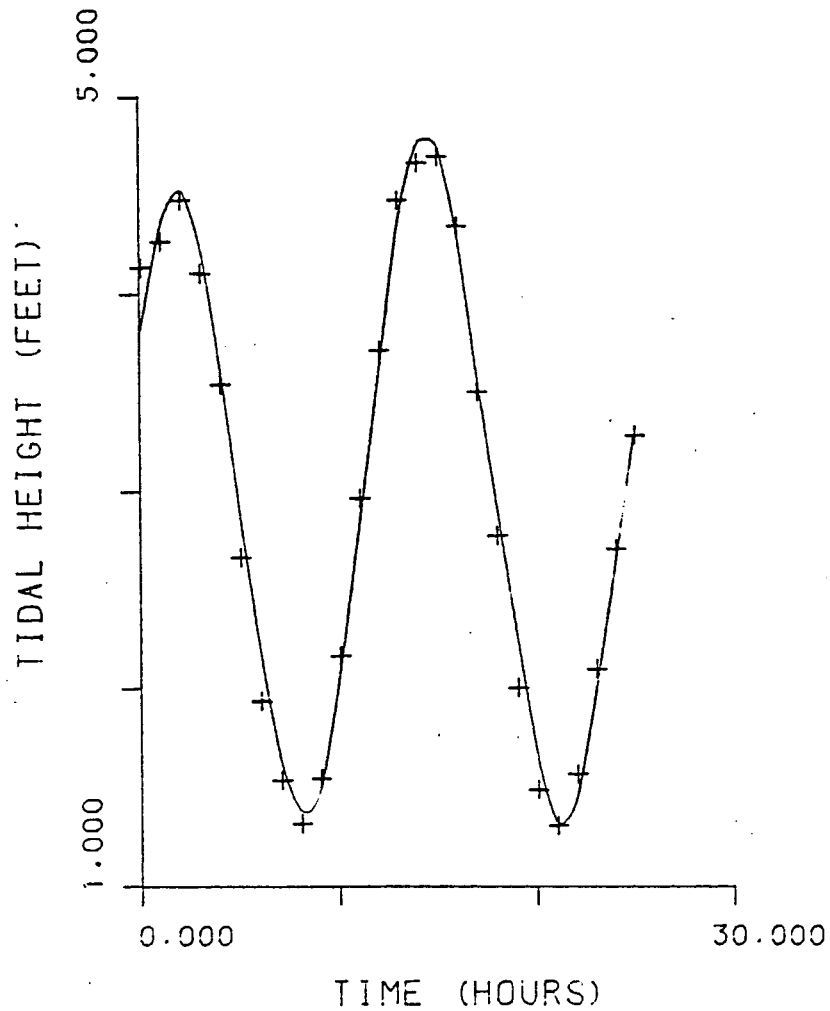


FIGURE 14

Tidal Height versus Time - Nummy Island Gage

TIDAL HEIGHT VS TIME  
 SHELLBED LANDING GAGE  
 + - OBSERVED MLW HEIGHT  
 - - COMPUTED MLW HEIGHT

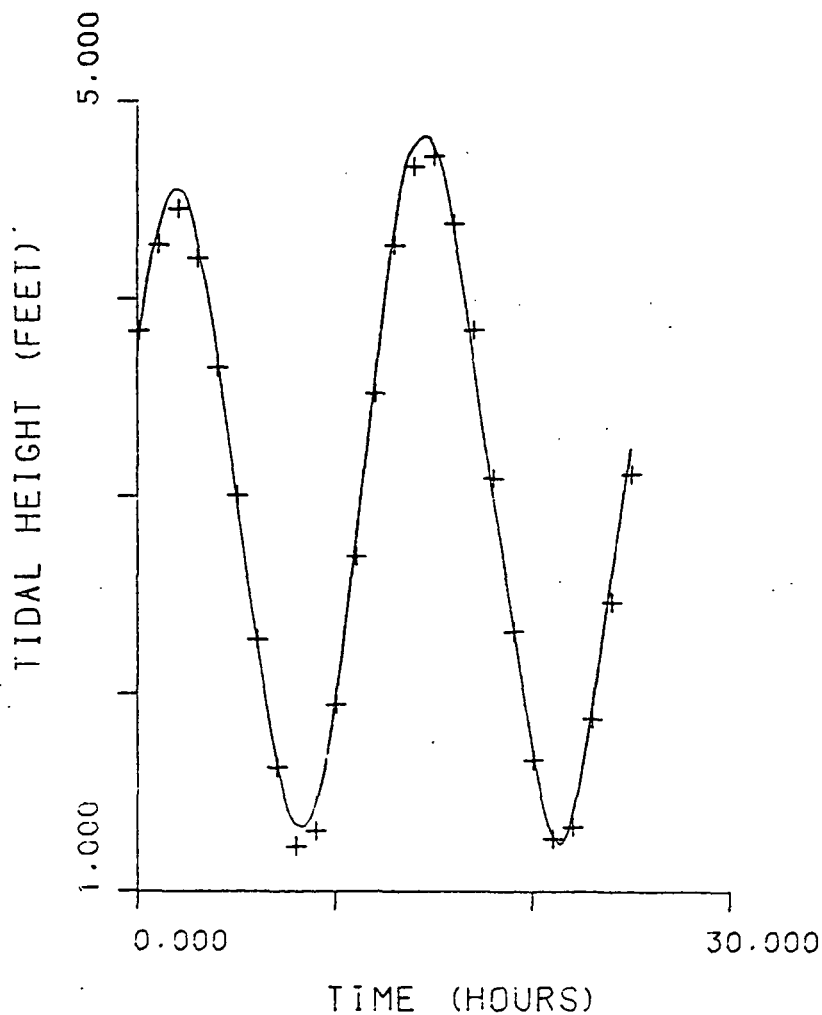


FIGURE 15  
 Tidal Height versus Time - Shellbed Landing Gage

TIDAL HEIGHT VS TIME  
 GREAT CHANNEL GAGE  
 + - OBSERVED MLW HEIGHT  
 - - COMPUTED MLW HEIGHT

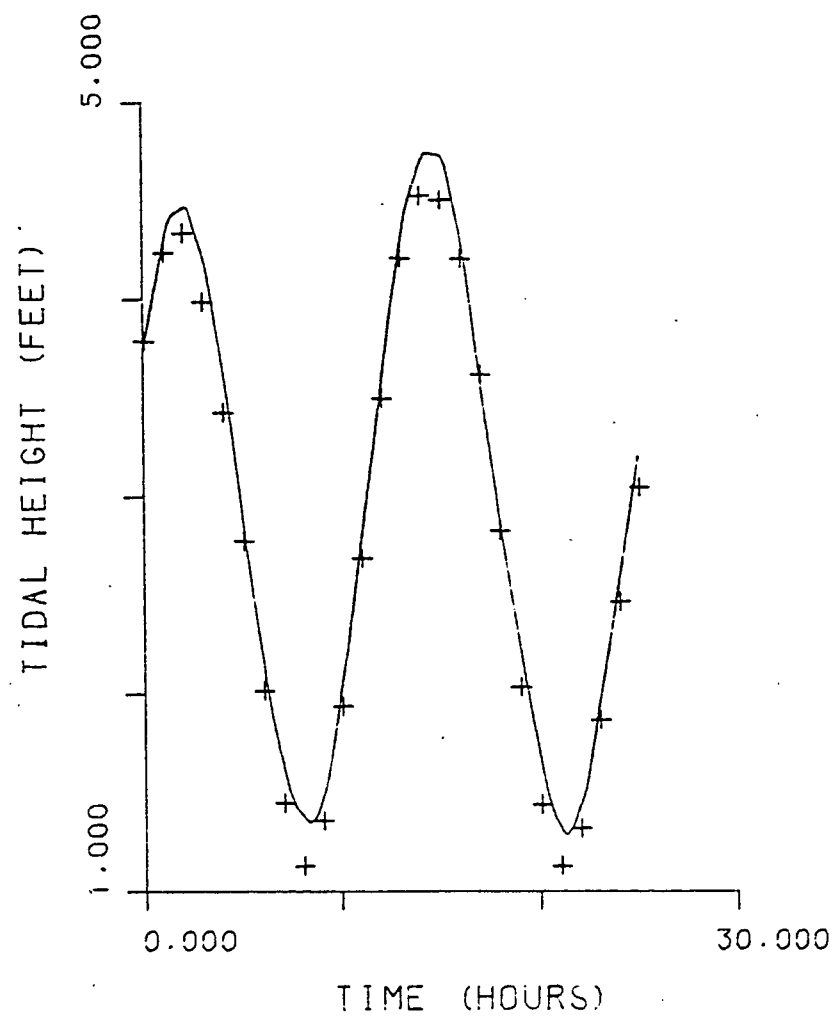


FIGURE 16

Tidal Height versus Time - Great Channel Gage

TIDAL HEIGHT VS TIME  
 GREAT SOUND GAGE  
 + - OBSERVED MLW HEIGHT  
 - - COMPUTED MLW HEIGHT

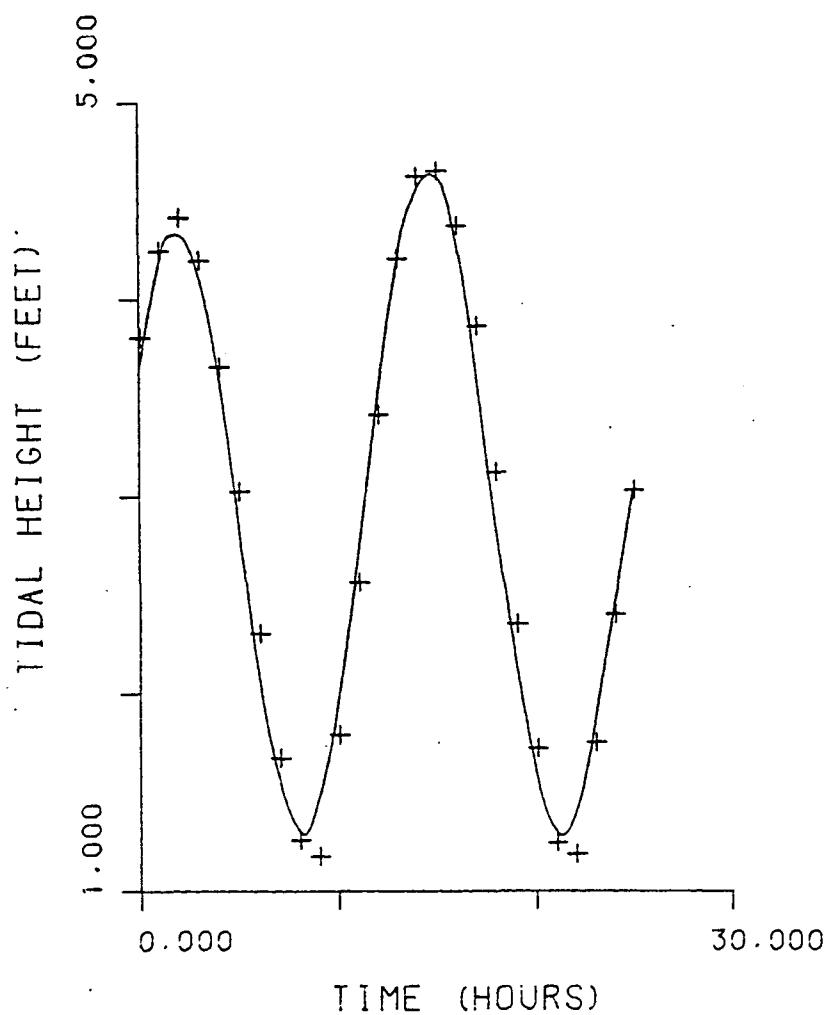


FIGURE 17

Tidal Height versus Time - Great Sound Gage

water heights of the Sandy Hook tide unadjusted. Had these values been lowered about 0.1 feet, reproduction of the low values would have been much better. Problems with the highs are fine tuning ones, and some adjustment of friction factors may help, but greatly improved reproduction of observed tidal heights is not likely to be achieved.

Concerning the flows and flow measurements predicted by the coarse grid, it is clearly evident that the grid is too coarse to accurately predict the flows in the system. In locations such as Sunset Lake, Townsend Inlet, and Great Channel, channels that are actually 500 feet wide and up to 30 feet deep are modeled as being 2000 feet wide and eight feet deep. As a result, these channels may be too efficient and permit too much water to pass. The fact that Sunset Lake is constantly higher than Townsend Inlet drives the flow through the system as observed. In reality, much of this head might be lost in the constricted channel connecting Sunset Lake with Richardson and Grassy Sounds. At this point, velocity or discharge measurements are needed to permit further refinement of the coarse grid.

Despite these shortcomings, as this is a neap tide day, an order of magnitude estimate for the minimum tidal prism for Hereford Inlet can be obtained from these results. The maximum positive volume occurs at the change from flood to ebb tide. Likewise, the most negative volume corresponds to the change from ebb to flood tide. Thus, the difference between these two values represents the volume of the tidal prism for the ebb tide.



Using the data for the first tidal cycle and taking the most positive volume minus the most negative volume, an estimate for the ebb tidal prism is:

$$1.3 \cdot 10^8 \text{ ft}^3 - (-4.7 \cdot 10^8) \text{ ft}^3 = 6.0 \cdot 10^8 \text{ ft}^3$$

Applying this procedure to the second tidal cycle yields:

$$1.6 \cdot 10^8 \text{ ft}^3 - (-5.5 \cdot 10^8) \text{ ft}^3 = 8.1 \cdot 10^8 \text{ ft}^3$$

Similarly, the tidal prism for the flood tide can be computed by taking the most positive volume from the second tidal cycle minus the most negative volume from the first, as this difference represents the total volume which flowed in through the inlet. This calculation yields:

$$1.6 \cdot 10^8 \text{ ft}^3 - (-4.7 \cdot 10^8) \text{ ft}^3 = 6.3 \cdot 10^8 \text{ ft}^3$$

The tidal prism for other tidal cycles is expected to be greater than these values.

#### 4.2 Jenkins Sound Fine Grid

The Jenkins Sound fine grid is shown in Fig. 18. The output of the model is found in Appendix 4.

Beginning at 2400 hours the tide is rising, and the sound is filling. Between 2400 and 0100 hours inundation occurs in the areas set at elevation 4.0 to 4.1 feet, as can be seen by comparing the two flow patterns and noticing that some of the marsh symbols have

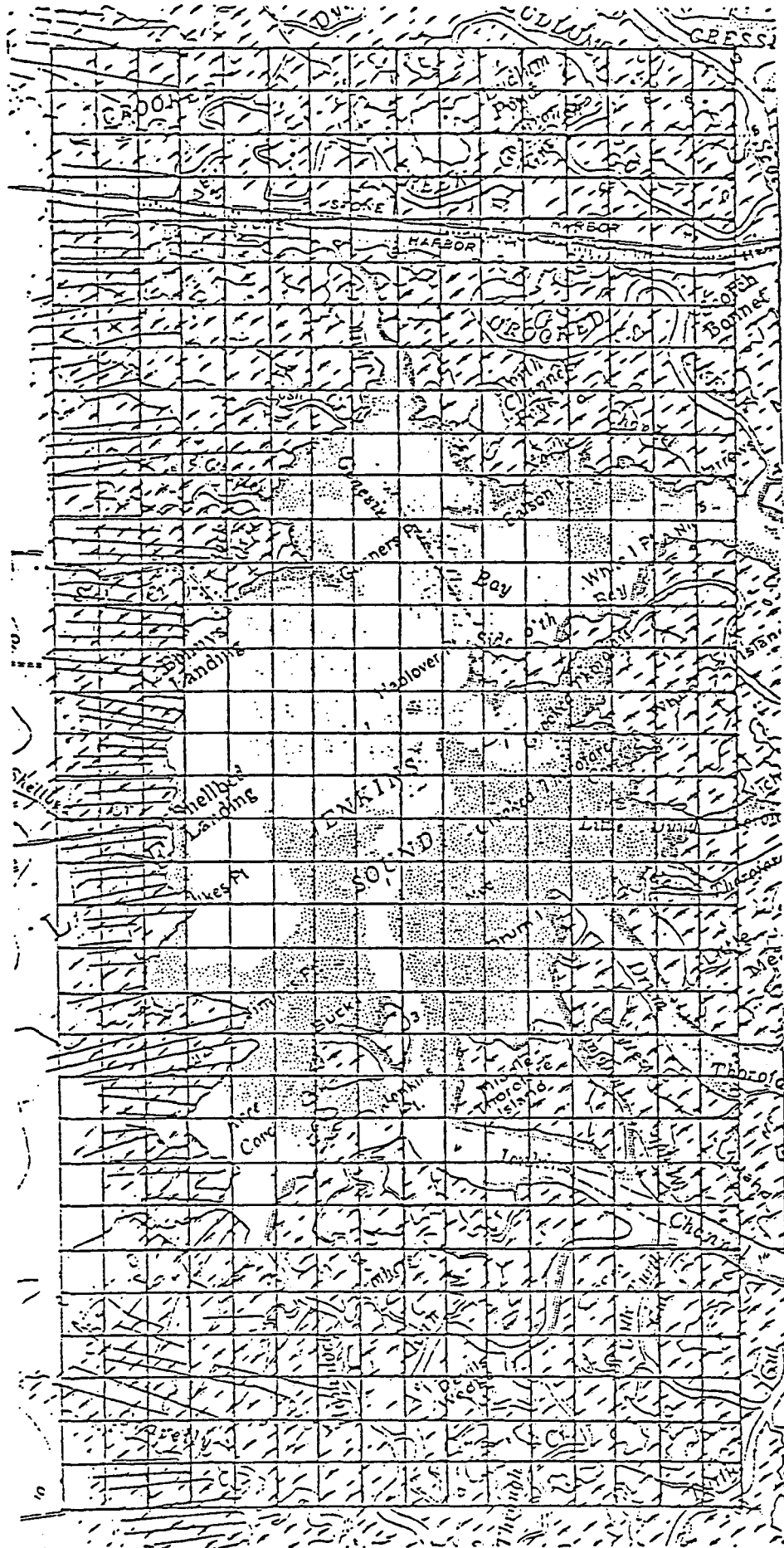


FIGURE 18  
 Jenkins Sound Fine Grid  
 -50-

disappeared. At 0200 hours high tide is reached, and then the sound begins draining. By 0400 hours, the tidal heights are below 4.0 feet, and the inundated areas become dry once again, as indicated by the return of the marsh symbols. Draining continues until low tide at 0800 hours, after which filling begins. The rate of filling increases through the maximum flood tide about 1100 hours, and decreases to zero near 1500 hours. Thereafter, draining begins, and the cycle repeats.

The inflow and outflow of the tidal cycle is readily evident in Fig. 19, which shows the sum of the flow rates with time through the grid's four forcing cells. The corresponding volume versus time graph is Fig. 20. From Fig. 20, it can be seen that zero net exchange occurs at 1218 hours or about nine minutes before the end of a typical cycle. The net outflow at the end of the second cycle is  $1.7 \cdot 10^8$  cubic feet.

The computed and observed tidal heights are compared in Fig. 21. Reproduction is accurate, except at low tide. This reflects the inadequacy of the input data as generated by the coarse grid in this range.

Comparison of flow rates, volumes, and tidal heights for the coarse and fine grid models of Jenkins Sound are made in Figs. 22 to 24. The flow rates show consistency between them, although at the change of tide, the magnitude of the coarse grid flow is usually slightly larger than that of the fine grid. This is reflected in the volume versus time comparison, where the coarse grid volumes are larger, but the zero crossings are quite close. The computed tidal heights show no discernable difference.

FLOW RATE VS TIME  
JENKINS SOUND FINE GRID

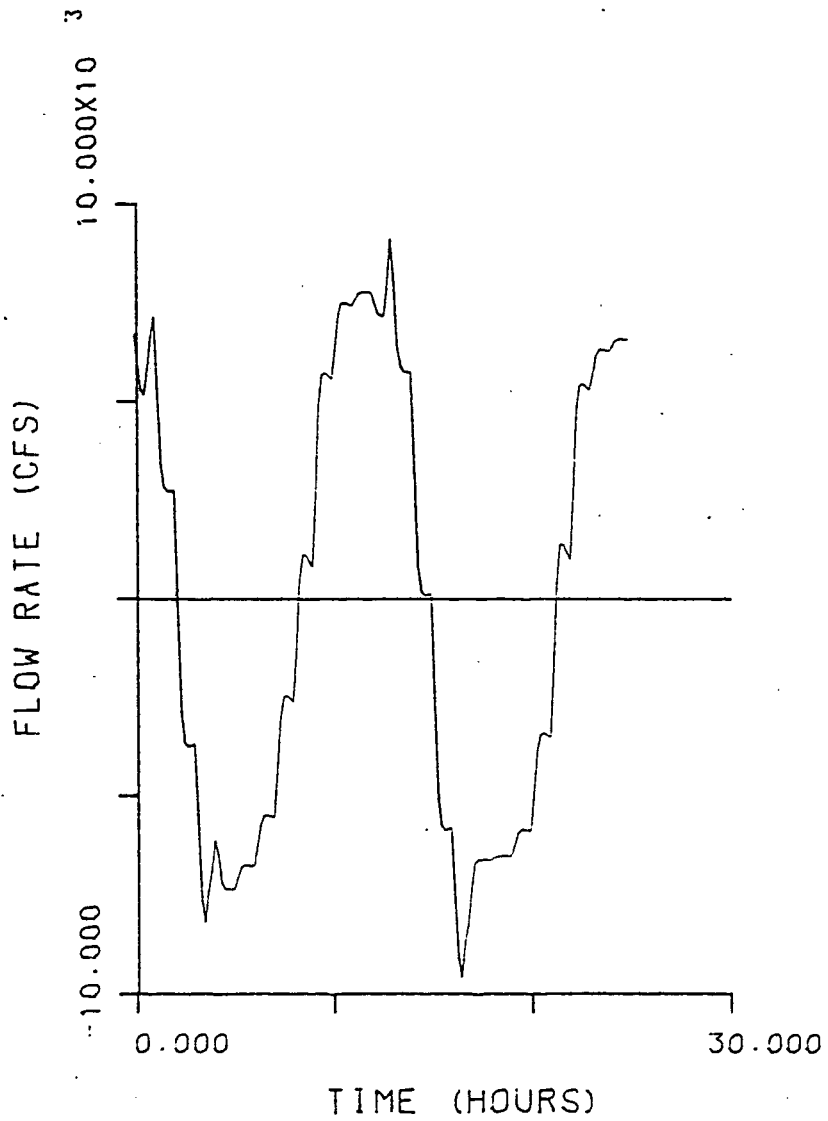


FIGURE 19

Flow Rate versus Time - Jenkins Sound Fine Grid

VOLUME VS TIME  
JENKINS SOUND FINE GRID

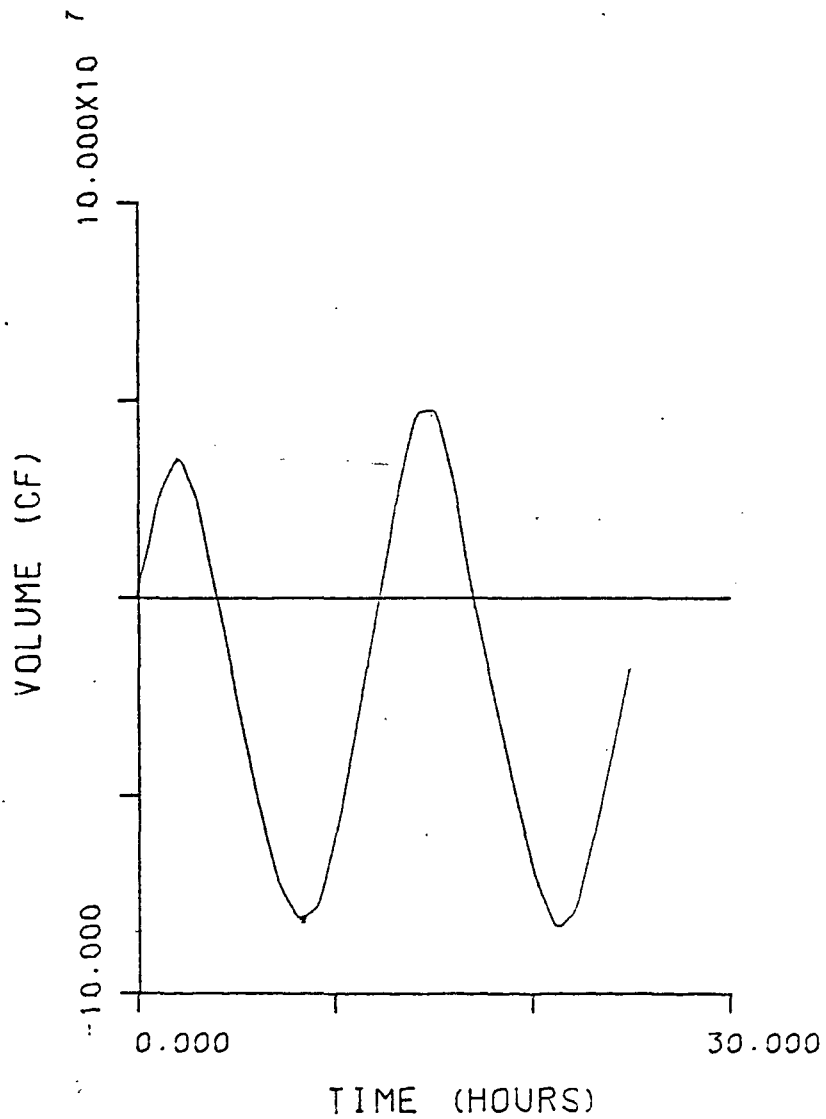


FIGURE 20

Volume versus Time - Jenkins Sound Fine Grid

TIDAL HEIGHT VS TIME  
 JENKINS SOUND FINE GRID  
 + - OBSERVED MLW HEIGHT  
 - - COMPUTED MLW HEIGHT

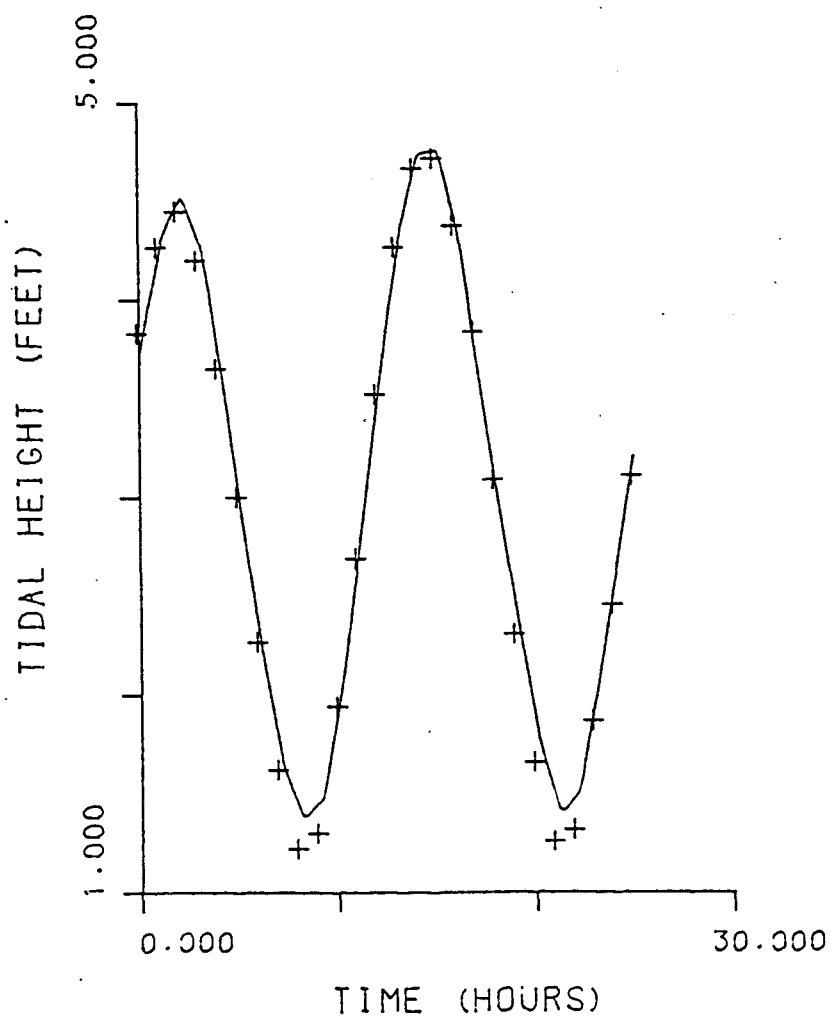


FIGURE 21

Tidal Height versus Time - Jenkins Sound Fine Grid

# FLOW RATE VS TIME JENKINS SOUND GRIDS

- 1 - FINE GRID MODEL
- 2 - COARSE GRID MODEL

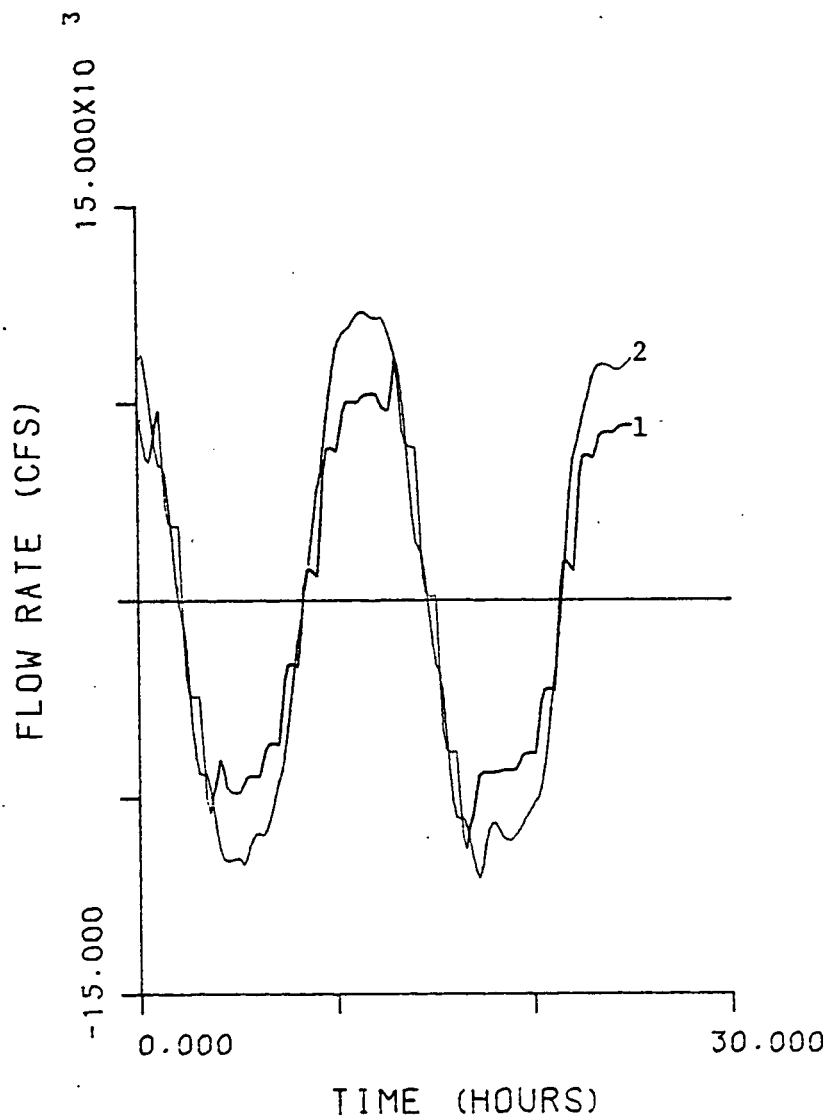


FIGURE 22

Flow Rate versus Time - Jenkins Sound Grids

# VOLUME VS TIME JENKINS SOUND GRIDS

- 1 - FINE GRID MODEL
- 2 - COARSE GRID MODEL

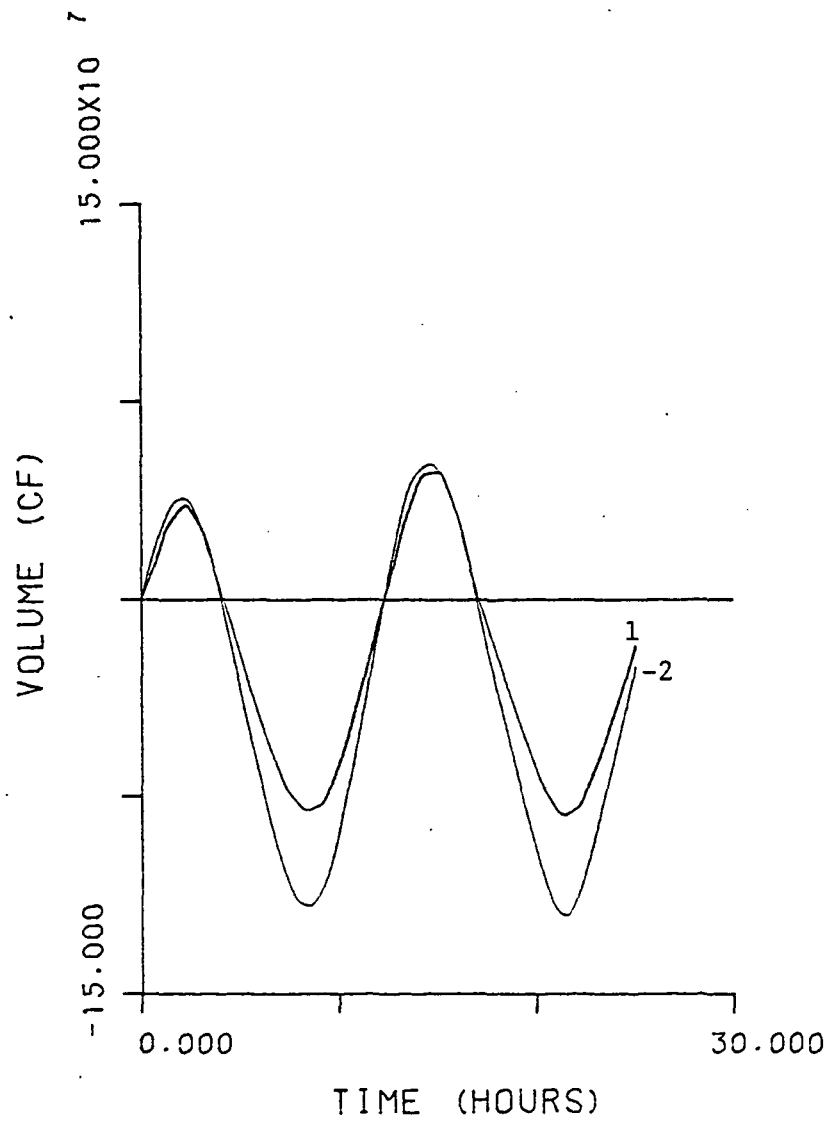


FIGURE 23

Volume versus Time - Jenkins Sound Grids



# TIDAL HEIGHT VS TIME JENKINS SOUND GAGE

- + - OBSERVED MLW HEIGHT
- 1 - FINE GRID COMPUTED HT
- 2 - COARSE GRID COMPUTED HT

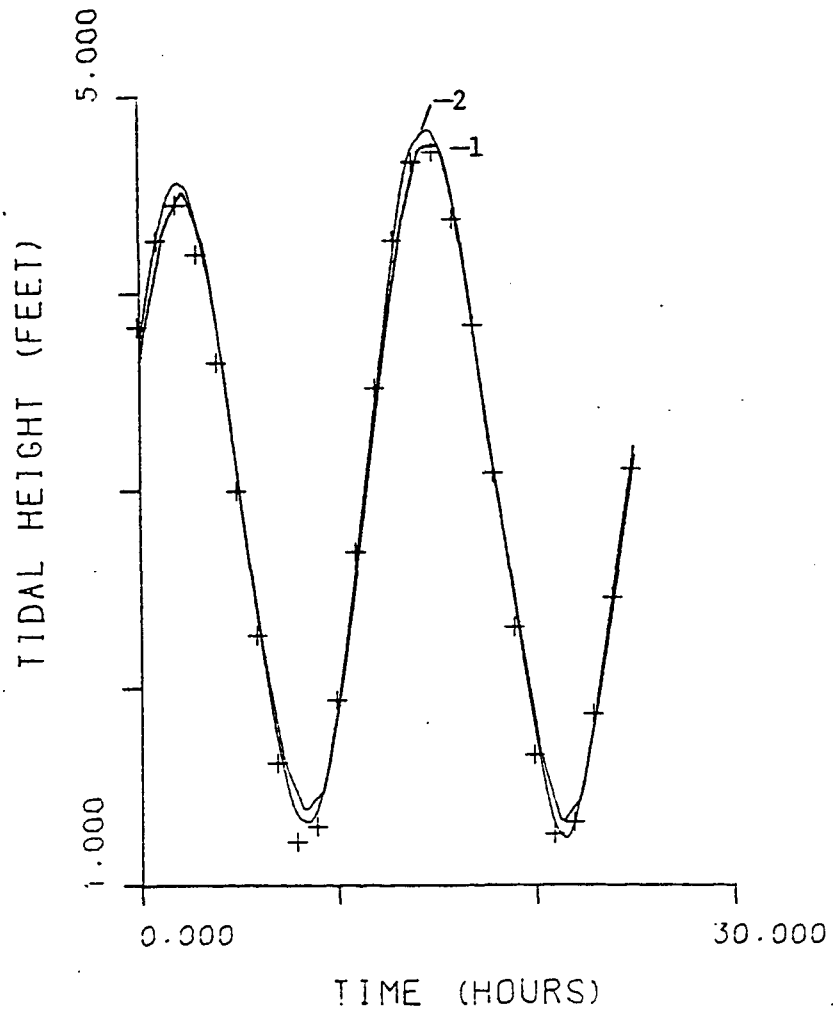


FIGURE 24

Tidal Height versus Time - Jenkins Sound Gage

This agreement between the coarse and fine grids of Jenkins Sound is expected. In this instance, the coarse grid configuration reasonably represents the true geometry, in that one 2000 foot wide, six foot deep channel to Jenkins Sound in the coarse grid is equalled by four 500 foot wide, six foot deep channels in the fine grid. This is not the case with the other grids, where the coarse grid is less representative of the actual geometry.

#### 4.3 Great Sound Fine Grid

The Great Sound modeling area is shown in Fig. 25. The output from the grid is contained in Appendix 5.

The simulation presented by the Great Sound fine grid model is initially similar to that of the coarse grid, with Great Sound being filled from both Great Channel and Townsend Inlet. As with the Jenkins Sound fine model, inundation begins at four foot elevation sometime between 2400 and 0100 hours.

By 0200 hours, the fine grid indicates flow up Great Channel, through Great Sound, and out Townsend Inlet, as was observed in the coarse grid model. At 0300 hours, the fine grid shows a near slack condition in Great Channel, in contrast to the flow up Great Channel to Great Sound predicted by the coarse grid. Both models show drainage out of Townsend Inlet.

Through the rest of the falling tide period, 0400 - 0800 hours, the two models disagree as to the direction of flow in Great Channel.



The fine grid indicates flow out of Great Sound and down Great Channel, while the coarse grid shows flow up Great Channel into Great Sound. This difference is undoubtedly due to the higher head loss across Great Sound in the fine grid, as compared to that in the coarse grid. This increased head loss results from the shallower depths and more irregular geometry of the fine grid as compared to the coarse grid. Hence, it is easier for the water to flow out at Great Channel in the fine grid than to flow across Great Sound and out at Townsend Inlet as seen in the coarse grid model. (It should be noted the circular flow pattern found in the lower left corner of the fine grid between 0700 and 0900 hours is a computation anomaly and is due to the fact that it is easier for the water to circulate between these deeper, lower friction cells than to flow into the adjacent, higher friction, shallower cells. This type of circulation pattern would not be observed in nature over this portion of the tidal cycle.)

As the tide rises, the sound again fills from both Great Channel and Townsend Inlet. By high tide at 1400 hours, the inundatable areas have again been flooded. Hereafter, the pattern repeats through the next cycle.

Comparisons of the flows for the fine grid at Townsend Inlet and Great Channel are shown in Fig. 26. This graph indicates predominantly inflow at Great Channel and outflow at Townsend Inlet. While the forms of the hydrographs are similar, the inflow through Great Channel is nearly twice the inflow of Townsend Inlet at its maximums.

FLOW RATE VS TIME  
GREAT SOUND FINE GRID

- 1 - FLOW AT TOWNSEND INLET
- 2 - FLOW IN GREAT CHANNEL

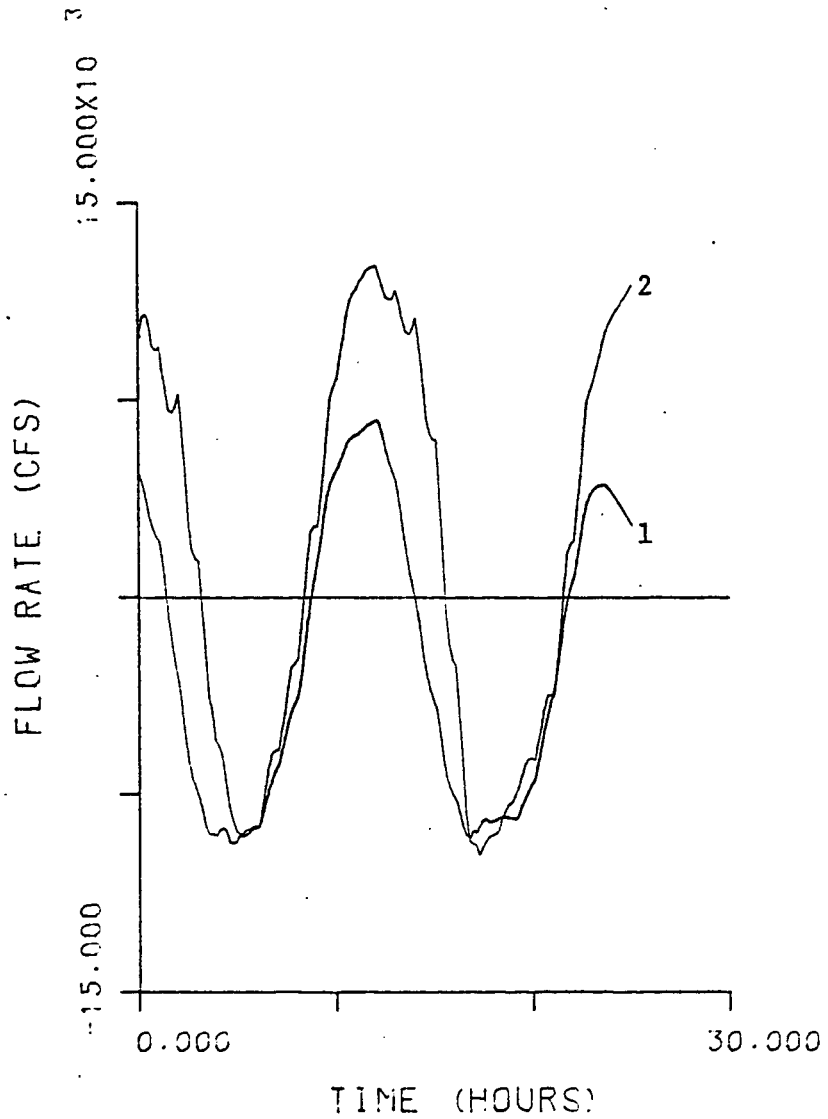


FIGURE 26

Flow Rate versus Time - Great Sound Fine Grid

The two locations experience similar peak outflows. This translates to a net inflow past Great Channel and net outflow past Townsend Inlet, as shown in Fig. 27.

Comparisons of coarse and fine grid flows at Townsend Inlet is shown in Fig. 28. It can be seen that, although the forcing cell at Townsend Inlet in the coarse grid is four times as wide as the corresponding cell in the fine grid, and both are at the same depth, the flow rate is not four times as large, but only two to three times greater. This results from the technique used in Eq. (2) to compute the flow, which relates the flow in the cell to the difference between the tidal heights across the cell boundary. Due to the non-linearity of the equations, the resulting flows are not linearly proportional. The volumes corresponding to the flows of Fig. 28 are shown in Fig. 29.

At Great Channel, Fig. 30, the fine grid shows more variability in direction than does the coarse grid. This draining and filling is what would be anticipated, rather than the flow-through condition experienced in the coarse grid. The corresponding volume vs. time graphs are in Fig. 31, which indicate both grids experience a net inflow at Great Channel. The magnitude of this net inflow is much less for the fine grid, however.

The tidal heights computed by the fine grid are shown in Fig. 32. The figure shows favorable reproduction, except at the extremes, although a slight time lag of about ten minutes is observed.

VOLUME VS TIME  
GREAT SOUND FINE GRID

- 1 - VOL PAST TOWNSEND INLET
- 2 - VOL PAST GREAT CHANNEL
- 3 - TOTAL VOLUME

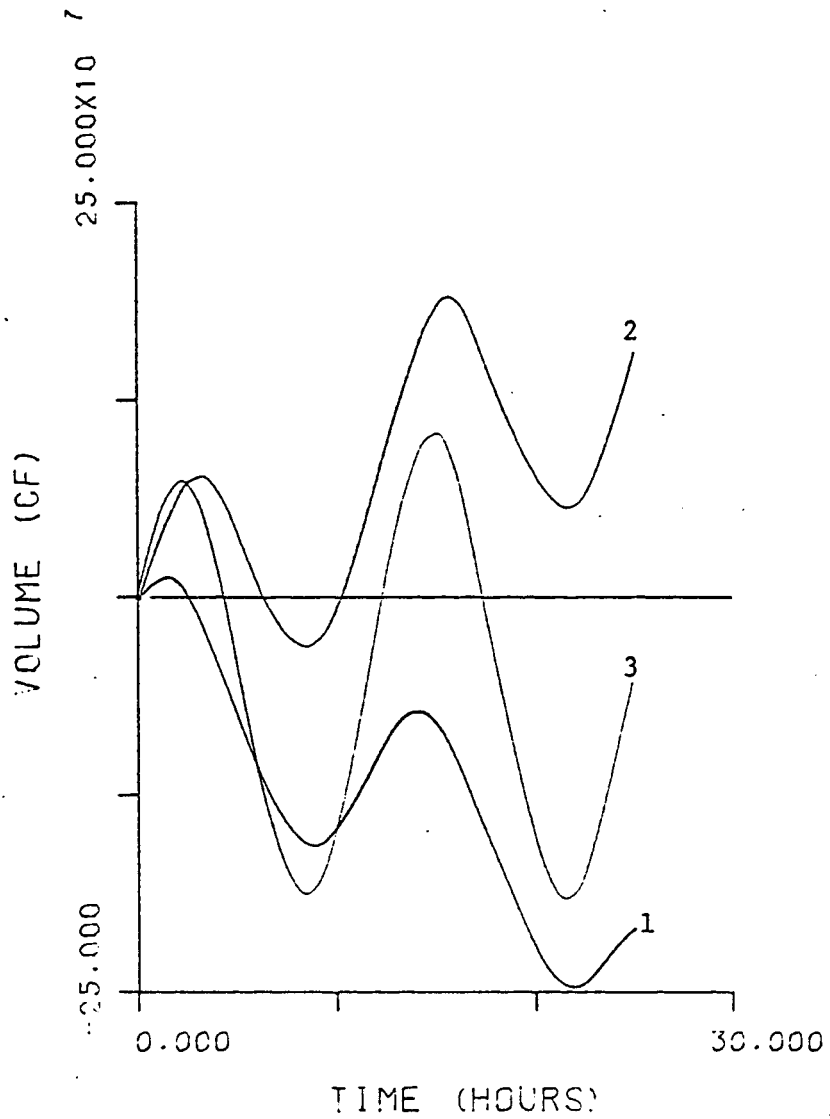


FIGURE 27

Volume versus Time - Great Sound Fine Grid

FLOW RATE VS TIME  
TOWNSEND INLET

- 1 - FINE GRID MODEL
- 2 - COARSE GRID MODEL

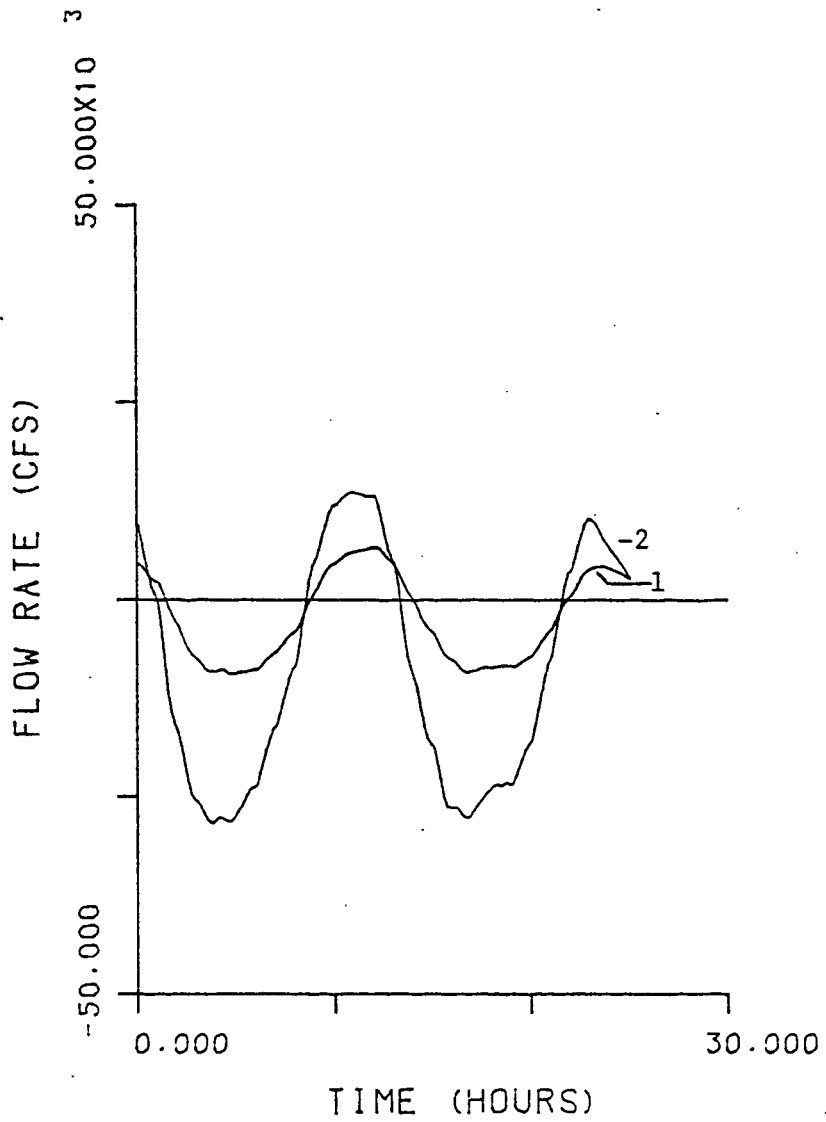


FIGURE 28

Flow Rate versus Time - Townsend Inlet



VOLUME VS TIME  
TOWNSEND INLET

- 1 - FINE GRID MODEL
- 2 - COARSE GRID MODEL

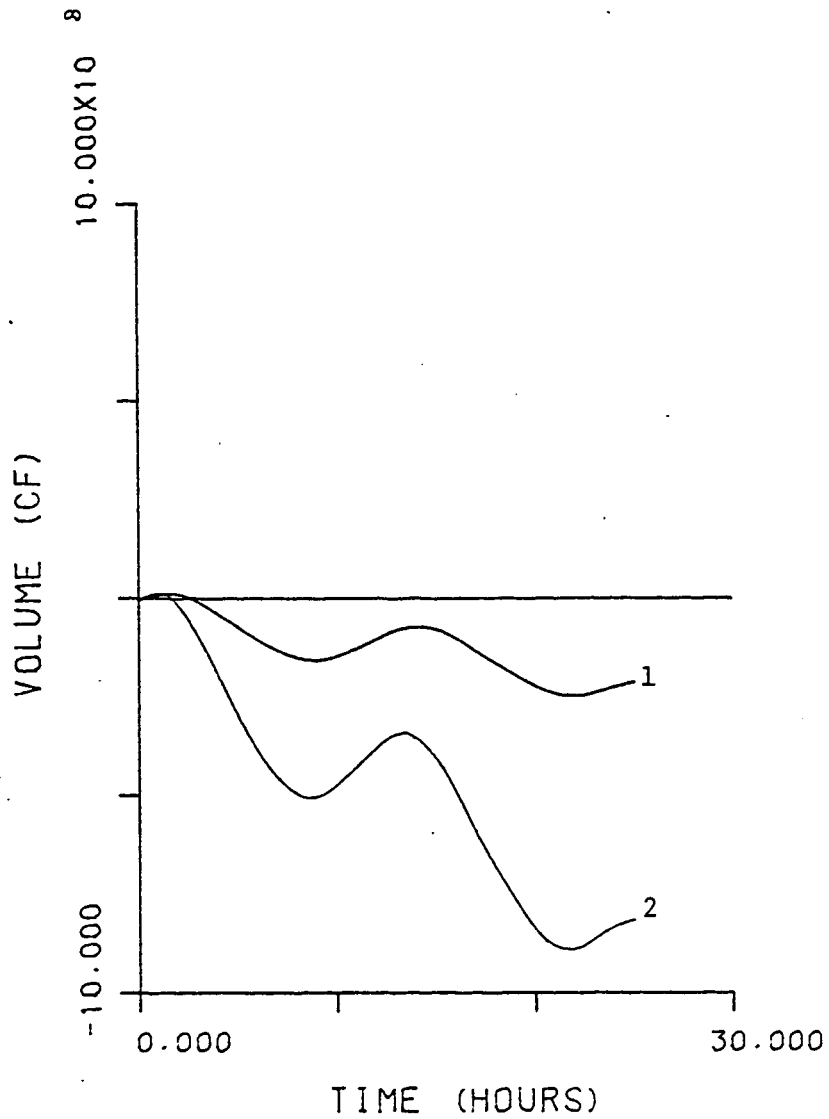


FIGURE 29

Volume versus Time - Townsend Inlet

# FLOW RATE VS TIME GREAT CHANNEL

- 1 - FINE GRID MODEL
- 2 - COARSE GRID MODEL

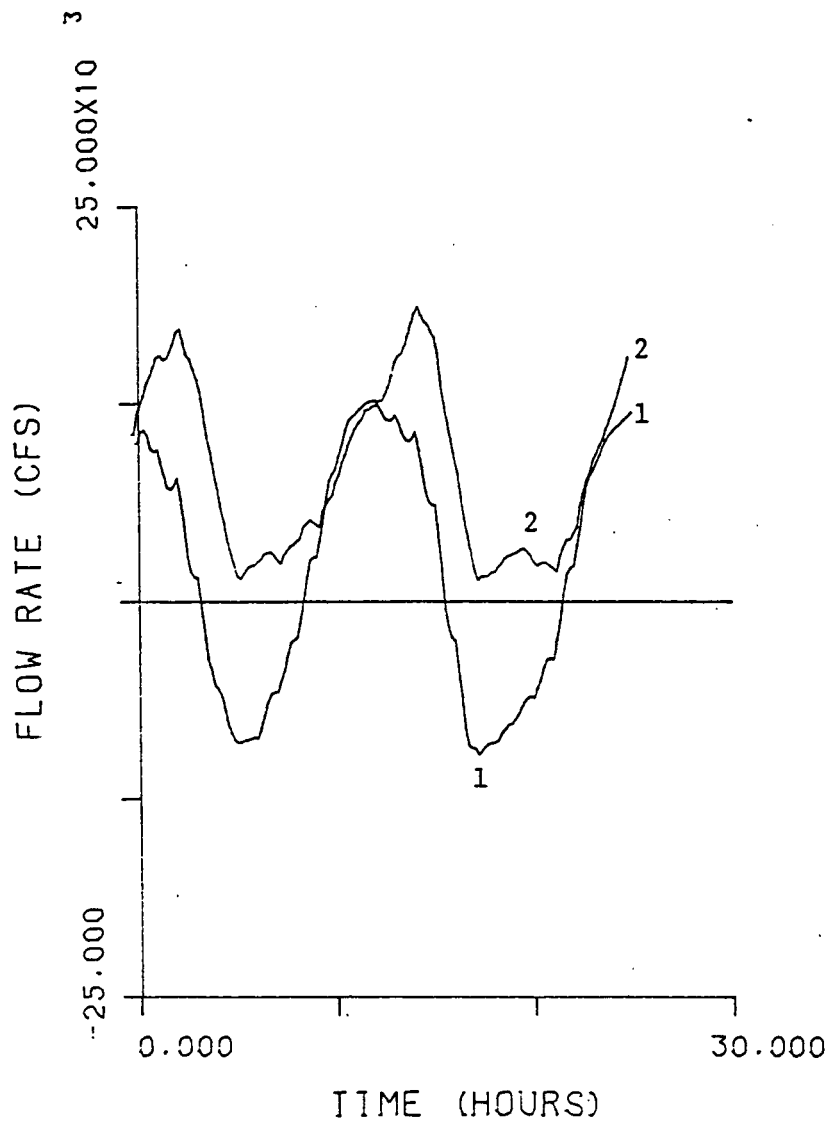


FIGURE 30  
Flow Rate versus Time - Great Channel

VOLUME VS TIME  
GREAT CHANNEL

- 1 - FINE GRID MODEL
- 2 - COARSE GRID MODEL

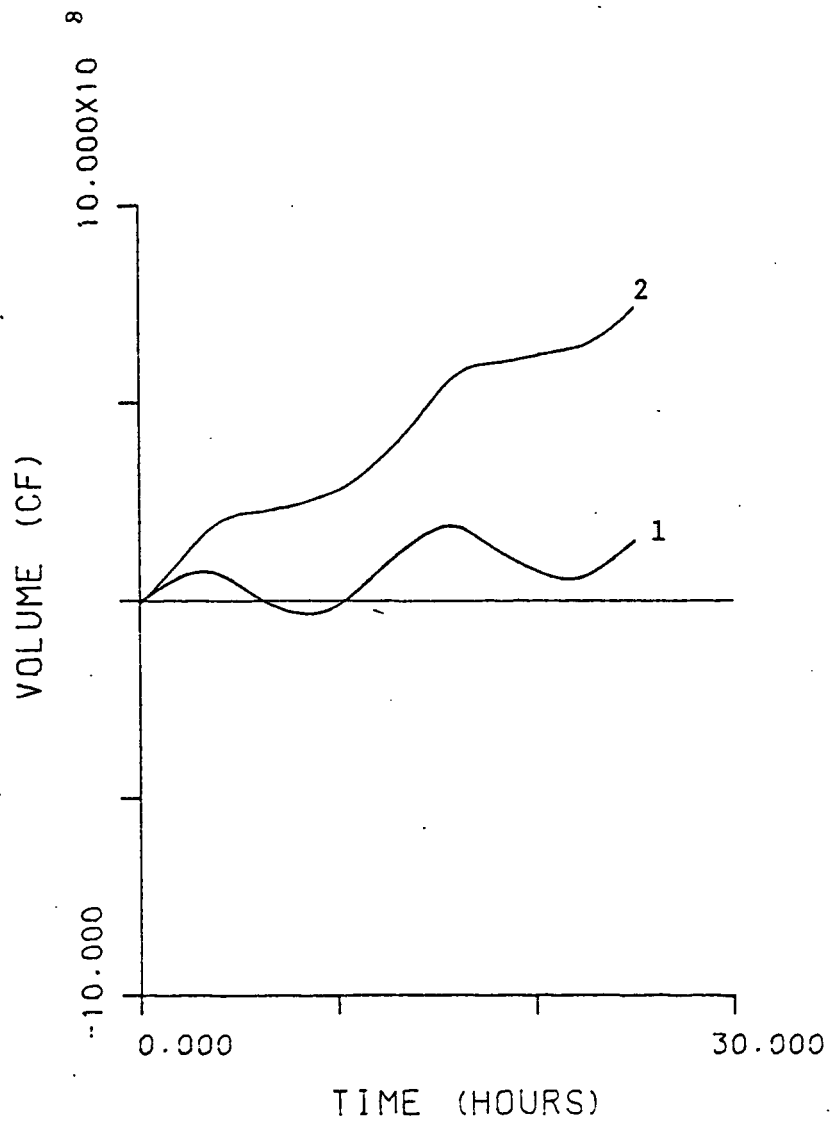


FIGURE 31  
Volume versus Time - Great Channel

TIDAL HEIGHT VS TIME  
 GREAT SOUND FINE GRID  
 + - OBSERVED MLW HEIGHT  
 - - COMPUTED MLW HEIGHT

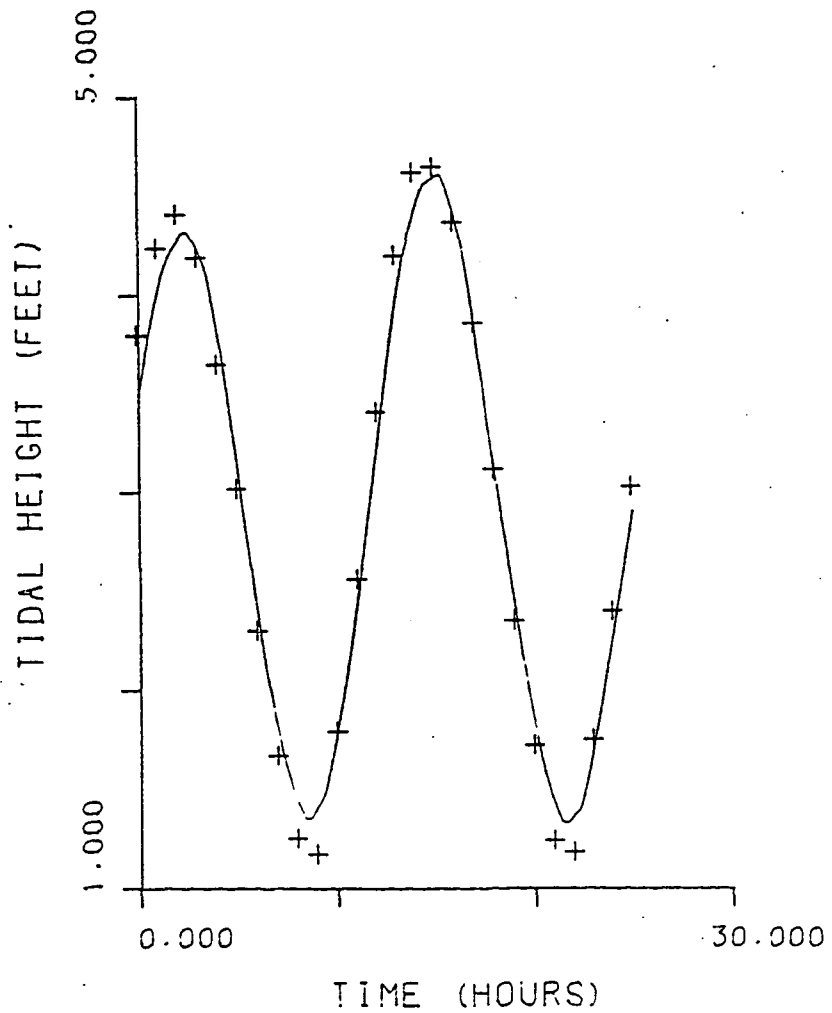


FIGURE 32

Tidal Height versus Time - Great Sound Fine Grid

Comparison of the computed heights by the coarse and fine grids is made in Fig. 33, where it can be seen that the coarse grid simulation is the slightly better of the two.

#### 4.4 Richardson and Grassy Sound Fine Grid

The third fine grid model run was for Richardson and Grassy Sounds. The coarse and fine grids for this area shows significant differences (see Fig. 34). In the coarse grid, Richardson Sound has only one inlet/outlet, while in the fine grid, at least five cells feed it, including Old Turtle Thorofare, which is not included in the coarse grid. In the fine grid, the sounds are more irregular in shape, with most of the small, interconnecting channels represented. In the coarse grid, most of this detail is missing. The output from this fine grid is contained in Appendix 6.

At the start of the simulation period the models disagree as to the flow pattern. The coarse grid predicts flow from Sunset Lake, through the Intercoastal Waterway and down to Nummy Island. The fine grid, however, predicts flow in at both Sunset Lake and Nummy Island. This filling pattern continues until 0200 hours when high tide is reached. During the filling process the lower elevation inundation cells change from dry to wet.

After high tide, the fine grid model predicts the sounds will drain past both Sunset Lake and Nummy Island, in contrast to the flow-through condition presented by the coarse grid. This drainage

# TIDAL HEIGHT VS TIME GREAT SOUND GAGE

- + - OBSERVED MLW HEIGHT
- 1 - FINE GRID COMPUTED HT
- 2 - COARSE GRID COMPUTED HT

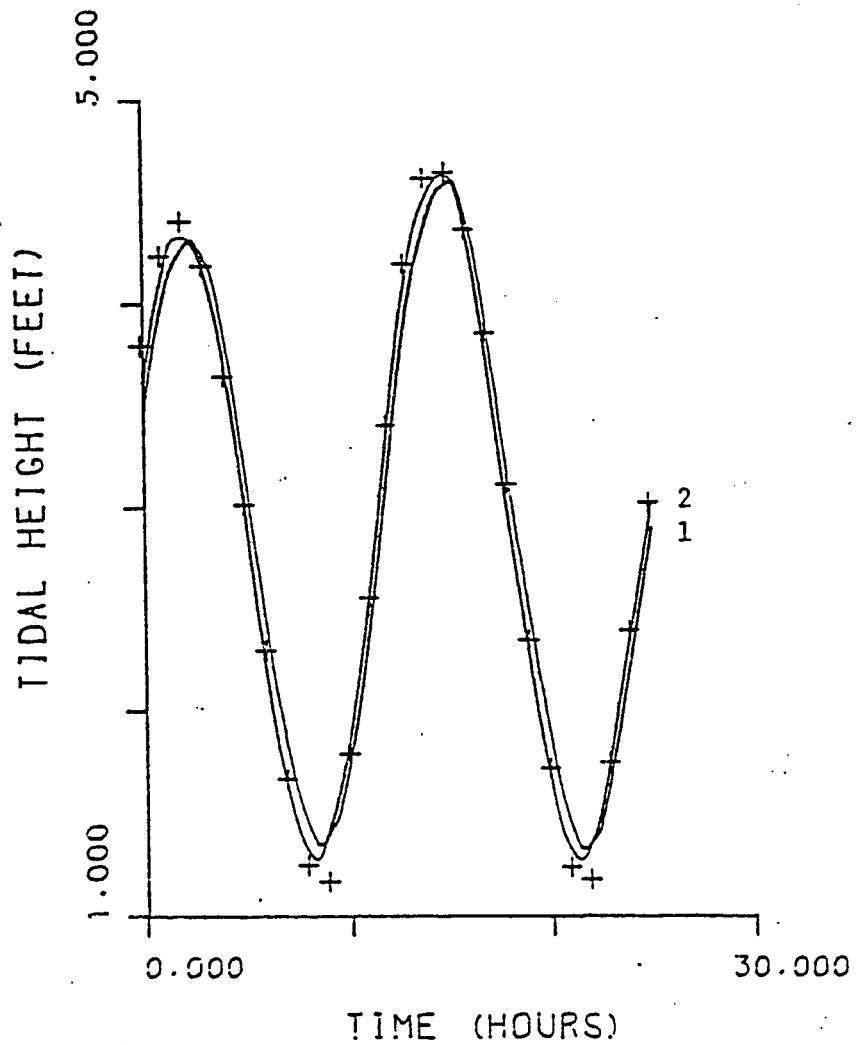


FIGURE 33

Tidal Height versus Time - Great Sound Gage

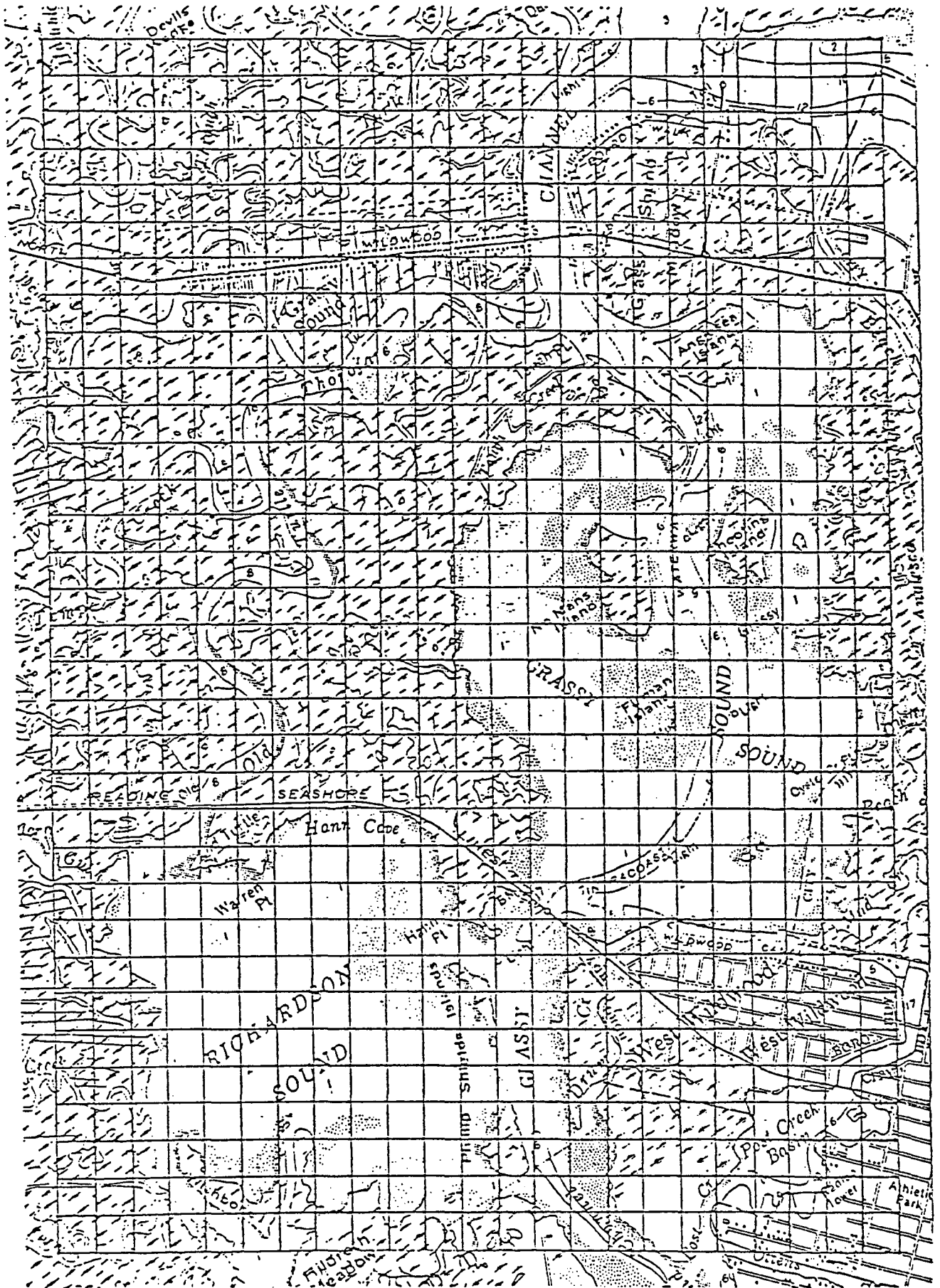


FIGURE 34

Grassy and Richardson Sound Fine Grid

pattern continues until low tide at 0800 hours, and filling begins by 0900 hours. The large flows indicated near the entrance to Richardson Sound during the draining process are again an anomaly similar to that observed with the Great Sound fine grid and do not exist in reality.

Filling begins shortly after low water and continues until just past high tide. This time the sounds are filled from both directions in both grids. Inundation again occurs in the fine grid when the water levels begin exceeding four feet. The flow pattern then repeats over the next tidal cycle.

The flow rates through the forcing cells at Sunset Lake and Nummy Island are shown in Fig. 35, and the corresponding net volumes in Fig. 36. The flow-through bias of the coarse grid is evident in these figures. Comparisons of the flow rates and volumes between the coarse and fine grids at these same locations are presented in Figs. 37 to 40.

The tidal heights predicted by the fine grid for Old Turtle Thorofare and West Wildwood are shown in Figs. 41 and 42. The results show lags of 45 minutes to an hour between computed and observed results. Such phasing indicates it is difficult for the water to enter and leave the sounds. This can be caused by shallow depths with high friction factors, resulting in restricted flow. The lags should be reduced with additional fine tuning. Comparisons with the coarse grid results are presented in Figs. 43 and 44, which show the coarse grid is more accurate in predicting water levels at these two locations.



FLOW RATE VS TIME  
GRASSY AND RICHARDSON  
SOUND FINE GRID MODEL  
1 - FLOW AT NUMMY ISLAND  
2 - FLOW AT SUNSET LAKE

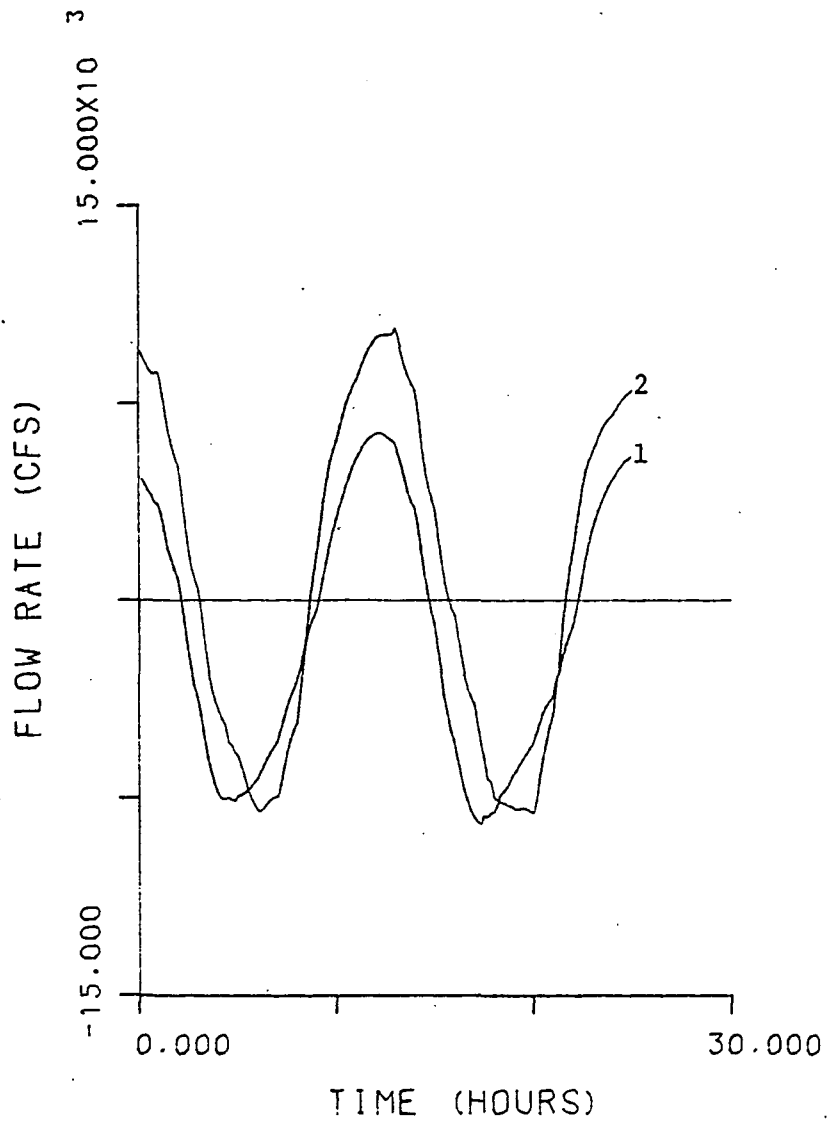


FIGURE 35

Flow Rate versus Time - Grassy and Richardson Sound Fine Grid Model

VOLUME VS TIME  
 GRASSY AND RICHARDSON  
 SOUND FINE GRID MODEL  
 1 - VOL PAST NUMMY ISLAND  
 2 - VOL PAST SUNSET LAKE  
 3 - TOTAL VOLUME

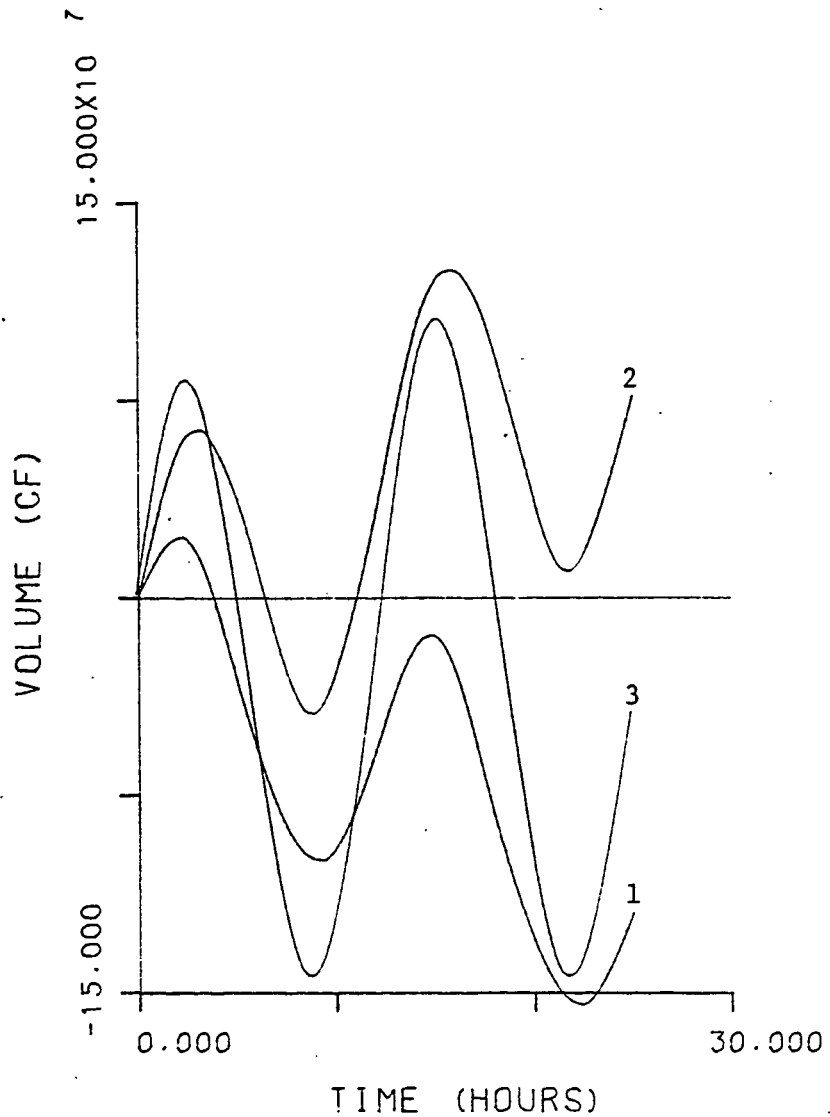


FIGURE 36

Volume versus Time - Grassy and Richardson Sound Fine Grid Model

# FLOW RATE VS TIME SUNSET LAKE.

- 1 - FINE GRID MODEL
- 2 - COARSE GRID MODEL

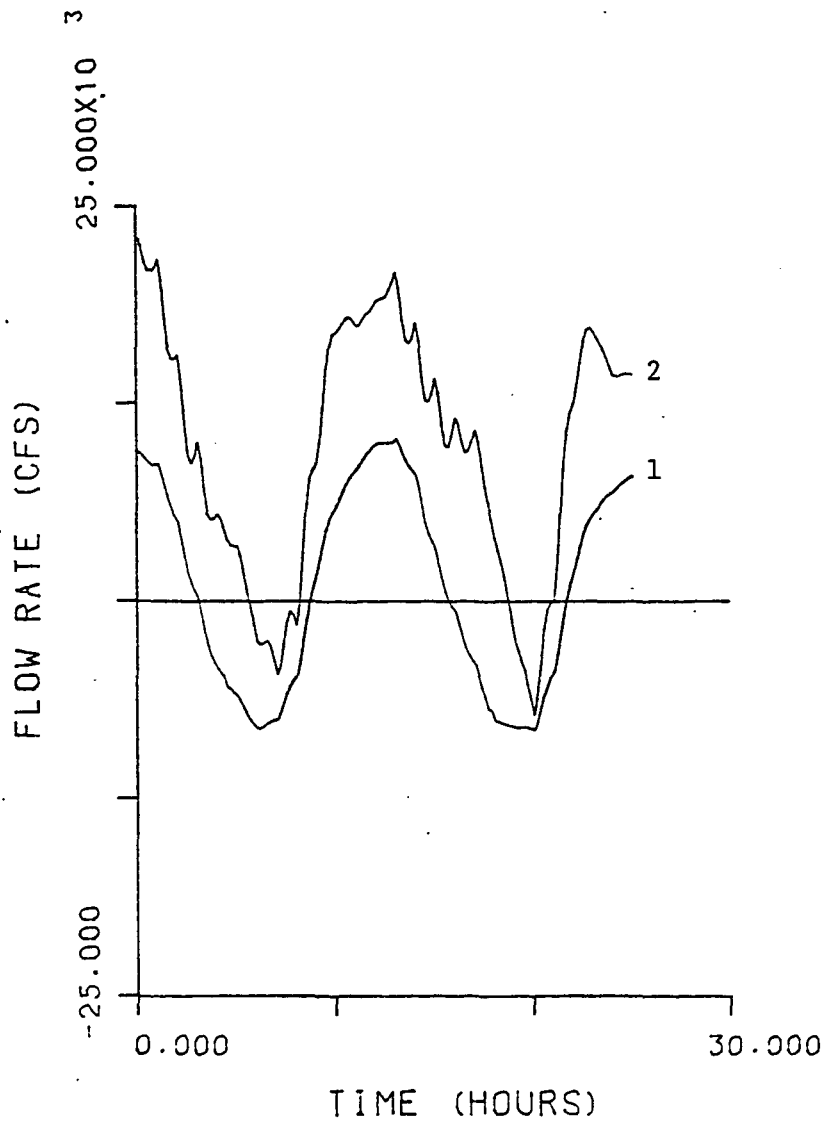


FIGURE 37

Flow Rate versus Time - Sunset Lake

# VOLUME VS TIME SUNSET LAKE.

- 1 - FINE GRID MODEL
- 2 - COARSE GRID MODEL

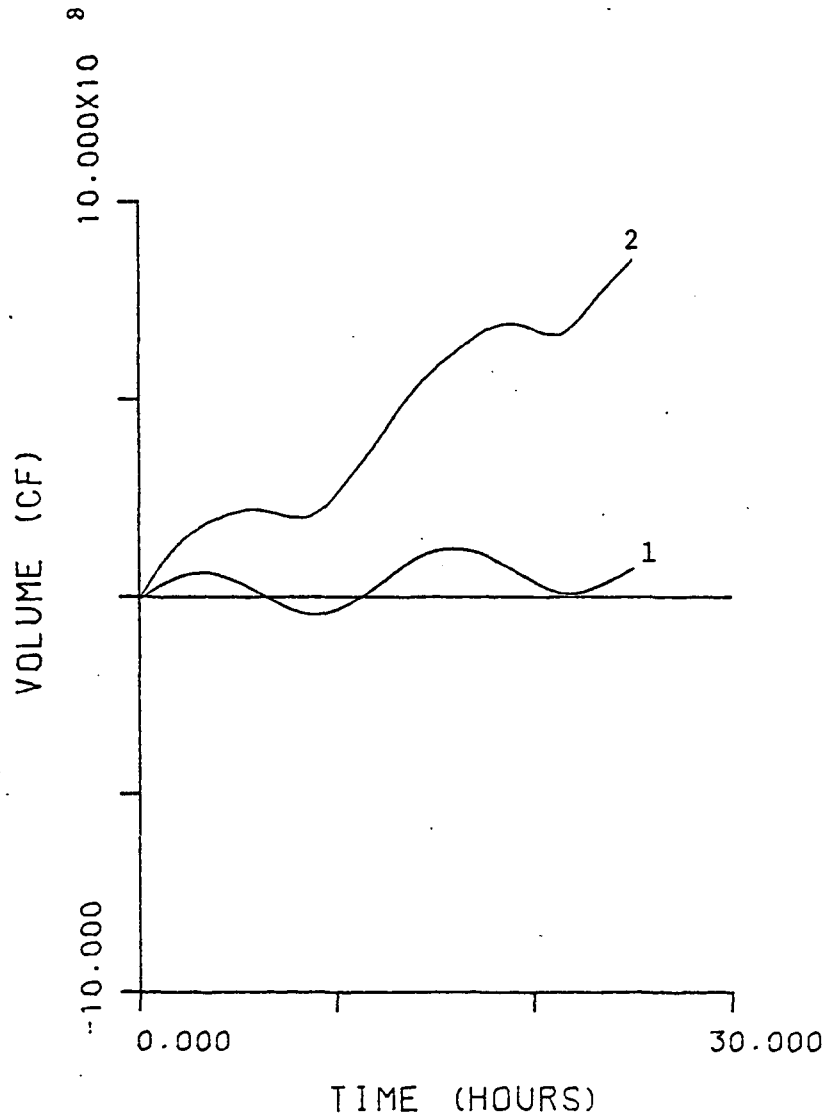


FIGURE 38  
Volume versus Time - Sunset Lake

FLOW RATE VS TIME  
NUMMY ISLAND.

- 1 - FINE GRID MODEL
- 2 - COARSE GRID MODEL

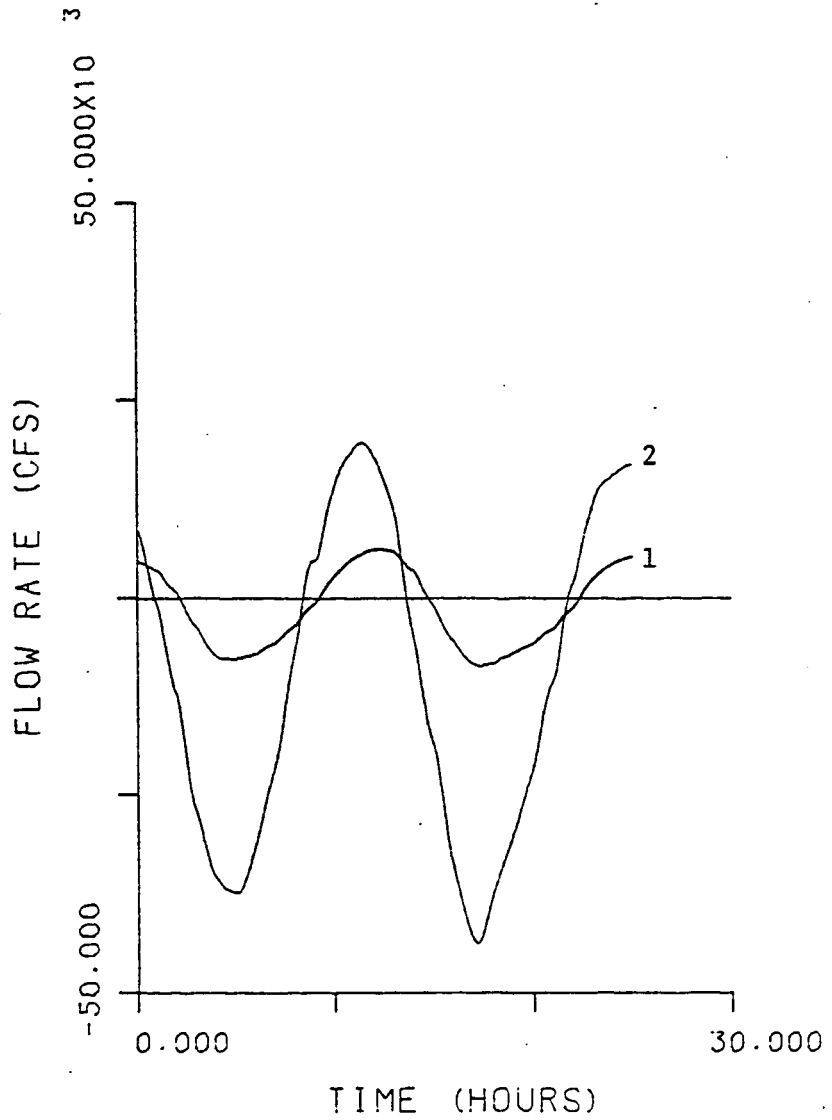


FIGURE 39

Flow Rate versus Time - Nummy Island

VOLUME VS TIME  
NUMMY ISLAND.

- 1 - FINE GRID MODEL
- 2 - COARSE GRID MODEL

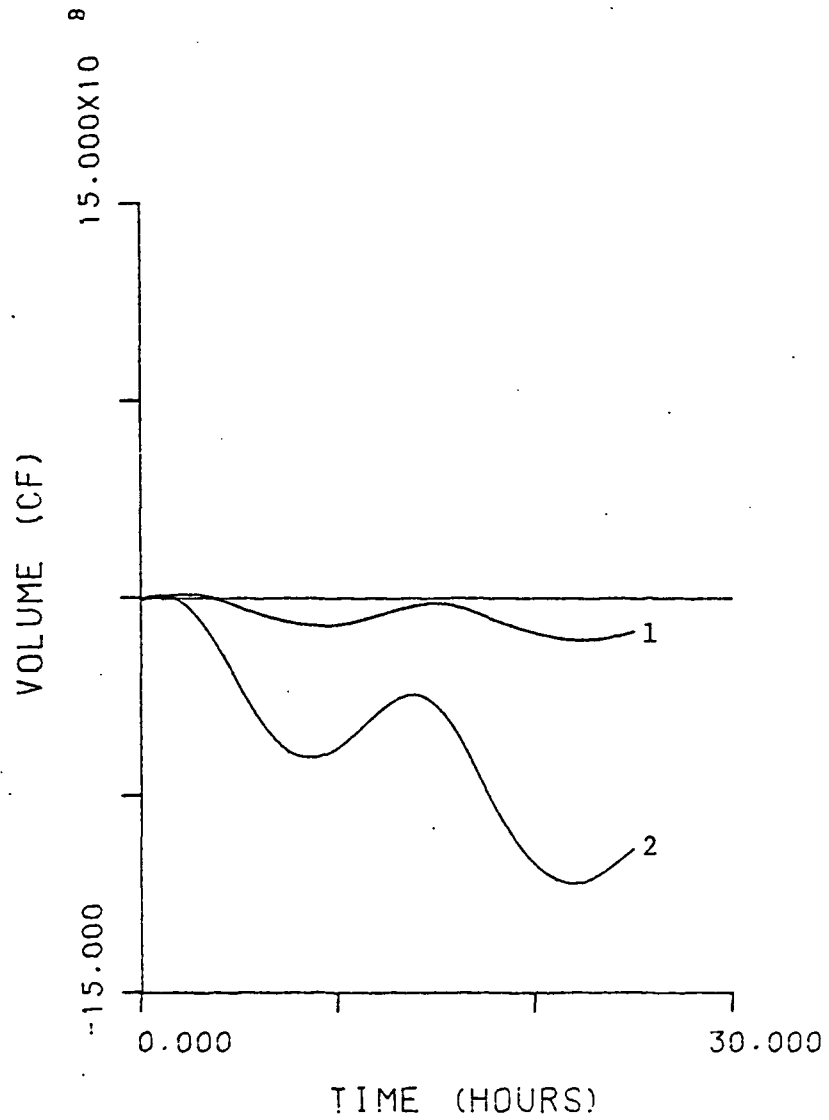


FIGURE 40  
Volume versus Time - Nummy Island

TIDAL HEIGHT VS TIME  
 OLD TURTLE THOROFARE  
 RICHARDSON AND GRASSY  
 SOUND FINE GRID MODEL  
 + - OBSERVED MLW HEIGHT  
 - - COMPUTED MLW HEIGHT

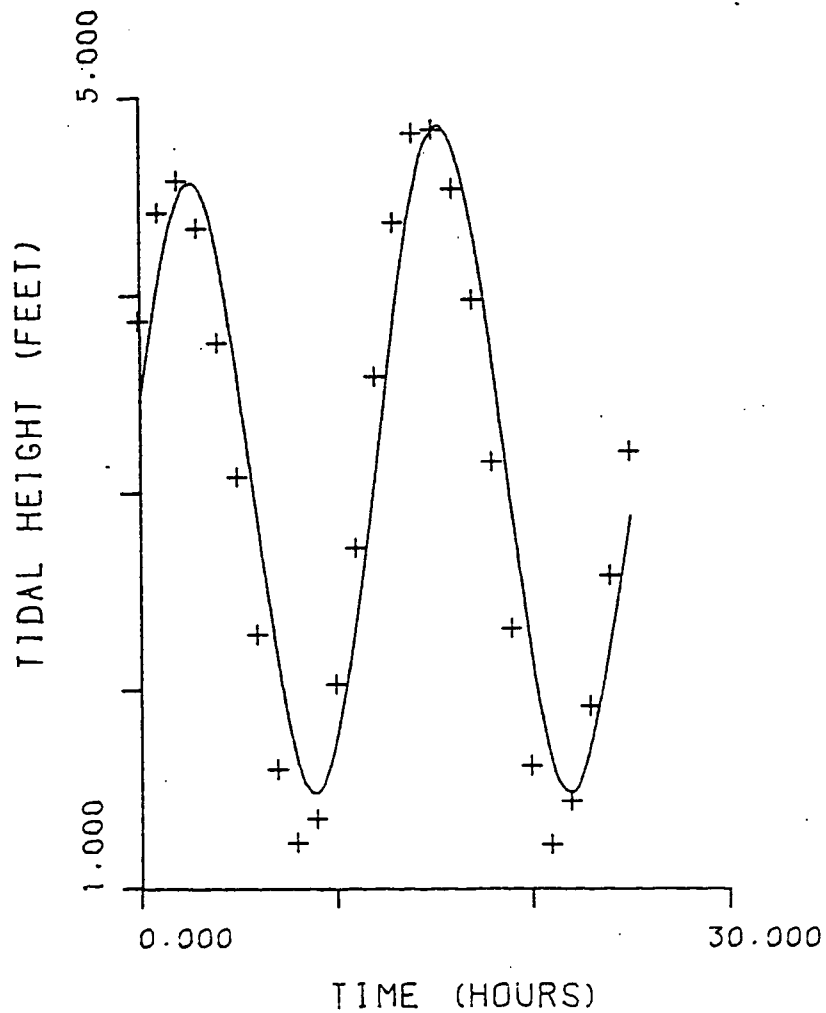


FIGURE 41

Tidal Height versus Time - Old Turtle Thorofare - Richardson  
 and Grassy Sound Fine Grid Model

TIDAL HEIGHT VS TIME  
 WEST WILDWOOD GAGE  
 RICHARDSON AND GRASSY  
 SOUND FINE GRID MODEL  
 + - OBSERVED MLW HEIGHT  
 - - COMPUTED MLW HEIGHT

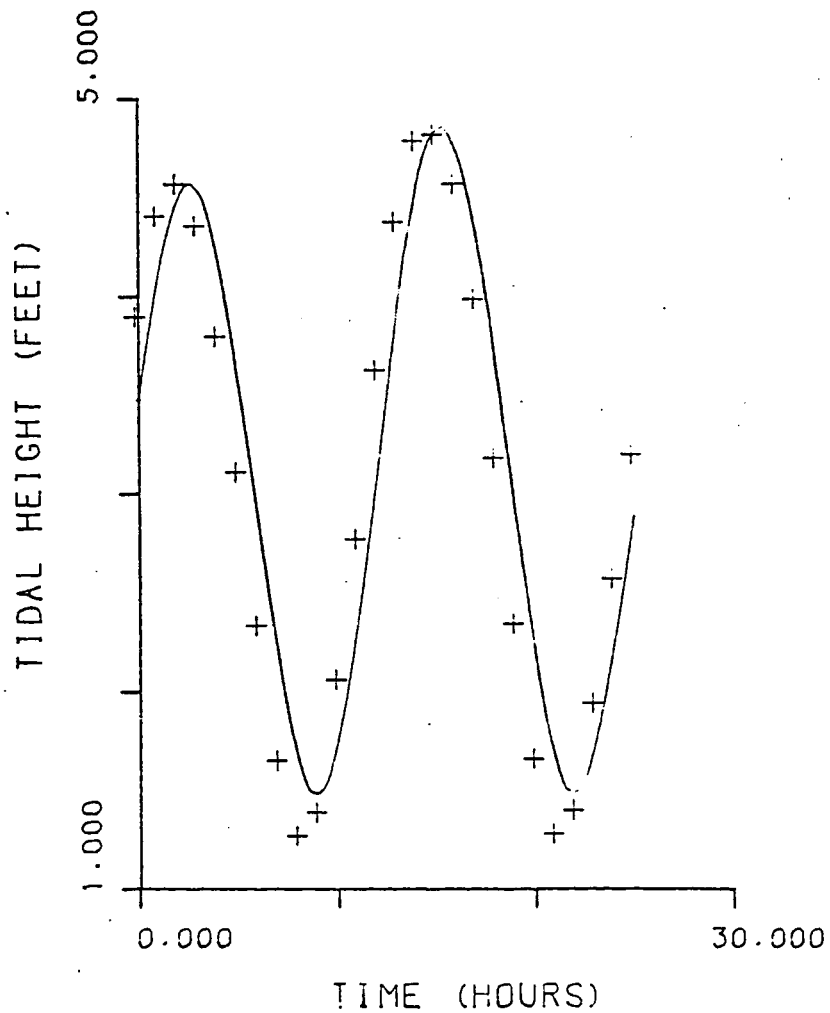


FIGURE 42

Tidal Height versus Time - West Wildwood Gage - Richardson  
 and Grassy Sound Fine Grid Model



# TIDAL HEIGHT VS TIME OLD TURTLE THOROFARE

- + - OBSERVED MLW HEIGHT
- 1 - FINE GRID COMPUTED HT
- 2 - COARSE GRID COMPUTED HT

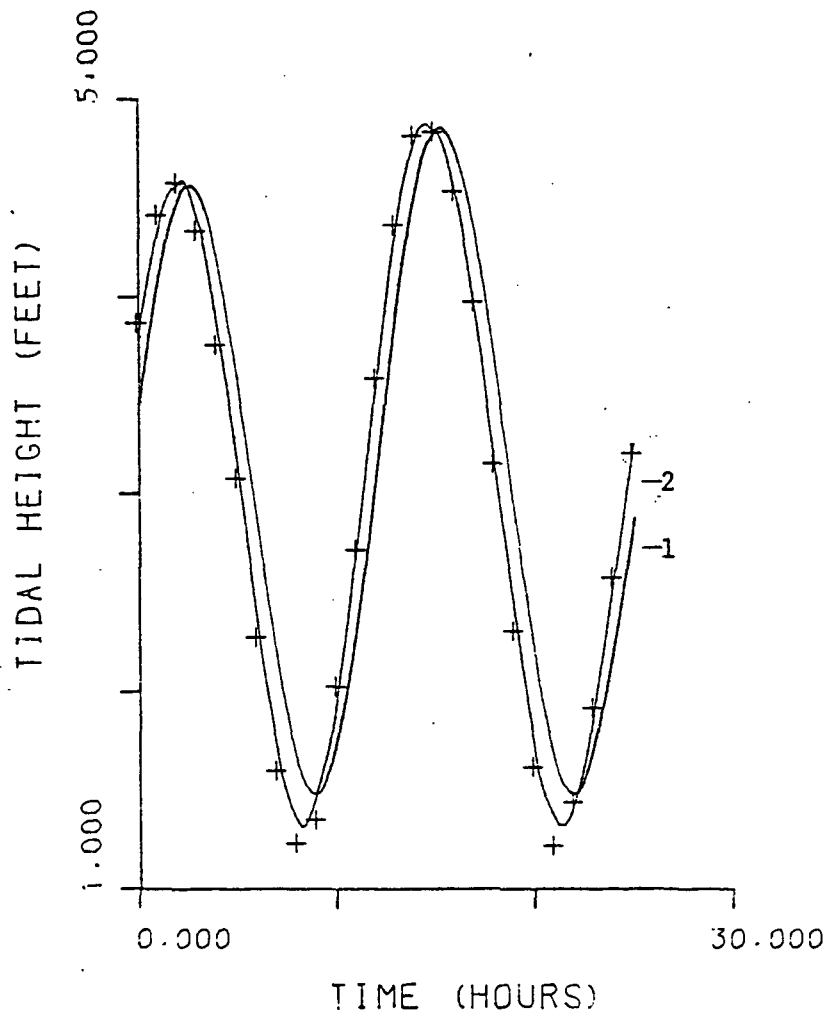


FIGURE 43

Tidal Height versus Time - Old Turtle Thorofare

# TIDAL HEIGHT VS TIME WEST WILDWOOD GAGE

- + - OBSERVED MLW HEIGHT
- 1 - FINE GRID COMPUTED HT
- 2 - COARSE GRID COMPUTED HT

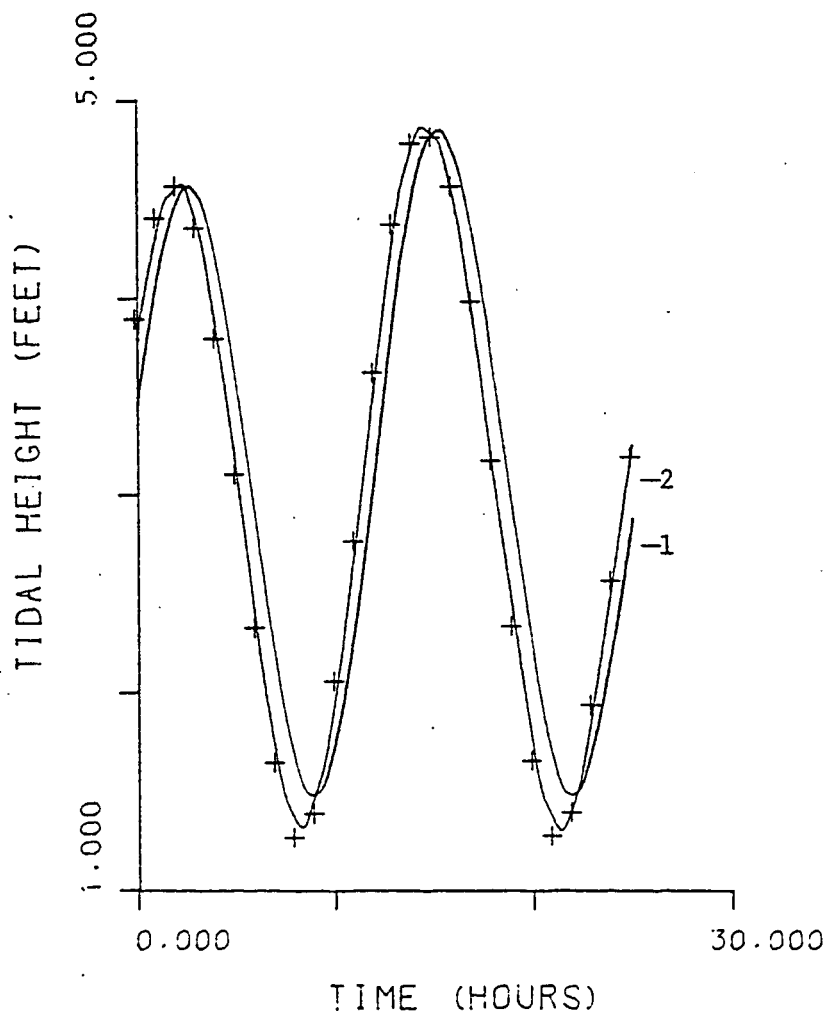


FIGURE 44

Tidal Height versus Time - West Wildwood Gage

#### 4.5 Comments

Overall, the reproduction of observed tidal heights is accurate. Discrepancies at the extremes and phase differences between observed and computed heights are matters of fine tuning and not believed to be a shortcoming in the model. The quality of the computed flows remains questionable, however, as no field measurements are available for comparison. Once flow measurements are available and the models are calibrated to predict both tidal height and discharge, it is anticipated the fine grid models will provide more accurate results than will the coarse grid model, as they better represent the true geometry.

## 5. SUMMARY, CONCLUSIONS, AND RECOMMENDATIONS

### 5.1 Summary

The explicit, two-dimensional finite difference model HYDTID was applied to the Hereford Inlet bay system and used to predict the system's hydrodynamic response to applied forcing tides. The model predicts flow magnitudes in the x and y directions and the tidal height in each cell by solving the vertically averaged momentum and continuity equations within the constraints of the initial and boundary conditions.

Initially, a coarse grid model, with a cell size of 2000 ft. on a side, crudely represented the true geometry, but was able to encompass the entire study area. This model was forced from the north near Townsend Inlet and the south at Sunset Lake by observed records at these locations. From the east the model was forced by a tide derived from the Sandy Hook record. The simulated tidal heights and flows were refined through adjustment of cell depth and friction, through modification of the Hereford Inlet tide, and by varying the amount of storage permitted in the inundatable areas.

As finalized, the coarse model did not require inundatable areas to accurately reproduce the six known tidal records lying within the system. At specific locations the predicted tidal heights were then used as the boundary conditions to force finer grid models. These finer grids were located in Jenkins Sound, Great Sound, and Richardson and Grassy Sounds.

The finer grids can more accurately represent the true geometry, and with further fine tuning, should be able to predict the observed tidal heights more accurately. The results were readily affected by small changes in cell depth, roughness, and boundary definition.

Due to the lack of field data, none of the models are yet calibrated to predict discharge. Thus, the flow patterns predicted in the grids are not necessarily accurate, and may, therefore, be correct only as an order of magnitude estimate.

## 5.2 Conclusions

These restrictions lead to the following conclusions for this study:

1. The flow field cannot be accurately defined until the model is calibrated using field discharge measurements.
2. The model does accurately predict tidal heights when properly calibrated.
3. The neap tidal prism for ebb and flood flow in Hereford Inlet is at least  $6 \cdot 10^8 \text{ ft}^3$ .

## 5.3 Recommendations for Future Study

This modeling effort was intended to be a first step in the study of the hydraulics of the Hereford Inlet-bay system. Until the model is calibrated to predict discharge, however, it is of only limited usefulness. Therefore, a recommendation for future study is to calibrate the model to predict both tidal height and discharge.

The preferred way to perform the calibration would be to collect a complete set of hydraulic data over a full tidal cycle. This would involve simultaneous measurements of tidal heights, discharge, and bottom elevations in Great Channel and near Nummy Island at their previous gaging locations, and measurements in new locations at Hereford Inlet, at Long Reach (in lieu of Townsend Inlet) and in Grassy Sound Channel (in lieu of Sunset Lake). Concurrent tidal height measurements, only, would need to be taken at the previous gage locations at Old Turtle Thorofare, West Wildwood, Jenkins Sound, and Great Sound. This would provide a complete set of consistent data with which to calibrate the model.

Recognizing that this would be involved and expensive, a less sophisticated alternative would be to take only the discharge measurements and then relate them to tidal heights through historical records. Using a bimodal Fourier series or similar technique, amplitude factors and phase differences could be determined relating each record to the Sandy Hook record. Sandy Hook is convenient, because it is a permanent installation and is always available. By applying the amplitude factors and phase differences to the Sandy Hook tide, the desired records at any other time could be approximated. The Hereford Inlet record could then be derived from the Sandy Hook and Nummy Island records. With this data the model could then be tuned to reproduce the observed discharges and the predicted elevations.

Once calibrated to predict both discharge and tidal height, the model would then be useful for predicting system response under varying tidal conditions. Application to sediment and contaminant transport is also possible.

## 6. ACKNOWLEDGMENTS

This effort was a Fritz Engineering Laboratory project sponsored by the Fleischmann Foundation grant awarded to the Wetlands Institute, Stone Harbor, New Jersey. Dr. Vince Guida is the Institute's director, and I appreciate the opportunity he has afforded me in carrying out this research.

Drs. Richard Weisman and Gerard Lennon served as faculty advisors for the project. They provided invaluable assistance in directing the effort. I am deeply indebted to them for their suggestions, comments, and guidance.

I must acknowledge the support I have received from Dr. Robert Johnson, Director of the Water Resources Division, Dr. David VanHorn, Chairman of the Civil Engineering Department, and Dr. Lynn Beedle, Director of Fritz Engineering Laboratory, not only in this effort, but throughout my stay at Lehigh. Also, Dr. Jerry King, Dean of the Graduate School and personal friend, was a source of inspiration throughout the endeavor. Mrs. Dorothy Fielding, Mrs. Ruth Grimes, and Mrs. Catherine Miller assisted with the typing of the manuscript.

The computer program HYDTID was provided by the Coastal Engineering Research Center, Ft. Belvoir, Virginia. Implementing resources were furnished by the Lehigh University Computing Center. The cooperation of these organizations was greatly appreciated.

Lastly, I must recognize the never ending love displayed by my wife, Kathleen. In recognition of this love, I dedicate this paper to her.



## 7. REFERENCES

- Brown, E. I., "Inlets on Sandy Coasts," Proceedings of the American Society of Civil Engineers, Vol. LIV, 1928, pp. 505-553.
- Bruun, P. and Gerritsen, F., Stability of Coastal Inlets, North Holland Publishing Company, Amsterdam, 1960.
- Caccese, L. A. and Spies, H. R., "Barnegat Inlet Nature Prevails," Coastal Sediments '77, Fifth Symposium of the Waterway, Port, Coastal, and Ocean Division, 1977, pp. 305-310.
- Chow, V. T., Open-Channel Hydraulics, McGraw Hill Book Company, New York, 1959.
- Czerniak, M. T., "Inlet Interaction and Stability Theory Verification," Coastal-Sediments '77, Fifth Symposium of the Waterway, Port, Coastal, and Ocean Division, 1977, pp. 754-771.
- Dronkers, J. J., Tidal Computations in Rivers and Coastal Waters, John Wiley and Sons, Inc., New York City, 1964.
- Escoffier, F. F., "The Stability of Tidal Inlets," Shore and Beach, Vol. 8, No. 4, 1940, pp. 114-115.
- Escoffier, F. F., "Hydraulics and Stability of Tidal Inlets," GITI Report 13, U. S. Army Corps of Engineers, Coastal Engineering Research Center, Fort Belvoir, VA, and U. S. Army Engineer Waterways Experiment Station, Vicksburg, MS, August 1977.
- Harris, D. L. and Bodine, B. R., "Comparison of Numerical and Physical Hydraulic Models, Masonboro Inlet, North Carolina," GITI Report 6, U. S. Army Corps of Engineers, Coastal Engineering Research Center, Fort Belvoir, VA, and U. S. Army Engineer Waterways Experiment Station, Vicksburg, MS, June 1977.
- Hinwood, J. B. and Wallis, I. G., "Classification of Models of Tidal Waters," Journal of the Hydraulics Division, Vol. 101, October 1977a, pp. 1315-1331.
- Hinwood, J. B. and Wallis, I. B., "Classification of Models of Tidal Waters," Journal of the Hydraulics Division, Vol. 101, November 1975b, pp. 1405-1421.

- Huval, C. J. and Wintergerst, G. L., "Simplified Numerical (Lumped Parameter) Simulation", App. 4, GITI Report 6, Comparison of Numerical and Physical Hydraulic Models, Masonboro Inlet, North Carolina, U. S. Army Corps of Engineers, Coastal Engineering Research Center, Fort Belvoir, VA., and U. S. Army Engineer Waterways Experiment Station, Vicksburg, MS, June 1977.
- Jarrett, J. T., "Tidal Prism-Inlet Area Relationships", GITI Report 3, U. S. Army, Corps of Engineers, Coastal Engineering Research Center, Fort Belvoir, VA., and U. S. Army Engineer Waterways Experiment Station, Vicksburg, MS, February 1976.
- Keulegan, G. H., "A Formula for the Calculation of the Tidal Discharge Through an Inlet", Bulletin of the Beach Erosion Board, Vol. 4, No. 1, January 1951, pp. 15-29.
- Keulegan, G. H., "Tidal Flow in Entrances: Water Level Fluctuations of Basins in Communication with Seas", Technical Bulletin No. 14, Committee on Tidal Hydraulics, U. S. Army, Corps of Engineers, Vicksburg, MS, July 1967.
- Lamb, H., Hydrodynamics, 6th Ed., Dover, New Jersey, 1932.
- Masch, F. D., Brandes, R. J., and Reagan, J. D., "Numerical Simulation of Hydrodynamics (WRE)", Vol. 1, App. 2, GITI Report 6, Comparison of Numerical and Physical Models, Masonboro Inlet, North Carolina, U. S. Army, Corps of Engineers, Coastal Engineering Research Center, Fort Belvoir, VA., and U. S. Army Waterways Experiment Station, Vicksburg, MS, June 1977a.
- Masch, F. D., Brandes, R. J., and Reagan, J. D., "Numerical Simulation of Hydrodynamics (WRE)", Vol. 2, App. 2, GITI Report 6, Comparison of Numerical and Physical Models, Masonboro Inlet, North Carolina, U. S. Army Corps of Engineers, Coastal Engineering Research Center, Fort Belvoir, VA., and U. S. Army Waterways Experiment Station, Vicksburg, MS, June 1977b.
- O'Brien, M. P., "Estuary Tidal Prism Related to Entrance Areas", Civil Engineering, Vol. 1, No. 8, 1931, pp. 738-739.
- O'Brien, M. P., "Equilibrium Flow Areas of Tidal Inlets on Sandy Coasts", Journal of Waterways and Harbors Division, Vol. 95, No. WW1, February 1969, pp. 43-52.
- O'Brien, M. P. and Dean, R. G., "Hydraulics and Sedimentary Stability of Coastal Inlets", Proceedings of the 13th Coastal Engineering Conference, 1972, pp. 761-780.

Oliveira, I. B., "Natural Flushing Ability in Tidal Inlets",  
Proceedings of the Twelfth Conference on Coastal Engineering,  
1970, pp. 1827-1845.

Reid, R. O. and Bodine, B. R., "Numerical Model for Storm Surges in  
Galveston Bay", Journal of the Waterways and Harbors Division,  
Vol. 94, No. WW1, February 1968, pp. 53-57.

Seelig, W. N., Harris, D. L., and Herchenroder, B. E., "A Spatially  
Integrated Numerical Model of Inlet Hydraulics", GITI Report 14,  
U. S. Army, Corps of Engineers, Coastal Engineering Research  
Center, Fort Belvoir, VA., and U. S. Army Engineer Waterways  
Experiment Station, Vicksburg, MS, November 1977.

"Tide Tables, High and Low Water Predictions, East Coast of North  
and South America, including Greenland", National Ocean Survey,  
Washington, D. C., 1978.

Van de Kreeke, J., "Water-Level Fluctuations and Flow in Tidal Inlets",  
Journal of the Waterways and Harbors Division, Vol. 193, No. WW4,  
November 1967, pp. 97-106.

APPENDICES

APPENDIX 1:

Tidal Hydrodynamic Equations

The basic equations governing fluid flow are the Navier-Stokes equations, which express the conservation of momentum in viscous Newtonian fluids, and the continuity equation, which expresses the conservation of fluid mass. The solution of tidal hydraulics problems involving the Navier-Stokes equations is inconvenient due to their generality and nonlinear nature.

In an effort to simplify their solution, Harris and Bodine (1977) present a manipulation of the equations into a form better suited to tidal computations. The resulting equations stress the principal phenomena and provide some insight into the nature of the secondary terms which are subsequently neglected. Basing their development on the assumption that sea water is incompressible, Reid and Bodine proceed to partition the tidal flow into large and small scale flows, and then average these resulting flows over time and space. The governing equations with groups of terms indicated by letters are:

x and y momentum:

$$\underbrace{\frac{\partial q_x}{\partial t}}_A = \underbrace{\frac{-q_x}{d} \cdot \frac{\partial q_x}{\partial x} - \frac{q_y}{d} \frac{\partial q_x}{\partial y}}_B + \underbrace{\Omega q_y}_C - \underbrace{gd \frac{\partial h}{\partial x}}_D - \underbrace{gd S_{ex}}_E + \underbrace{K V_w^2 \cos \psi}_F \quad (1)$$

$$\underbrace{\frac{\partial q_y}{\partial t}} = \underbrace{\frac{-q_x}{d} \cdot \frac{\partial q_y}{\partial x} - \frac{q_y}{d} \frac{\partial q_y}{\partial y}} - \underbrace{\Omega q_x} - \underbrace{gd \frac{\partial h}{\partial y}} - \underbrace{gd S_{ey}} + \underbrace{K V_w^2 \sin \psi} \quad (2)$$

continuity:

$$\underbrace{\frac{\partial h}{\partial \tau}}_G = - \underbrace{\frac{\partial q_x}{\partial x} - \frac{\partial q_y}{\partial y}}_H + \underbrace{(r - e)}_I \quad (3)$$

In these equations  $q_x$ ,  $q_y$ ,  $h$ ,  $d$ ,  $r$ , and  $e$  are defined in Section 2.1. In addition,  $\Omega$  is the coriolis parameter;  $S_{ex}$  and  $S_{ey}$  represent the bottom friction;  $K$  is a dimensionless wind stress coefficient;  $V_w$  is a measure of the wind speed; and  $\psi$  is the angle between the wind direction and the  $x$  axis, measured clockwise from North

In the momentum equations the terms labeled A are the unsteady terms and represent the change of flow with time; terms B are the convective acceleration terms and measure the inertia of the water; terms C are the coriolis terms which result from the use of a rotating coordinate system; terms D describe the slope of the water surface and the resulting pressure forces which drive the flow; terms E express the loss of momentum due to bottom friction as a function of Manning's  $n$ ; and terms F represent the exchange of momentum at the water surface due to wind stresses. In the continuity equation term G represents the rate at which the water surface rises or falls; terms H measure the rate at which the water converges or diverges horizontally; and term I the net excess of precipitation over evaporation.

The explicit finite difference scheme applied to the equations is a time centered one in which computations of flows and water levels are performed in "leap frog" fashion. Superscript notation indicates the time level in the following manner:

- t-1 : the previous time level (t - Δt/2)  
t : the current time level (t)  
t+1 : the next time level (t + Δt/2)  
t+2 : two subsequent levels (t + Δt)

Applying the difference scheme to the terms in the x momentum equation yields:

$$\frac{\partial q_x}{\partial t} = \frac{q_x^{t+1}(i,j) - q_x^{t-1}(i,j)}{\Delta t} \quad (4)$$

$$\frac{q_x}{d} \frac{\partial q_x}{\partial x} = \frac{q_x^{t+1}(i,j)}{d_x} \cdot \frac{q_x^{t-1}(i+1,j) - q_x^{t-1}(i-1,j)}{2 \Delta x} \quad (5)$$

where

$$d_x = \frac{d^t(i,j) + d^t(i+1,j)}{2} \quad (6)$$

$$\frac{q_y}{d} \cdot \frac{\partial q_x}{\partial y} = \frac{\bar{q}_y}{d_x} \cdot \frac{q_x^{t-1}(i,j+1) - q_x^{t-1}(i,j-1)}{2 \Delta y} \quad (7)$$

where

$$\begin{aligned} \bar{q}_y = \frac{1}{4} [q_y^{t-1}(i,j) + q_y^{t-1}(i+1,j) \\ + q_y^{t-1}(i,j-1) + q_y^{t-1}(i+1,j-1)] \end{aligned} \quad (8)$$

$$- \Omega q_y = - \overline{\Omega q_y} \quad (9)$$

$$- g d \frac{\partial h}{\partial x} = - g d_x \cdot \frac{[h^t(i+1,j) - h^t(i,j)]}{\Delta x} \quad (10)$$

$$g d S_{ex} = \frac{g \cdot n_x^2}{(2.21) \cdot d_x^{4/3}} \cdot [q_x^{t+1}(i,j) \cdot \overline{q/d}] \quad (11)$$

where

$$n_x = \frac{n(i,j) + n(i+1,j)}{2} \quad (12)$$

and

$$\overline{q/d} = \frac{[(q_x^{t-1}(i,j))^2 + (\overline{q_y})^2]^{1/2}}{d_x} \quad (13)$$

In these expressions the only unknown is  $q_x^{t+1}$ , the flow per unit width in the x direction at the next time step. Combining the terms according to Eq. (1) and solving for  $q_x^{t+1}$ , the following explicit relation is obtained:

$$\begin{aligned} q_x^{t+1}(i,j) = & [q_x^{t-1}(i,j) - \Delta t \cdot \frac{\overline{q_y}}{d_x} \cdot \frac{q_x^{t-1}(i,j+1) - q_x^{t-1}(i,j-1)}{2 \Delta y} \\ & + \Delta t \overline{\Omega q_y} - \Delta t g d_x \frac{h^t(i+1,j) - h^t(i,j)}{\Delta x} \\ & + \Delta t K V_w^2 \cos \psi ] / C_{fx} \end{aligned} \quad (14)$$

where

$$C_{fx} = 1 + \frac{\Delta t}{d_x} \cdot \frac{q_x^{t-1}(i+1,j) - q_x^{t-1}(i-1,j)}{2 \Delta x} + \frac{g n_x^2 \Delta t}{2.21 d_x^{4/3}} [\overline{q/d}] \quad (15)$$

Similarly, using finite differences on the y momentum equation yields:

$$\begin{aligned}
 q_y^{t+1}(i,j) = & [q_y^{t-1}(i,j) - \Delta t \frac{\bar{q}_x}{d_y} \cdot \frac{q_y^{t-1}(i+1,j) - q_y^{t-1}(i-1,j)}{2 \Delta x} \\
 & - \Delta t \Omega \bar{q}_x - \Delta t g d_y \frac{h^t(i,j+1) - h^t(i,j)}{\Delta y} \\
 & + \Delta t K v_w^2 \sin \psi] / C_{fy}
 \end{aligned} \tag{16}$$

where

$$C_{fy} = 1 + \frac{\Delta t}{d_y} \cdot \frac{q_y^{t-1}(i,j+1) - q_y^{t-1}(i,j-1)}{2 \Delta y} + \frac{g n_y^2 \Delta t}{2.21 \cdot d_y^{4/3}} [\bar{q}/d] \tag{17}$$

$$d_y = \frac{d^t(i,j) + d^t(i,j+1)}{2} \tag{18}$$

$$\begin{aligned}
 \bar{q}_x = & \frac{1}{4} [q_x^{t-1}(i,j) + q_x^{t-1}(i,j+1) + q_x^{t-1}(i-1,j) \\
 & + q_x^{t-1}(i-1,j+1)]
 \end{aligned} \tag{19}$$

$$n_y = \frac{n(i,j) + n(i,j+1)}{2} \tag{20}$$

$$\frac{\bar{q}}{d} = \frac{[(\bar{q}_x)^2 + (q_y^{t-1}(i,j))^2]^{1/2}}{d_y} \tag{21}$$



Lastly, the unknown water level,  $h$ , can be found from the continuity equation and the two flows per unit width just computed as follows:

$$\frac{\partial h}{\partial t} = \frac{h^{t+2}(i,j) - h^t(i,j)}{\Delta t} \quad (22)$$

$$\frac{\partial q_x}{\partial x} = \frac{q_x^{t+1}(i,j) - q_x^{t+1}(i-1,j)}{\Delta x} \quad (23)$$

$$\frac{\partial q_y}{\partial y} = \frac{q_y^{t+1}(i,j) - q_y^{t+1}(i,j-1)}{\Delta y} \quad (24)$$

Combining these terms in the form of Eq. (3) and solving for  $h^{t+2}$  yields:

$$h(i,j)^{t+2} = h^t(i,j) - \Delta t \frac{q_x^{t+1}(i,j) - q_x^{t+1}(i-1,j)}{\Delta x} - \Delta t \frac{q_y^{t+1}(i,j) - q_y^{t+1}(i,j-1)}{\Delta y} + \Delta t (r - e) \quad (25)$$

The leap frog nature of the calculations results in the difference  $(q_x^{t+1} - q_x^{t-1})$  and  $(q_y^{t+1} - q_y^{t-1})$  being centered on the  $t$  time level and the difference  $(h^{t+2} - h^t)$  being centered on the  $t+1$  time level. In an explicit scheme, because the time steps are quite small, using different time levels should not produce significant error.

In the preceding expressions, cell (i,j) was assumed to be an open water cell and was free to communicate with adjacent cells. When flow between adjacent cells is not permitted, the convective terms  $\frac{q_y}{d} \cdot \frac{\partial q_x}{\partial y}$  and  $\frac{q_x}{d} \cdot \frac{\partial q_y}{\partial x}$  must be reformulated to reflect the actual situation. This reformulation is accomplished by the convective flagging scheme mentioned in Section 3.2, which designates the appropriate calculation to be performed in the x and y directions. The two flags each range from one to four and indicate the following computations are to be performed:

<u>Flag Value</u>	<u>Type of Approximation</u>
1	Centered Difference
2	Zero
3	Forward Difference
4	Backward Difference

Mathematically, the following computations are accomplished:

x direction

Flag	Computation
------	-------------

1:	$\frac{q_y}{d} \cdot \frac{\partial q_x}{\partial y} = \frac{\bar{q}_y}{d_x} \frac{q_x^{t-1}(i,j+1) - q_x^{t-1}(i,j-1)}{2 \Delta y}$	(26)
----	--	------

2:	$\frac{q_y}{d} \cdot \frac{\partial q_x}{\partial y} = 0.$	(27)
----	--	------

Flag	Computation	
3:	$\frac{q_y}{d} \cdot \frac{\partial q_x}{\partial y} = \frac{\bar{q}_y}{d_x} \cdot \frac{q_x^{t-1}(i,j+1) - q_x^{t-1}(i,j)}{\Delta y}$	(28)

4:	$\frac{q_y}{d} \cdot \frac{\partial q_x}{\partial y} = \frac{\bar{q}_y}{d_x} \cdot \frac{q_x^{t-1}(i,j) - q_x^{t-1}(i,j-1)}{\Delta y}$	(29)
----	--	------

y direction

Flag	Computation	
1:	$\frac{q_x}{d} \cdot \frac{\partial q_y}{\partial x} = \frac{\bar{q}_x}{d_y} \cdot \frac{q_y^{t-1}(i+1,j) - q_y^{t-1}(i-1,j)}{2 \Delta x}$	(30)

2:	$\frac{q_x}{d} \cdot \frac{\partial q_y}{\partial x} = 0.$	(31)
----	--	------

3:	$\frac{q_x}{d} \cdot \frac{\partial q_y}{\partial x} = \frac{\bar{q}_x}{d_y} \cdot \frac{q_y^{t-1}(i+1,j) - q_y^{t-1}(i,j)}{\Delta x}$	(32)
----	--	------

4:	$\frac{q_x}{d} \cdot \frac{\partial q_y}{\partial x} = \frac{\bar{q}_x}{d_y} \cdot \frac{q_y^{t-1}(i,j) - q_y^{t-1}(i,j-1)}{\Delta x}$	(33)
----	--	------

The physical situations corresponding to the 16 possible two digit flags are displayed in Fig. 6, Section 3.2.

APPENDIX 2: Tidal Data

	O SH	A	O HI	A	O SSL	A	O TI	A	O OTT	A	O WW	A	O NI	A	O SBL	A	O GC	A	O GS	A
25 Aug																				
2400	6.62	4.15	--	3.98	4.85	4.13	5.07	3.73	4.34	3.88	6.38	3.91	5.15	4.14	4.34	3.84	7.18	3.79	4.07	3.81
26 Aug																				
0100	7.13	4.66	-	4.45	5.38	4.66	5.49	4.15	4.89	4.43	6.89	4.42	5.28	4.27	4.78	4.28	7.63	4.24	4.55	4.25
0200	7.28	4.81	-	4.56	5.51	4.79	5.41	4.07	5.05	4.59	7.05	4.58	5.49	4.48	4.96	4.46	7.73	4.34	4.72	4.43
0300	6.82	4.35	-	4.14	5.26	4.54	5.06	3.72	4.81	4.35	6.84	4.37	5.12	4.11	4.71	4.21	7.38	3.99	4.50	4.20
0400	6.01	3.54	-	3.38	4.64	3.92	4.52	3.18	4.23	3.77	6.28	3.81	4.56	3.55	4.16	3.66	6.82	3.43	3.96	3.66
0500	5.12	2.65	-	2.53	3.91	3.19	3.77	2.43	3.55	3.09	5.59	3.12	3.68	2.67	3.51	3.01	6.17	2.78	3.33	3.03
0600	4.47	2.00	-	1.92	3.01	2.29	3.03	1.69	2.75	2.29	4.81	2.34	2.95	2.94	2.78	2.28	5.41	2.02	2.61	2.31
0700	3.98	1.51	-	1.47	2.33	1.61	2.65	1.31	2.07	1.61	4.13	1.66	2.55	1.54	2.13	1.63	4.84	1.45	1.98	1.68
0800	3.85	1.38	-	1.38	2.03	1.31	2.52	1.18	1.70	1.24	3.75	1.28	2.33	1.32	1.73	1.23	4.52	1.13	1.56	1.26
0900	4.09	1.62	-	1.58	2.36	1.64	2.89	1.55	1.82	1.36	3.87	1.40	2.56	1.55	1.81	1.31	4.75	1.36	1.48	1.18
1000	4.86	2.39	-	2.31	2.98	2.26	3.47	2.13	2.50	2.04	4.54	2.07	3.18	2.17	2.45	1.95	5.33	1.94	2.10	1.80
1100	5.73	3.26	-	3.14	3.73	3.01	4.20	2.86	3.19	2.73	5.25	2.79	3.98	2.97	3.20	2.70	6.08	2.69	2.87	2.57
1200	6.52	4.05	-	3.89	4.58	3.86	5.00	3.66	4.06	3.60	6.11	3.64	4.73	3.72	4.03	3.53	6.89	3.50	3.72	3.42
1300	7.23	4.76	-	4.55	5.35	4.63	5.55	4.21	4.84	4.38	6.86	4.39	5.49	4.48	4.78	4.28	7.60	4.21	4.51	4.21
1400	7.56	5.09	-	4.84	5.76	5.04	5.73	4.39	5.29	4.83	7.27	4.80	5.68	4.67	5.18	4.68	7.92	4.53	4.93	4.63
1500	7.42	4.95	-	4.74	5.75	5.03	5.69	4.35	5.31	4.85	7.30	4.83	5.71	4.70	5.23	4.73	7.90	4.51	4.96	4.66
1600	6.76	4.29	-	4.11	5.42	4.70	5.25	3.91	5.01	4.55	7.05	4.58	5.36	4.35	4.89	4.39	7.60	4.21	4.68	4.38
1700	5.83	3.36	-	3.22	4.80	4.08	4.57	3.23	4.45	3.99	6.47	4.00	4.52	3.51	4.35	3.85	7.01	3.62	4.17	3.87
1800	5.18	2.71	-	2.61	3.90	3.18	3.83	2.49	3.63	3.17	5.66	3.19	3.79	2.78	3.60	3.10	6.22	2.83	3.43	3.13
1900	4.55	2.08	-	2.01	3.07	2.35	3.09	1.75	2.78	2.32	4.82	2.35	3.02	2.01	2.82	2.32	5.43	2.04	2.66	2.36
2000	3.99	1.52	-	1.49	2.31	1.59	2.63	1.29	2.09	1.63	4.14	1.67	2.50	1.49	2.17	1.67	4.83	1.44	2.03	1.73
2100	3.72	1.25	-	1.25	2.08	1.36	2.55	1.21	1.69	1.23	3.76	1.29	2.32	1.31	1.77	1.27	4.52	1.13	1.55	1.25
2200	4.03	1.56	-	1.52	2.37	1.65	2.79	1.45	1.91	1.45	3.88	1.41	2.58	1.57	1.83	1.33	4.71	1.32	1.49	1.19
2300	4.75	2.31	-	2.23	2.90	2.18	3.33	1.99	2.39	1.93	4.42	1.95	3.11	2.10	2.38	1.88	5.26	1.87	2.06	1.76
2400	5.53	3.06	-	2.91	3.50	2.78	3.86	2.52	3.05	2.59	5.05	2.58	3.72	2.71	2.97	2.47	5.86	2.47	2.71	2.41
27 Aug																				
0100	6.24	3.77	-	3.61	4.18	3.46	4.39	3.05	3.68	3.22	5.68	3.21	4.30	3.29	3.62	3.12	6.44	3.05	3.34	3.04

KEY TO APPENDIX 2

SH	Sandy Hook
HI	Hereford Inlet
SSL	Sunset Lake
TI	Townsend Inlet
OTT	Old Turtle Thorofare
WW	West Wildwood
NI	Nummy Island
SBL	Shellbed Landing
GC	Great Channel
GS	Great Sound
O	Observed tidal height
A	Adjusted tidal height

APPENDIX 3:

Flow Pattern: Coarse Grid

FLOW PATTERN FOR COARSE GRID

2400 HRS 25 AUG 1978

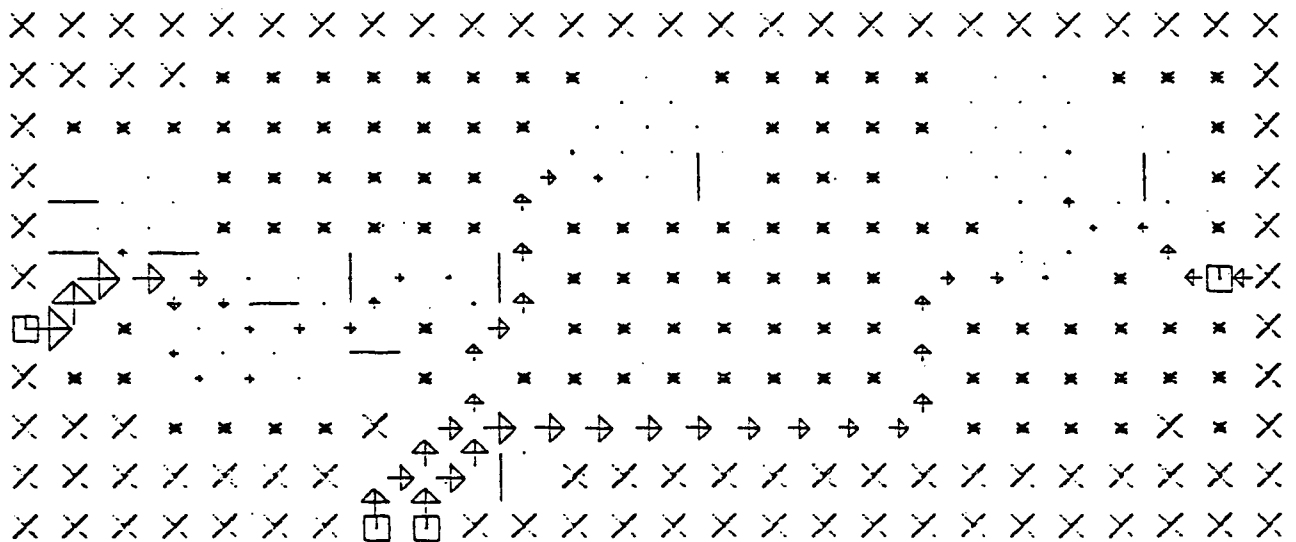
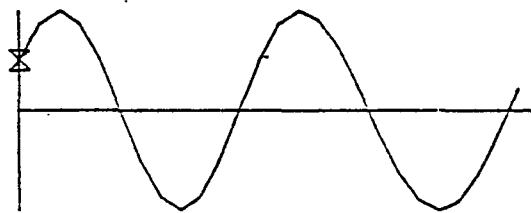
X - LAND CELL

\* - INUNDATION CELL

□ - FORCING CELL

- - NO FLOW BOUNDARY

SCALE - 100000. CFS / INCH



FLOW PATTERN FOR COARSE GRID

0100 HRS 26 AUG 1978

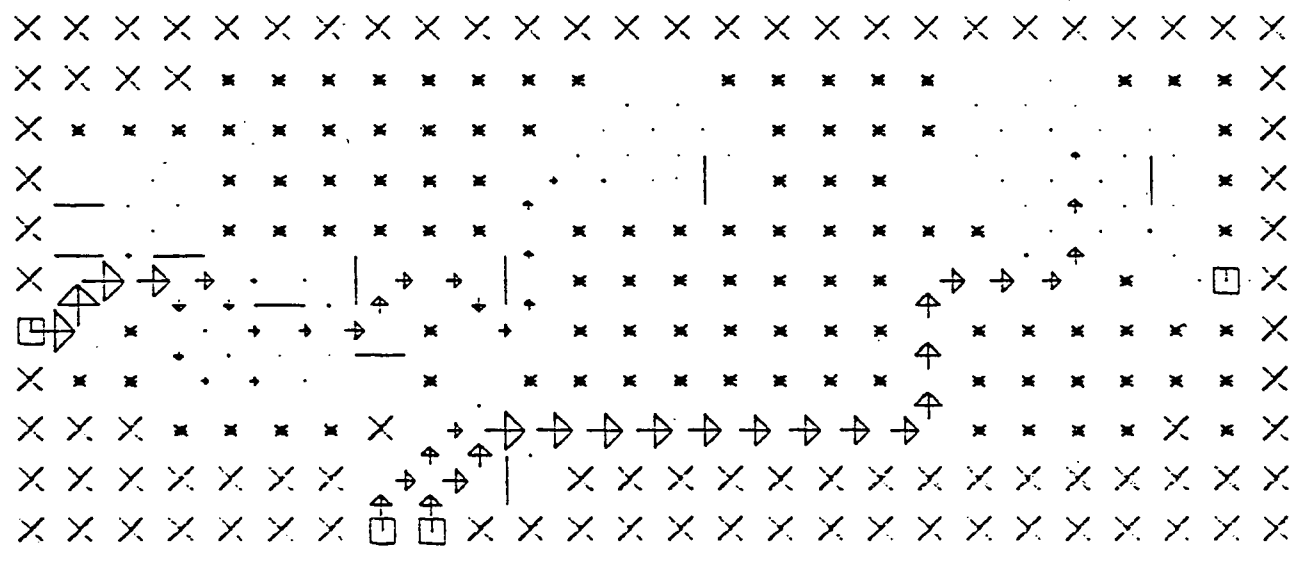
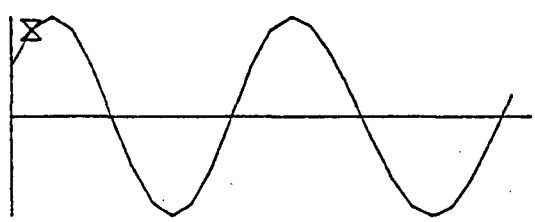
X - LAND CELL

\* - INUNDATION CELL

□ - FORCING CELL

- - NO FLOW BOUNDARY

SCALE - 100000. CFS / INCH





FLOW PATTERN FOR COARSE GRID

0200 HRS 26 AUG 1978

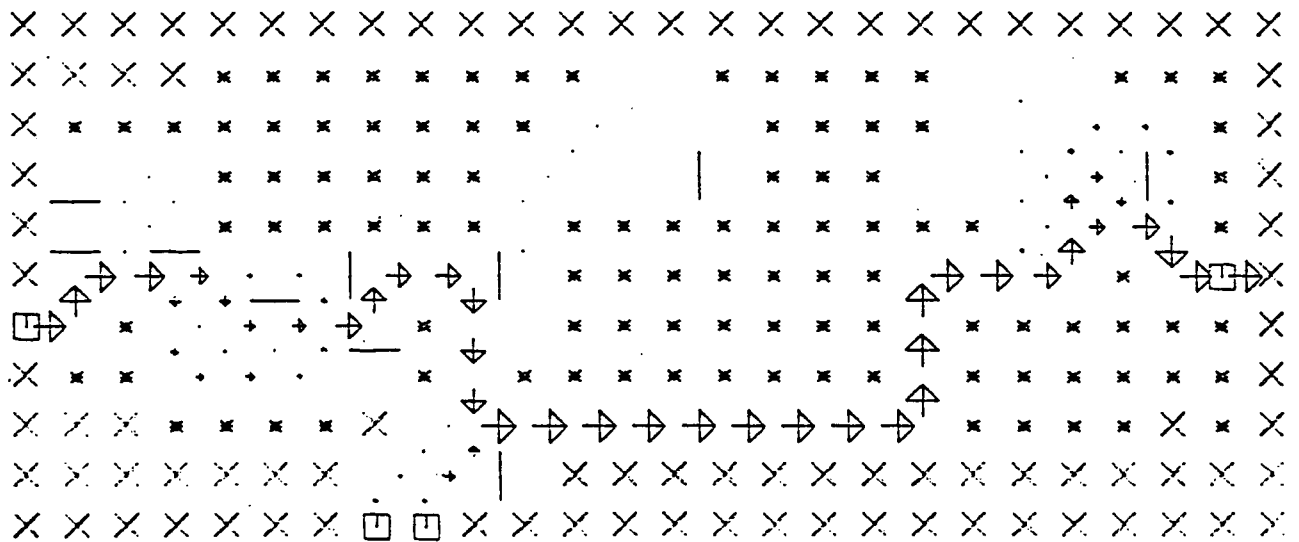
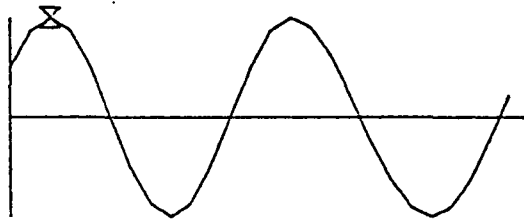
X - LAND CELL

\* - INUNDATION CELL

□ - FORCING CELL

- - NO FLOW BOUNDARY

SCALE - 100000. CFS / INCH



FLOW PATTERN FOR COARSE GRID

0300 HRS 26 AUG 1978

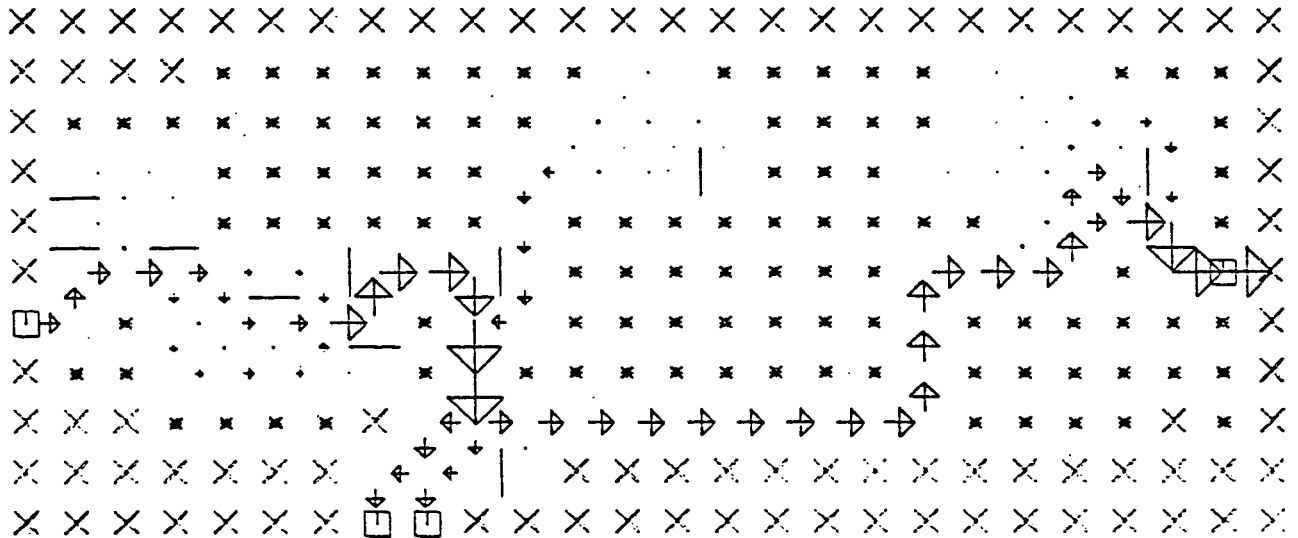
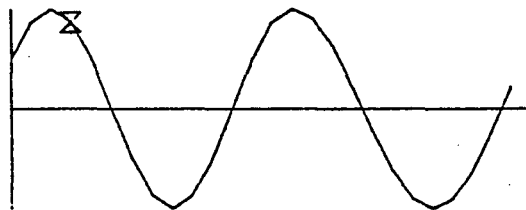
X - LAND CELL

\* - INUNDATION CELL

□ - FORCING CELL

- - NO FLOW BOUNDARY

SCALE - 100000. CFS / INCH



FLOW PATTERN FOR COARSE GRID

0400 HRS 26 AUG 1978

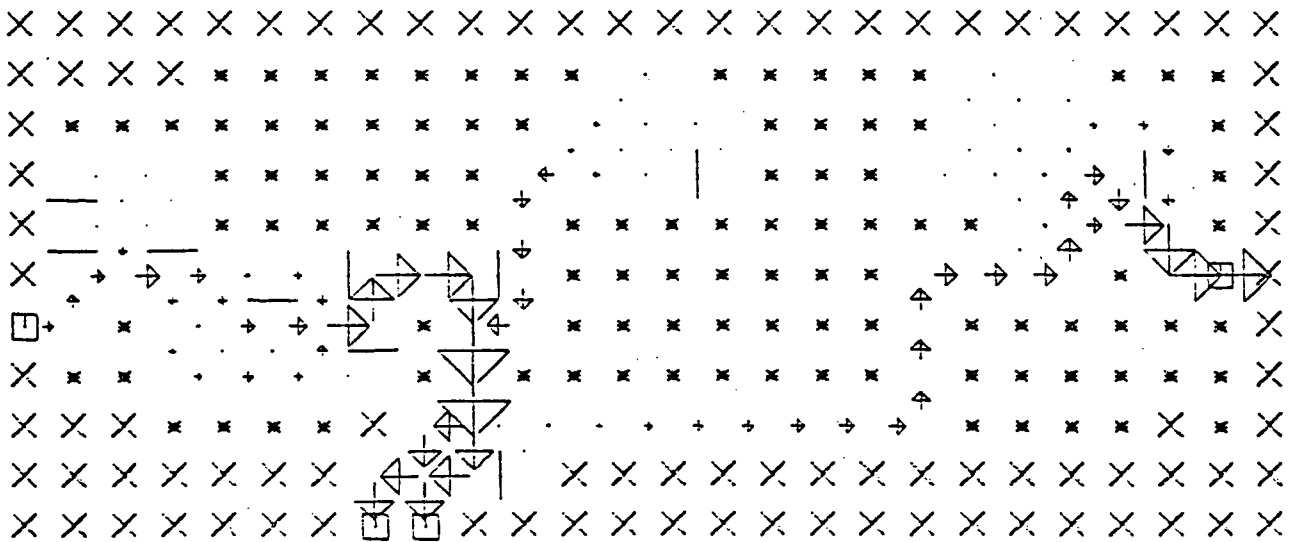
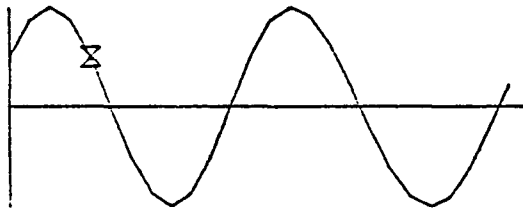
X - LAND CELL

\* - INUNDATION CELL

□ - FORCING CELL

- - NO FLOW BOUNDARY

SCALE - 100000 CFS / INCH



FLOW PATTERN FOR COARSE GRID

0500 HRS 26 AUG 1978

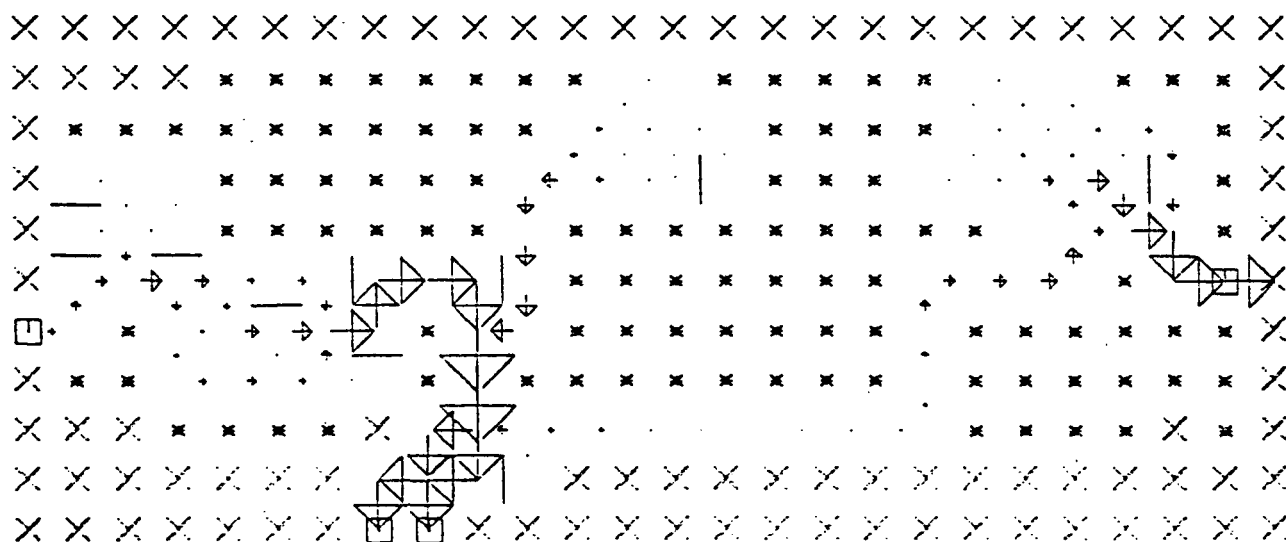
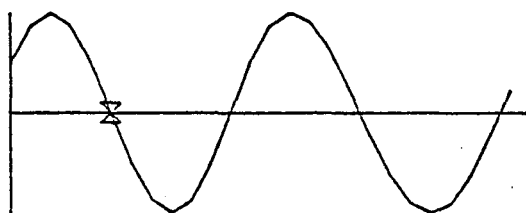
X - LAND CELL

\* - INUNDATION CELL

□ - FORCING CELL

- - NO FLOW BOUNDARY

SCALE - 100000. CFS / INCH



FLOW PATTERN FOR COARSE GRID

0600 HRS 26 AUG 1978

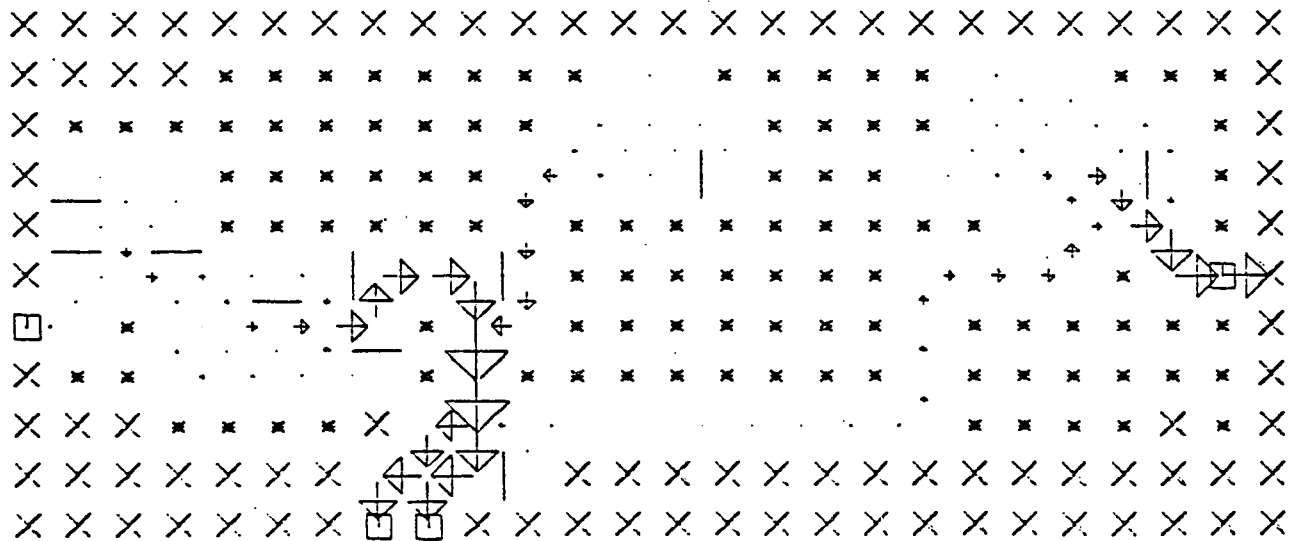
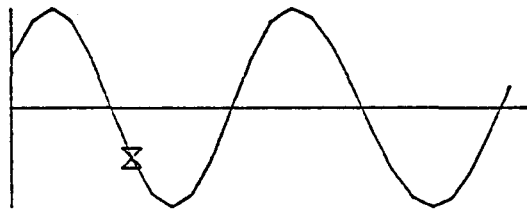
X - LAND CELL

\* - INUNDATION CELL

□ - FORCING CELL

- - NO FLOW BOUNDARY

SCALE - 100000. CFS / INCH



FLOW PATTERN FOR COARSE GRID

0700 HRS 26 AUG 1978

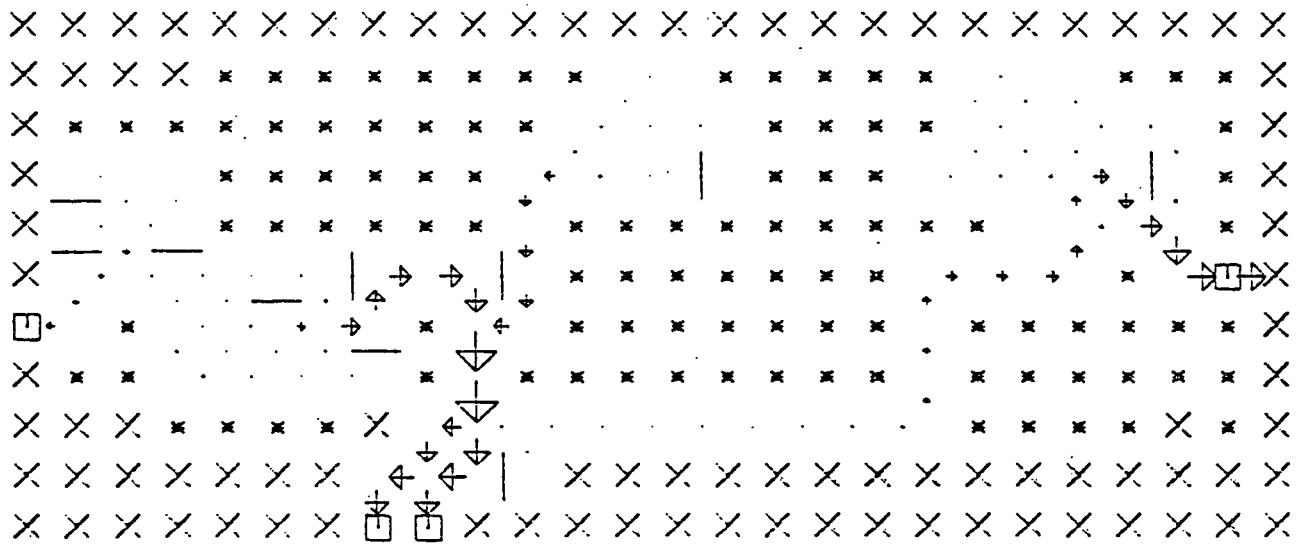
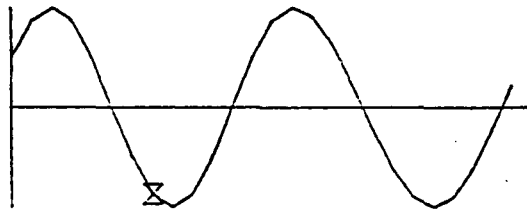
X - LAND CELL

\* - INUNDATION CELL

□ - FORCING CELL

- - NO FLOW BOUNDARY

SCALE - 100000. CFS / INCH



FLOW PATTERN FOR COARSE GRID

0800 HRS 26 AUG 1978

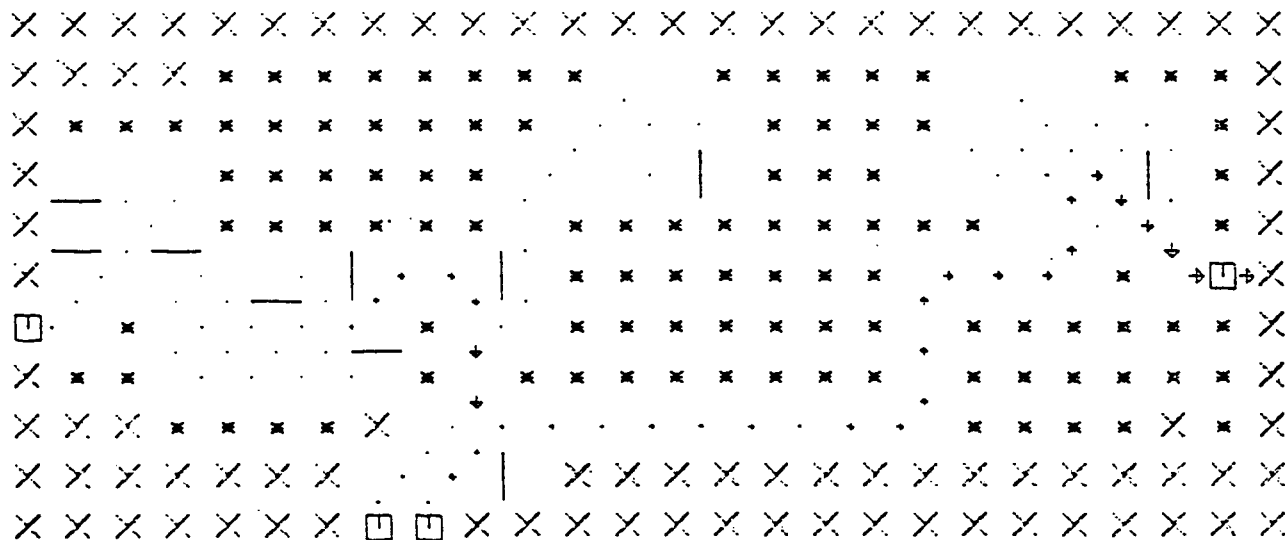
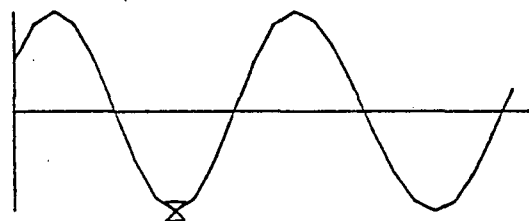
X - LAND CELL

\* - INUNDATION CELL

□ - FORCING CELL

- - NO FLOW BOUNDARY

SCALE - 100000. CFS / INCH



FLOW PATTERN FOR COARSE GRID

0900 HRS 26 AUG 1978

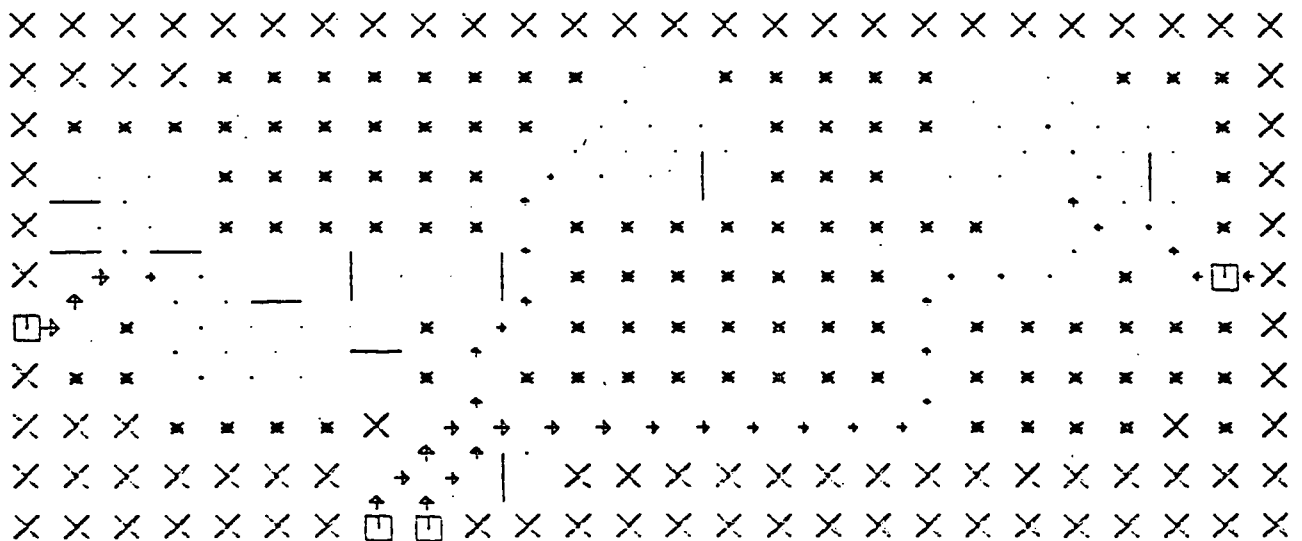
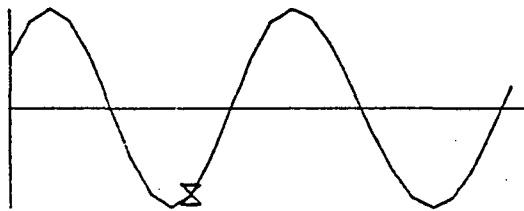
X - LAND CELL

\* - INUNDATION CELL

□ - FORCING CELL

- - NO FLOW BOUNDARY

SCALE - 100000. CFS / INCH





FLOW PATTERN FOR COARSE GRID

1000 HRS 26 AUG 1978

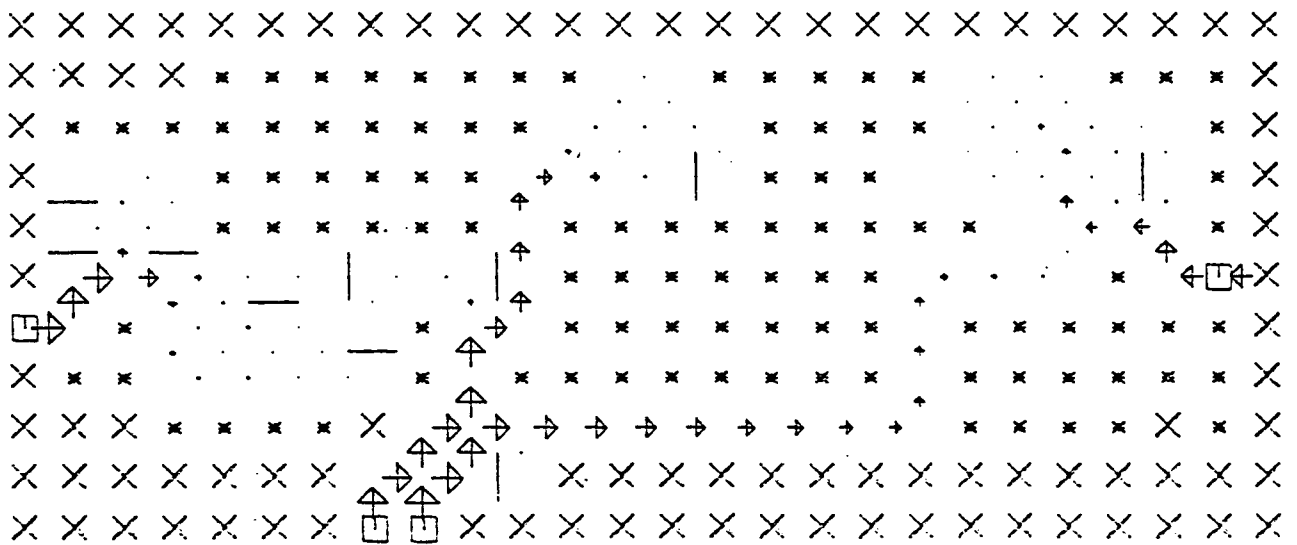
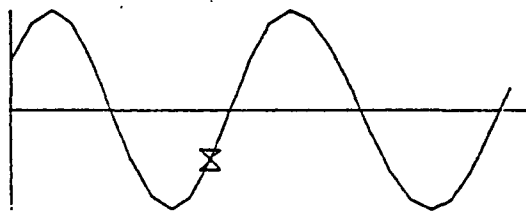
X - LAND CELL

\* - INUNDATION CELL

□ - FORCING CELL

- - NO FLOW BOUNDARY

SCALE - 100000. CFS / INCH

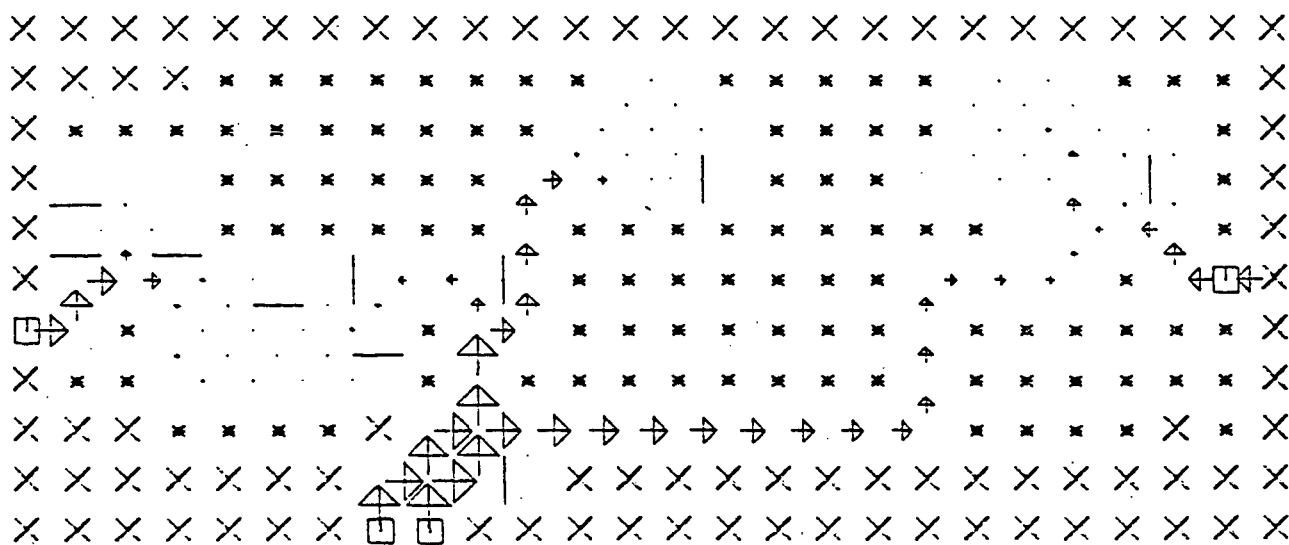
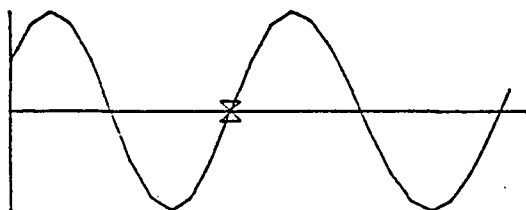


FLOW PATTERN FOR COARSE GRID

1100 HRS 26 AUG 1978

- X - LAND CELL
- \* - INUNDATION CELL
- - FORCING CELL
- - NO FLOW BOUNDARY

SCALE - 100000. CFS / INCH



FLOW PATTERN FOR COARSE GRID

1200 HRS 26 AUG 1978

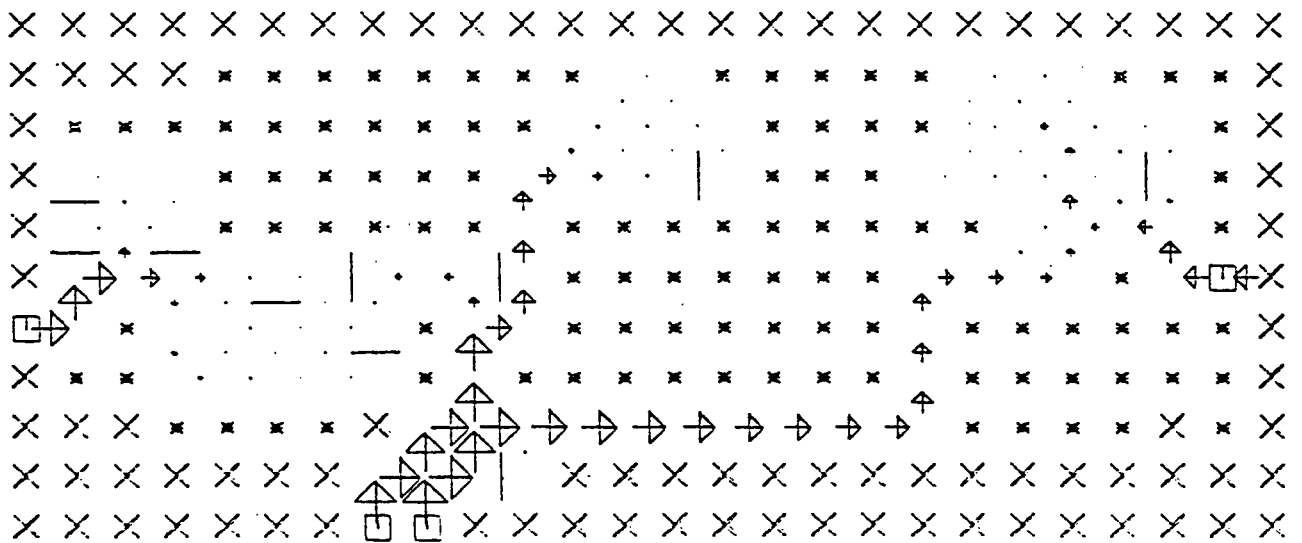
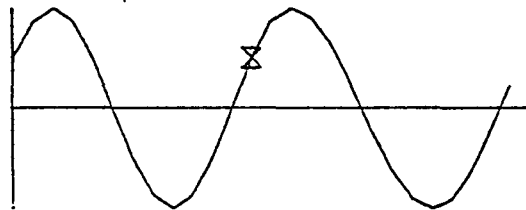
X - LAND CELL

\* - INUNDATION CELL

□ - FORCING CELL

- - NO FLOW BOUNDARY

SCALE - 100000. CFS / INCH



FLOW PATTERN FOR COARSE GRID

1300 HRS 26 AUG 1978

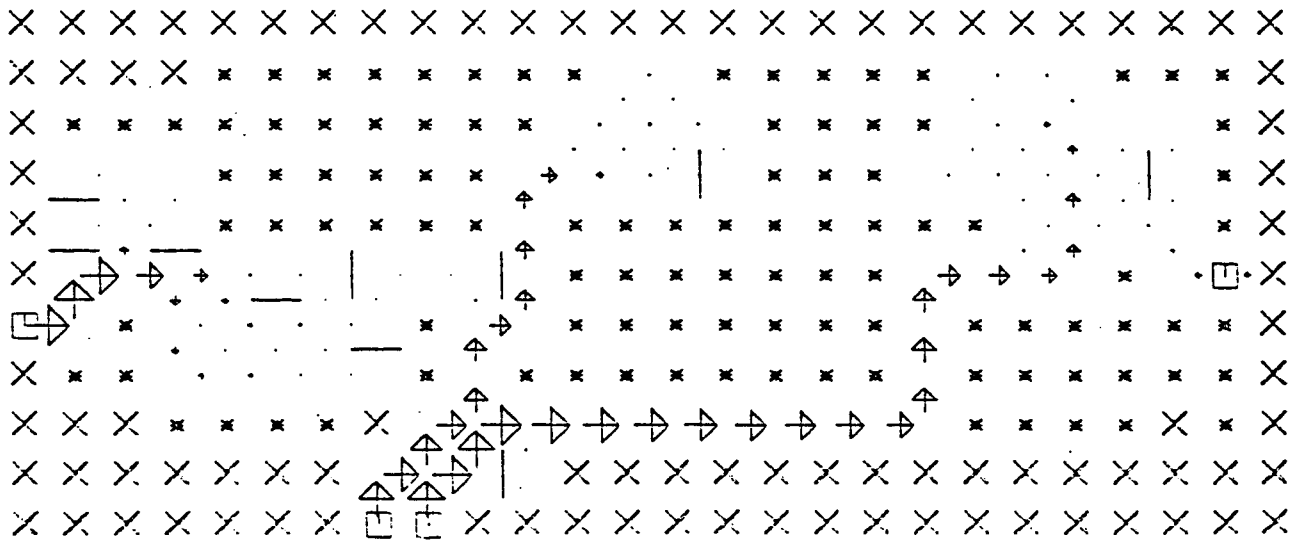
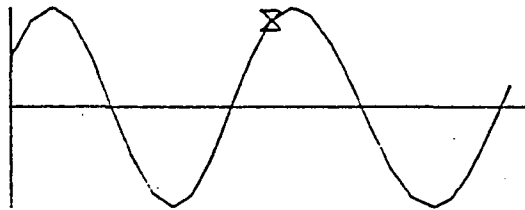
X - LAND CELL

\* - INUNDATION CELL

□ - FORCING CELL

- - NO FLOW BOUNDARY

SCALE - 100000. CFS / INCH



FLOW PATTERN FOR COARSE GRID

1400 HRS 26 AUG 1978

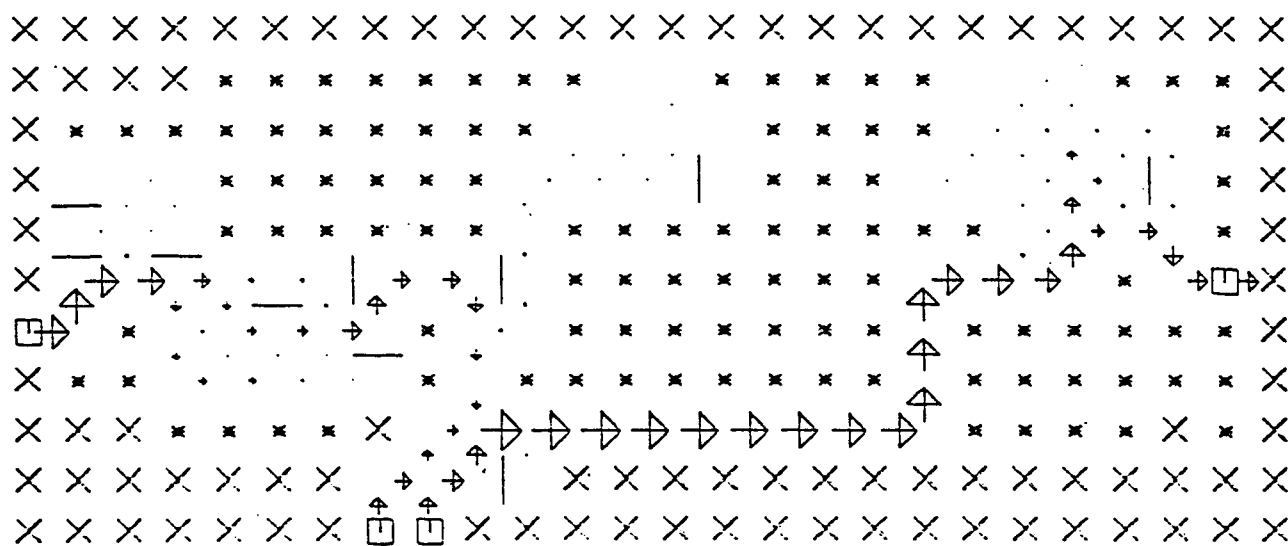
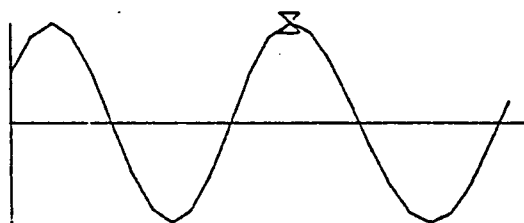
X - LAND CELL

\* - INUNDATION CELL

□ - FORCING CELL

- - NO FLOW BOUNDARY

SCALE - 100000. CFS / INCH

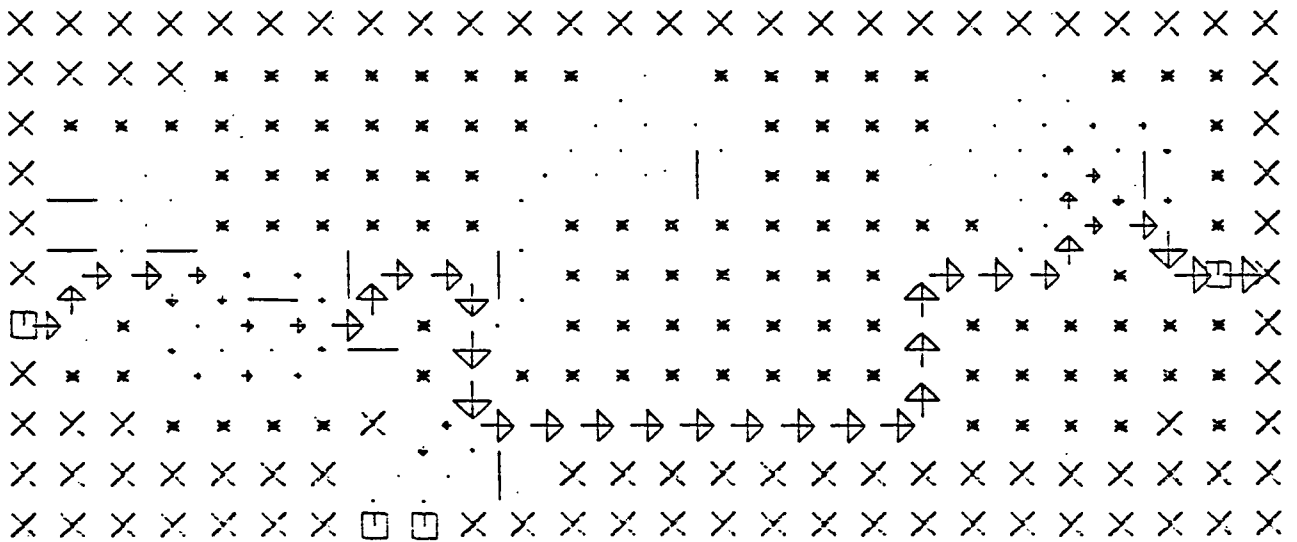
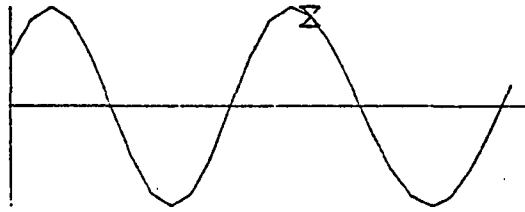


FLOW PATTERN FOR COARSE GRID

1500 HRS 26 AUG 1978

- X - LAND CELL
- \* - INUNDATION CELL
- - FORCING CELL
- - NO FLOW BOUNDARY

SCALE - 100000. CFS / INCH



FLOW PATTERN FOR COARSE GRID

1600 HRS 26 AUG 1978

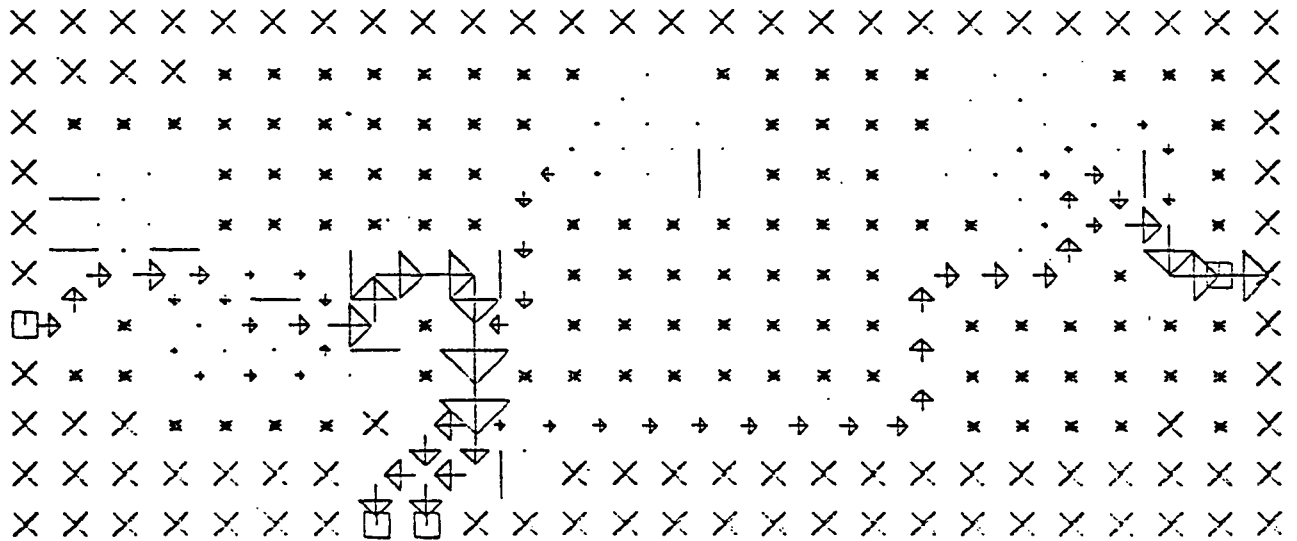
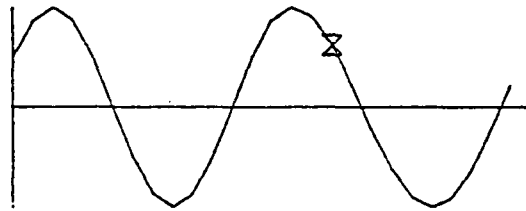
X - LAND CELL

\* - INUNDATION CELL

□ - FORCING CELL

- - NO FLOW BOUNDARY

SCALE - 100000. CFS / INCH



FLOW PATTERN FOR COARSE GRID

1700 HRS 26 AUG 1978

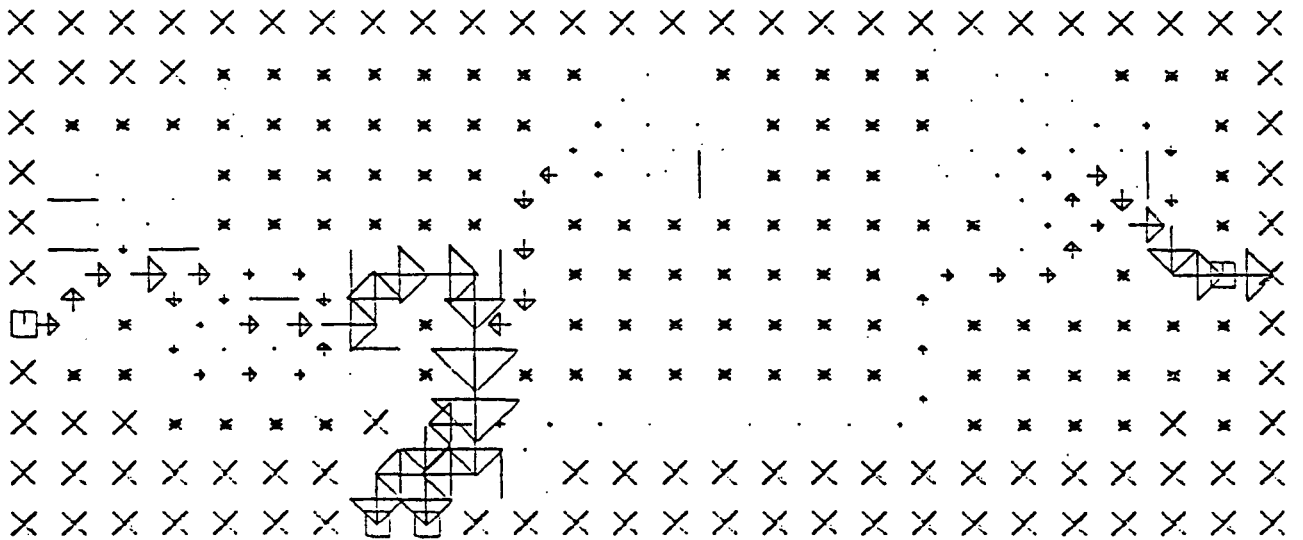
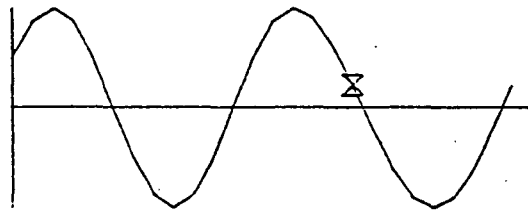
X - LAND CELL

\* - INUNDATION CELL

□ - FORCING CELL

- - NO FLOW BOUNDARY

SCALE - 100000. CFS / INCH





FLOW PATTERN FOR COARSE GRID

1800 HRS 26 AUG 1978

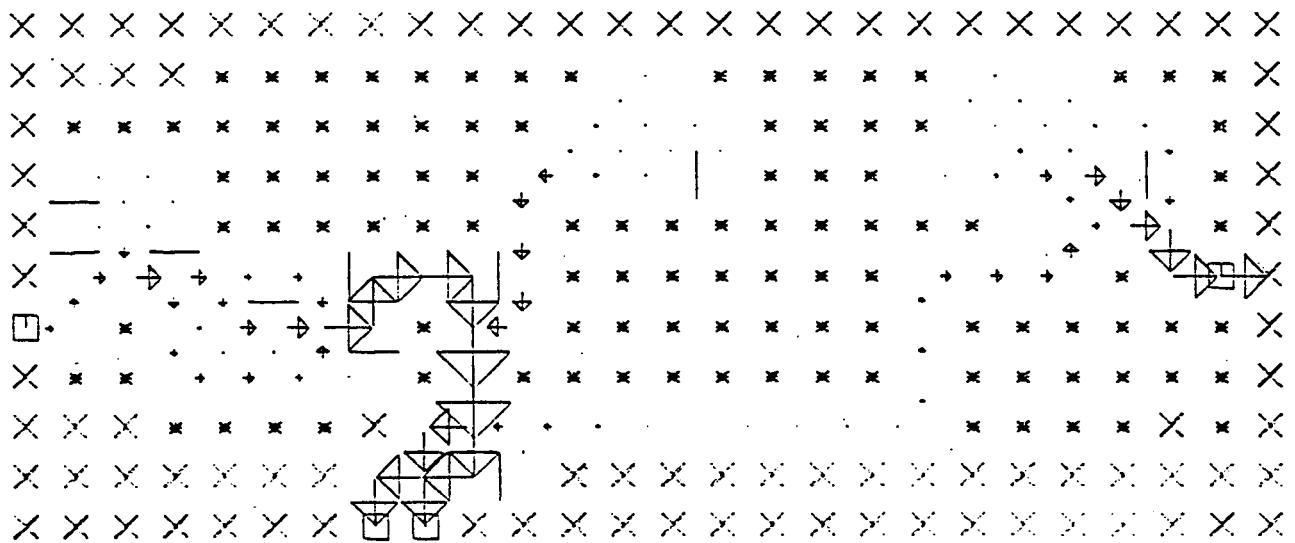
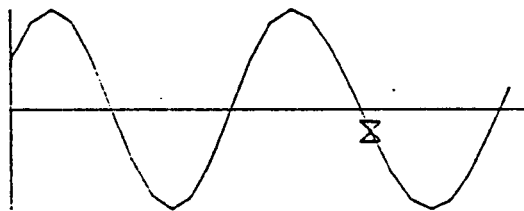
X - LAND CELL

\* - INUNDATION CELL

□ - FORCING CELL

- - NO FLOW BOUNDARY

SCALE - 100000. CFS / INCH

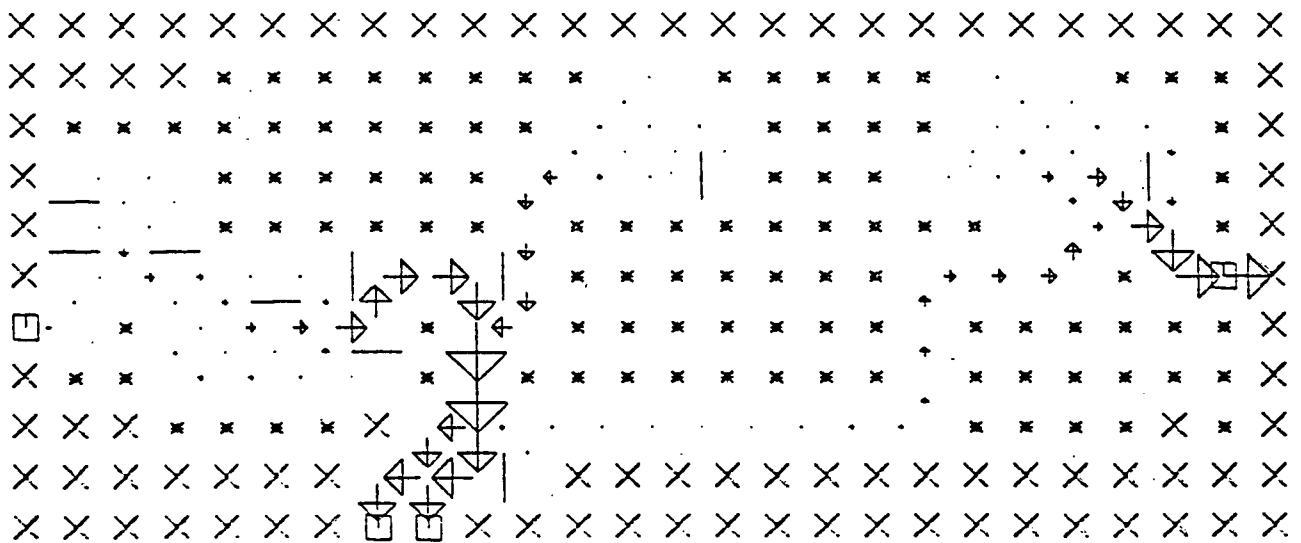
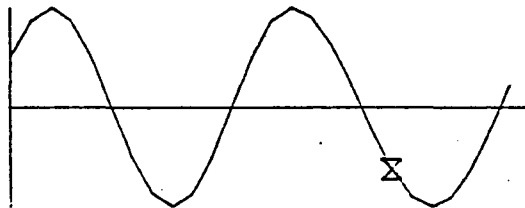


FLOW PATTERN FOR COARSE GRID

1900 HRS 26 AUG 1978

- X - LAND CELL
- \* - INUNDATION CELL
- - FORCING CELL
- - NO FLOW BOUNDARY

SCALE - 100000. CFS / INCH



FLOW PATTERN FOR COARSE GRID

2000 HRS 26 AUG 1978

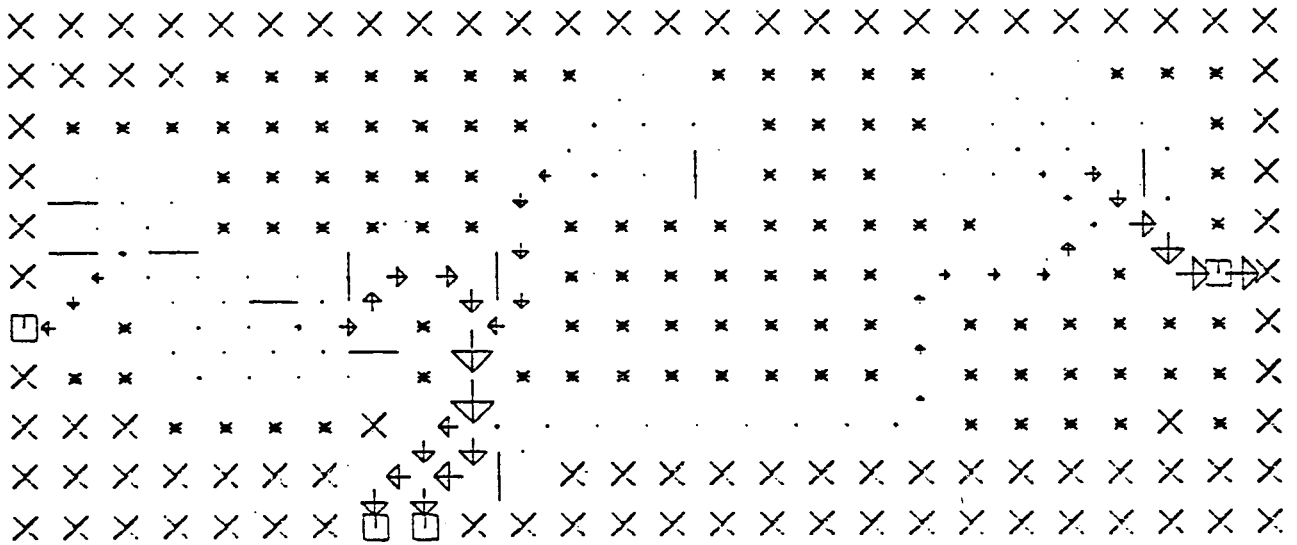
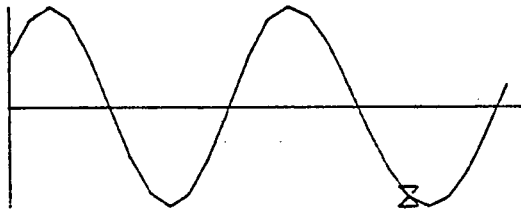
X - LAND CELL

\* - INUNDATION CELL

□ - FORCING CELL

- - NO FLOW BOUNDARY

SCALE - 100000. CFS / INCH



FLOW PATTERN FOR COARSE GRID

2100 HRS 26 AUG 1978

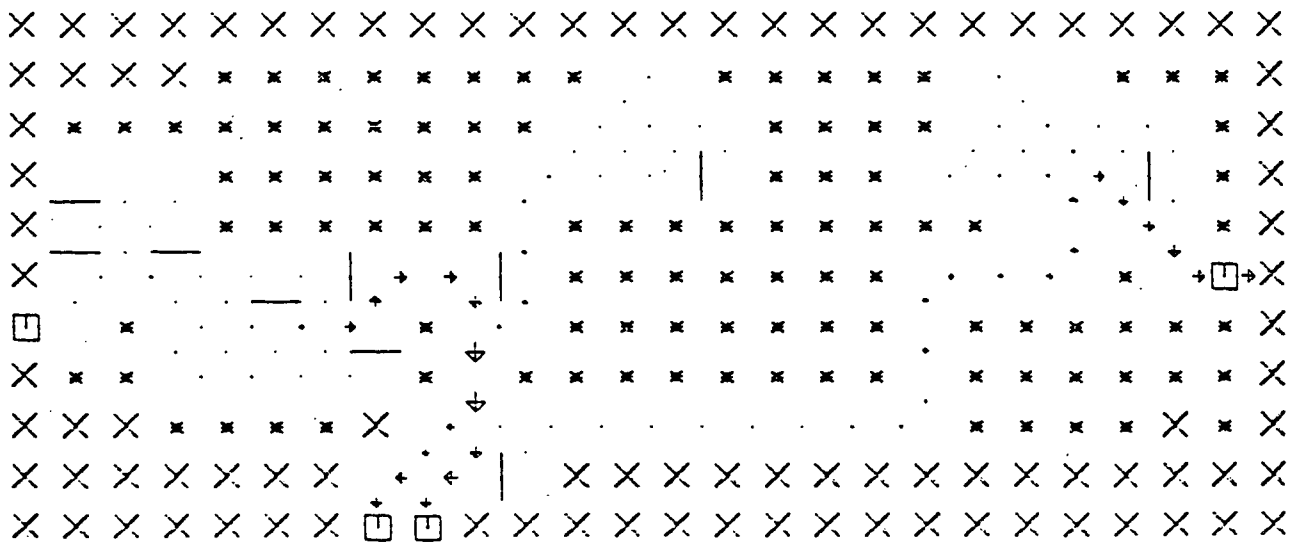
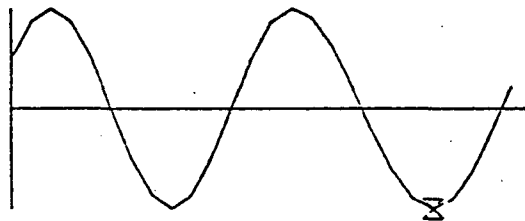
X - LAND CELL

\* - INUNDATION CELL

□ - FORCING CELL

- - NO FLOW BOUNDARY

SCALE - 100000. CFS / INCH



FLOW PATTERN FOR COARSE GRID

2200 HRS 26 AUG 1978

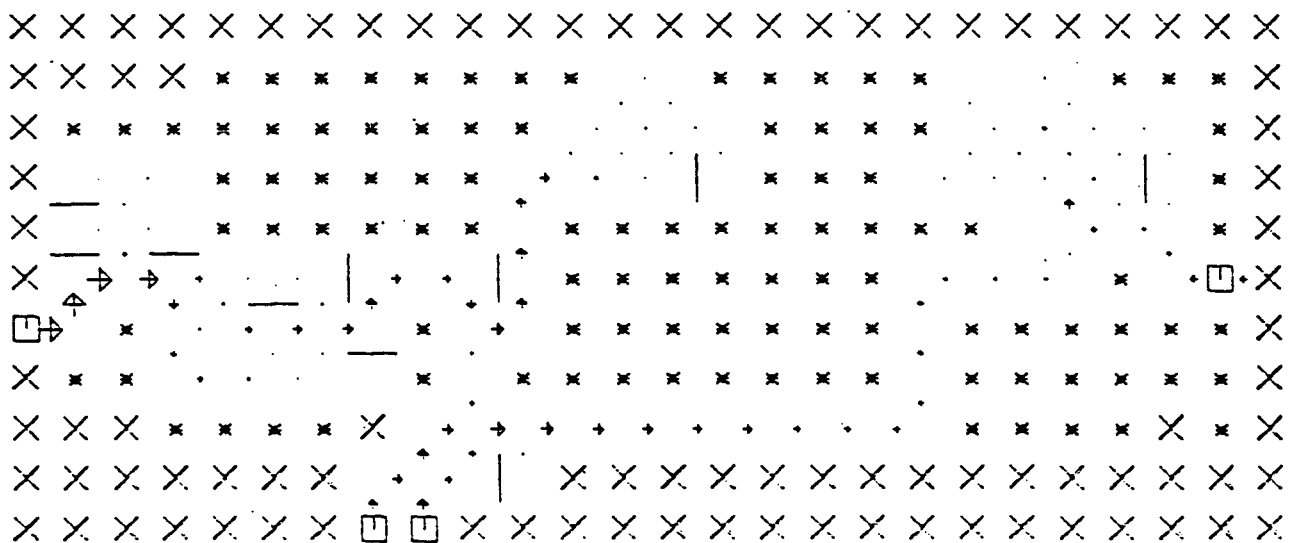
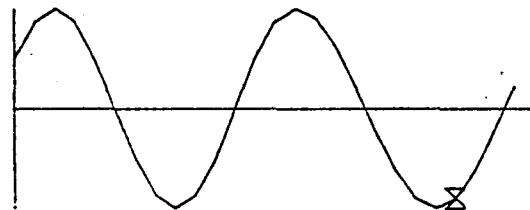
X - LAND CELL

\* - INUNDATION CELL

□ - FORCING CELL

- - NO FLOW BOUNDARY

SCALE - 100000. CFS / INCH



FLOW PATTERN FOR COARSE GRID

2300 HRS 26 AUG 1978

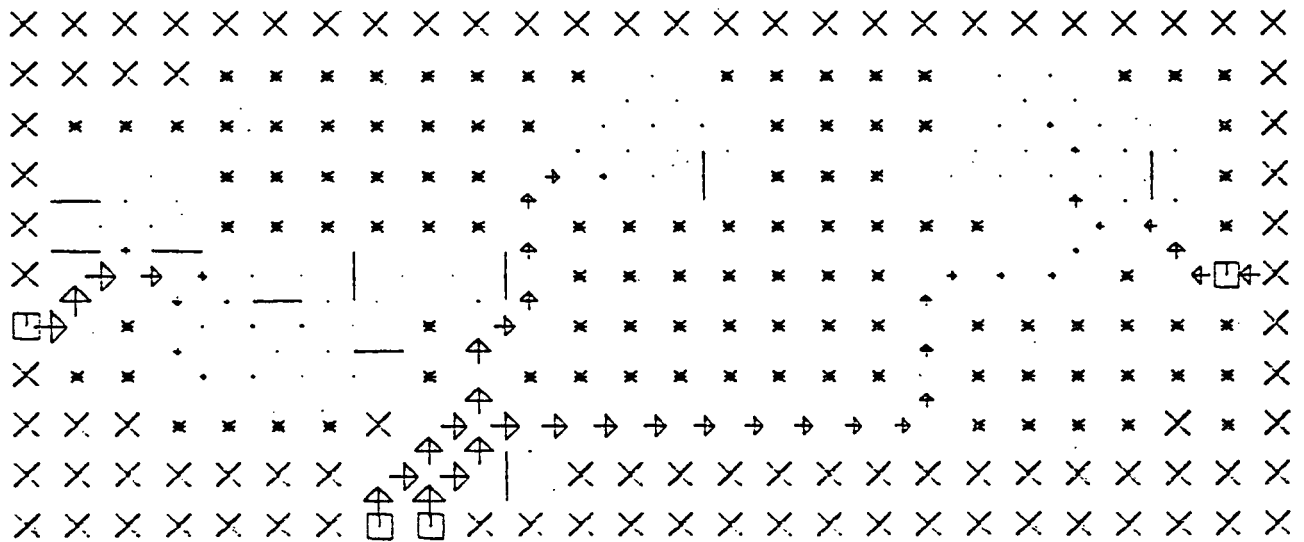
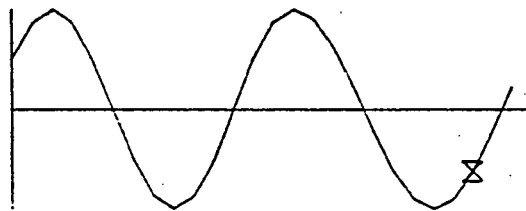
X - LAND CELL

\* - INUNDATION CELL

□ - FORCING CELL

- - NO FLOW BOUNDARY

SCALE - 100000. CFS / INCH



FLOW PATTERN FOR COARSE GRID

2400 HRS 26 AUG 1978

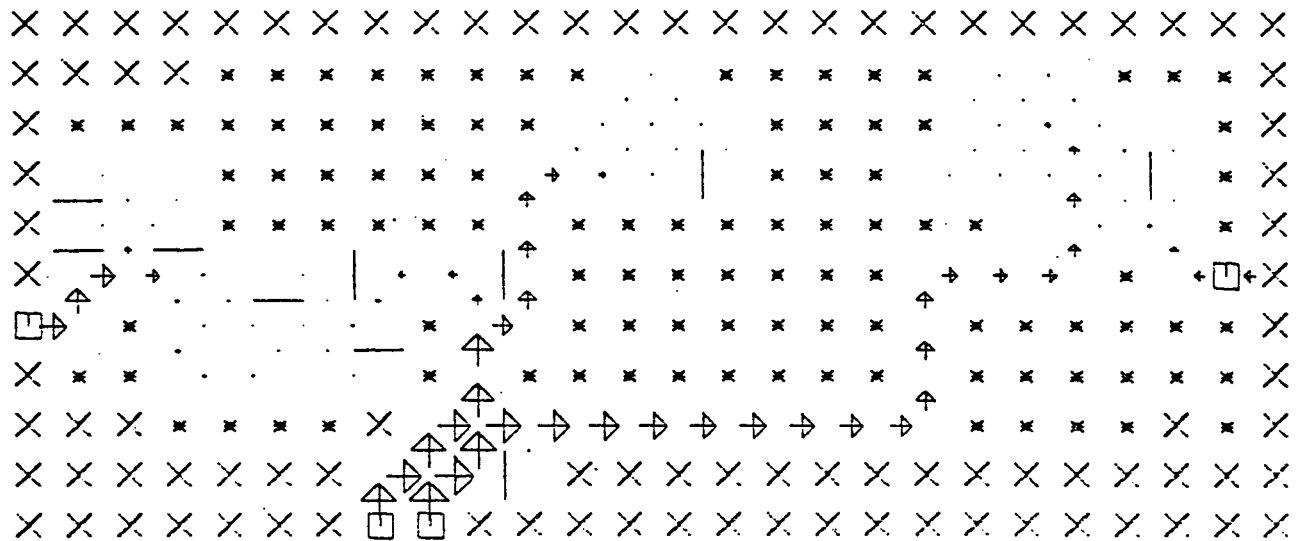
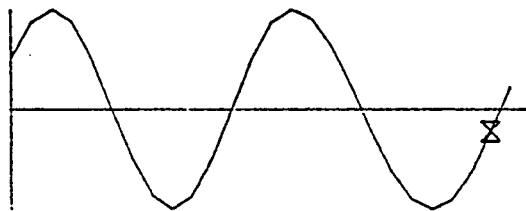
X - LAND CELL

\* - INUNDATION CELL

□ - FORCING CELL

- - NO FLOW BOUNDARY

SCALE - 100000. CFS / INCH



FLOW PATTERN FOR COARSE GRID

0100 HRS 27 AUG 1978

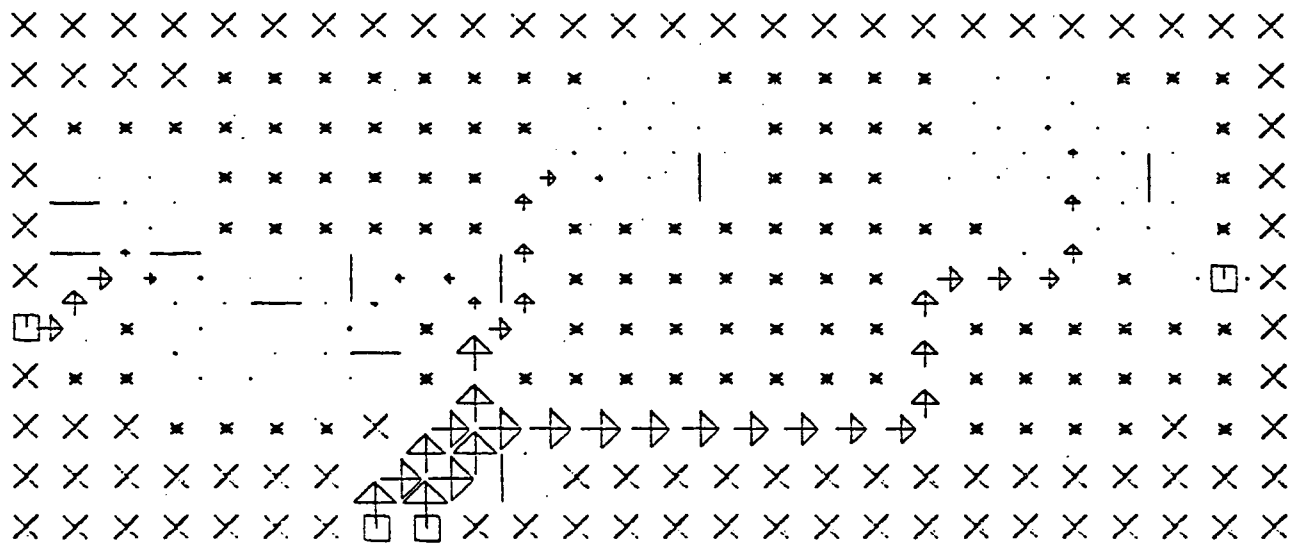
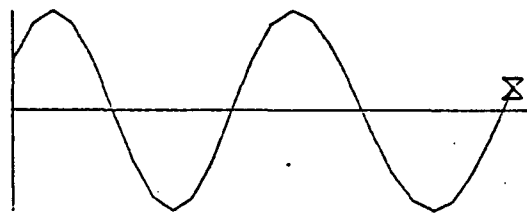
X - LAND CELL

\* - INUNDATION CELL

□ - FORCING CELL

- - NO FLOW BOUNDARY

SCALE - 100000. CFS / INCH





APPENDIX 4:

Flow Pattern: Jenkins Sound

FLOW PATTERN FOR JENKINS SOUND

2400 HRS 25 AUG 1978

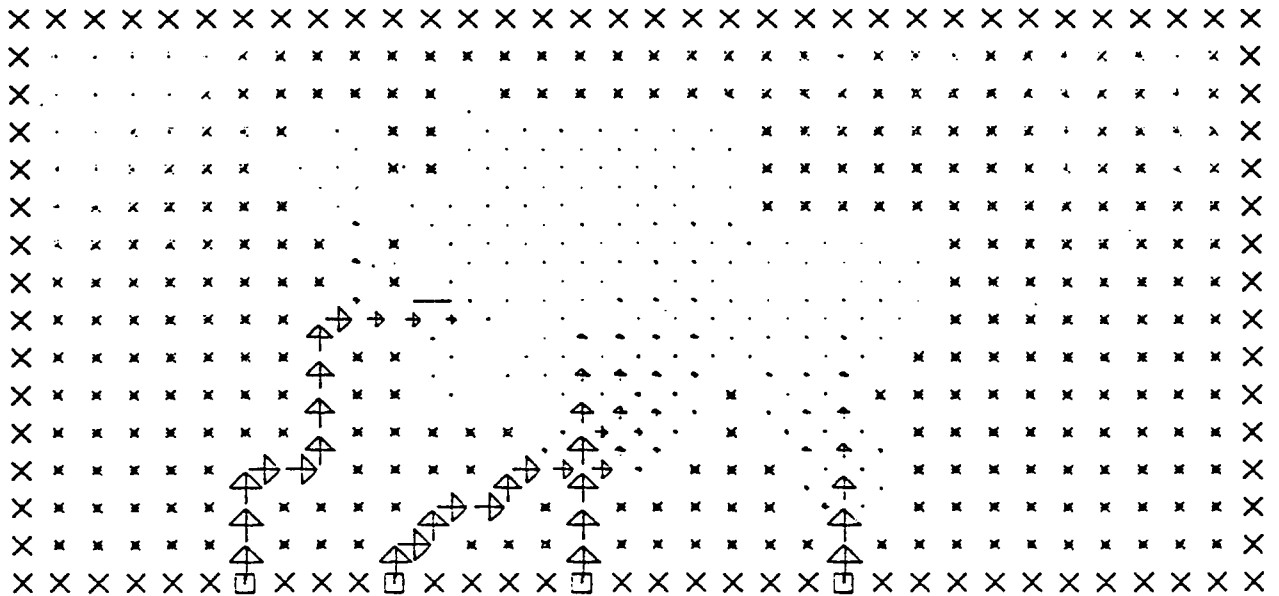
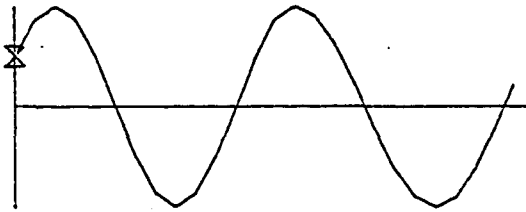
X - LAND CELL

\* - INUNDATION CELL

□ - FORCING CELL

- - NO FLOW BOUNDARY

SCALE - 10000. CFS / INCH

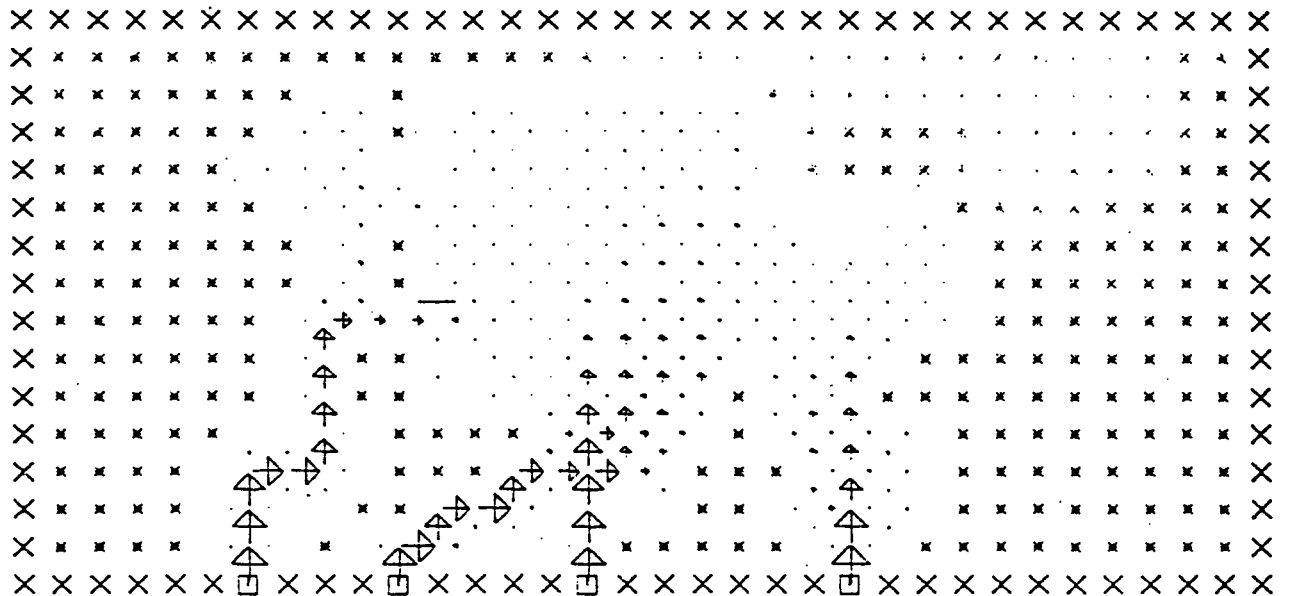
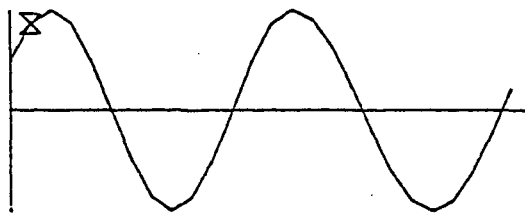


FLOW PATTERN FOR JENKINS SOUND

0100 HRS 26 AUG 1978

- X - LAND CELL
- \* - INUNDATION CELL
- - FORCING CELL
- - NO FLOW BOUNDARY

SCALE - 10000. CFS / INCH



FLOW PATTERN FOR JENKINS SOUND

0200 HRS 26 AUG 1978

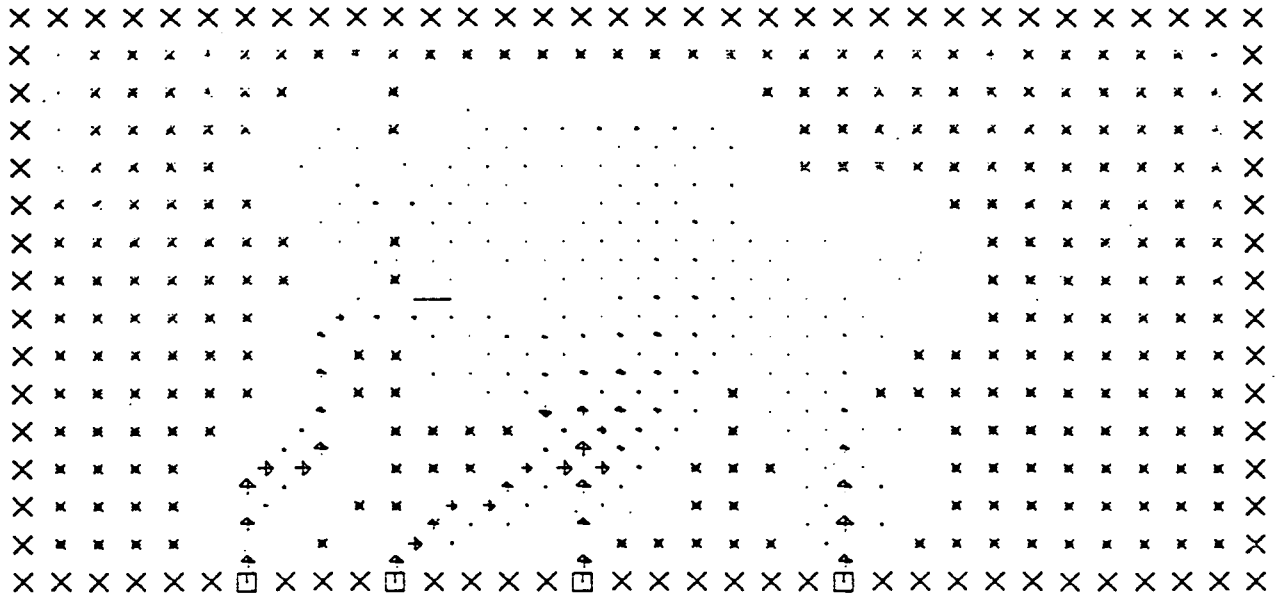
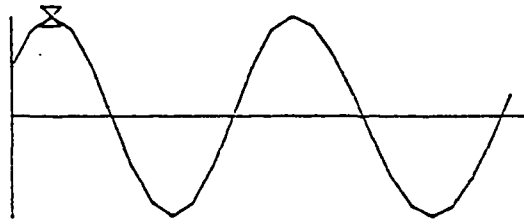
X - LAND CELL

\* - INUNDATION CELL

□ - FORCING CELL

- - NO FLOW BOUNDARY

SCALE - 10000. CFS / INCH



FLOW PATTERN FOR JENKINS SOUND

0300 HRS 26 AUG 1978

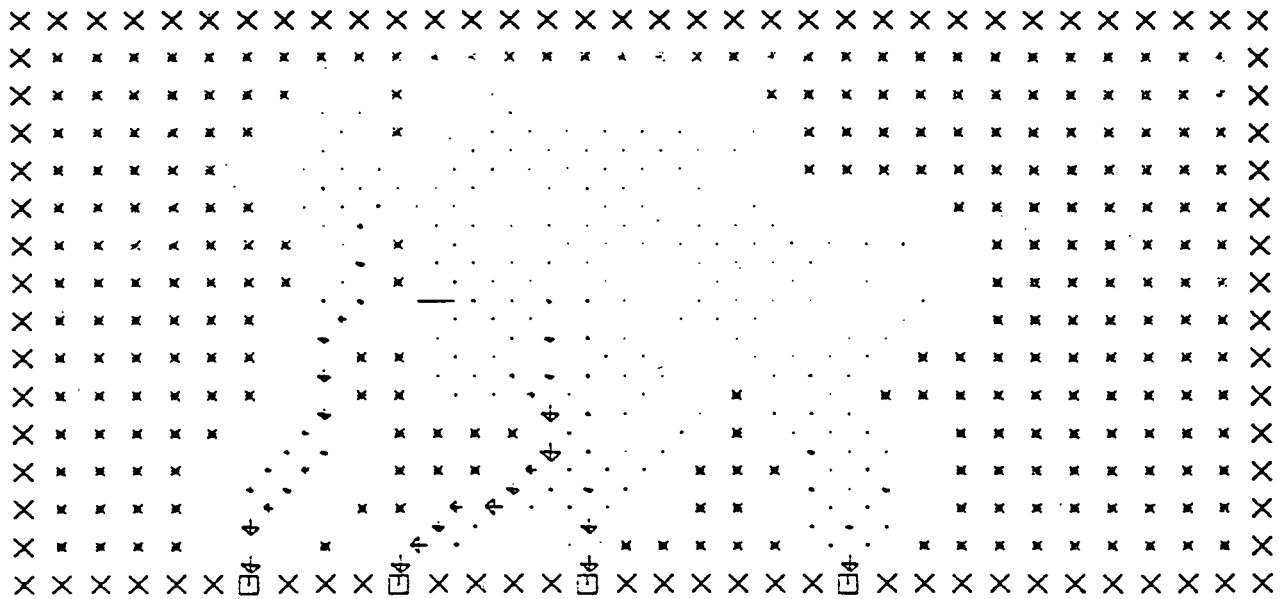
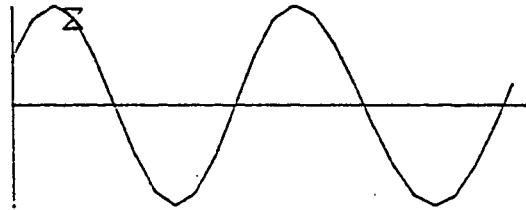
X - LAND CELL

\* - INUNDATION CELL

□ - FORCING CELL

- - NO FLOW BOUNDARY

SCALE - 10000. CFS / INCH



FLOW PATTERN FOR JENKINS SOUND

0400 HRS 26 AUG 1978

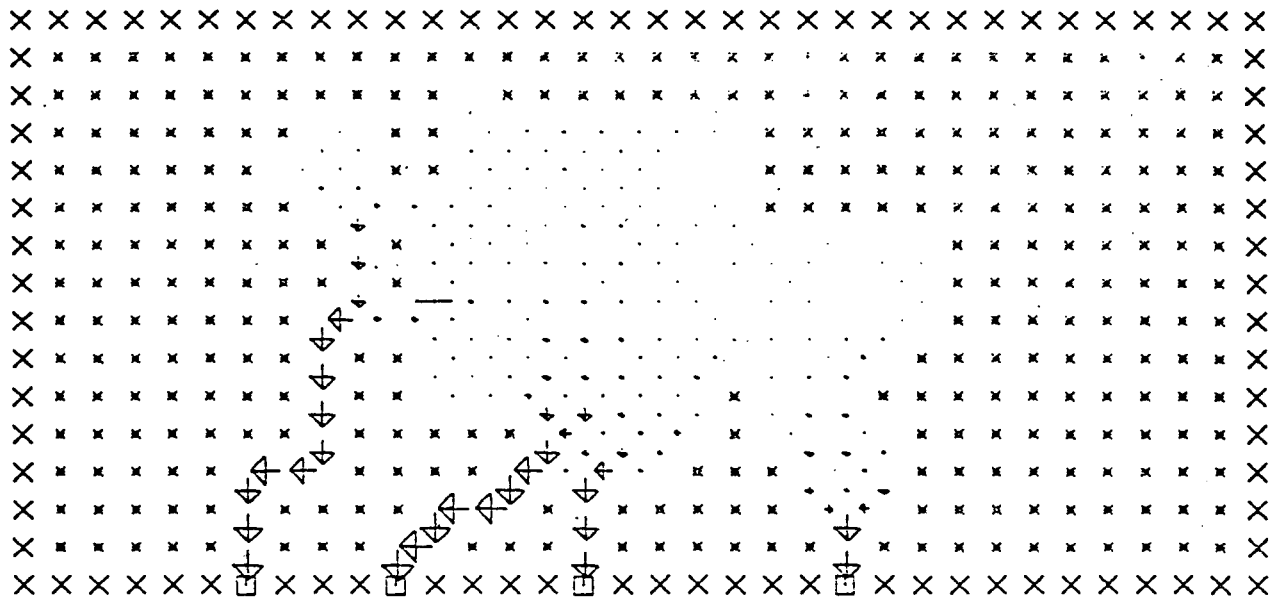
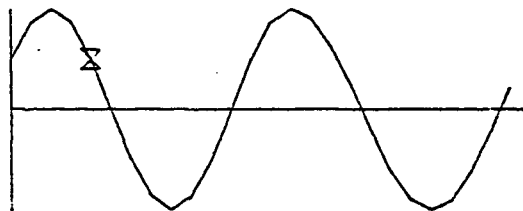
X - LAND CELL

\* - INUNDATION CELL

□ - FORCING CELL

- - NO FLOW BOUNDARY

SCALE - 10000. CFS / INCH



FLOW PATTERN FOR JENKINS SOUND

0500 HRS 26 AUG 1978

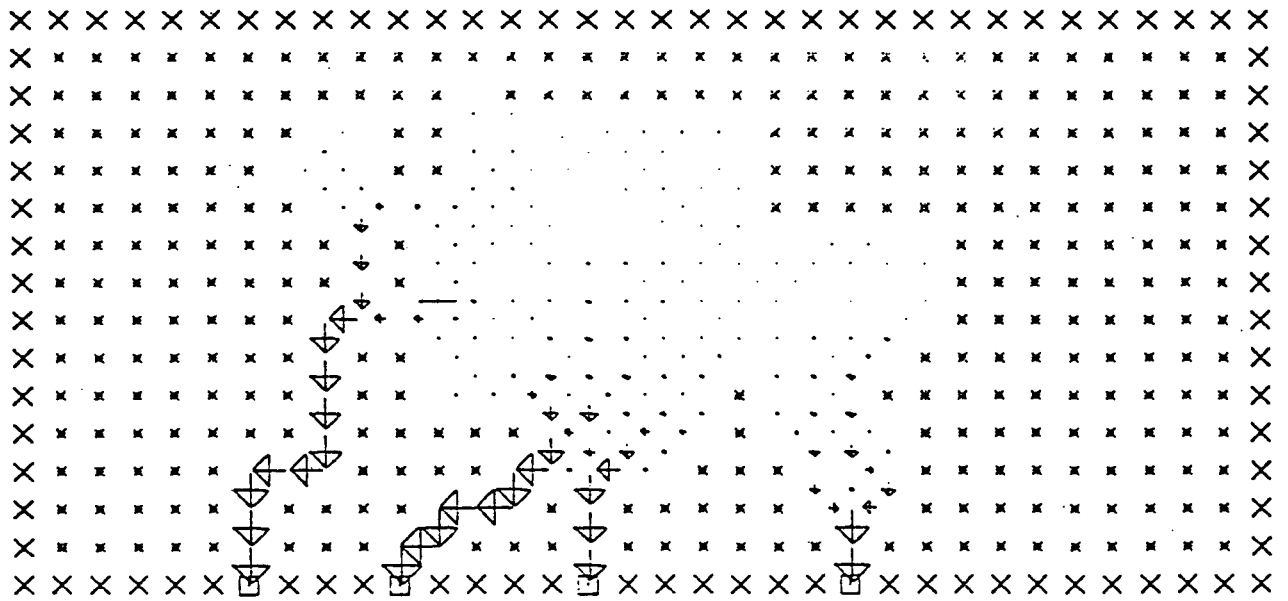
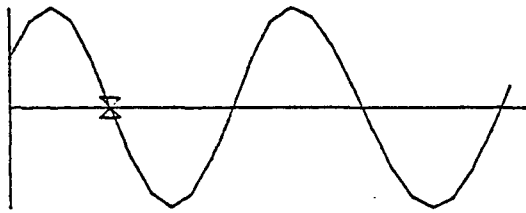
X - LAND CELL

\* - INUNDATION CELL

□ - FORCING CELL

- - NO FLOW BOUNDARY

SCALE - 10000. CFS / INCH.



FLOW PATTERN FOR JENKINS SOUND

0600 HRS 26 AUG 1978

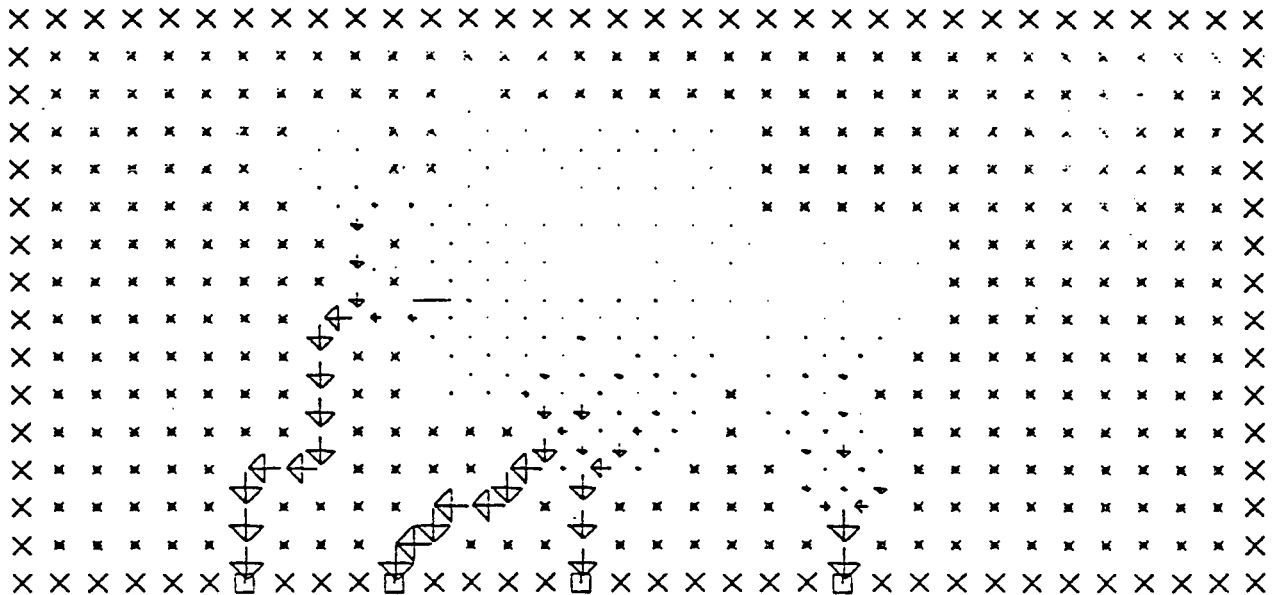
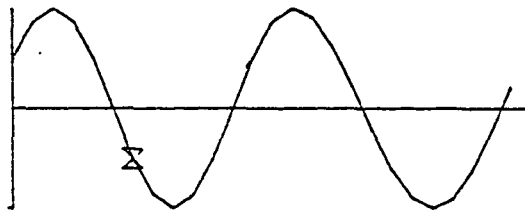
X - LAND CELL

\* - INUNDATION CELL

□ - FORCING CELL

- - NO FLOW BOUNDARY

SCALE - 10000. CFS / INCH





FLOW PATTERN FOR JENKINS SOUND

0700 HRS 26 AUG 1978

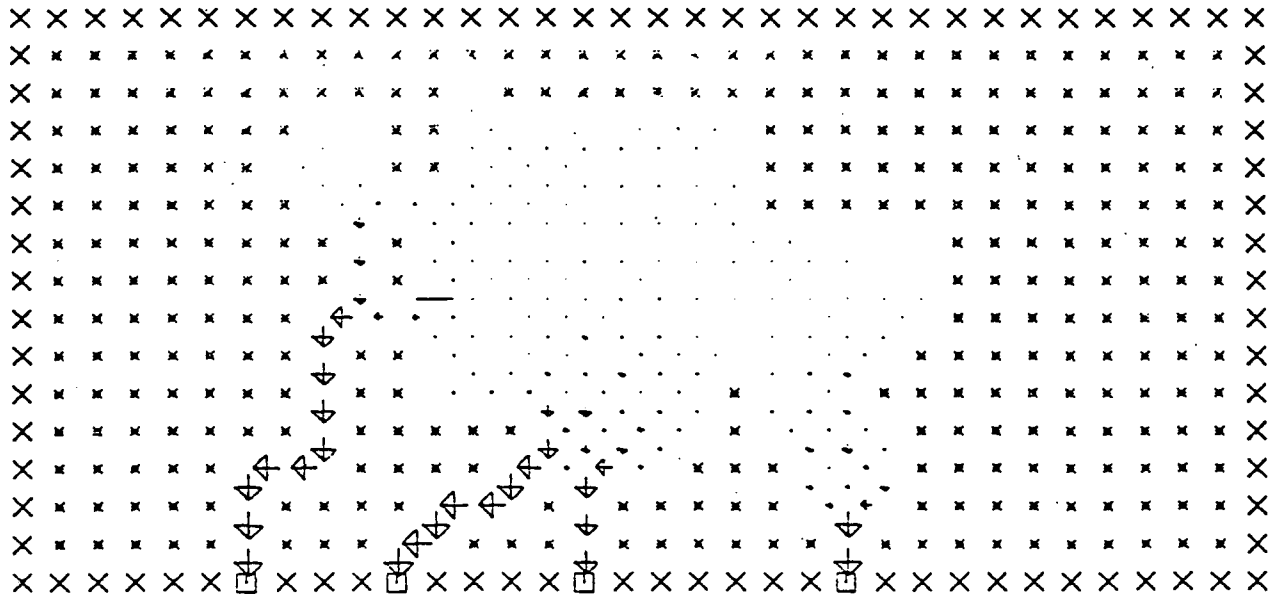
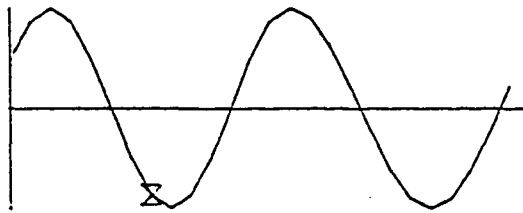
X - LAND CELL

\* - INUNDATION CELL

□ - FORCING CELL

- - NO FLOW BOUNDARY

SCALE - 10000. CFS / INCH



FLOW PATTERN FOR JENKINS SOUND

0800 HRS 26 AUG 1978

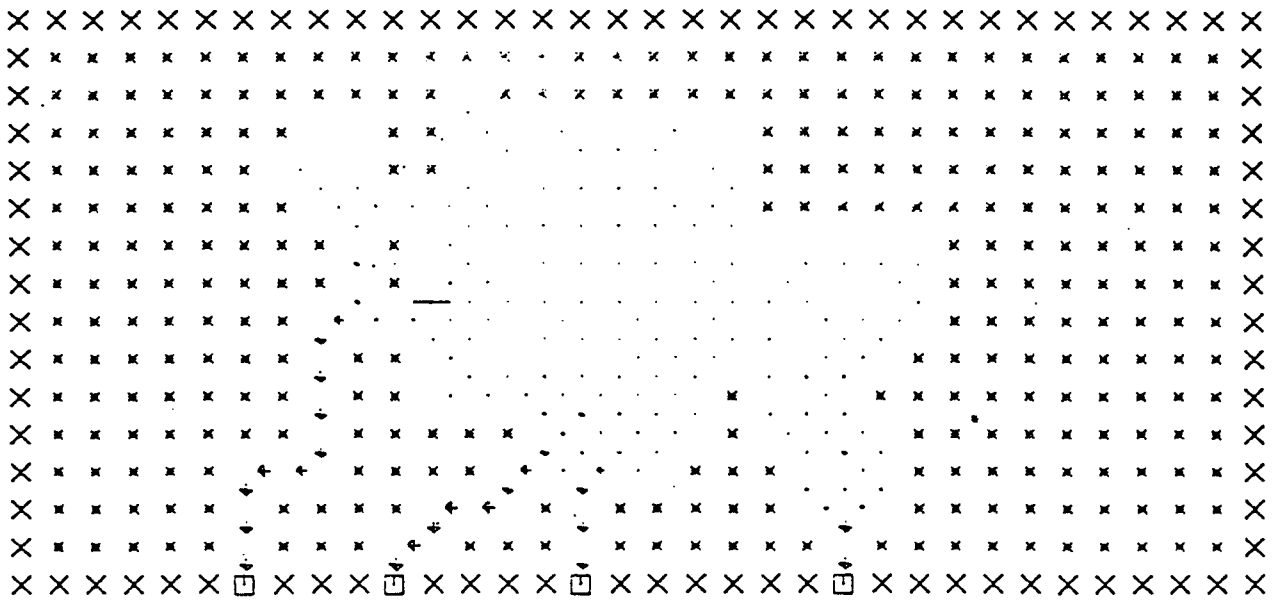
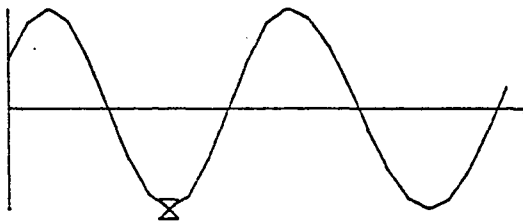
X - LAND CELL

\* - INUNDATION CELL

□ - FORCING CELL

- - NO FLOW BOUNDARY

SCALE - 10000. CFS / INCH



FLOW PATTERN FOR JENKINS SOUND

0900 HRS 26 AUG 1978

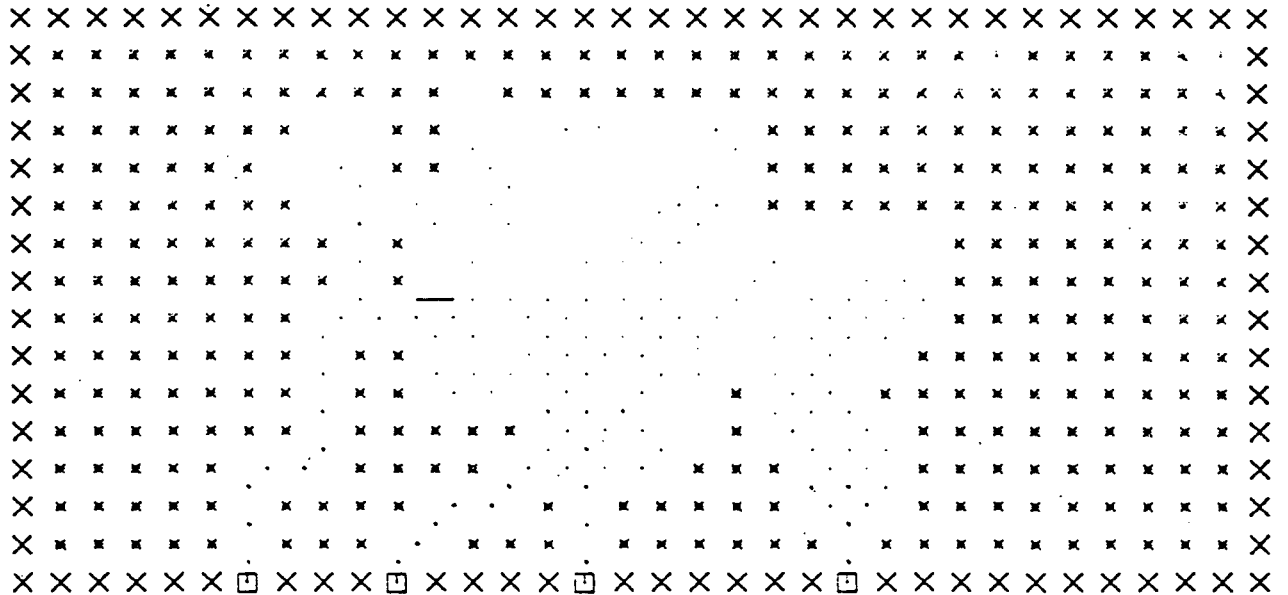
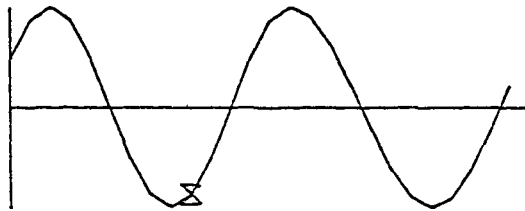
X - LAND CELL

\* - INUNDATION CELL

□ - FORCING CELL

- - NO FLOW BOUNDARY

SCALE - 10000. CFS / INCH



FLOW PATTERN FOR JENKINS SOUND

1000 HRS 26 AUG 1978

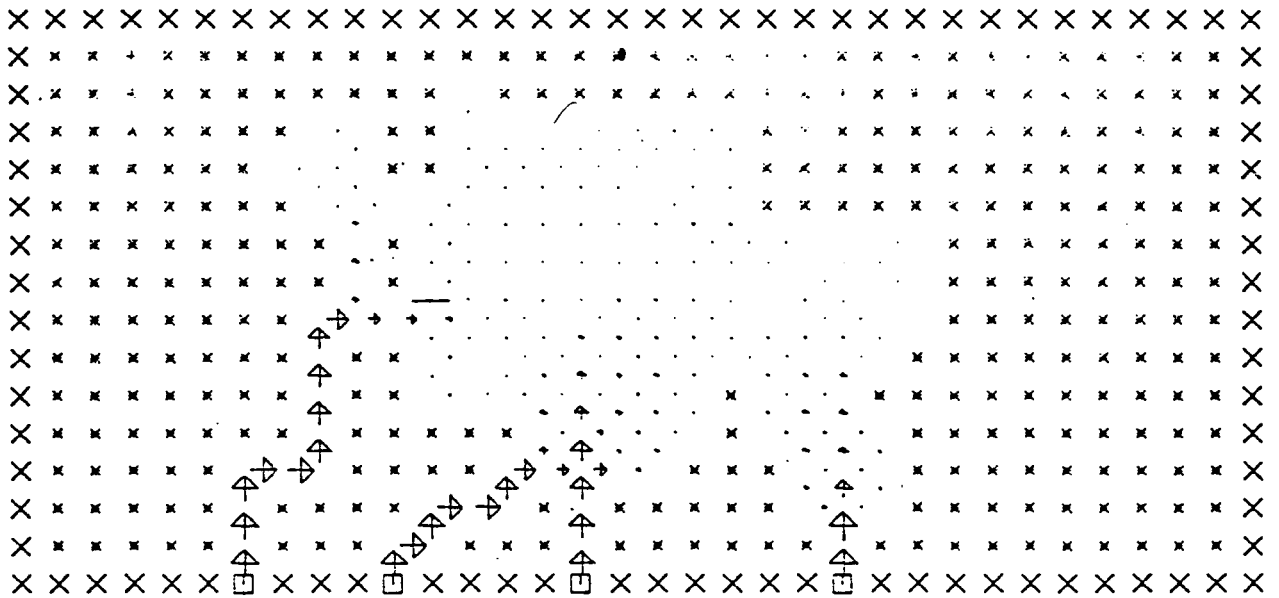
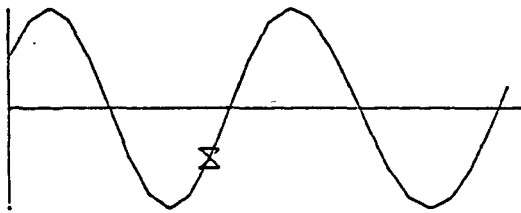
X - LAND CELL

\* - INUNDATION CELL

□ - FORCING CELL

- - NO FLOW BOUNDARY

SCALE - 10000. CFS / INCH



FLOW PATTERN FOR JENKINS SOUND

1100 HRS 26 AUG 1978

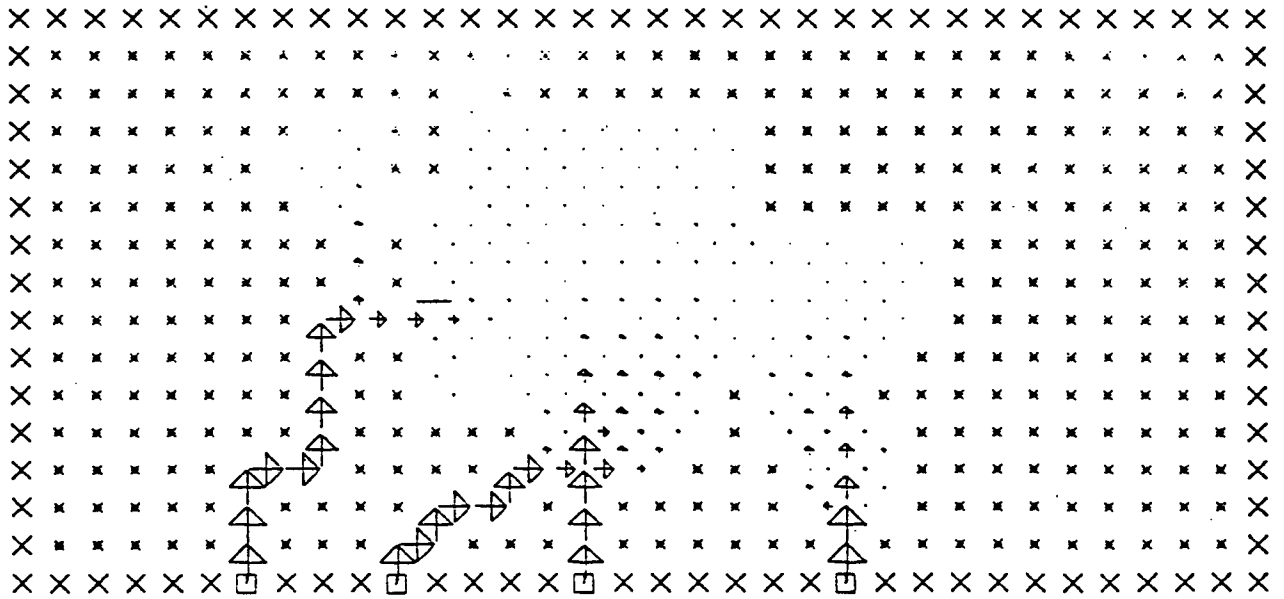
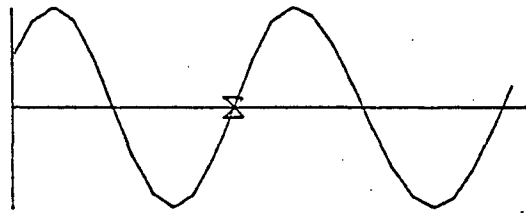
X - LAND CELL

\* - INUNDATION CELL

□ - FORCING CELL

- - NO FLOW BOUNDARY

SCALE - 10000. CFS / INCH



FLOW PATTERN FOR JENKINS SOUND

1200 HRS 26 AUG 1978

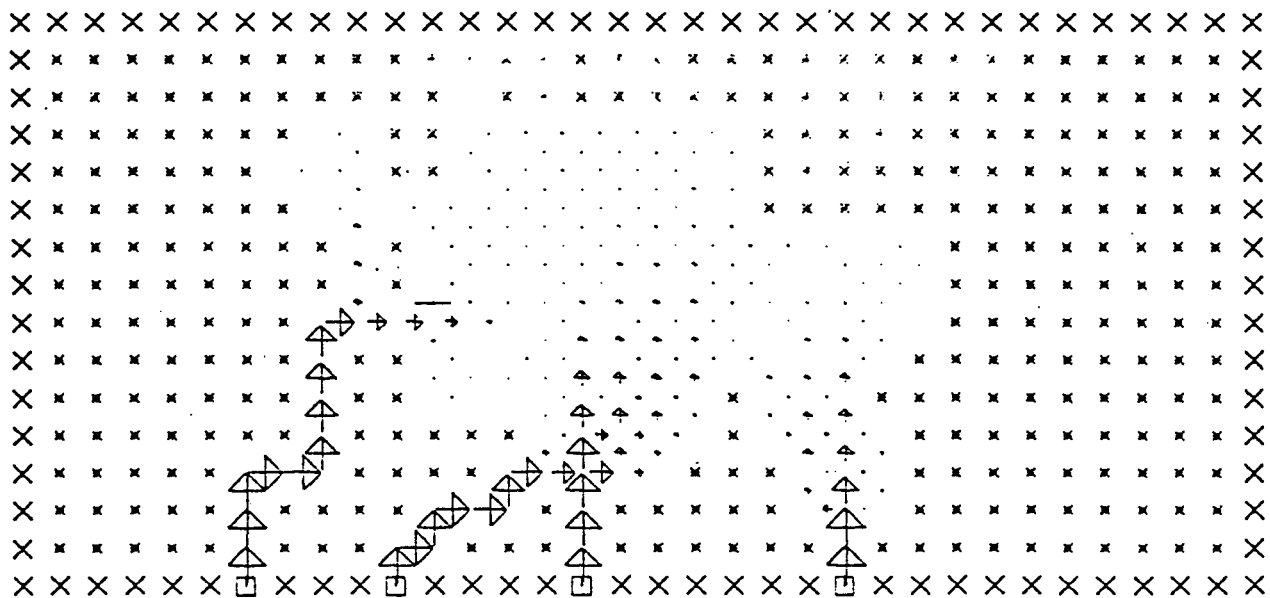
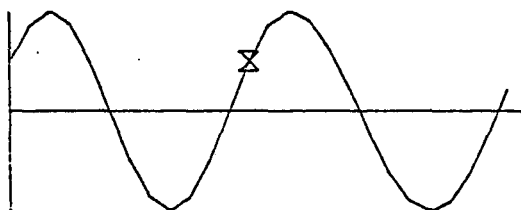
X - LAND CELL

\* - INUNDATION CELL

□ - FORCING CELL

- - NO FLOW BOUNDARY

SCALE - 10000. CFS / INCH



FLOW PATTERN FOR JENKINS SOUND

1300 HRS 26 AUG 1978

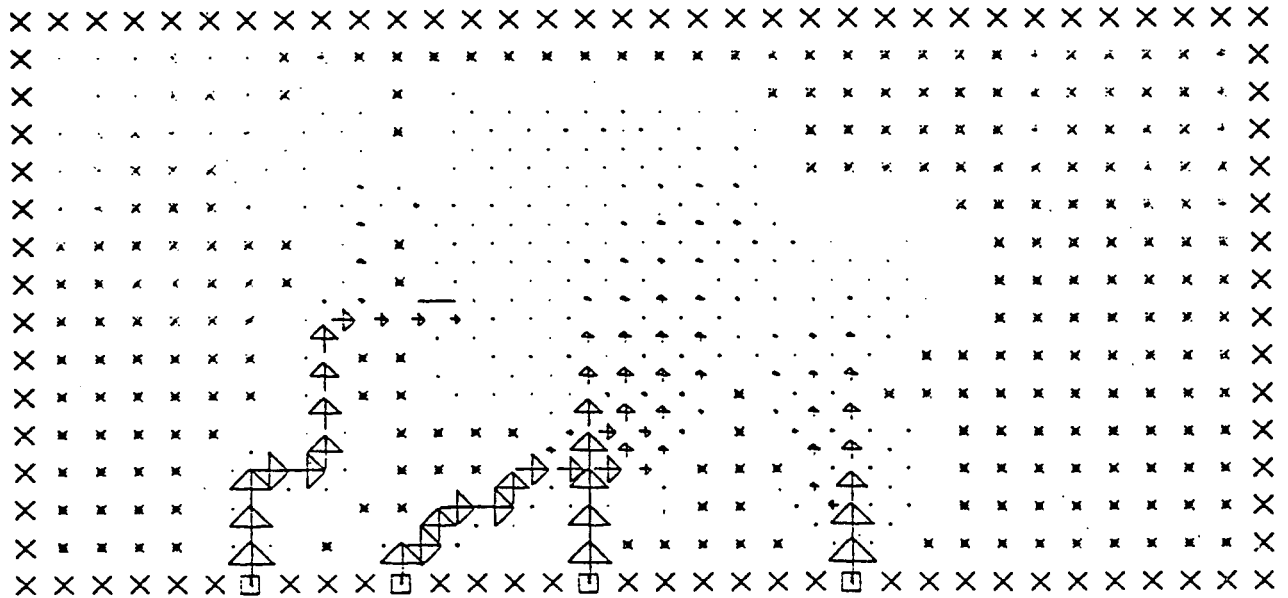
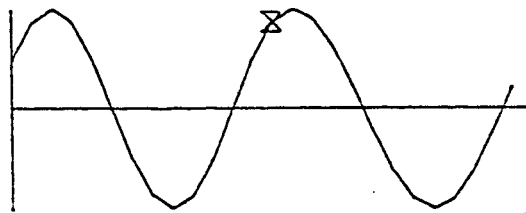
X - LAND CELL

\* - INUNDATION CELL

□ - FORCING CELL

- - NO FLOW BOUNDARY

SCALE - 10000. CFS / INCH



FLOW PATTERN FOR JENKINS SOUND

1400 HRS 26 AUG 1978

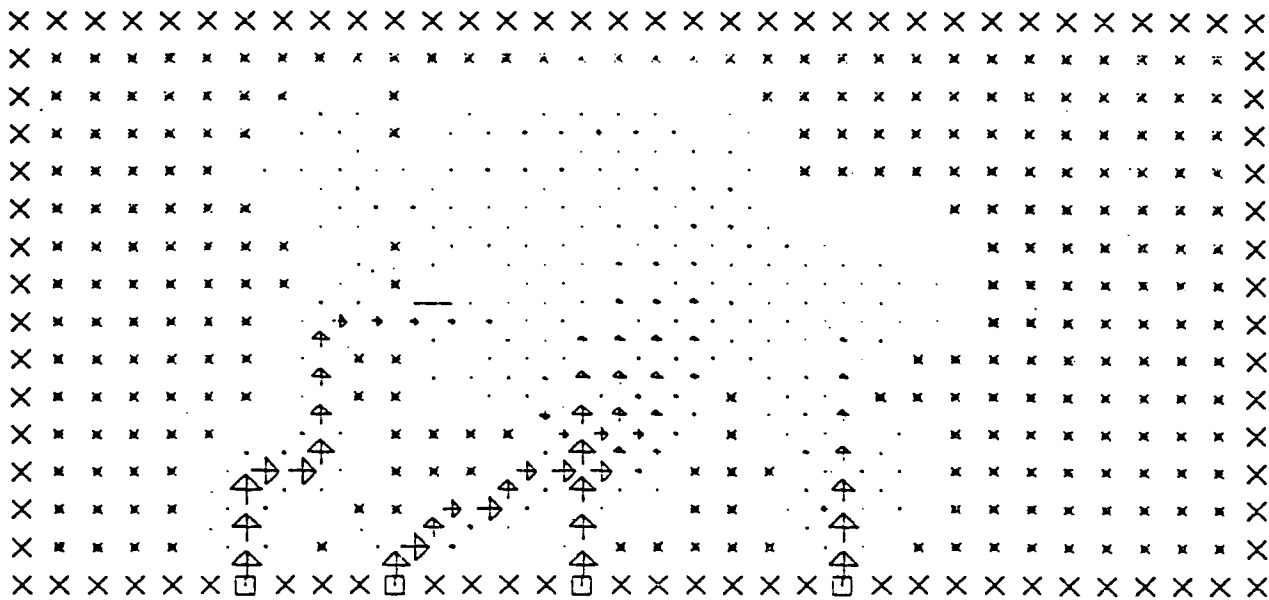
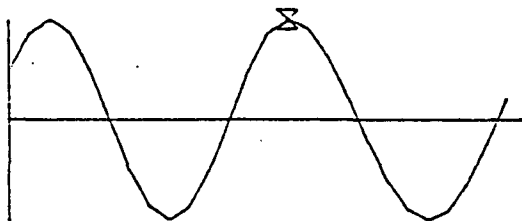
X - LAND CELL

\* - INUNDATION CELL

□ - FORCING CELL

- - NO FLOW BOUNDARY

SCALE - 10000. CFS / INCH



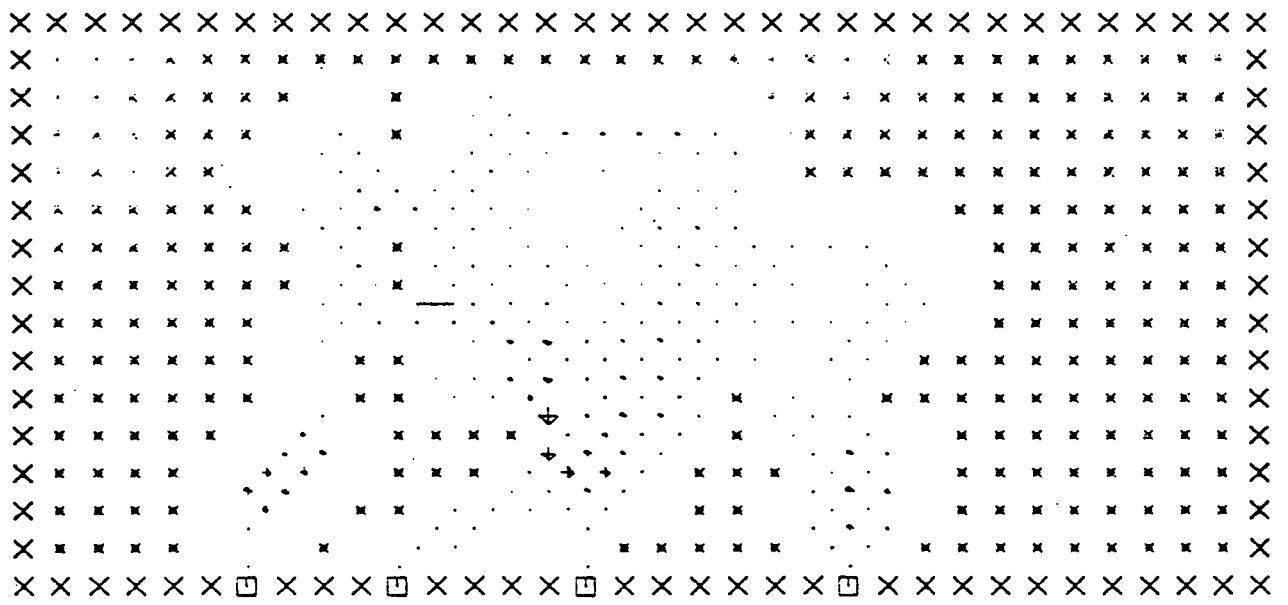
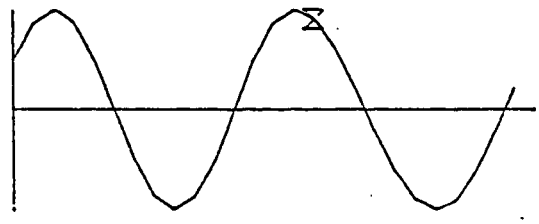


FLOW PATTERN FOR JENKINS SOUND

1500 HRS 26 AUG 1978

- X - LAND CELL
- \* - INUNDATION CELL
- - FORCING CELL
- - NO FLOW BOUNDARY

SCALE - 10000. CFS / INCH



FLOW PATTERN FOR JENKINS SOUND

1600 HRS 26 AUG 1978

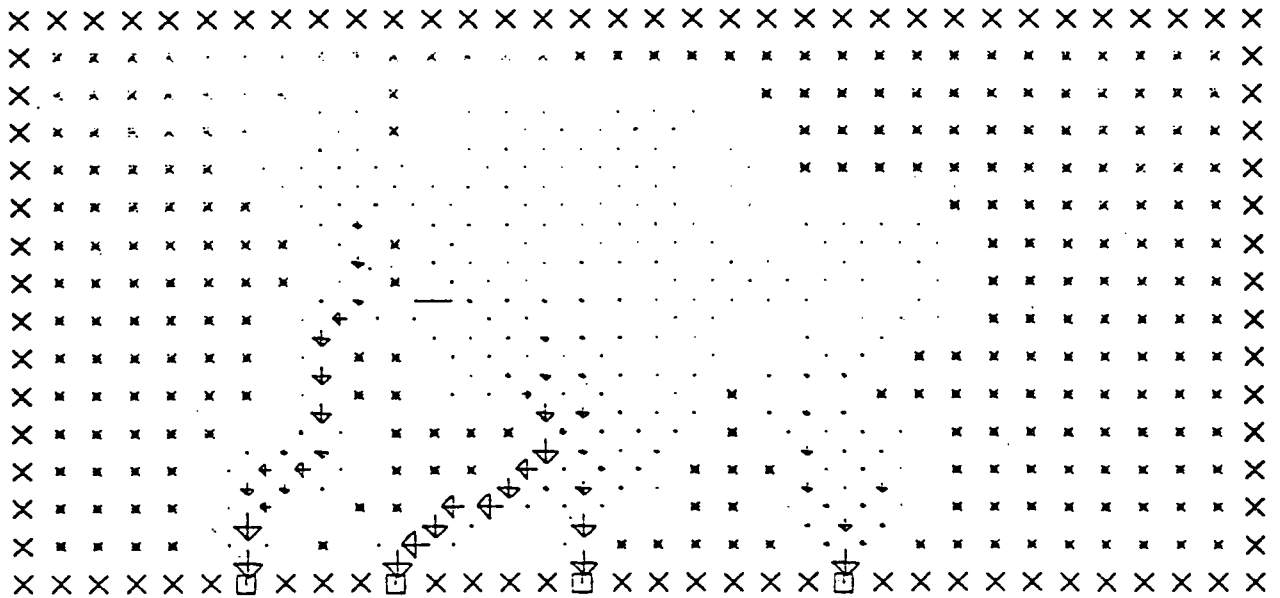
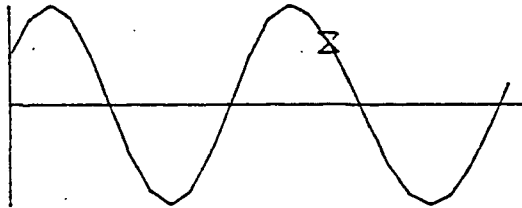
X - LAND CELL

\* - INUNDATION CELL

□ - FORCING CELL

- - NO FLOW BOUNDARY

SCALE - 10000. CFS / INCH

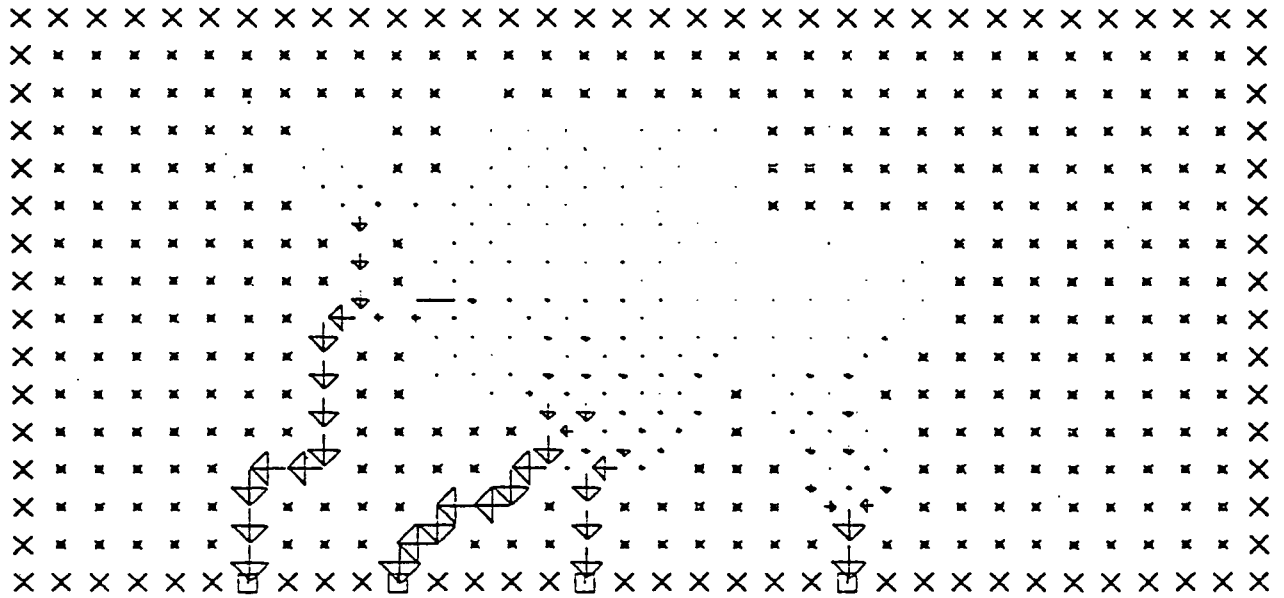
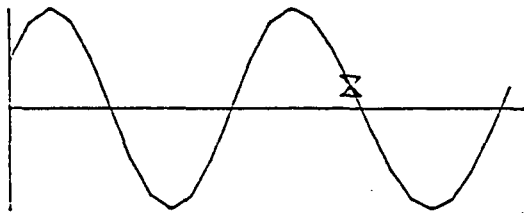


FLOW PATTERN FOR JENKINS SOUND

1700 HRS 26 AUG 1978

- X - LAND CELL
- \* - INUNDATION CELL
- - FORCING CELL
- - NO FLOW BOUNDARY

SCALE - 10000. CFS / INCH



FLOW PATTERN FOR JENKINS SOUND

1800 HRS 26 AUG 1978

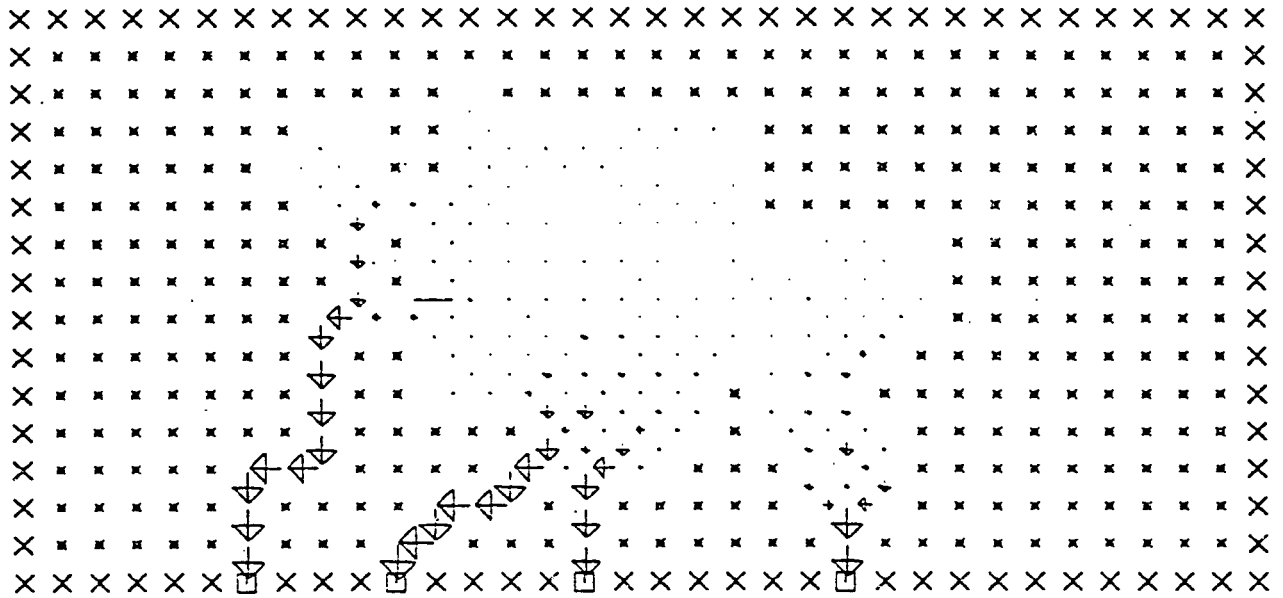
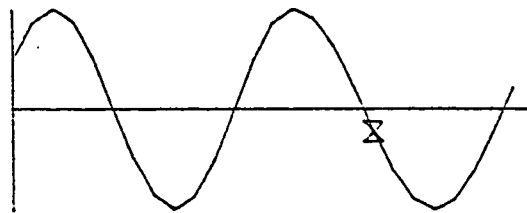
X - LAND CELL

\* - INUNDATION CELL

□ - FORCING CELL

- - NO FLOW BOUNDARY

SCALE - 10000. CFS / INCH



FLOW PATTERN FOR JENKINS SOUND

1900 HRS 26 AUG 1978

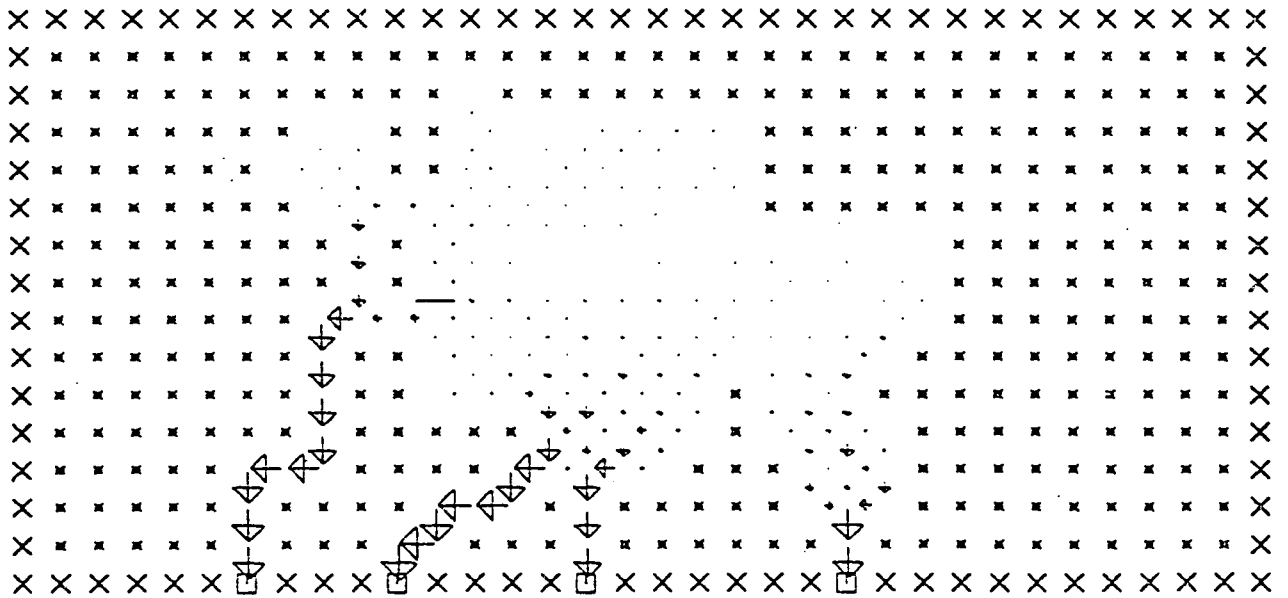
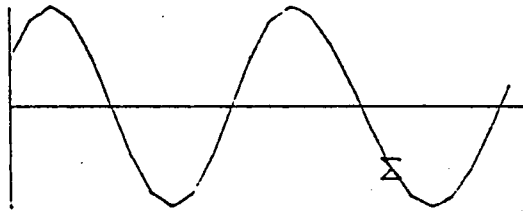
X - LAND CELL

\* - INUNDATION CELL

□ - FORCING CELL

- - NO FLOW BOUNDARY

SCALE - 10000. CFS / INCH



FLOW PATTERN FOR JENKINS SOUND

2000 HRS 26 AUG 1978

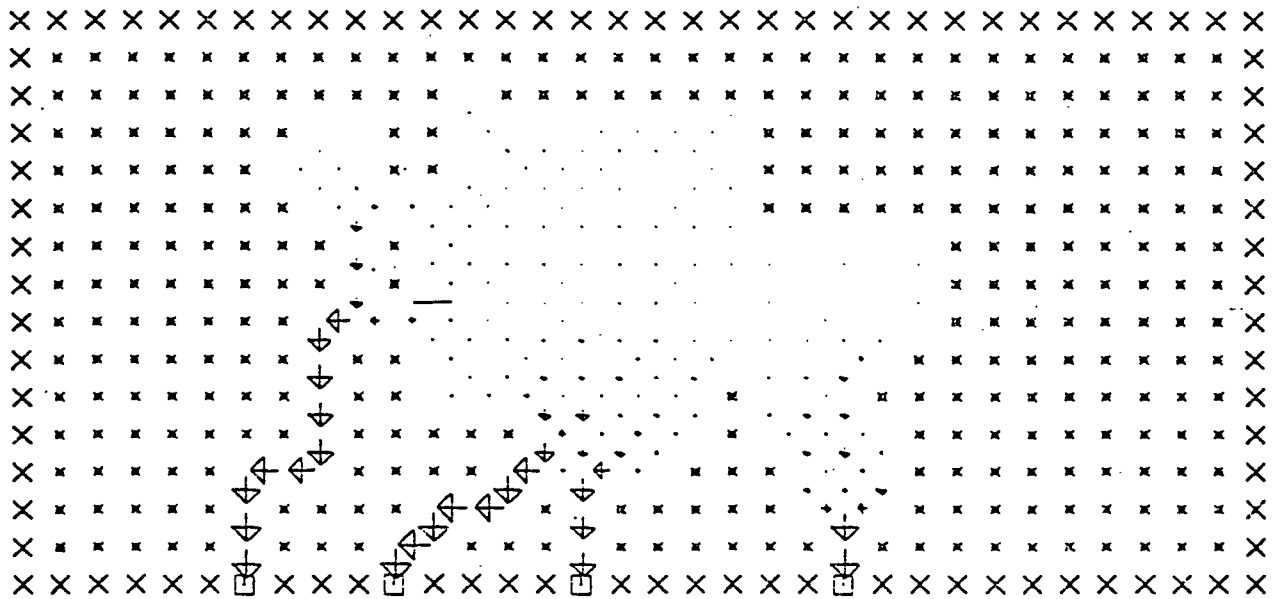
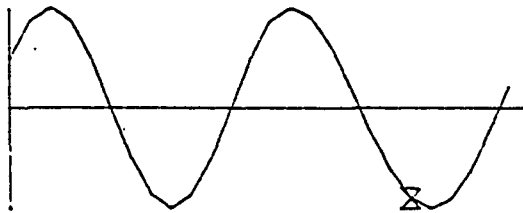
X - LAND CELL

\* - INUNDATION CELL

□ - FORCING CELL

- - NO FLOW BOUNDARY

SCALE - 10000. CFS / INCH



FLOW PATTERN FOR JENKINS SOUND

2100 HRS 26 AUG 1978

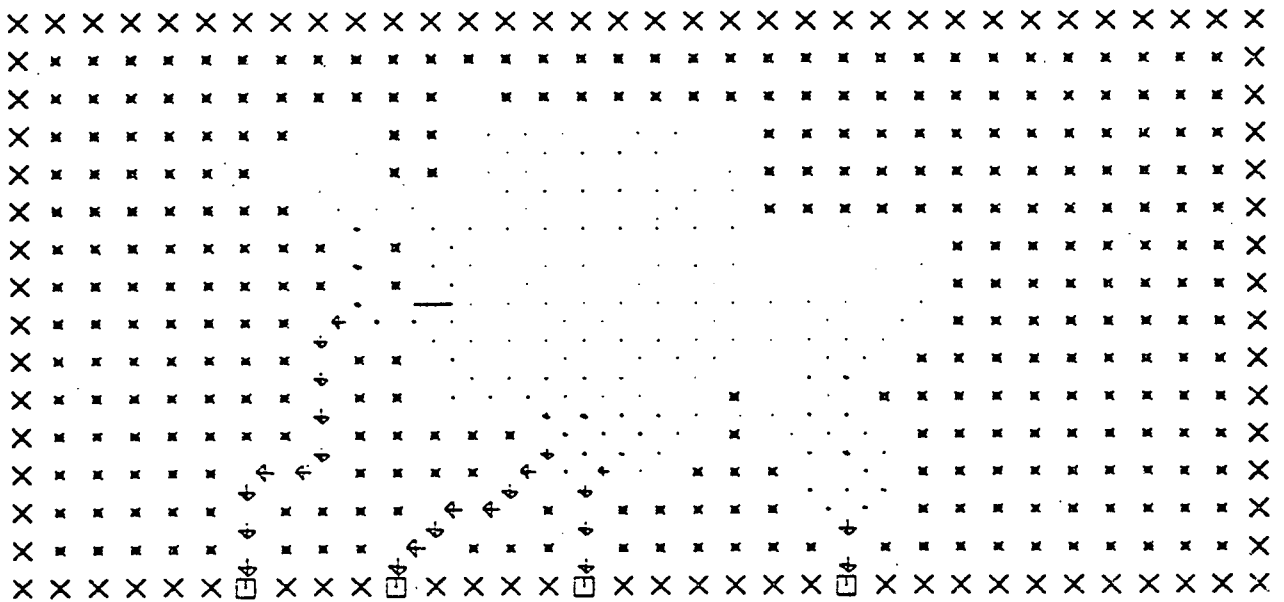
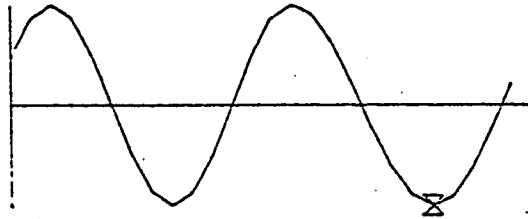
X - LAND CELL

\* - INUNDATION CELL

□ - FORCING CELL

- - NO FLOW BOUNDARY

SCALE - 10000. CFS / INCH.



FLOW PATTERN FOR JENKINS SOUND

2200 HRS 26 AUG 1978

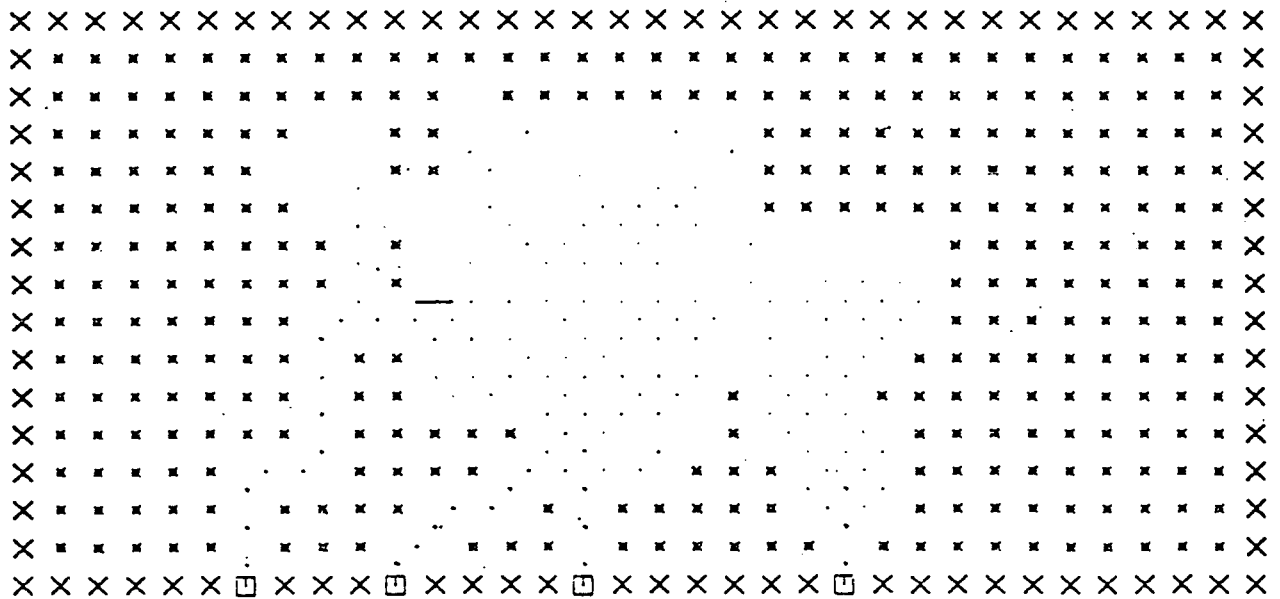
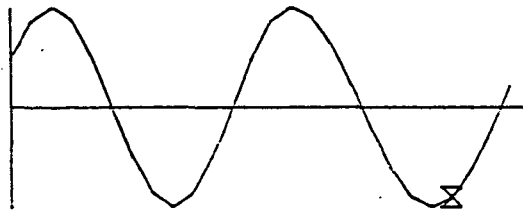
X - LAND CELL

\* - INUNDATION CELL

□ - FORCING CELL

- - NO FLOW BOUNDARY

SCALE - 10000. CFS / INCH





FLOW PATTERN FOR JENKINS SOUND

2300 HRS 26 AUG 1978

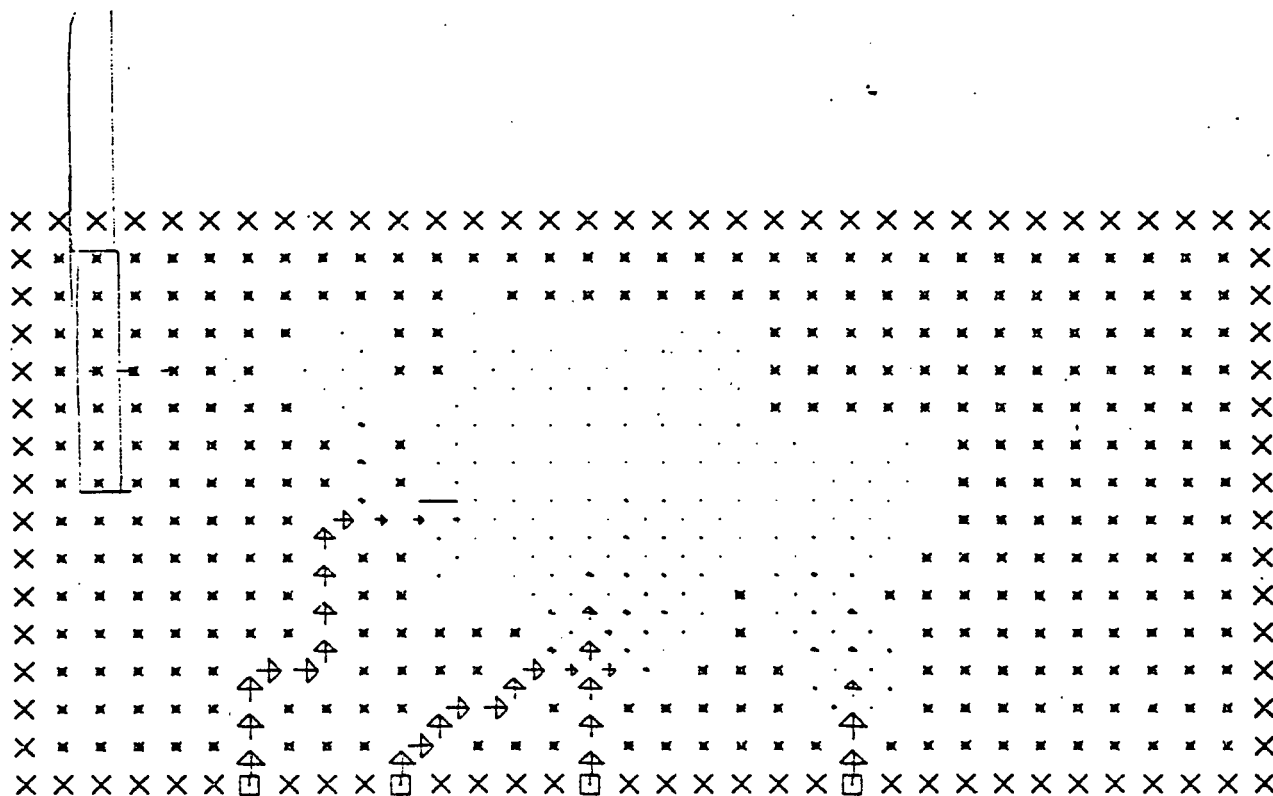
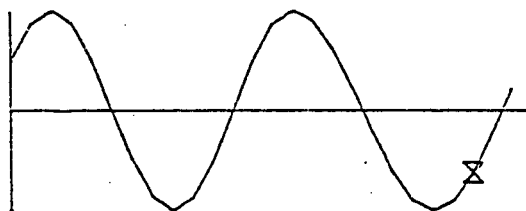
X - LAND CELL

\* - INUNDATION CELL

□ - FORCING CELL

- - NO FLOW BOUNDARY

SCALE - 10000. CFS / INCH



FLOW PATTERN FOR JENKINS SOUND

2400 HRS 26 AUG 1978

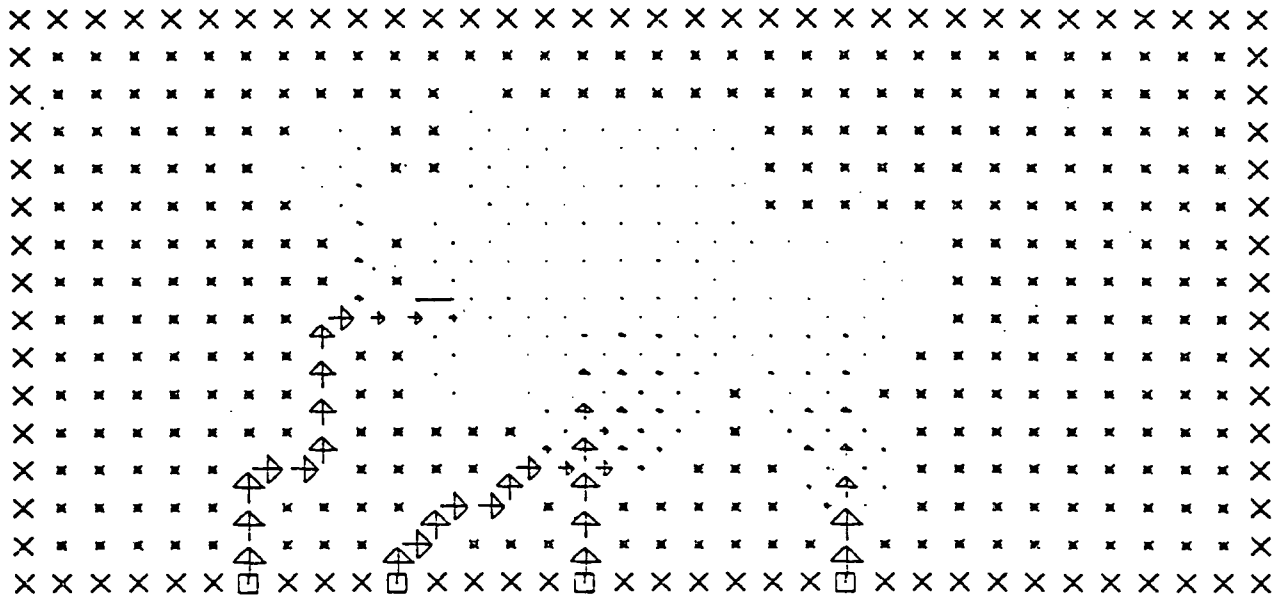
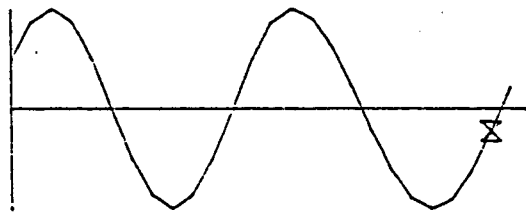
X - LAND CELL

\* - INUNDATION CELL

□ - FORCING CELL

- - NO FLOW BOUNDARY

SCALE - 10000. CFS / INCH



FLOW PATTERN FOR JENKINS SOUND

0100 HRS 27 AUG 1978

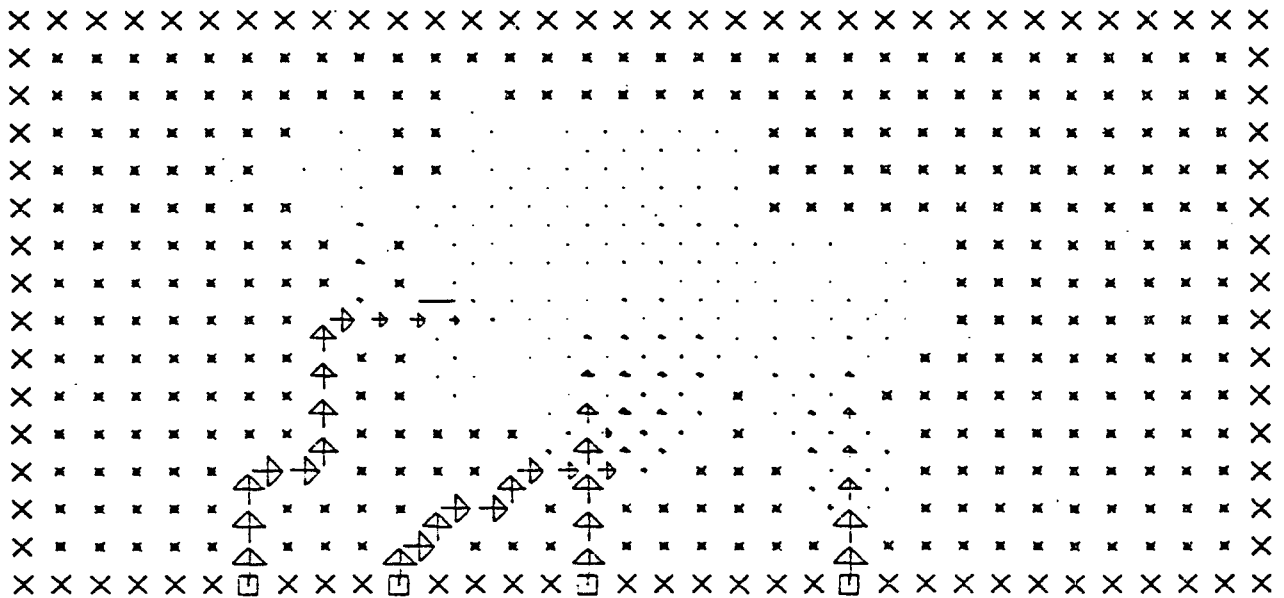
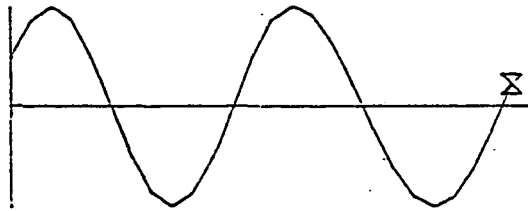
X - LAND CELL

\* - INUNDATION CELL

□ - FORCING CELL

- - NO FLOW BOUNDARY

SCALE - 10000. CFS / INCH



APPENDIX 5:

Flow Pattern: Great Sound

FLOW PATTERN FOR GREAT SOUND

2400 HRS 25 AUG 1978

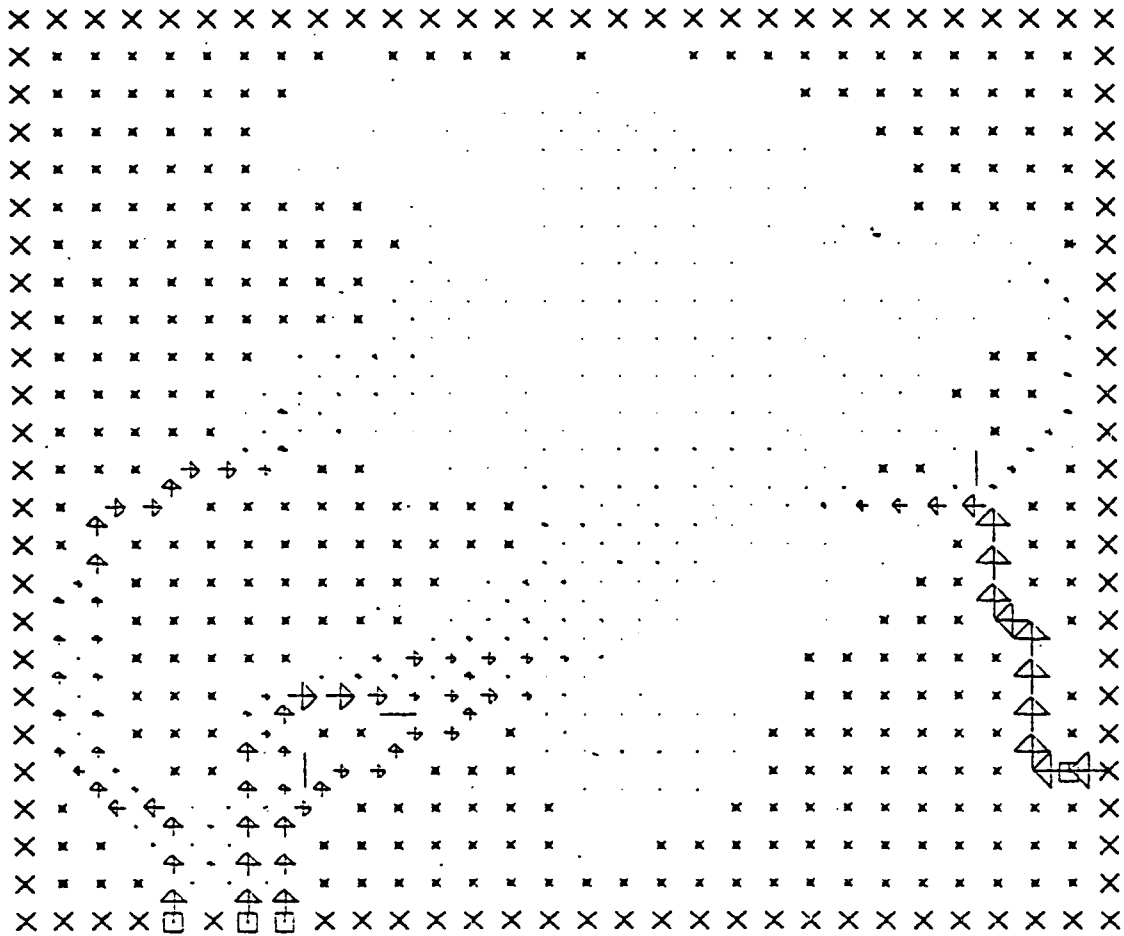
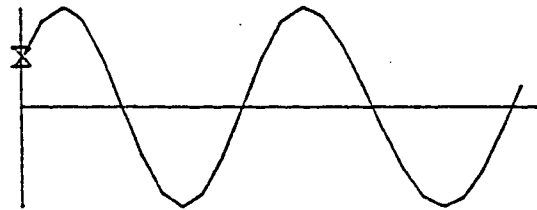
X - LAND CELL

\* - INUNDATION CELL

□ - FORCING CELL

- - NO FLOW BOUNDARY

SCALE - 25000. CFS / INCH

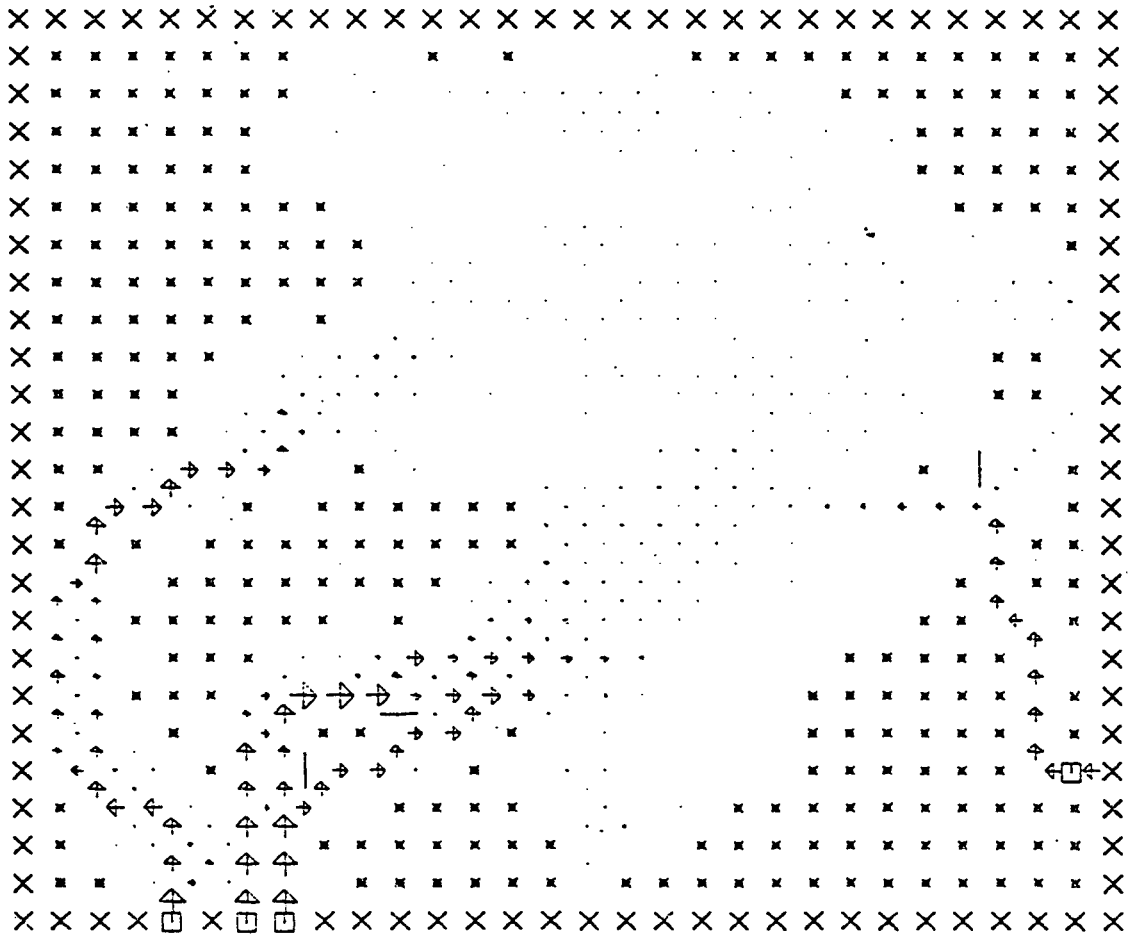
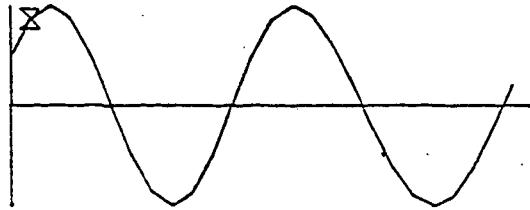


FLOW PATTERN FOR GREAT SOUND

0100 HRS 26 AUG 1978

- X - LAND CELL
- \* - INUNDATION CELL
- - FORCING CELL
- - NO FLOW BOUNDARY

SCALE - 25000. CFS / INCH



FLOW PATTERN FOR GREAT SOUND

0200 HRS 26 AUG 1978

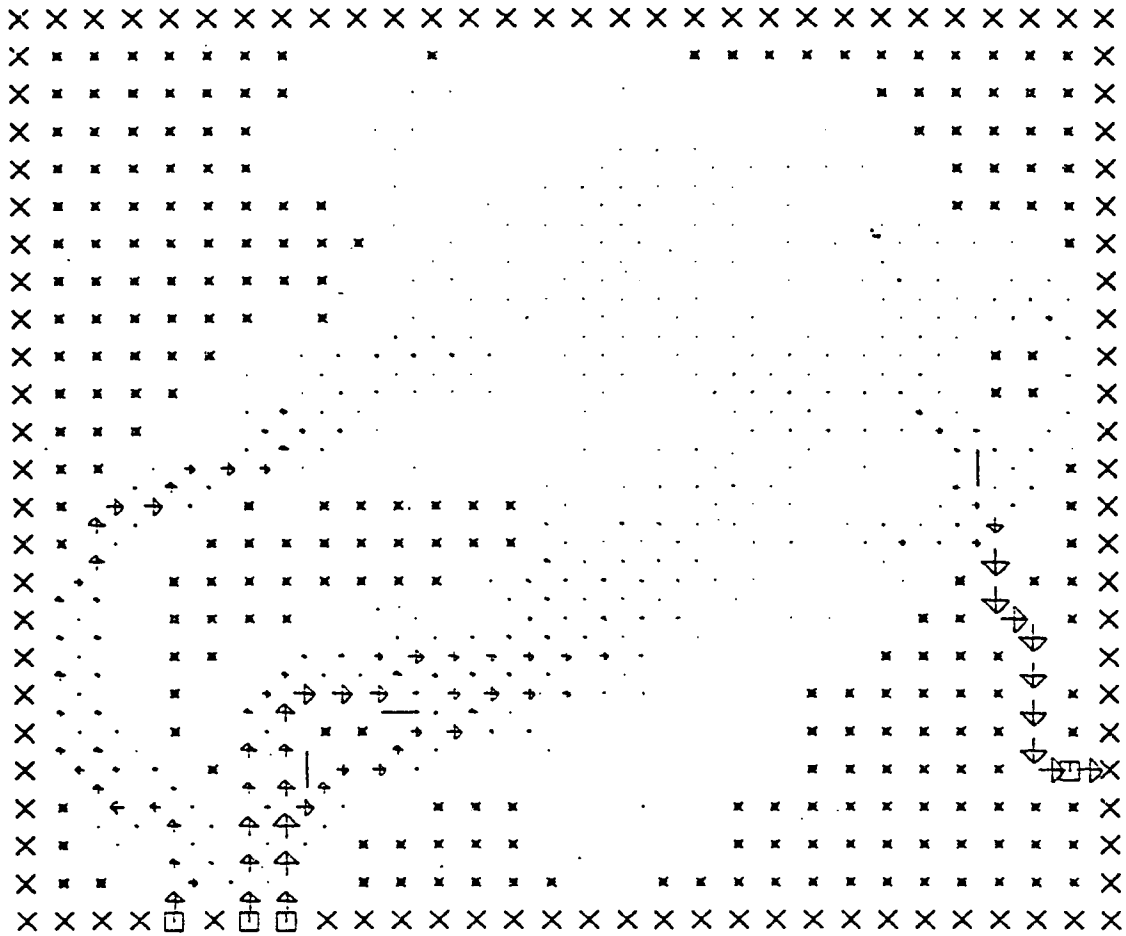
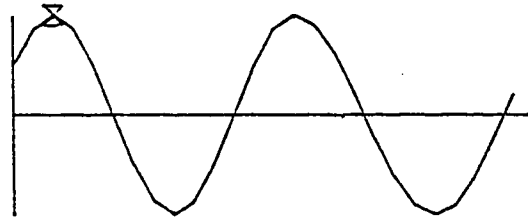
X - LAND CELL

\* - INUNDATION CELL

□ - FORCING CELL

- - NO FLOW BOUNDARY

SCALE - 25000. CFS / INCH

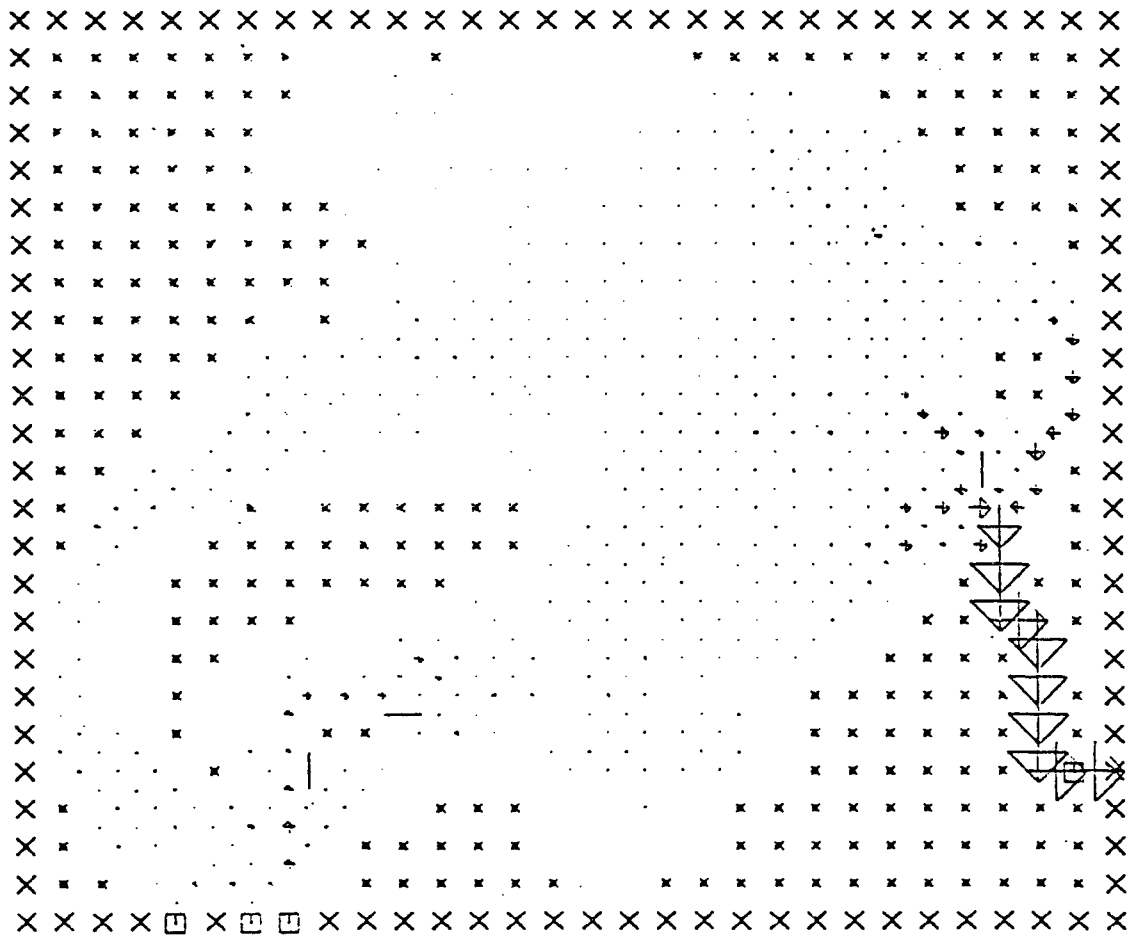
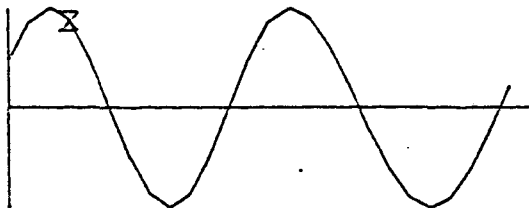


FLOW PATTERN FOR GREAT SOUND

0300 HRS 26 AUG 1978

- X - LAND CELL
- \* - INUNDATION CELL
- - FORCING CELL
- - NO FLOW BOUNDARY

SCALE - 25000. CFS / INCH





FLOW PATTERN FOR GREAT SOUND

0400 HRS 26 AUG 1978

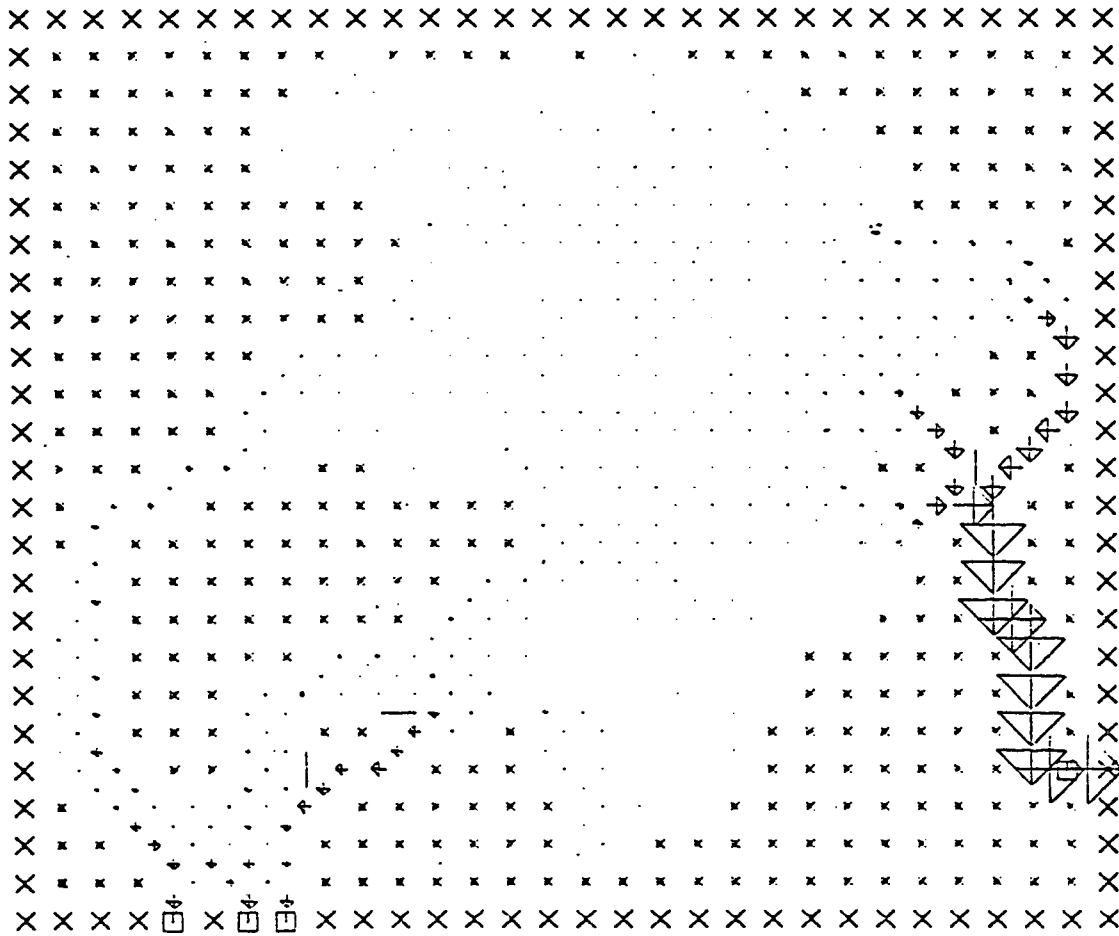
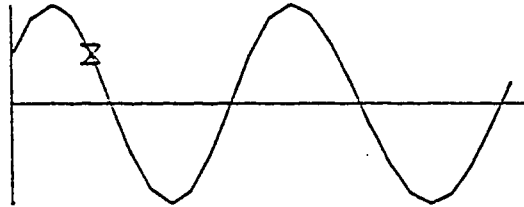
X - LAND CELL

\* - INUNDATION CELL

□ - FORCING CELL

- - NO FLOW BOUNDARY

SCALE - 25000. CFS / INCH

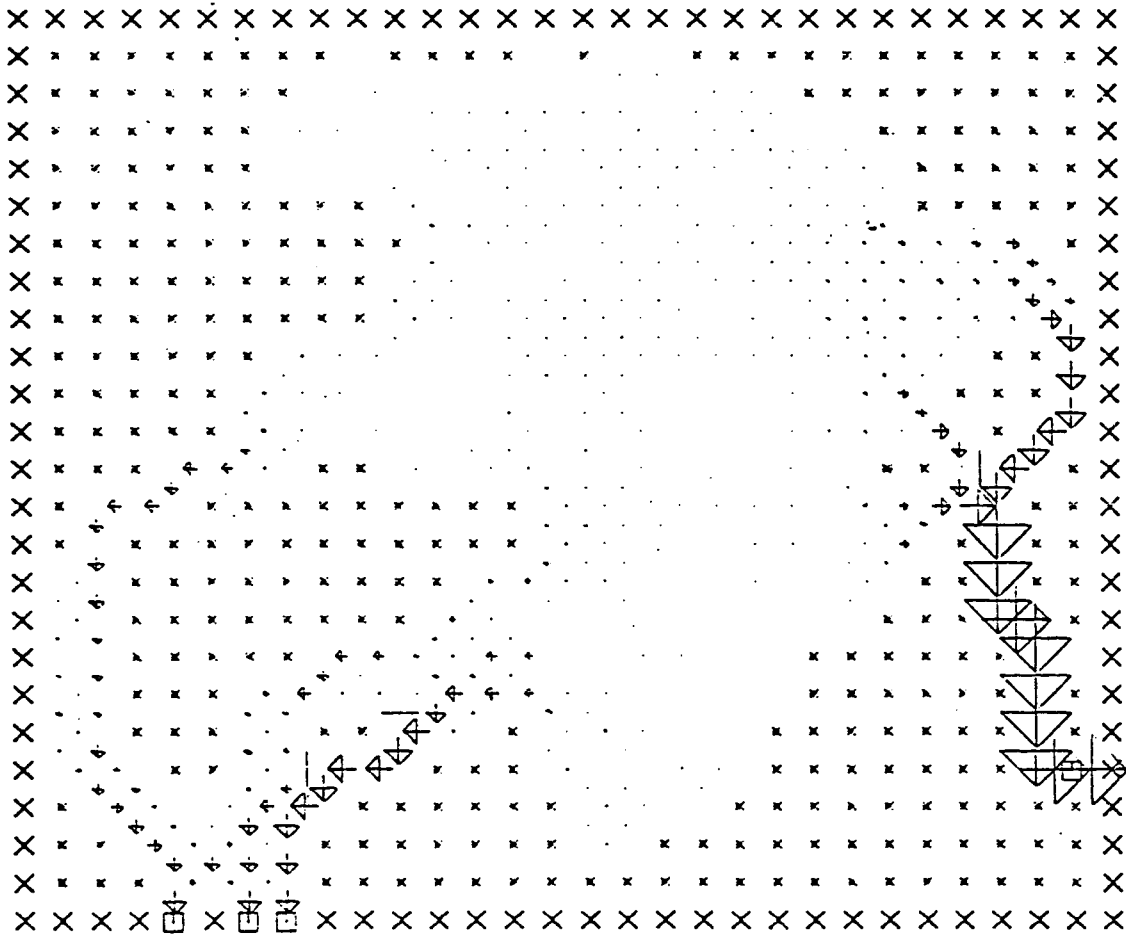
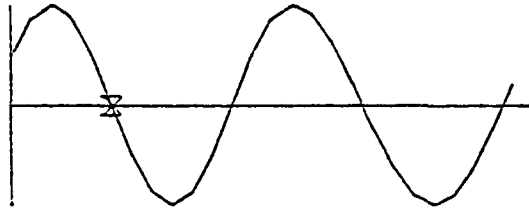


FLOW PATTERN FOR GREAT SOUND

0500 HRS 26 AUG 1978

- X - LAND CELL
- \* - INUNDATION CELL
- - FORCING CELL
- - NO FLOW BOUNDARY

SCALE - 25000. CFS / INCH



FLOW PATTERN FOR GREAT SOUND

0600 HRS 26 AUG 1978

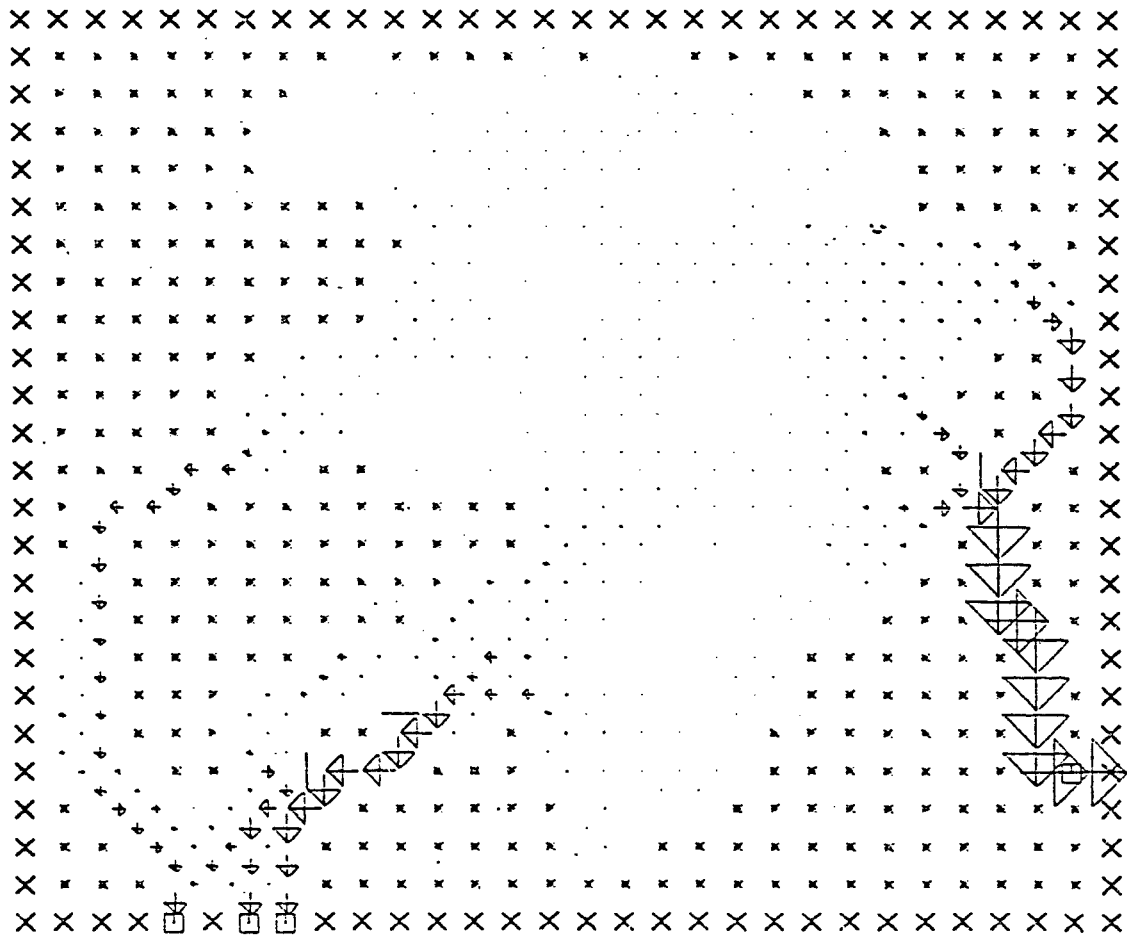
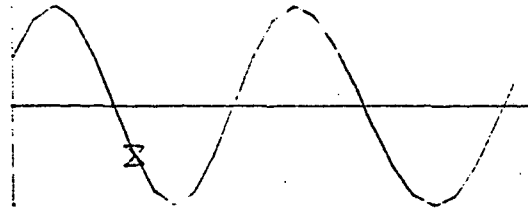
X - LAND CELL

\* - INUNDATION CELL

□ - FORCING CELL

- - NO FLOW BOUNDARY

SCALE - 25000. CFS / INCH

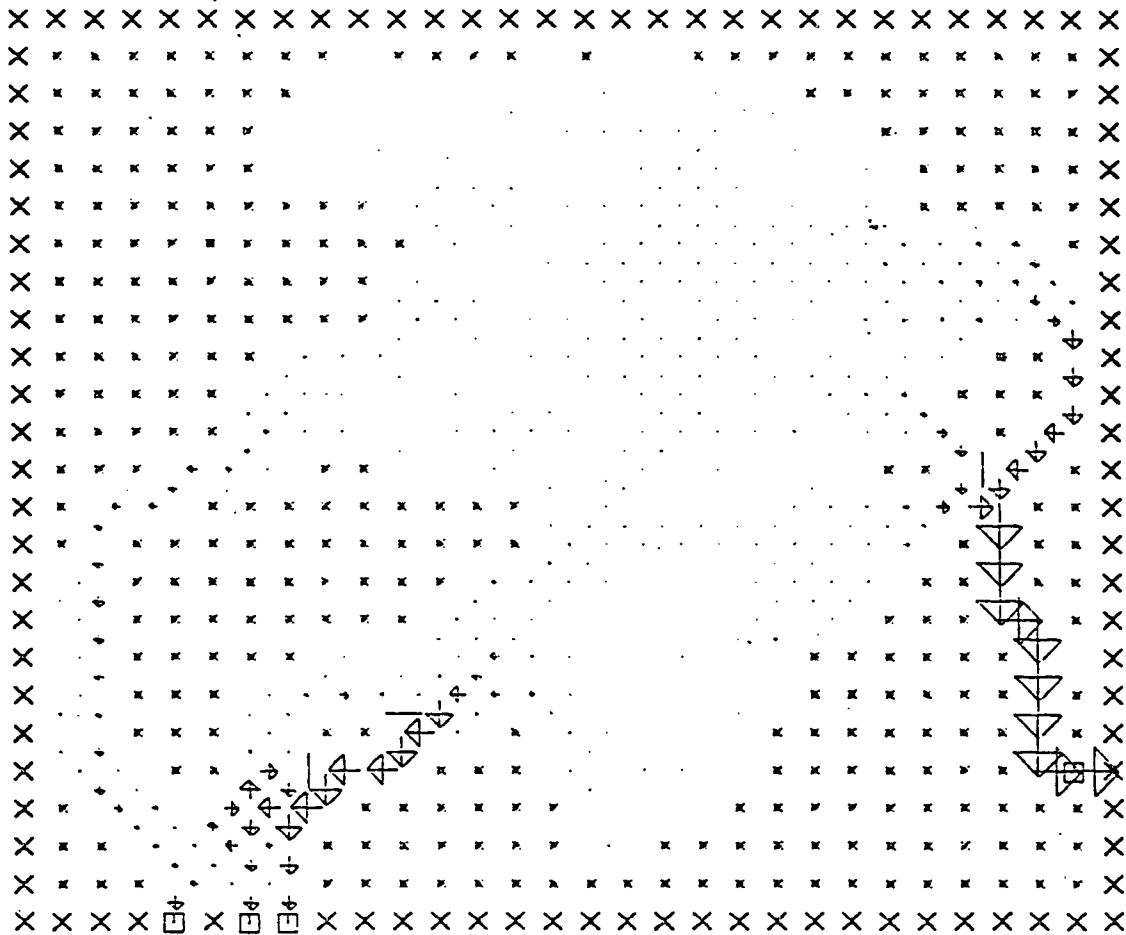
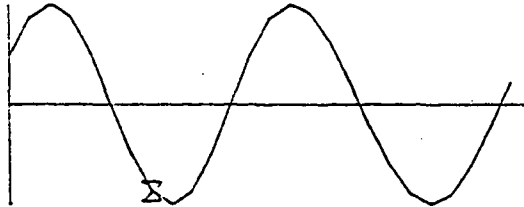


FLOW PATTERN FOR GREAT SOUND

0700 HRS 26 AUG 1978

- X - LAND CELL
- \* - INUNDATION CELL
- - FORCING CELL
- - NO FLOW BOUNDARY

SCALE - 25000. CFS / INCH



FLOW PATTERN FOR GREAT SOUND

0800 HRS 26 AUG 1978

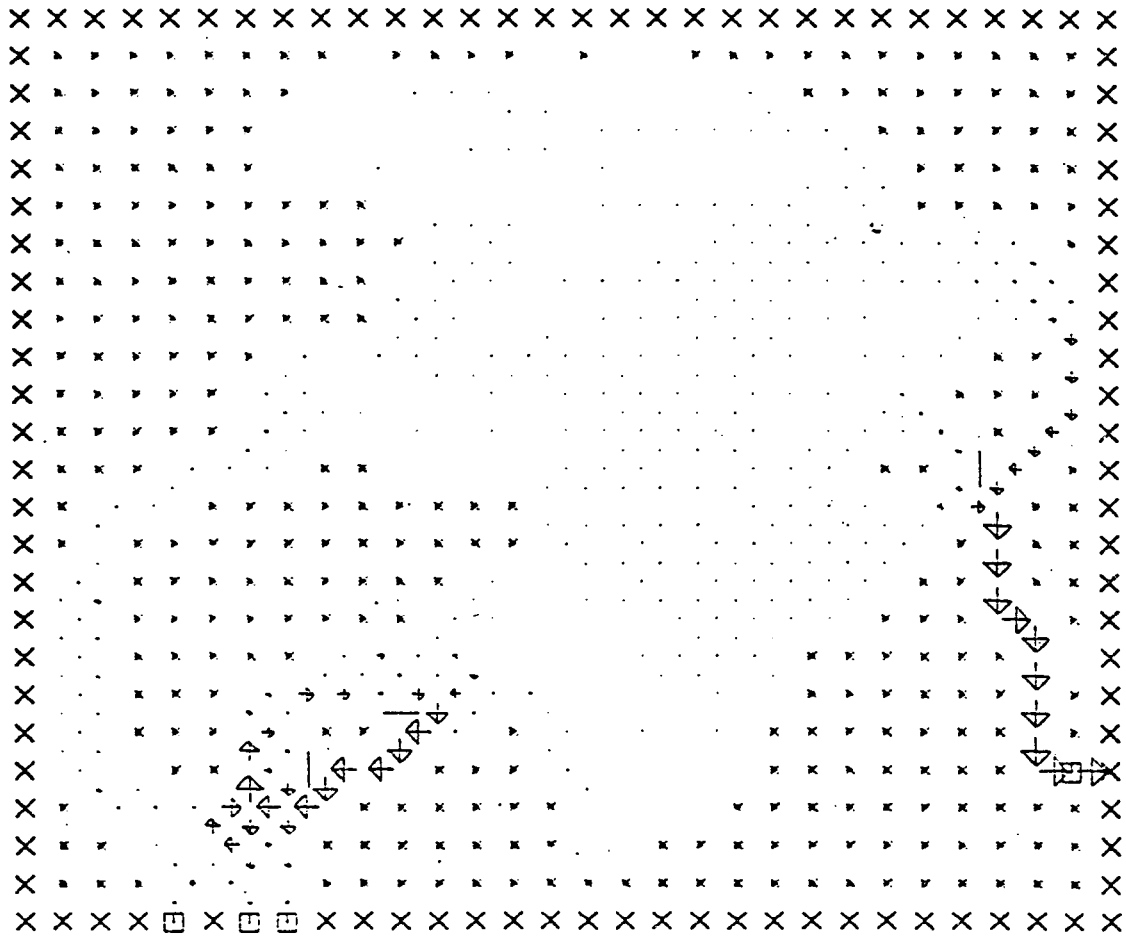
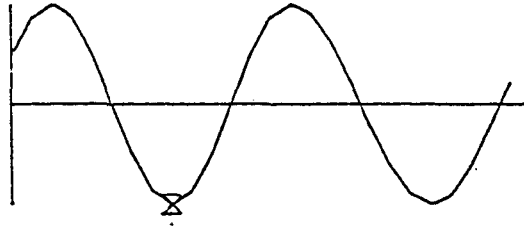
X - LAND CELL

\* - INUNDATION CELL

□ - FORCING CELL

- - NO FLOW BOUNDARY

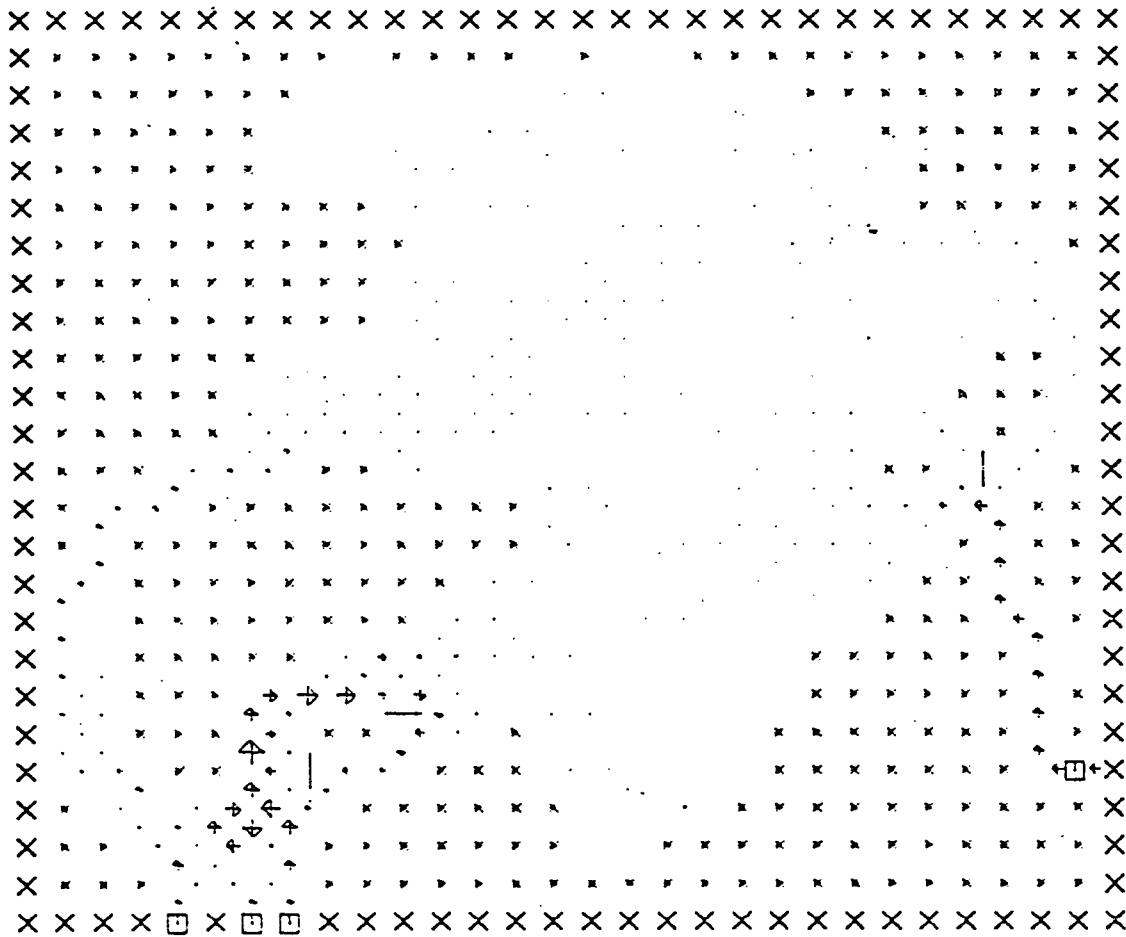
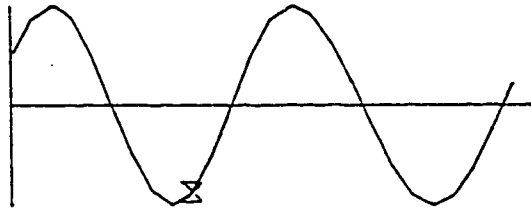
SCALE - 25000. CFS / INCH



FLOW PATTERN FOR GREAT SOUND

0900 HRS 25 AUG 1978

- X - LAND CELL
  - \* - INUNDATION CELL
  - - FORCING CELL
  - - NO FLOW BOUNDARY
- SCALE - 25000. CFS / INCH



FLOW PATTERN FOR GREAT SOUND

1000 HRS 26 AUG 1978

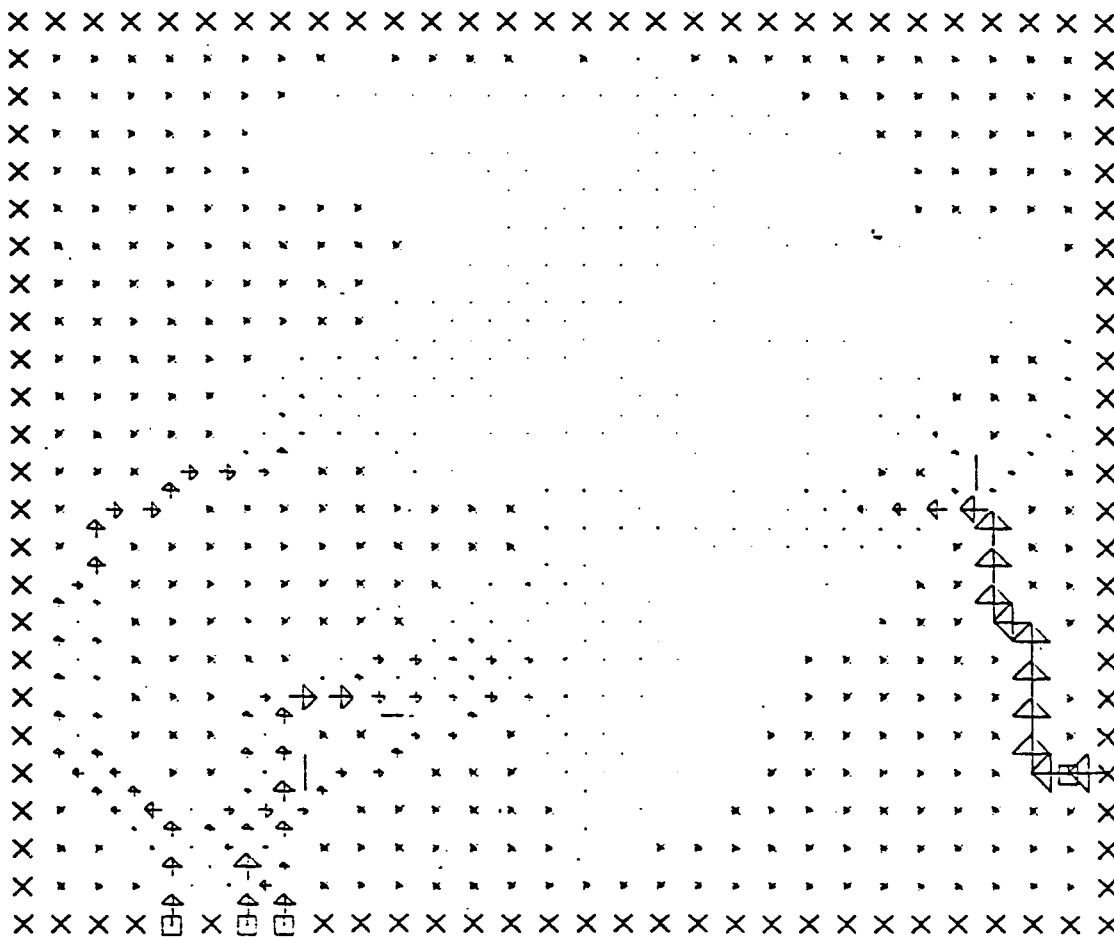
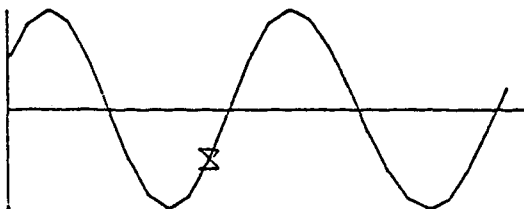
X - LAND CELL

\* - INUNDATION CELL

□ - FORCING CELL

- - NO FLOW BOUNDARY

SCALE - 25000. CFS / INCH



FLOW PATTERN FOR GREAT SOUND

1100 HRS 26 AUG 1978

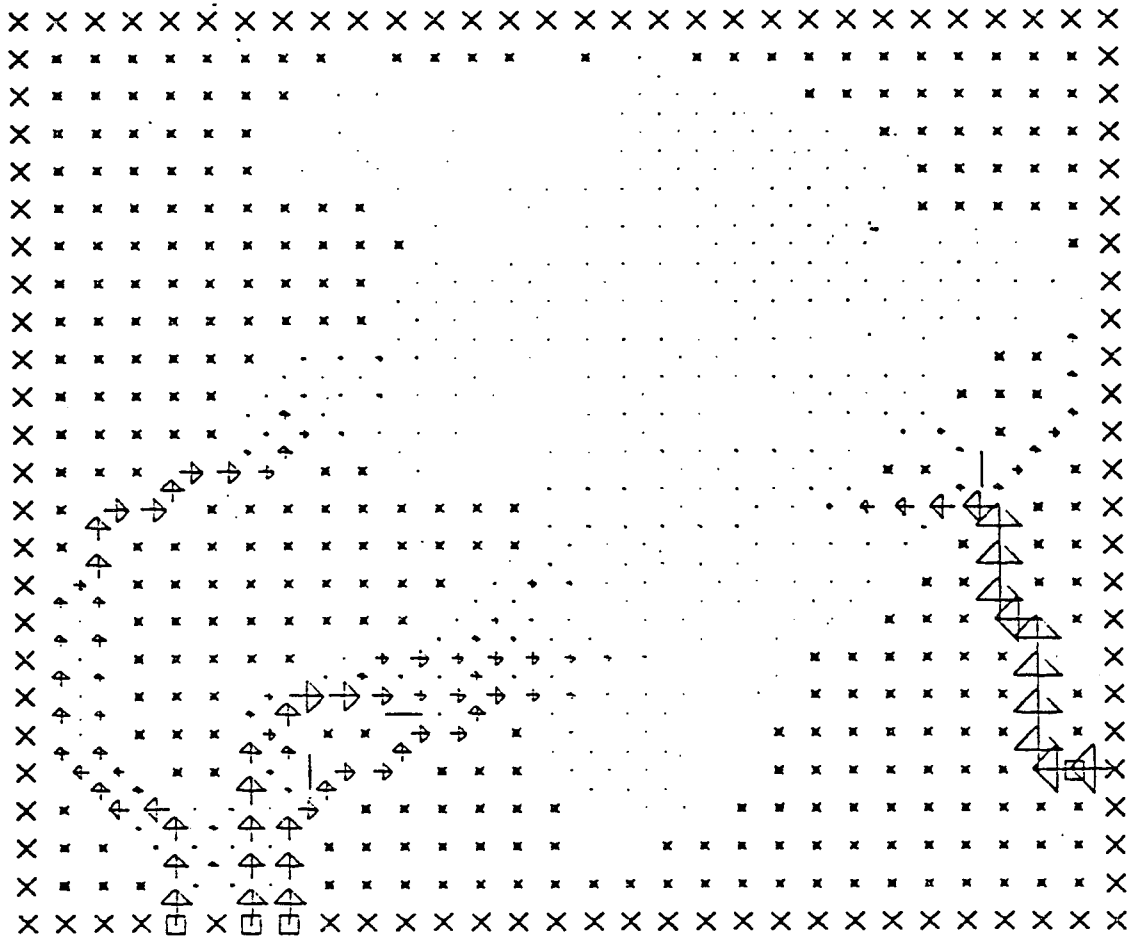
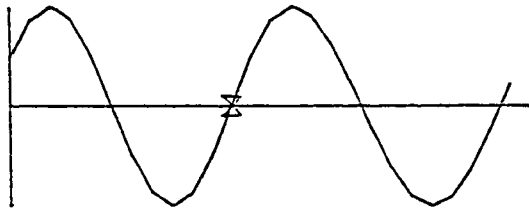
X - LAND CELL

\* - INUNDATION CELL

□ - FORCING CELL

- - NO FLOW BOUNDARY

SCALE - 25000. CFS / INCH





FLOW PATTERN FOR GREAT SOUND

1200 HRS 26 AUG 1978

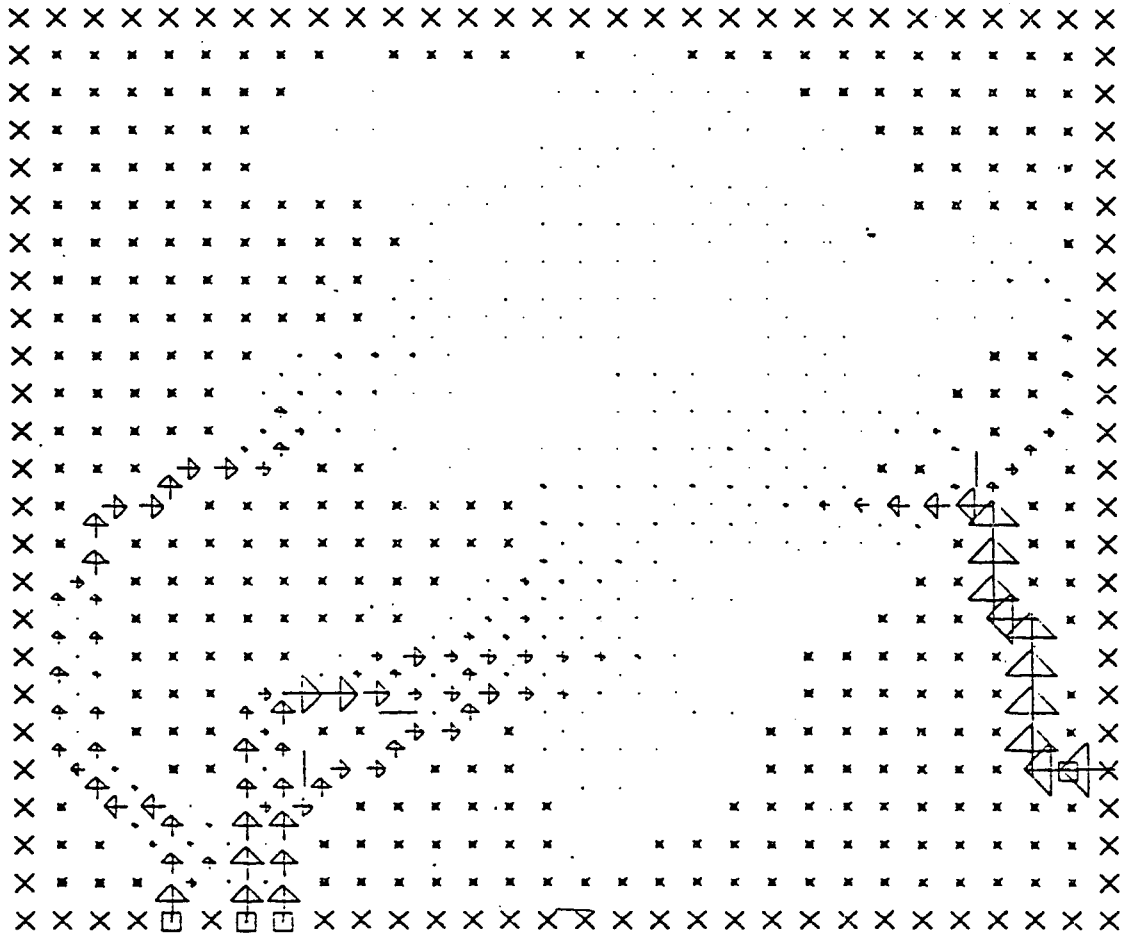
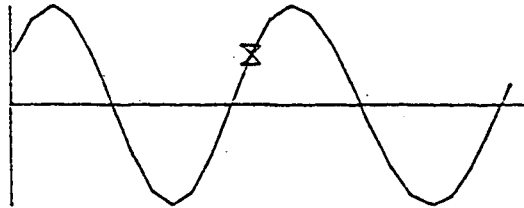
X - LAND CELL

\* - INUNDATION CELL

□ - FORCING CELL

- - NO FLOW BOUNDARY

SCALE - 25000. CFS / INCH



FLOW PATTERN FOR GREAT SOUND

1300 HRS 26 AUG 1978

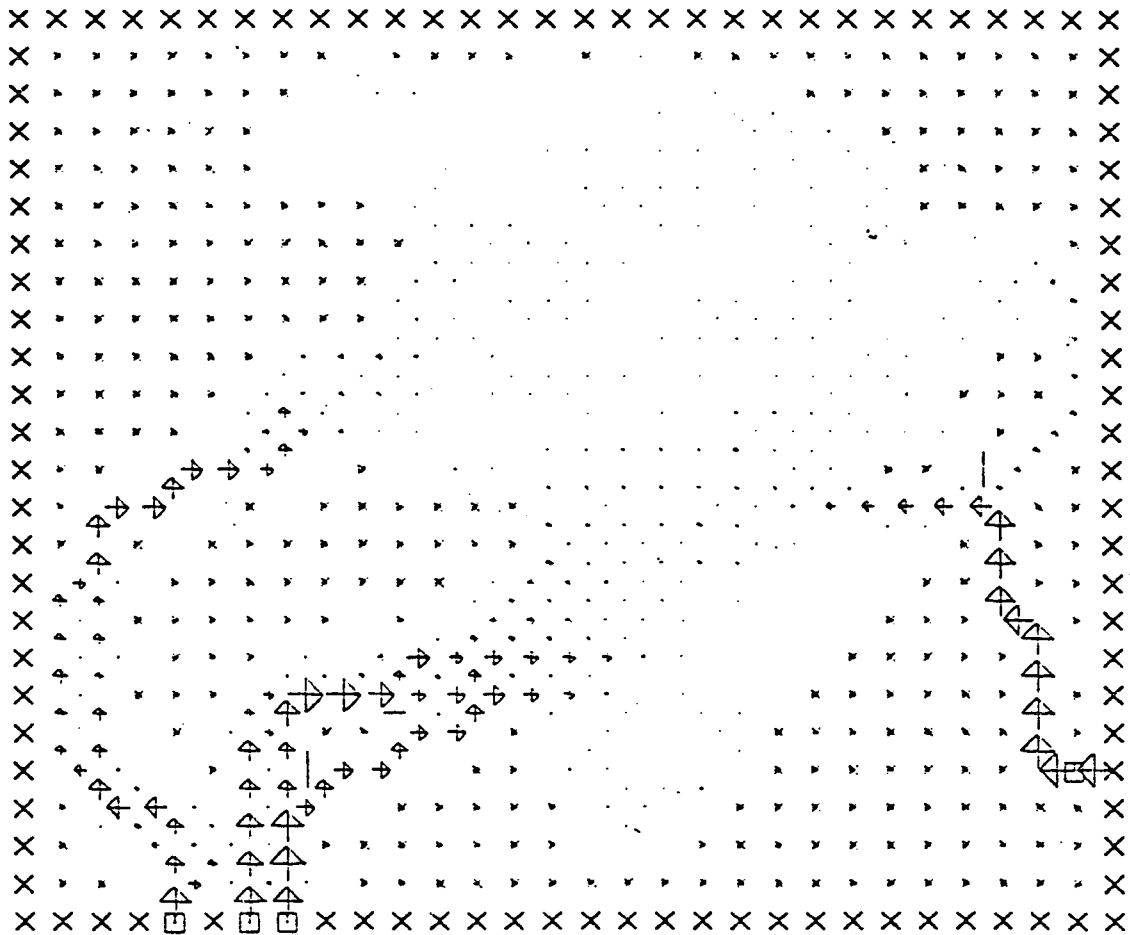
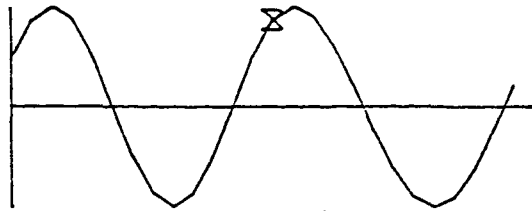
X - LAND CELL.

\* - INUNDATION CELL.

□ - FORCING CELL.

- - NO FLOW BOUNDARY

SCALE - 25000. CFS / INCH



FLOW PATTERN FOR GREAT SOUND

1400 HRS 26 AUG 1978

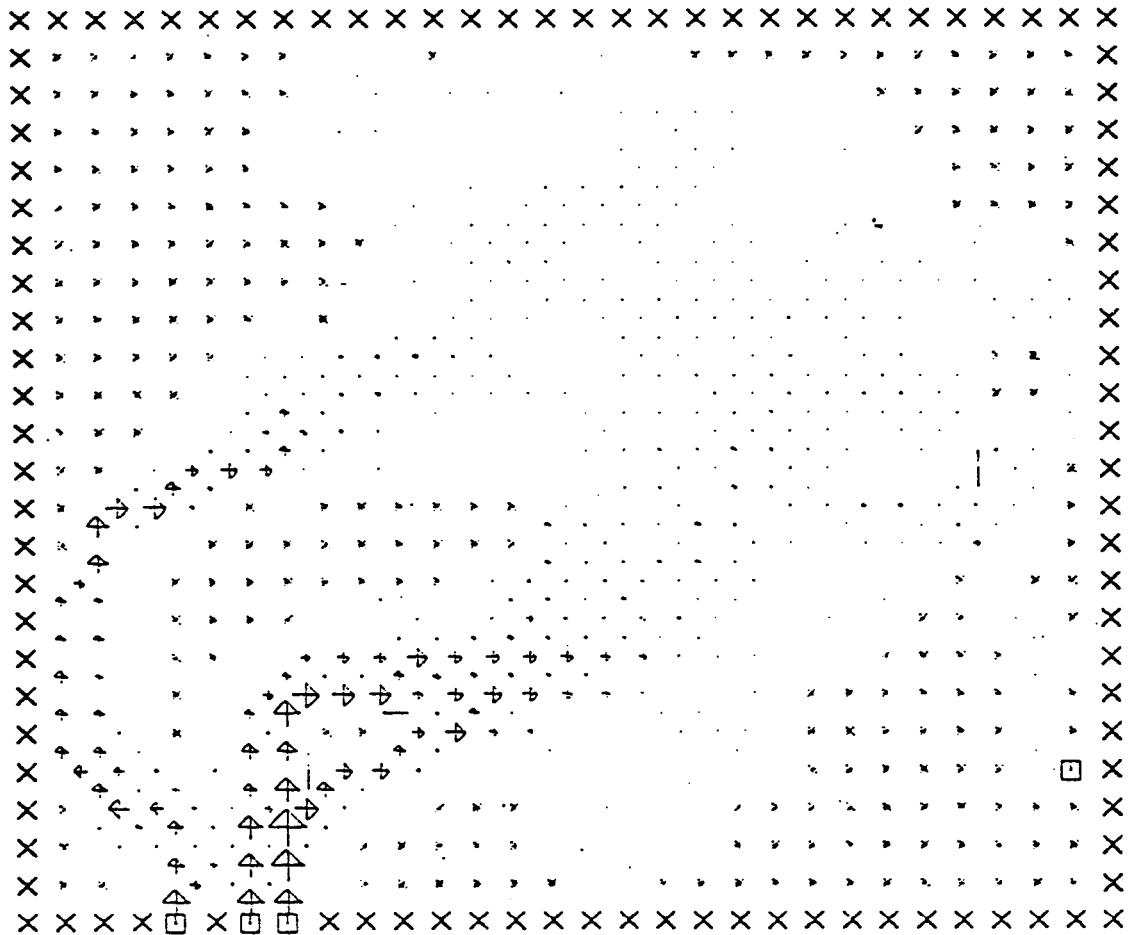
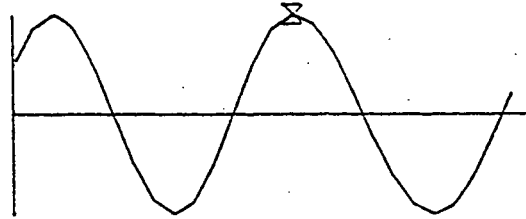
X - LAND CELL

\* - INUNDATION CELL

□ - FORCING CELL

- - NO FLOW BOUNDARY

SCALE - 25000. CFS / INCH

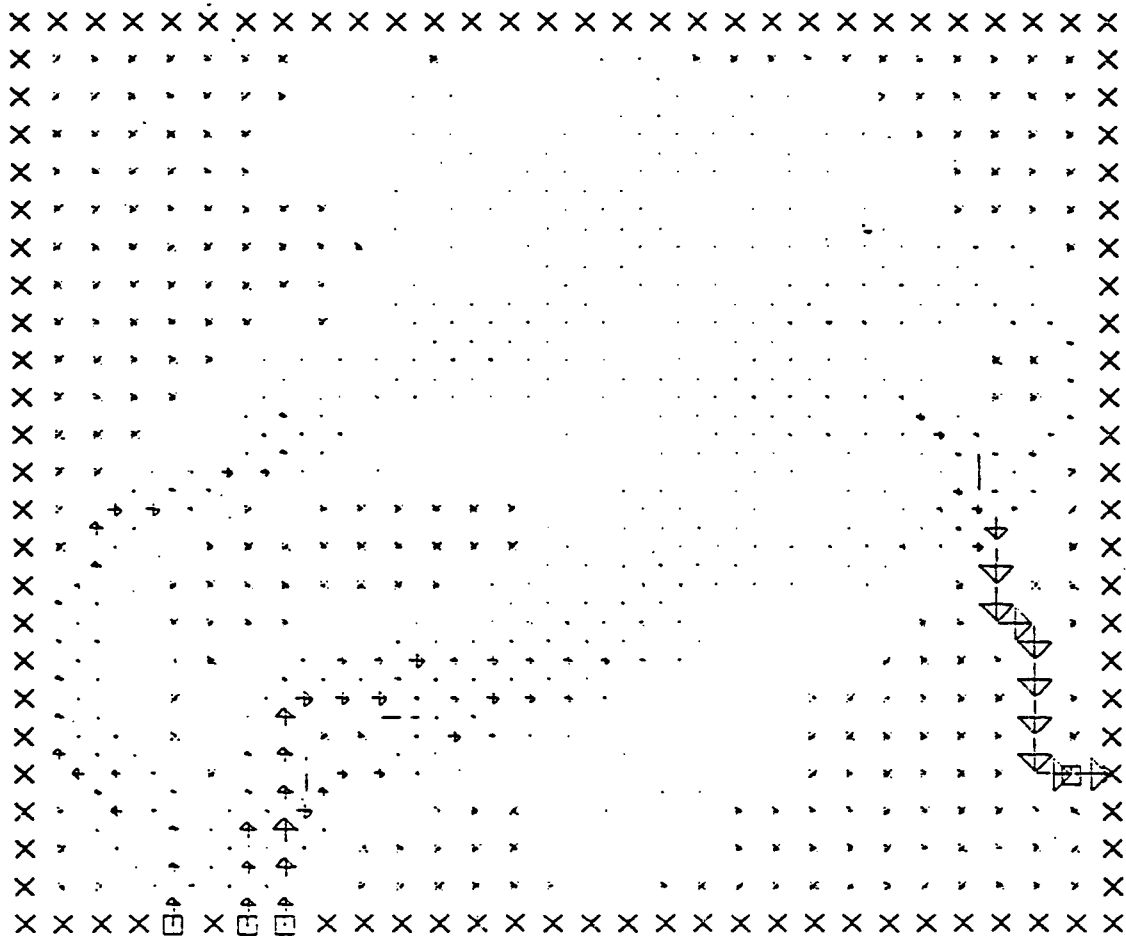
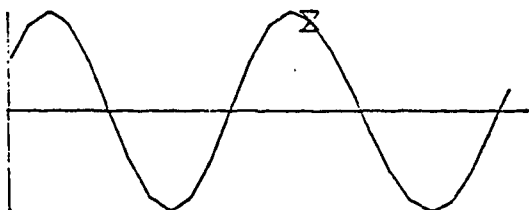


FLOW PATTERN FOR GREAT SOUND

1500 HRS 26 AUG 1978

- X - LAND CELL
- \* - INUNDATION CELL
- - FORCING CELL
- - NO FLOW BOUNDARY

SCALE - 25000. CFS / INCH



FLOW PATTERN FOR GREAT SOUND

1600 HRS 26 AUG 1978

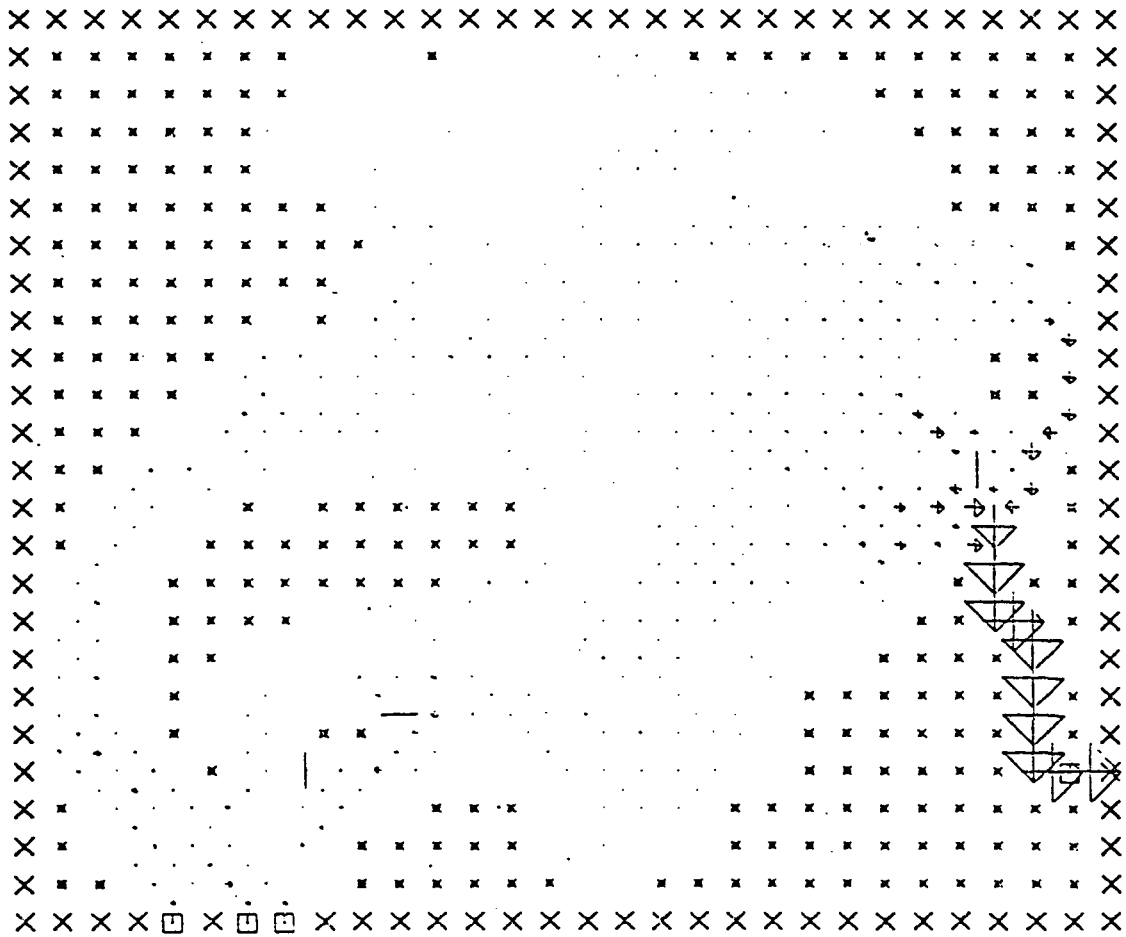
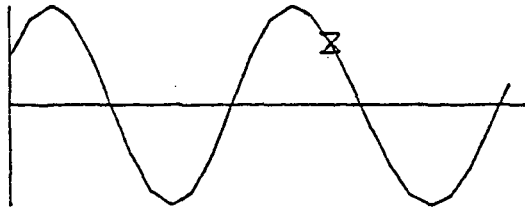
X - LAND CELL

\* - INUNDATION CELL

□ - FORCING CELL

- - NO FLOW BOUNDARY

SCALE - 25000. CFS / INCH

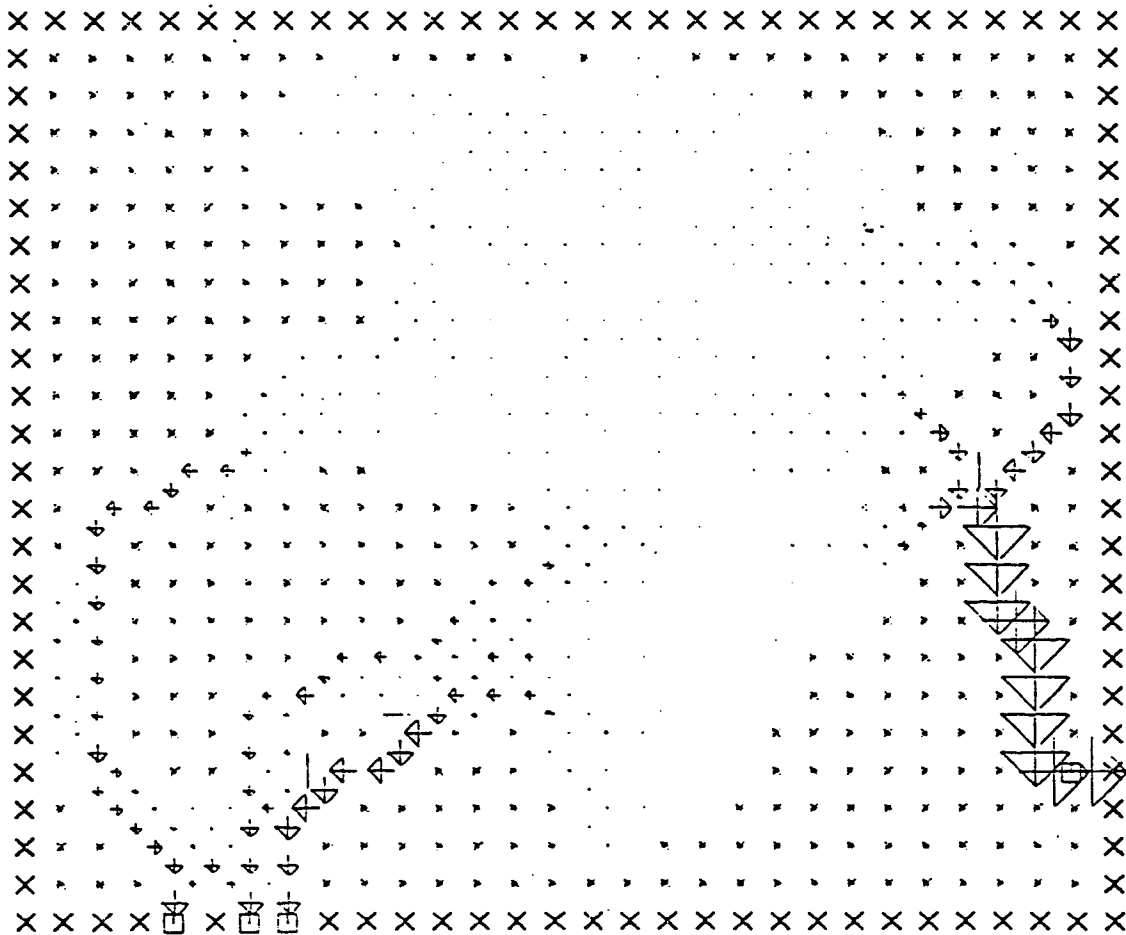
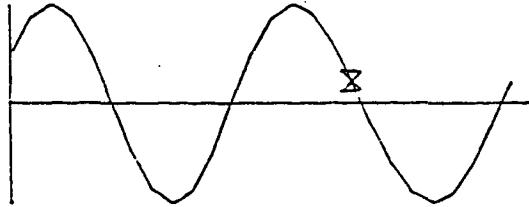


FLOW PATTERN FOR GREAT SOUND

1700 HRS 26 AUG 1978

- X - LAND CELL
- \* - INUNDATION CELL
- - FORCING CELL
- - NO FLOW BOUNDARY

SCALE - 25000. CFS / INCH



FLOW PATTERN FOR GREAT SOUND

1600 HRS 26 AUG 1978

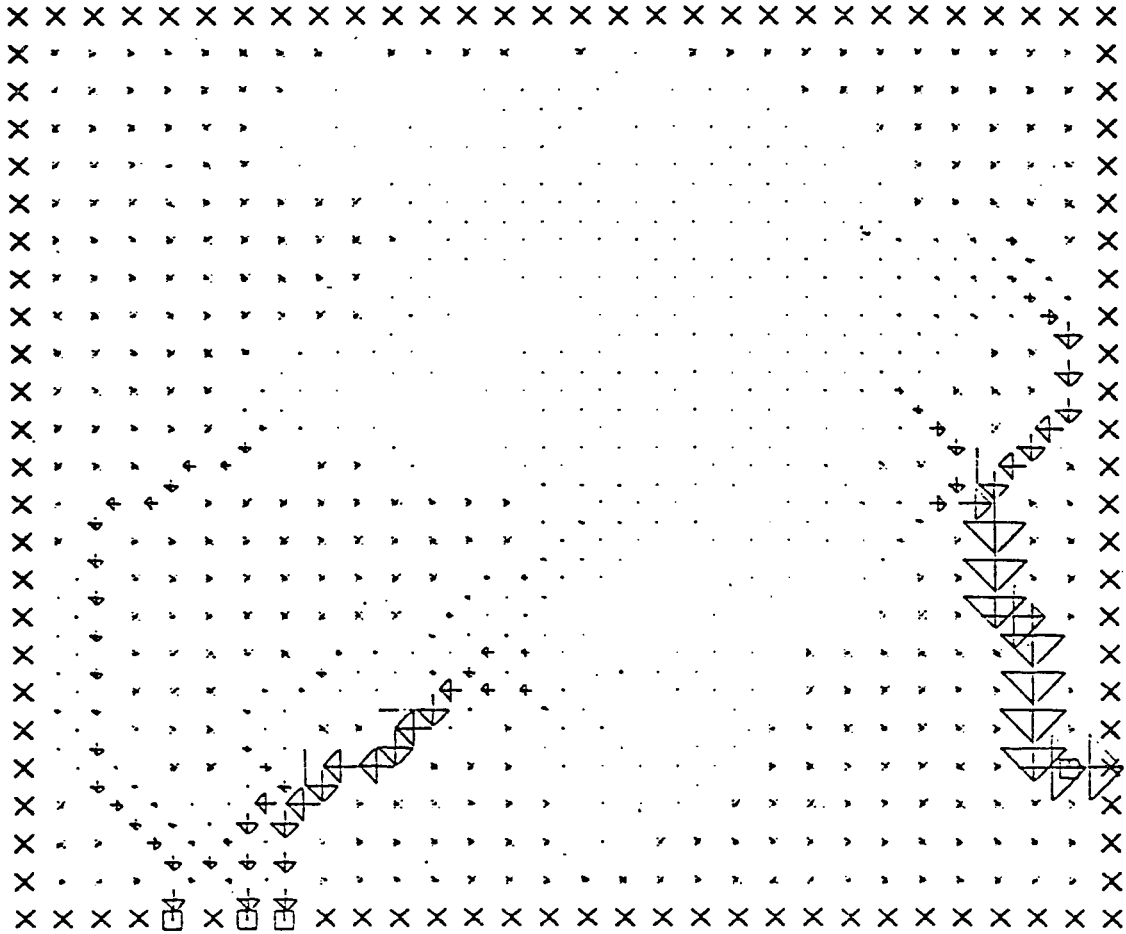
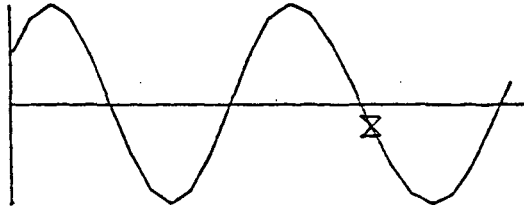
X - LAND CELL

\* - INUNDATION CELL

□ - FORCING CELL

- - NO FLOW BOUNDARY

SCALE - 25000. CFS / INCH



FLOW PATTERN FOR GREAT SOUND

1900 HRS 26 AUG 1978

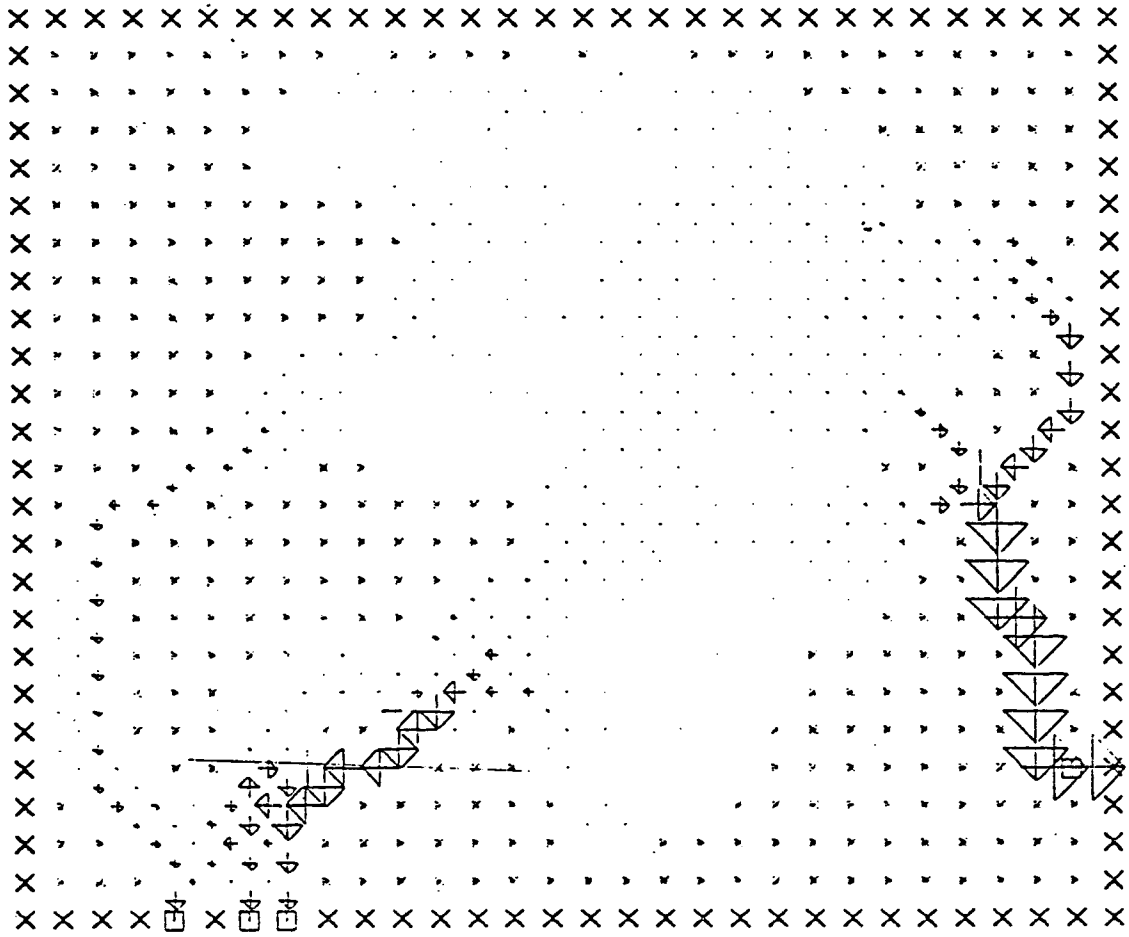
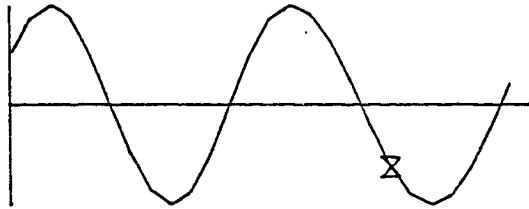
X - LAND CELL

\* - INUNDATION CELL

□ - FORCING CELL

- - NO FLOW BOUNDARY

SCALE - 25000. CFS / INCH





FLOW PATTERN FOR GREAT SOUND

2000 HRS 26 AUG 1978

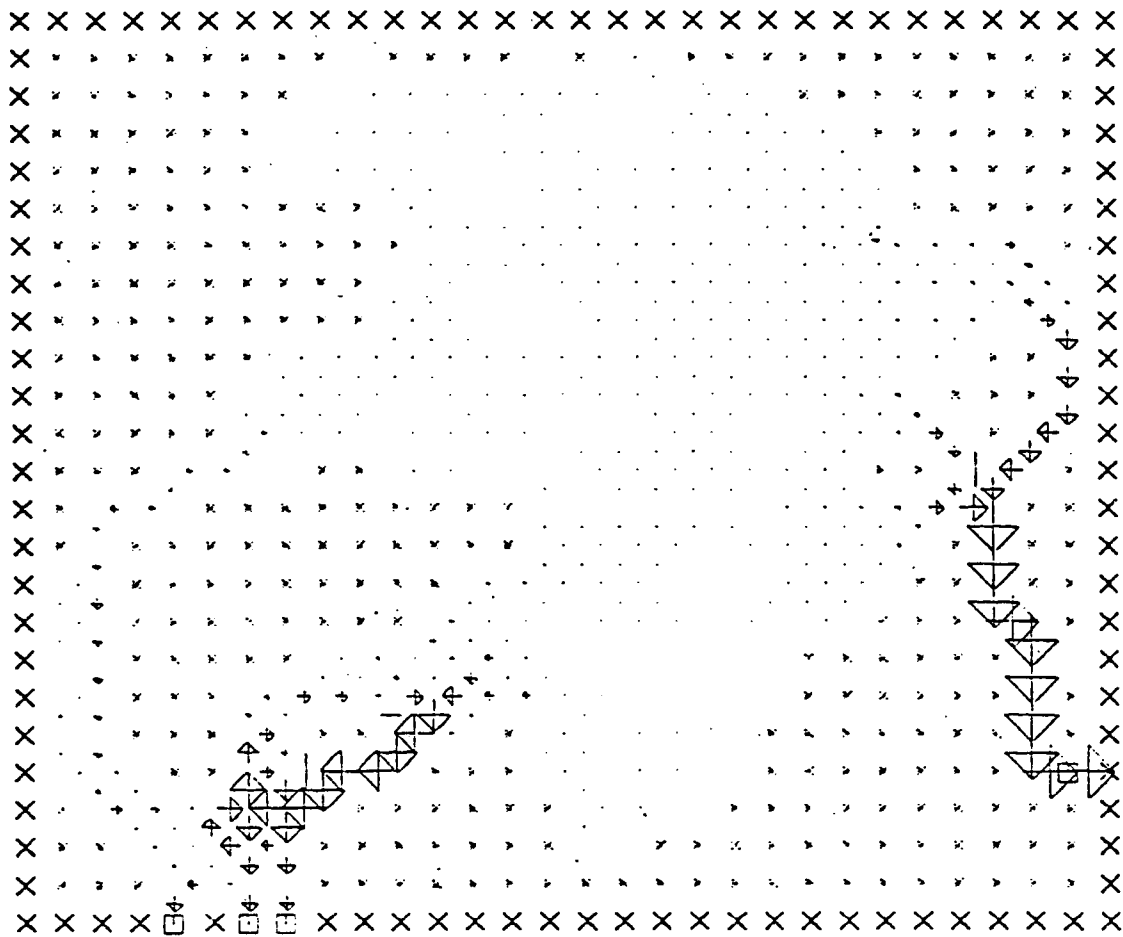
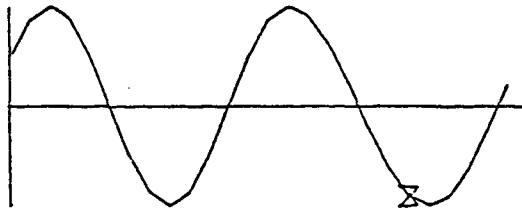
X - LAND CELL

\* - INUNDATION CELL

□ - FORCING CELL

- - NO FLOW BOUNDARY

SCALE - 25000. CFS / INCH



FLOW PATTERN FOR GREAT SOUND

2100 HRS 26 AUG 1978

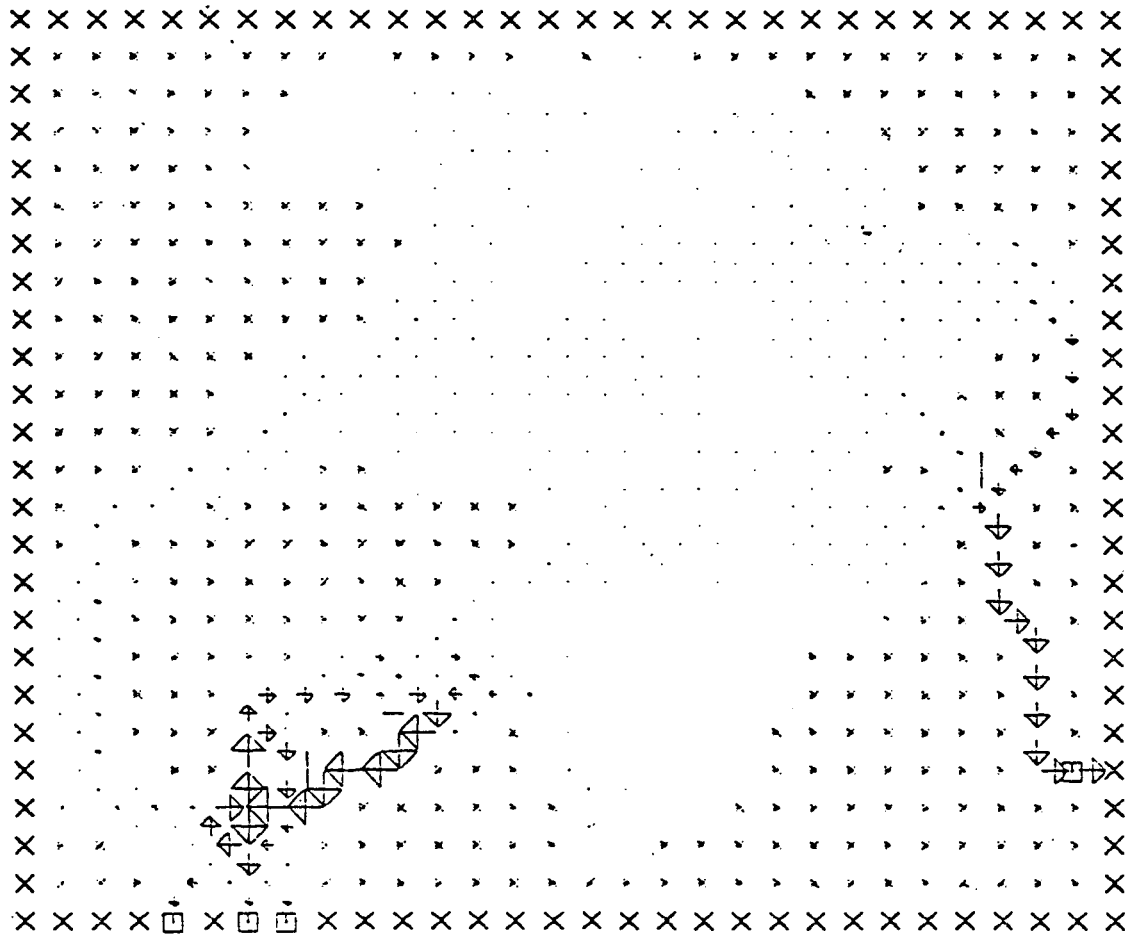
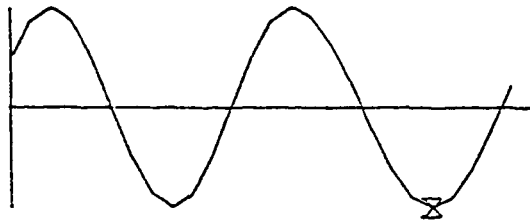
X - LAND CELL

\* - INUNDATION CELL

□ - FORCING CELL

- - NO FLOW BOUNDARY

SCALE - 25000. CFS / INCH

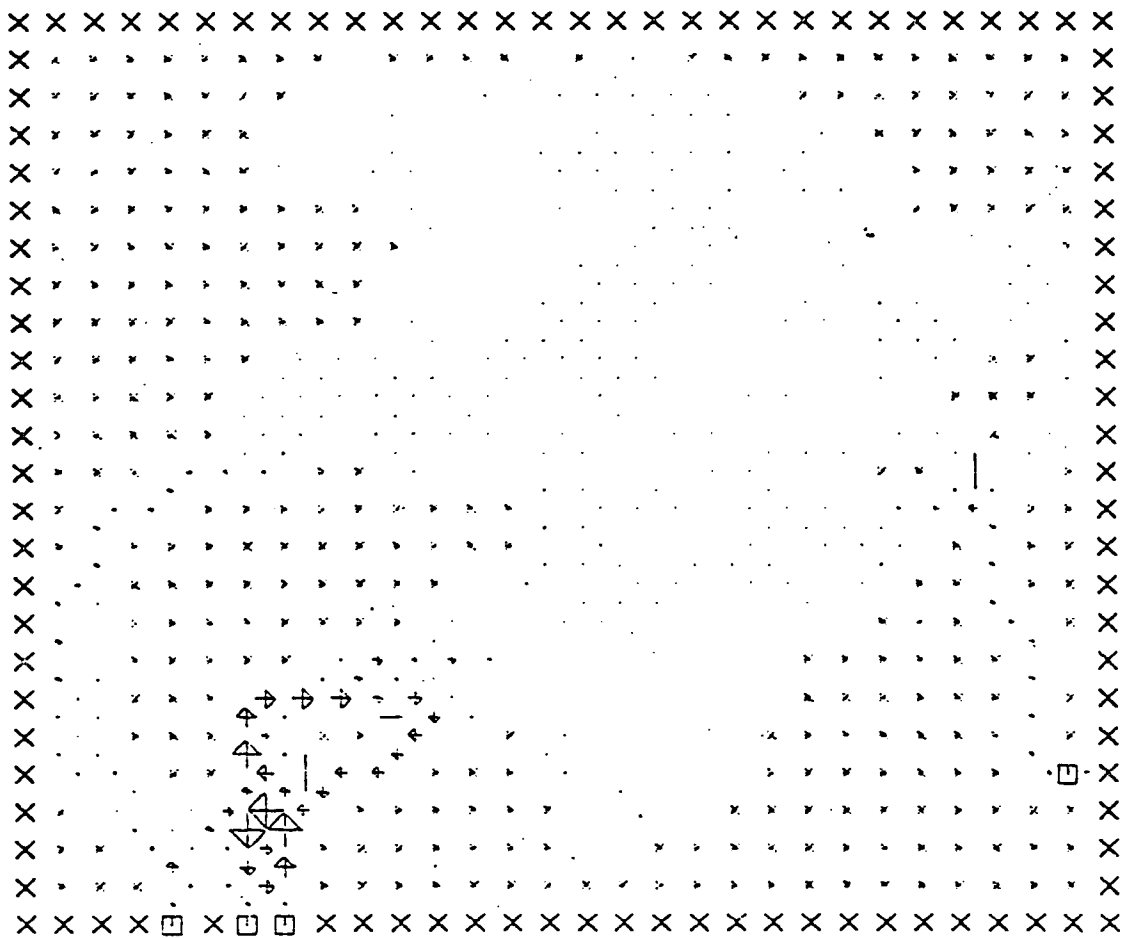
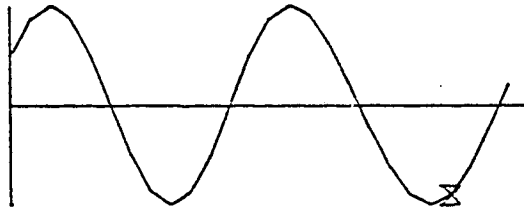


FLOW PATTERN FOR GREAT SOUND

2200 HRS 26 AUG 1978

- X - LAND CELL
- \* - INUNDATION CELL
- - FORCING CELL
- - NO FLOW BOUNDARY

SCALE - 25000. CFS / INCH



FLOW PATTERN FOR GREAT SOUND

2300. HRS 26 AUG 1978

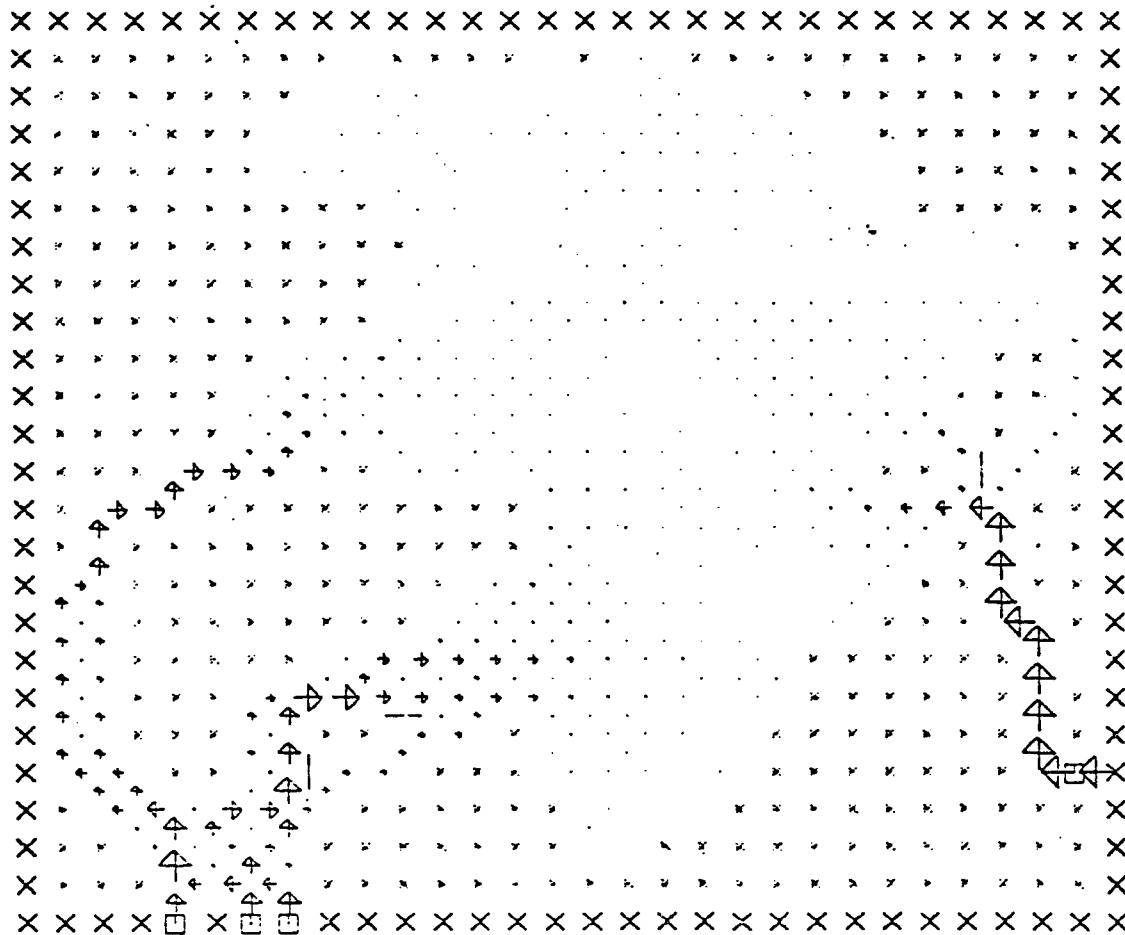
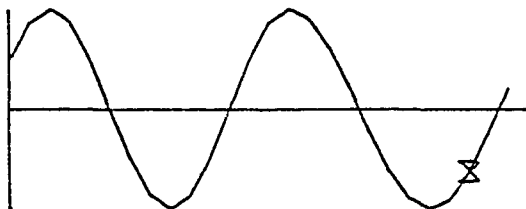
X - LAND CELL

\* - INUNDATION CELL

□ - FORCING CELL

- - NO FLOW BOUNDARY

SCALE - 25000. CFS / INCH

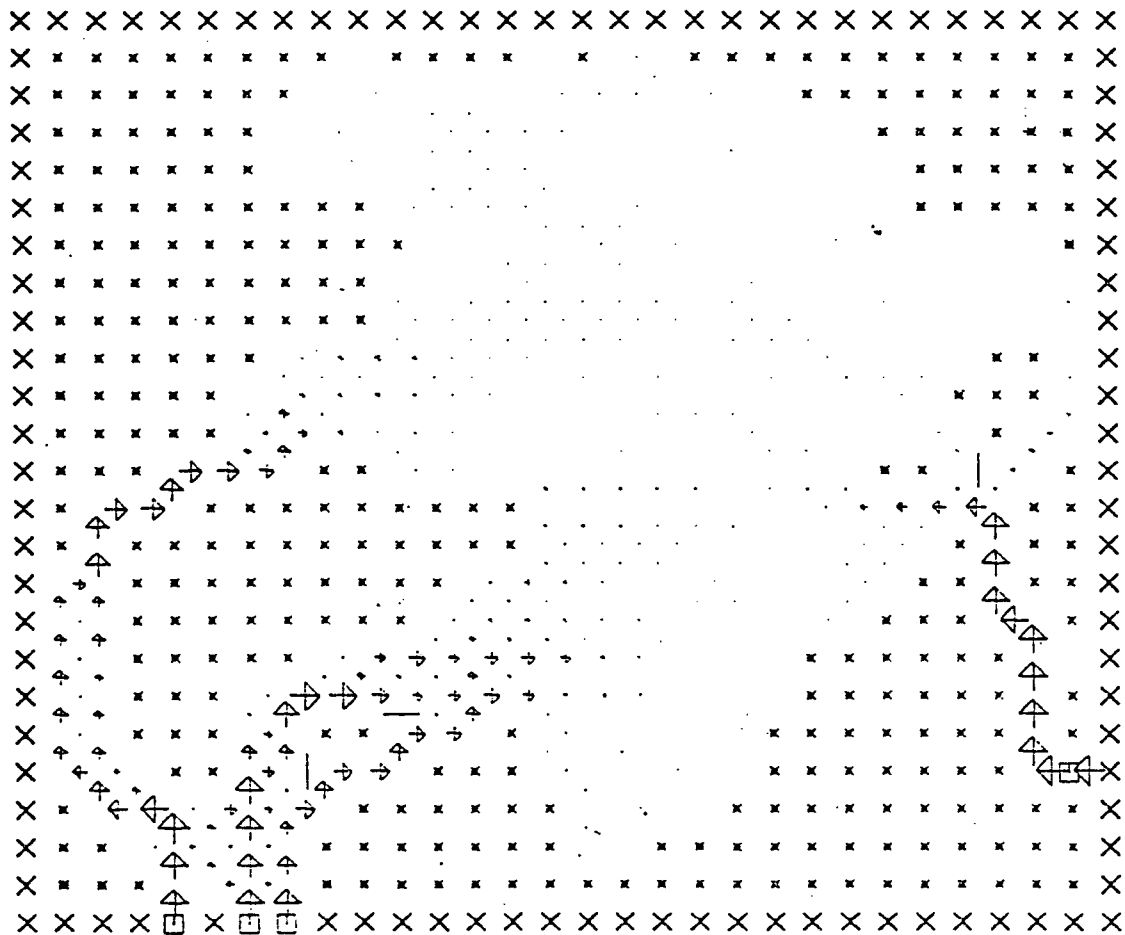
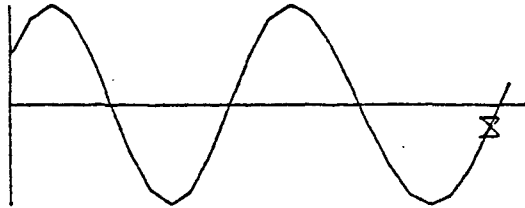


FLOW PATTERN FOR GREAT SOUND

2400 HRS 26 AUG 1978

- X - LAND CELL.
- \* - INUNDATION CELL.
- - FORCING CELL.
- - NO FLOW BOUNDARY

SCALE - 25000. CFS / INCH

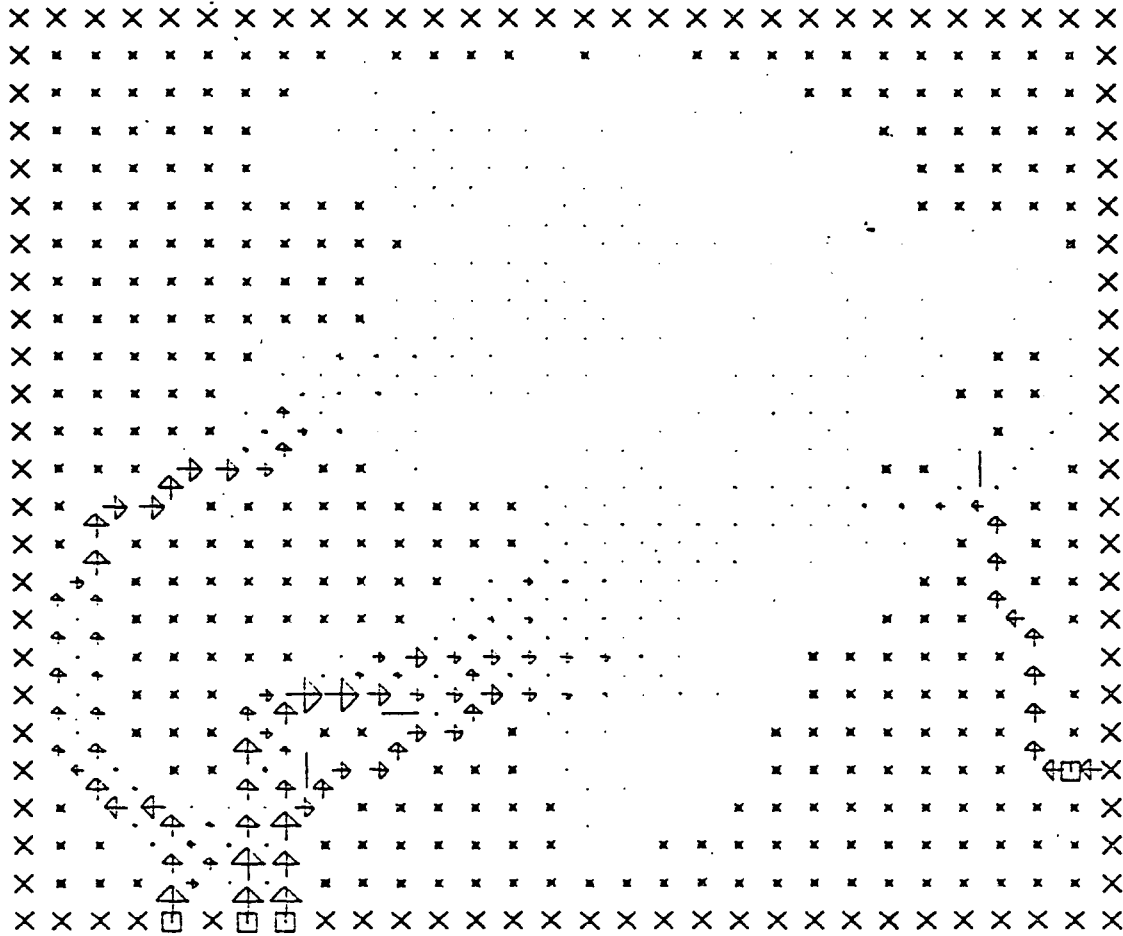
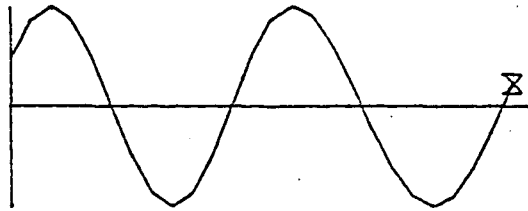


FLOW PATTERN FOR GREAT SOUND

0100 HRS 27 AUG 1978

- X - LAND CELL
- \* - INUNDATION CELL
- - FORCING CELL
- - NO FLOW BOUNDARY

SCALE - 25000. CFS / INCH



APPENDIX 6:

Flow Pattern: Grassy and Richardson Sounds

FLOW PATTERN FOR GRASSY

AND RICHARDSON SOUNDS

2400 HRS 25 AUG 1978

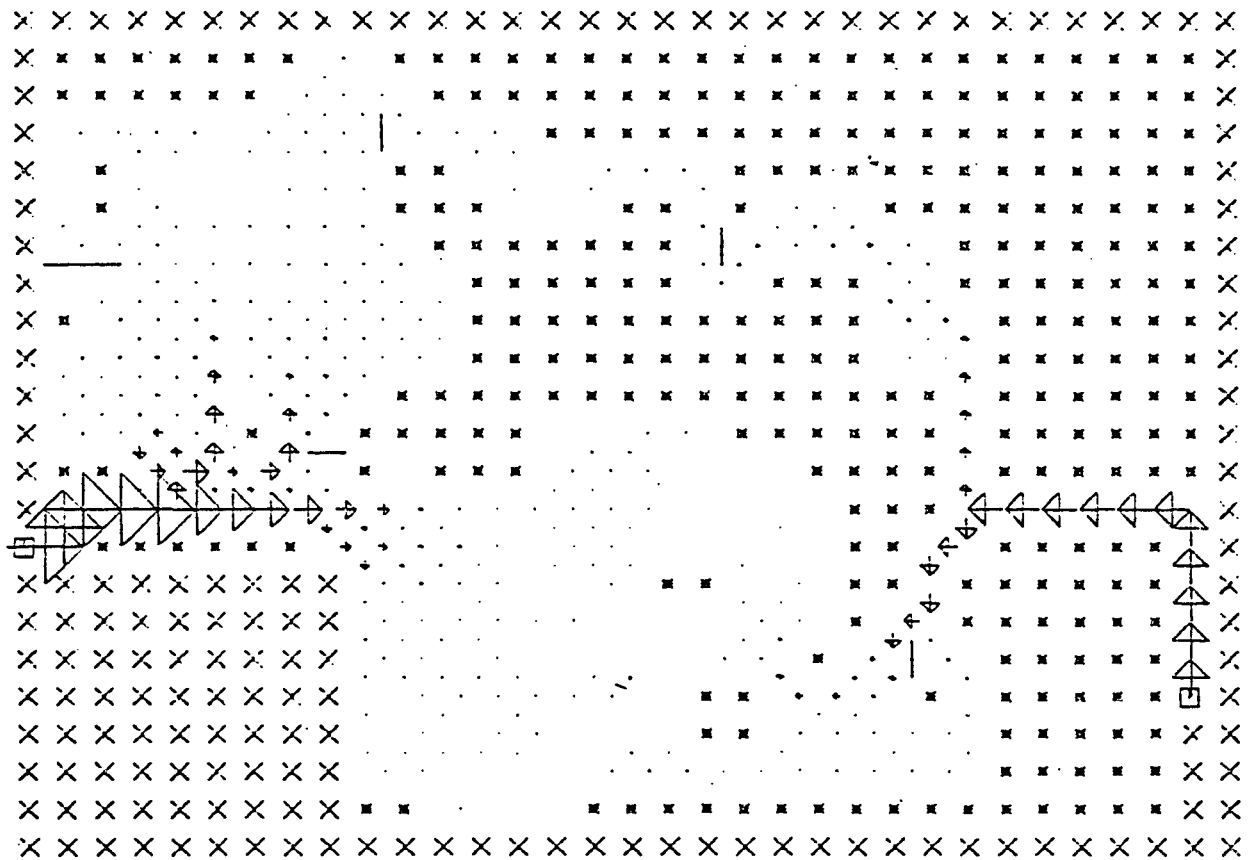
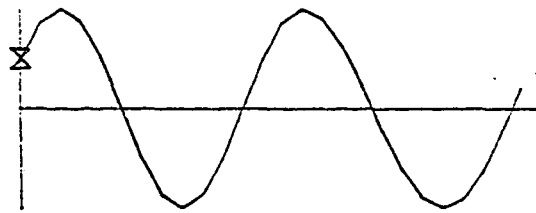
X - LAND CELL

\* - INUNDATION CELL

□ - FORCING CELL

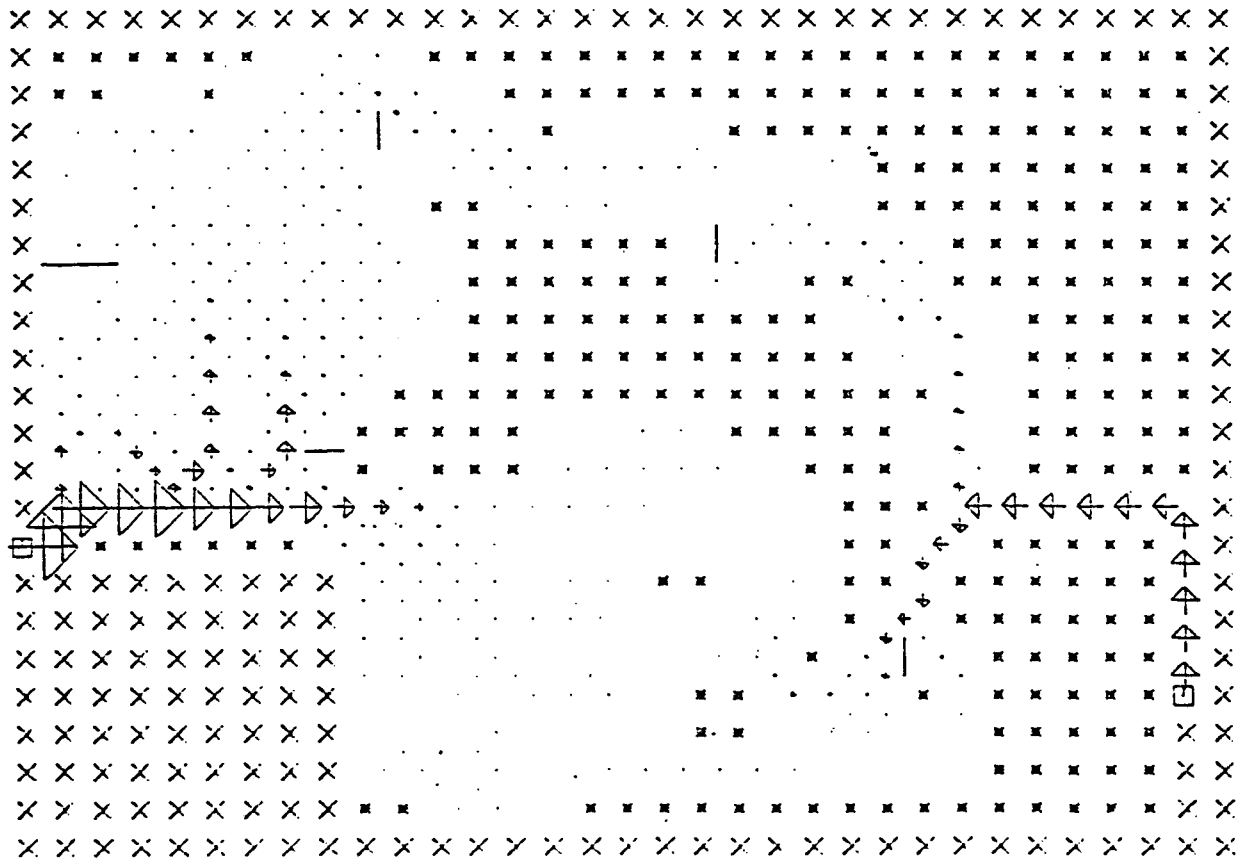
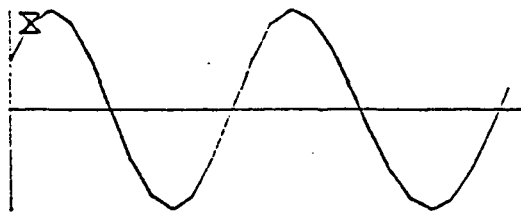
- - NO FLOW BOUNDARY

SCALE - 25000. CFS / INCH





FLOW PATTERN FOR GRASSY  
 AND RICHARDSON SOUNDS  
 0100 HRS 26 AUG 1978  
 X - LAND CELL  
 \* - INUNDATION CELL  
 □ - FORCING CELL  
 - - NO FLOW BOUNDARY  
 SCALE - 25000. CFS / INCH



FLOW PATTERN FOR GRASSY

AND RICHARDSON SOUNDS

0200 HRS 26 AUG 1978

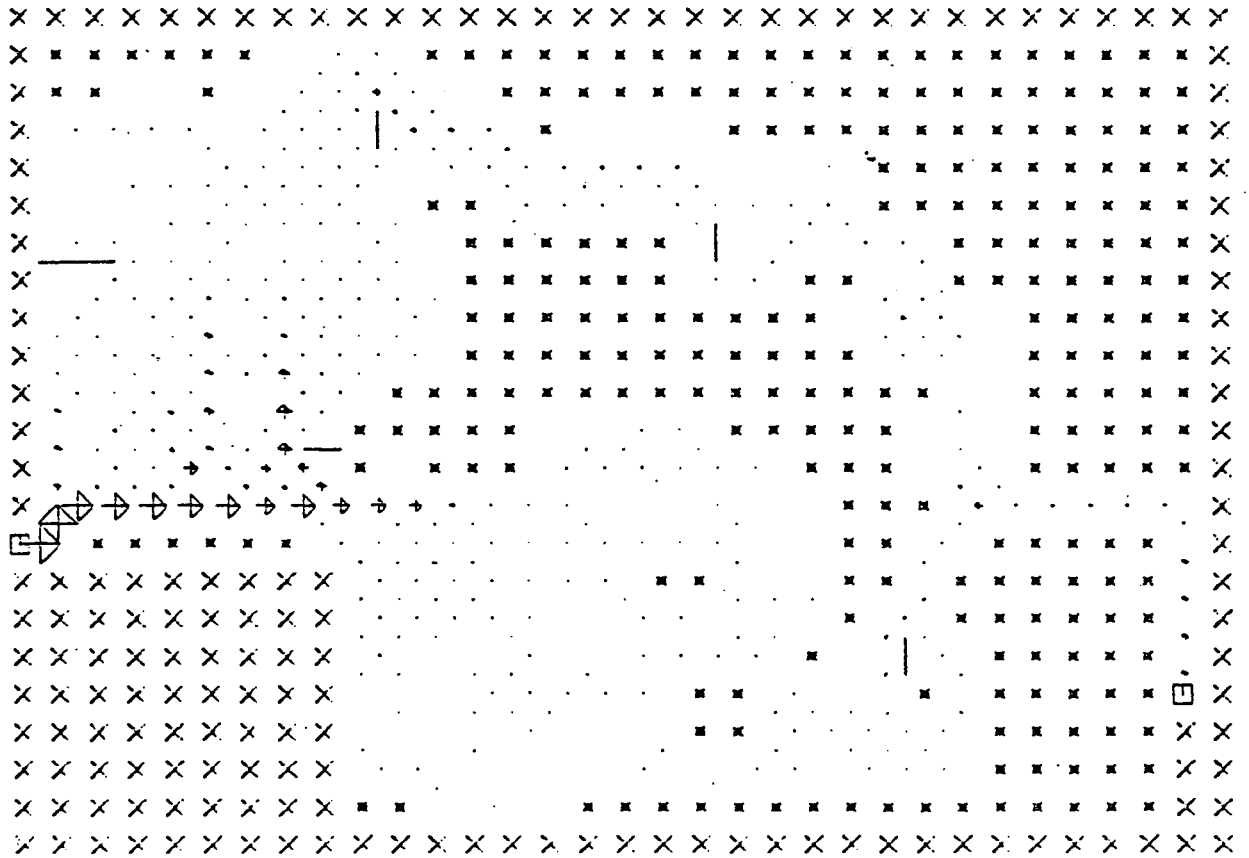
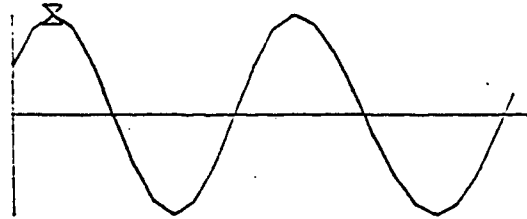
X - LAND CELL

\* - INUNDATION CELL

□ - FORCING CELL

- - NO FLOW BOUNDARY

SCALE - 25000. CFS / INCH



FLOW PATTERN FOR GRASSY

AND RICHARDSON SOUNDS

0300 HRS 26 AUG 1978

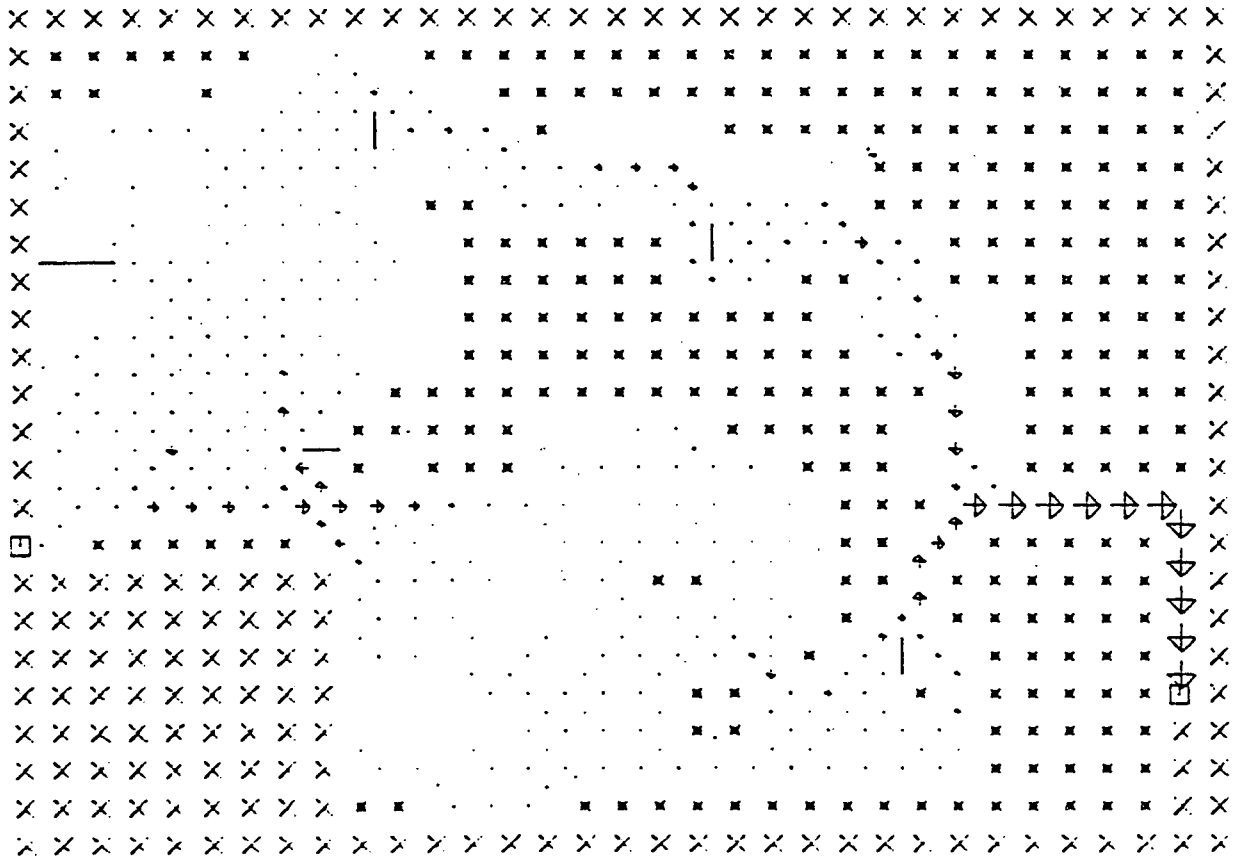
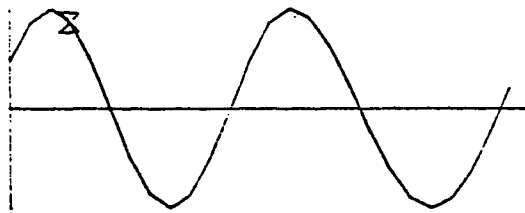
X - LAND CELL

\* - INUNDATION CELL

□ - FORCING CELL

- - NO FLOW BOUNDARY

SCALE - 25000. CFS / INCH



FLOW PATTERN FOR GRASSY  
AND RICHARDSON SOUNDS

0400 HRS 26 AUG 1978

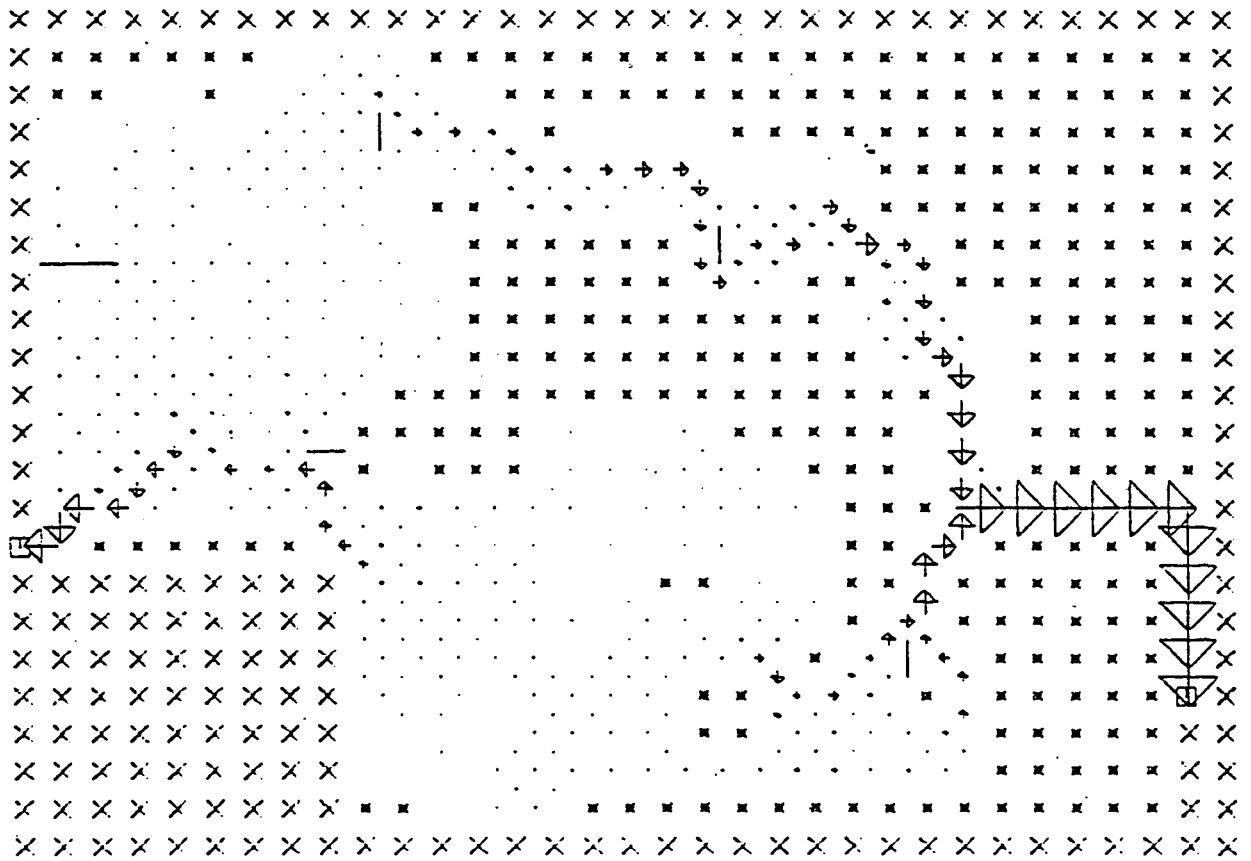
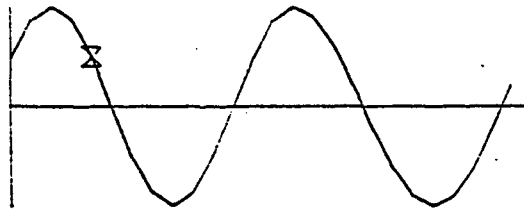
X - LAND CELL

\* - INUNDATION CELL

□ - FORCING CELL

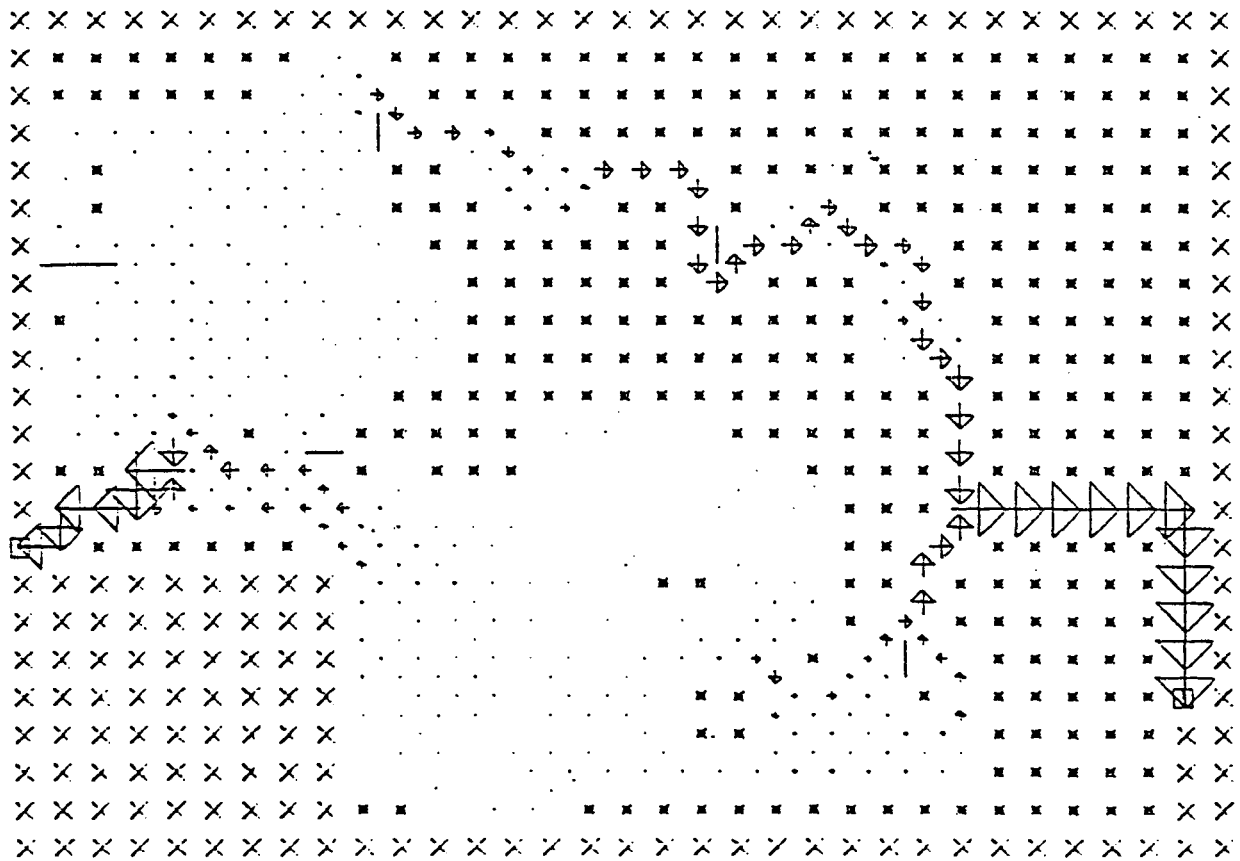
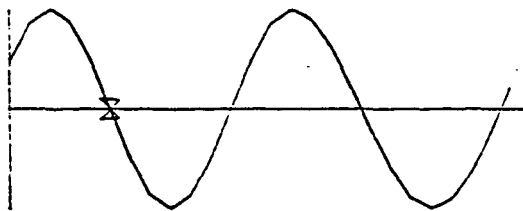
- - NO FLOW BOUNDARY

SCALE - 25000. CFS / INCH

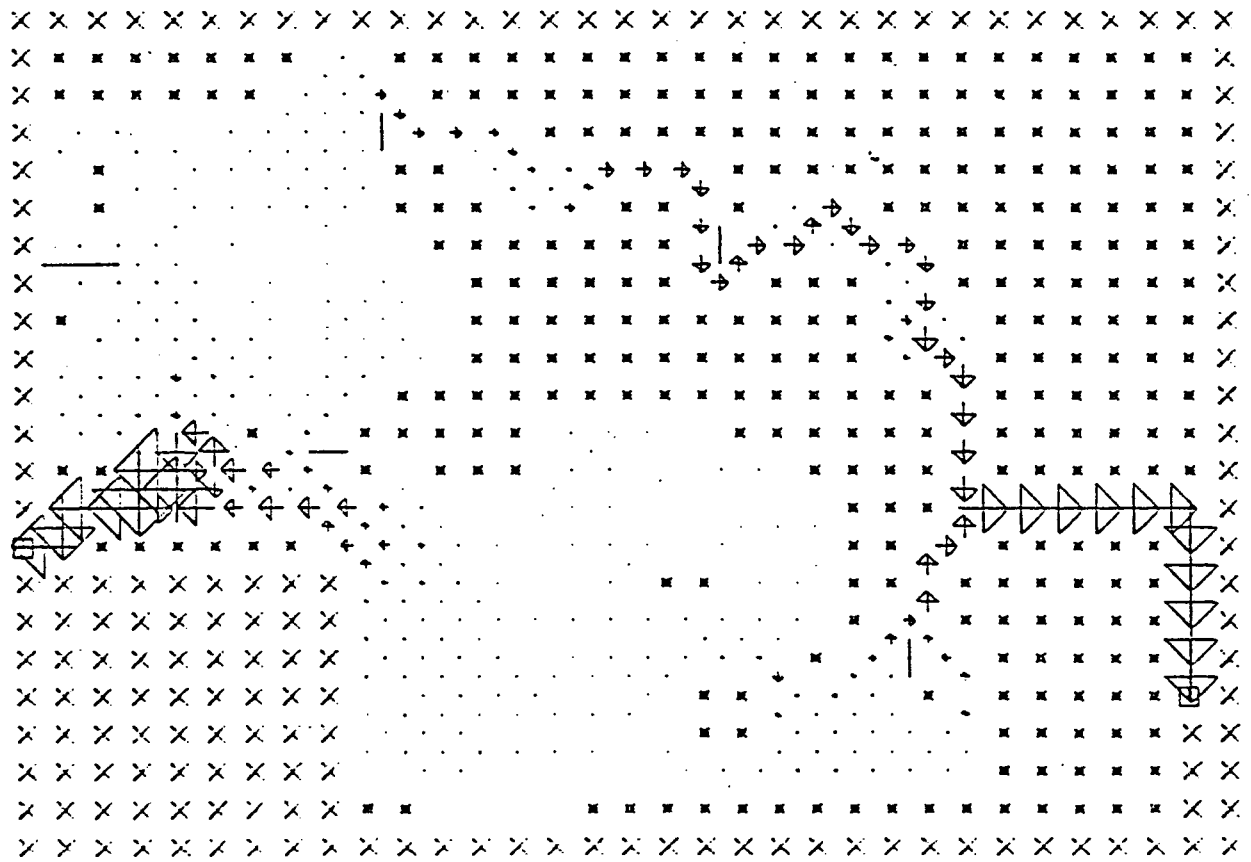
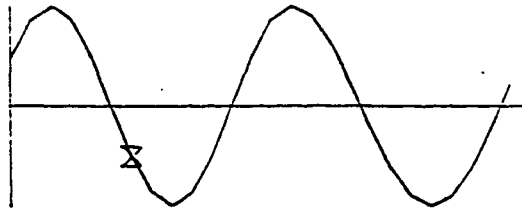


FLOW PATTERN FOR GRASSY  
AND RICHARDSON SOUNDS  
0500 HRS 26 AUG 1978

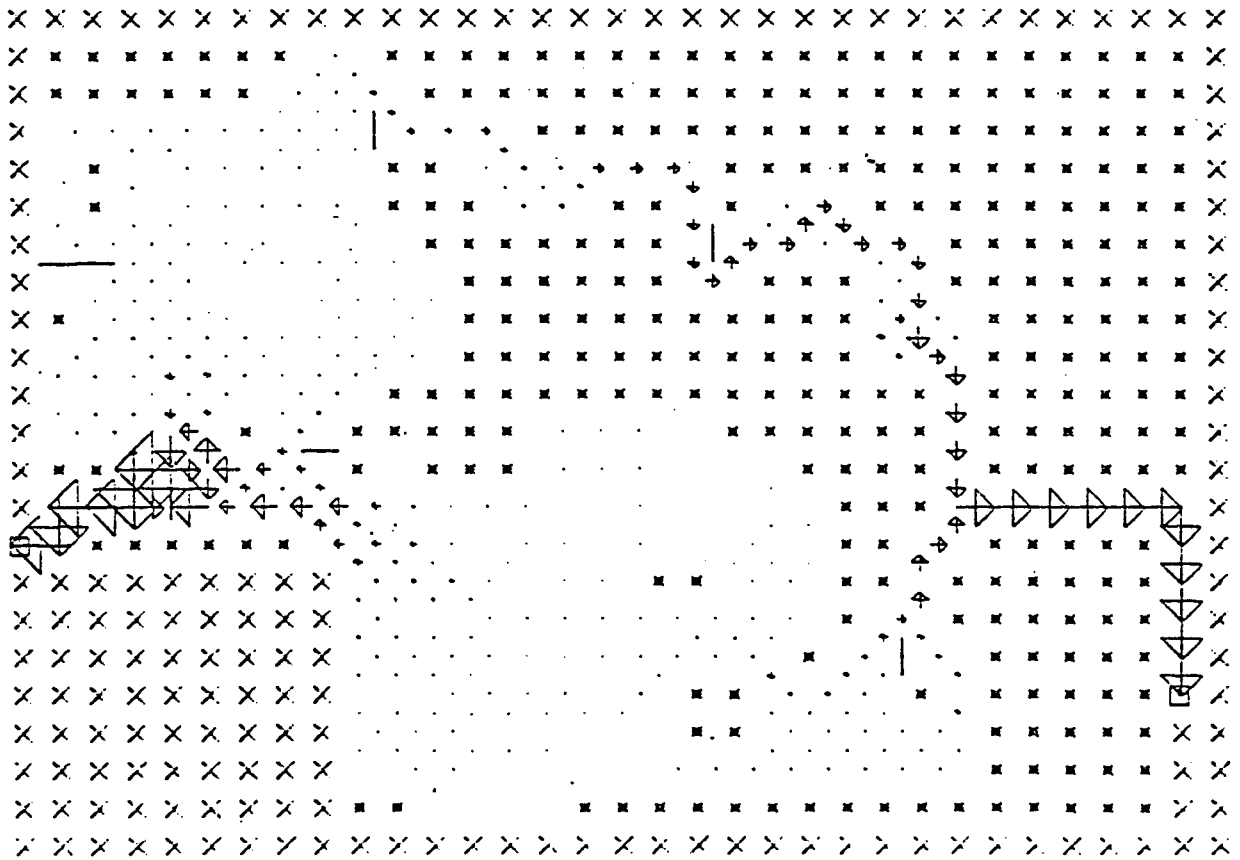
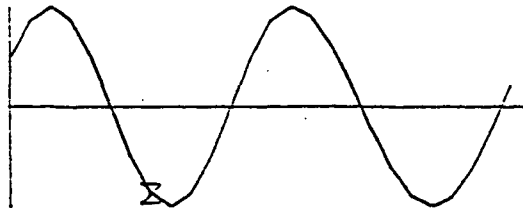
- X - LAND CELL
  - \* - INUNDATION CELL
  - - FORCING CELL
  - - NO FLOW BOUNDARY
- SCALE - 25000. CFS / INCH



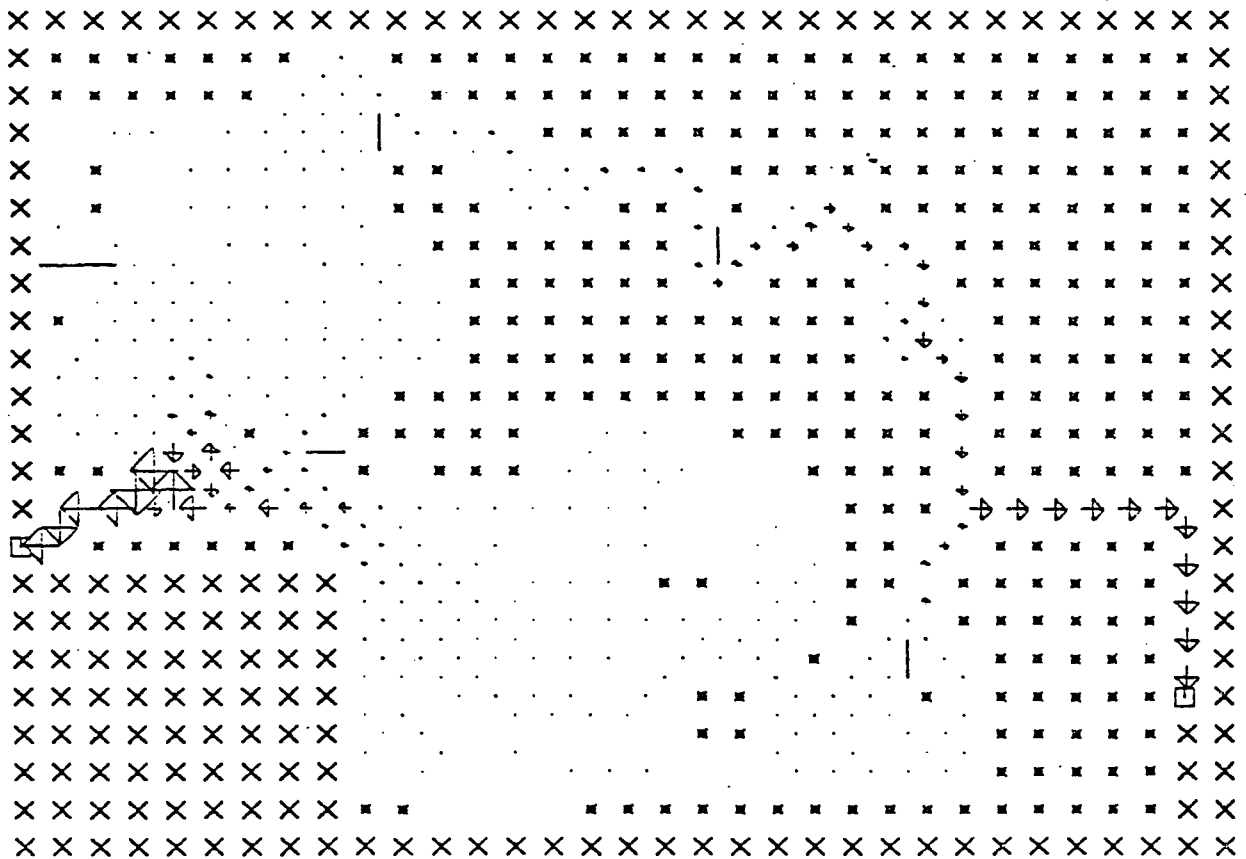
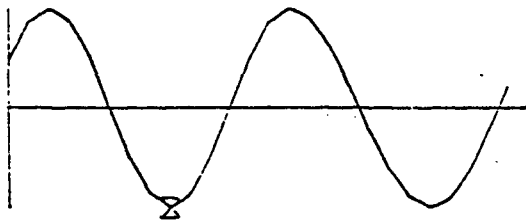
FLOW PATTERN FOR GRASSY  
 AND RICHARDSON SOUNDS  
 0600 HRS 26 AUG 1978  
 X - LAND CELL  
 \* - INUNDATION CELL  
 □ - FORCING CELL  
 - - NO FLOW BOUNDARY  
 SCALE - 25000. CFS / INCH



FLOW PATTERN FOR GRASSY  
 AND RICHARDSON SOUNDS  
 0700 HRS 26 AUG 1978  
 X - LAND CELL  
 \* - INUNDATION CELL  
 □ - FORCING CELL  
 - - NO FLOW BOUNDARY  
 SCALE - 25000. CFS / INCH



FLOW PATTERN FOR GRASSY  
 AND RICHARDSON SOUNDS  
 0800 HRS 26 AUG 1978  
 X - LAND CELL  
 \* - INUNDATION CELL  
 □ - FORCING CELL  
 - - NO FLOW BOUNDARY  
 SCALE - 25000. CFS / INCH





FLOW PATTERN FOR GRASSY

AND RICHARDSON SOUNDS

0900 HRS 26 AUG 1978

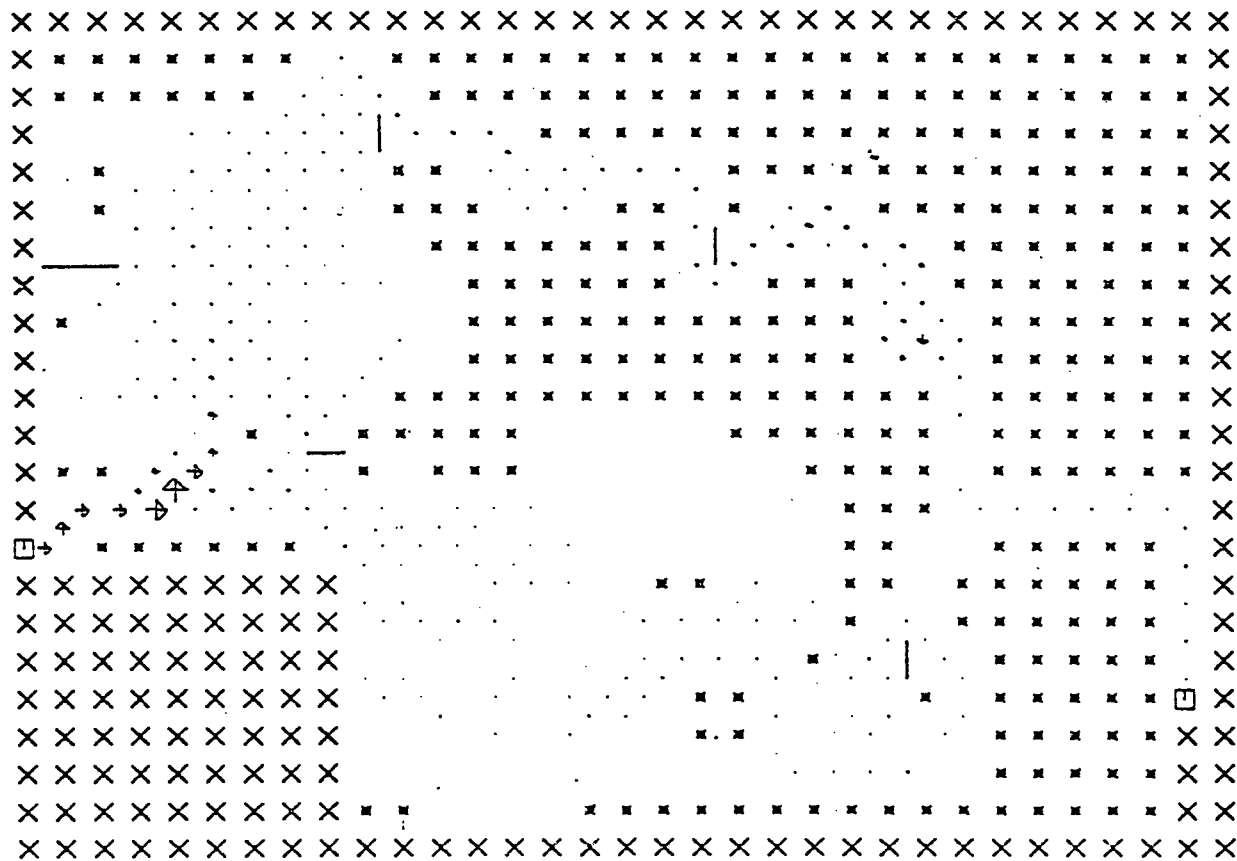
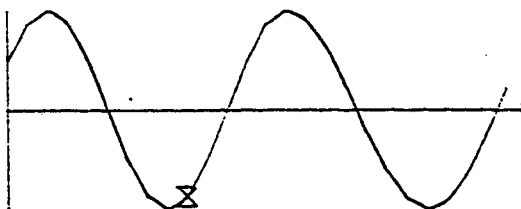
X - LAND CELL

\* - INUNDATION CELL

□ - FORCING CELL

- - NO FLOW BOUNDARY

SCALE - 25000. CFS / INCH



FLOW PATTERN FOR GRASSY

AND RICHARDSON SOUNDS

1000 HRS 26 AUG 1978

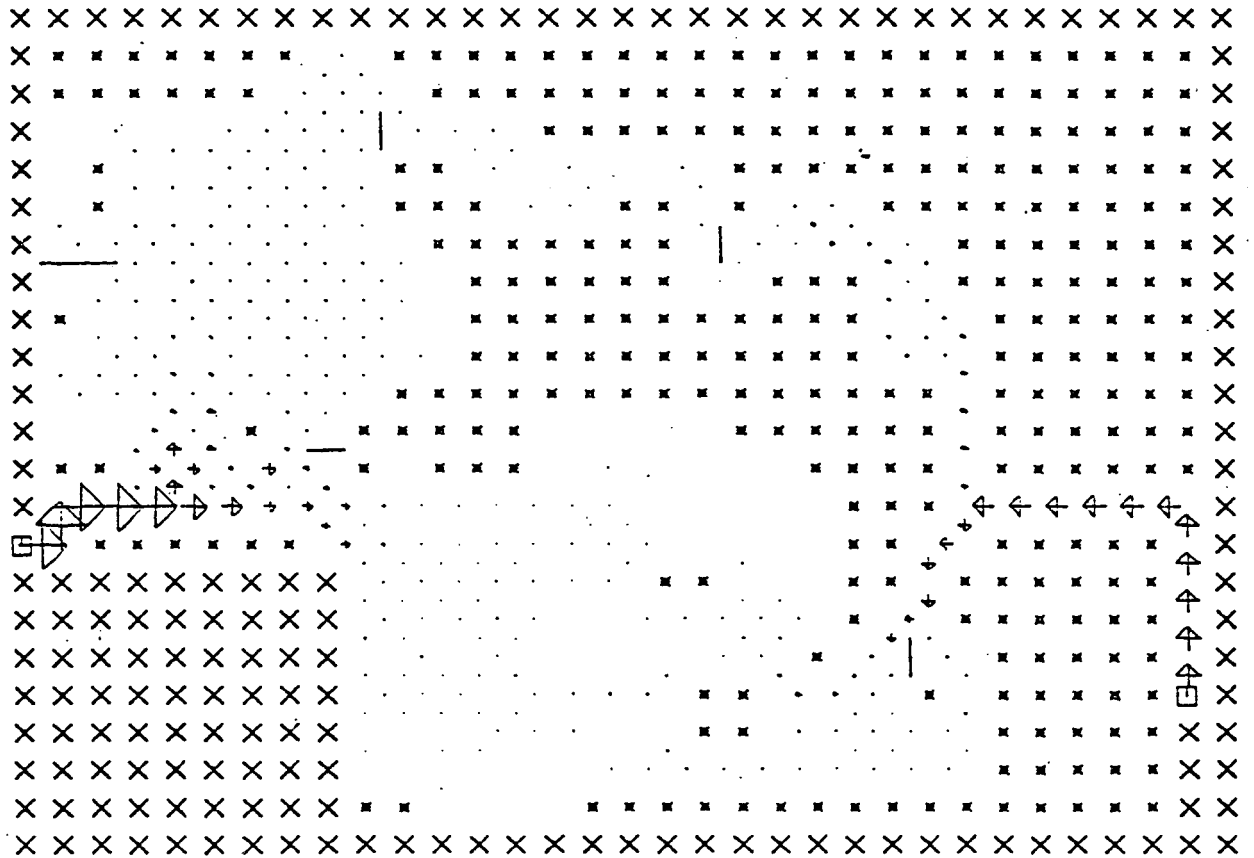
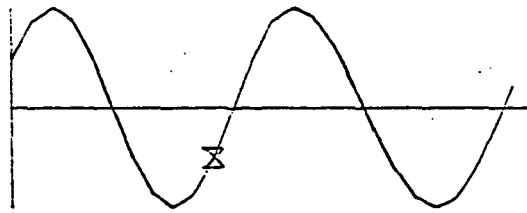
X - LAND CELL

\* - INUNDATION CELL

□ - FORCING CELL

- - NO FLOW BOUNDARY

SCALE - 25000. CFS / INCH



FLOW PATTERN FOR GRASSY

AND RICHARDSON SOUNDS

1100 HRS 26 AUG 1978

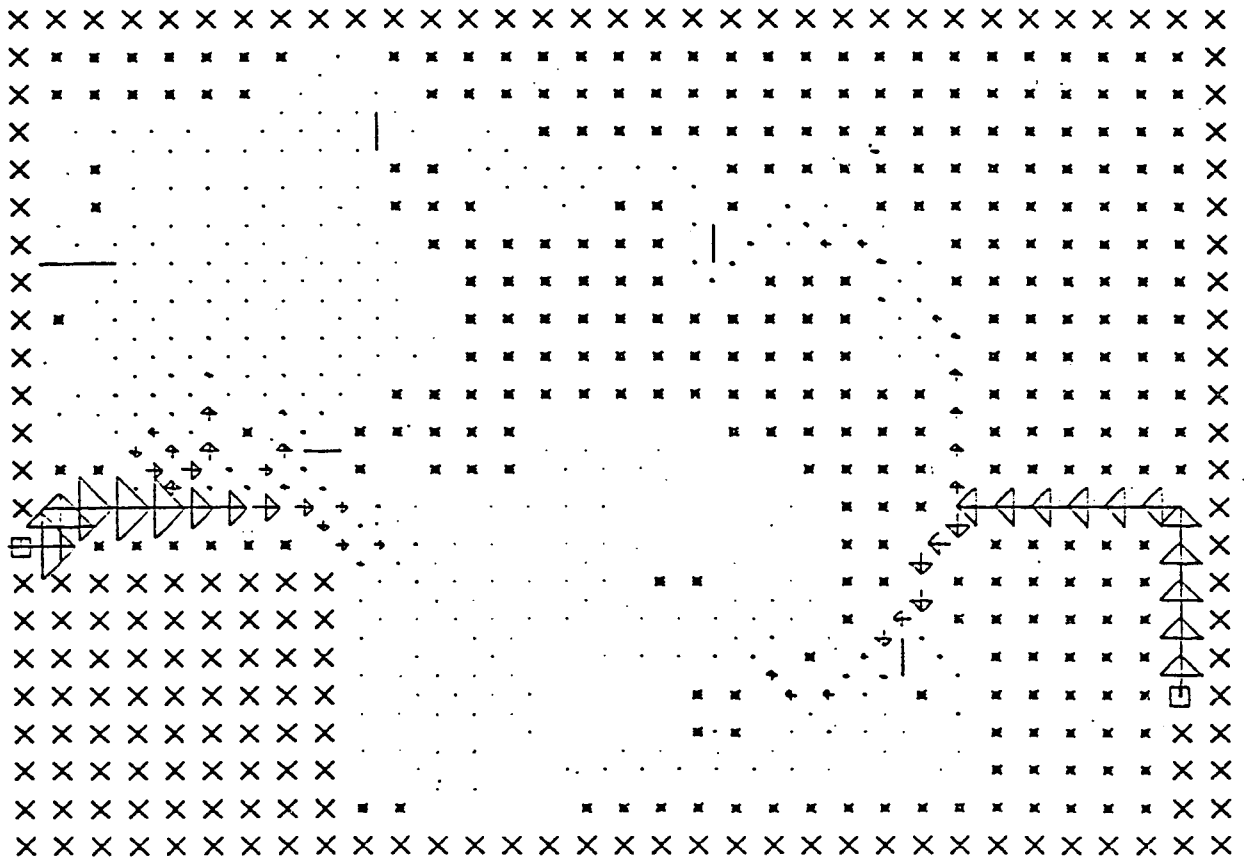
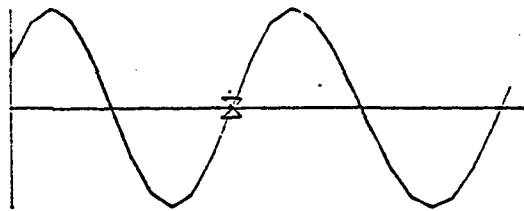
X - LAND CELL

\* - INUNDATION CELL

□ - FORCING CELL

- - NO FLOW BOUNDARY

SCALE - 25000. CFS / INCH

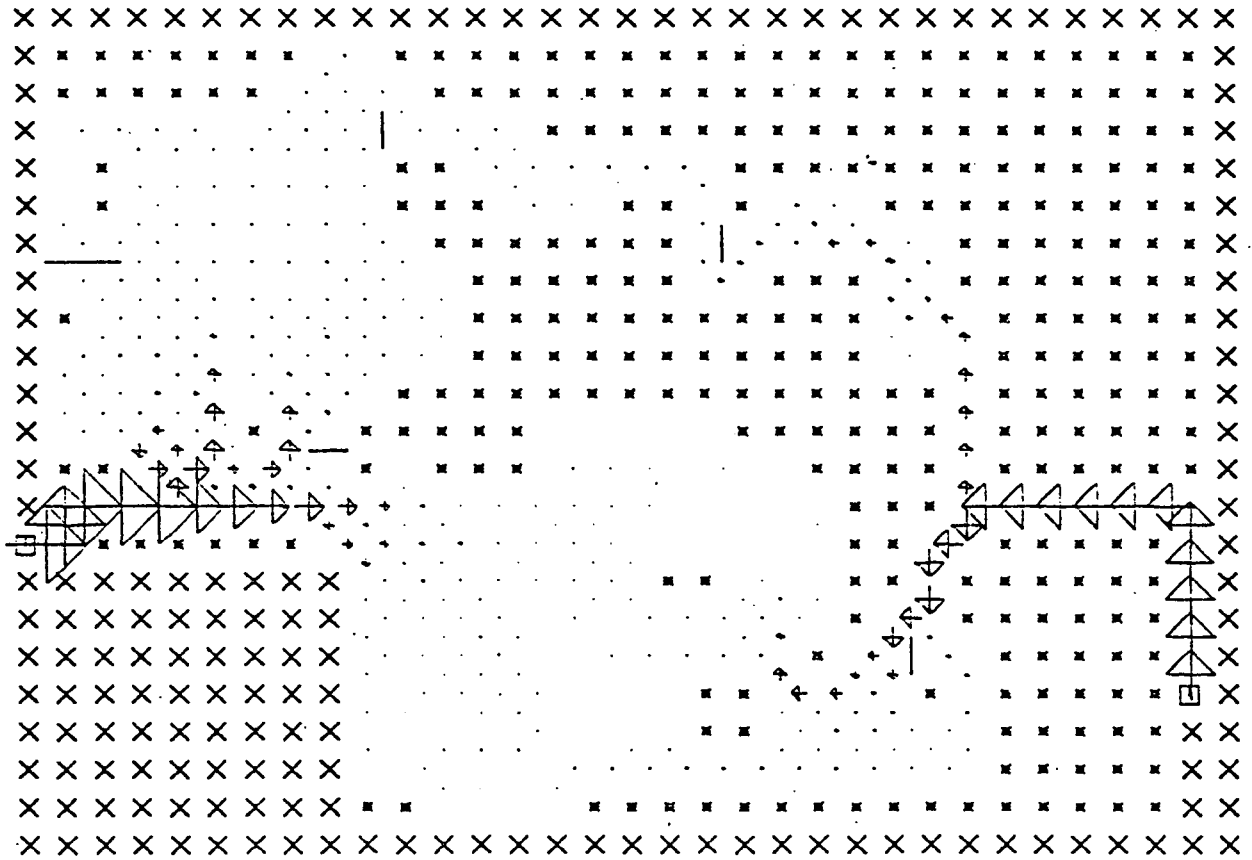
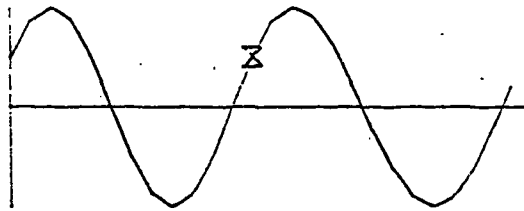


FLOW PATTERN FOR GRASSY  
AND RICHARDSON SOUNDS

1200 HRS 26 AUG 1978

- X - LAND CELL
- \* - INUNDATION CELL
- - FORCING CELL
- - NO FLOW BOUNDARY

SCALE - 25000. CFS / INCH



FLOW PATTERN FOR GRASSY

AND RICHARDSON SOUNDS

1300 HRS 26 AUG 1978

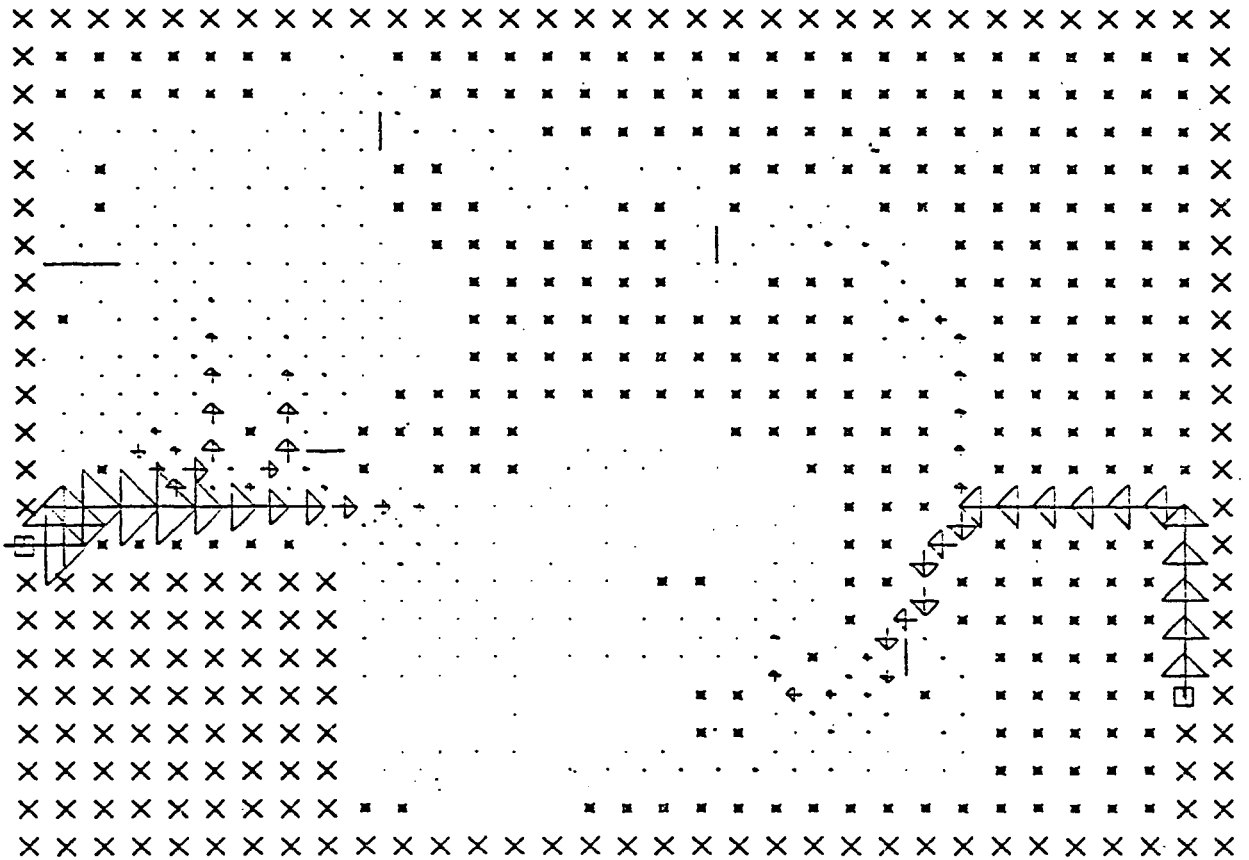
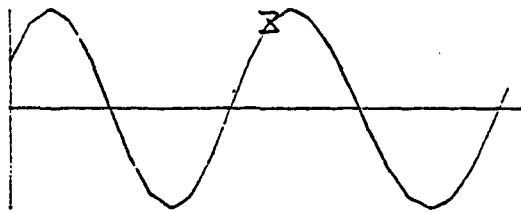
X - LAND CELL

\* - INUNDATION CELL

□ - FORCING CELL

- - NO FLOW BOUNDARY

SCALE - 25000. CFS / INCH



FLOW PATTERN FOR GRASSY

AND RICHARDSON SOUNDS

1400 HRS 26 AUG 1978

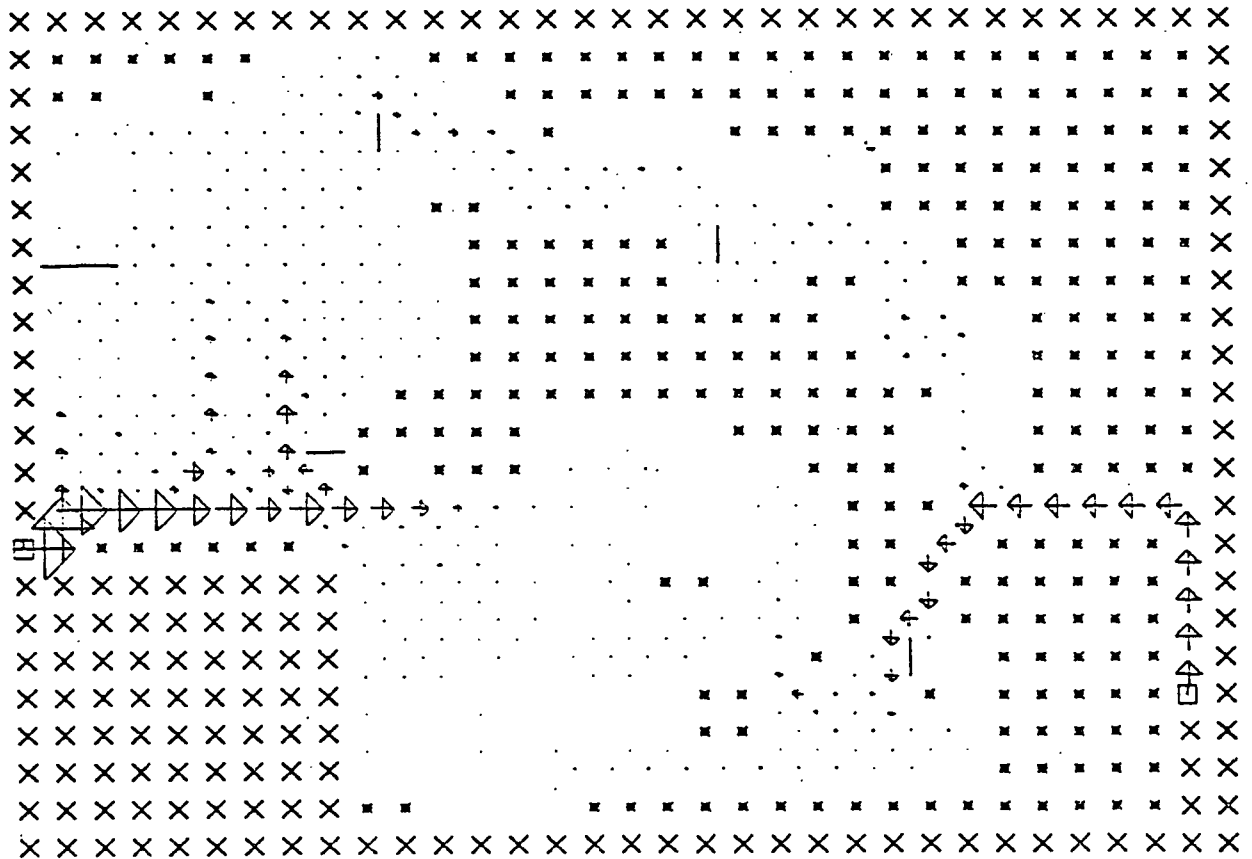
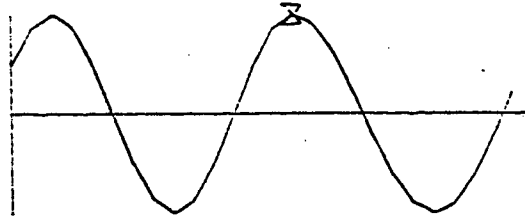
X - LAND CELL

\* - INUNDATION CELL

□ - FORCING CELL

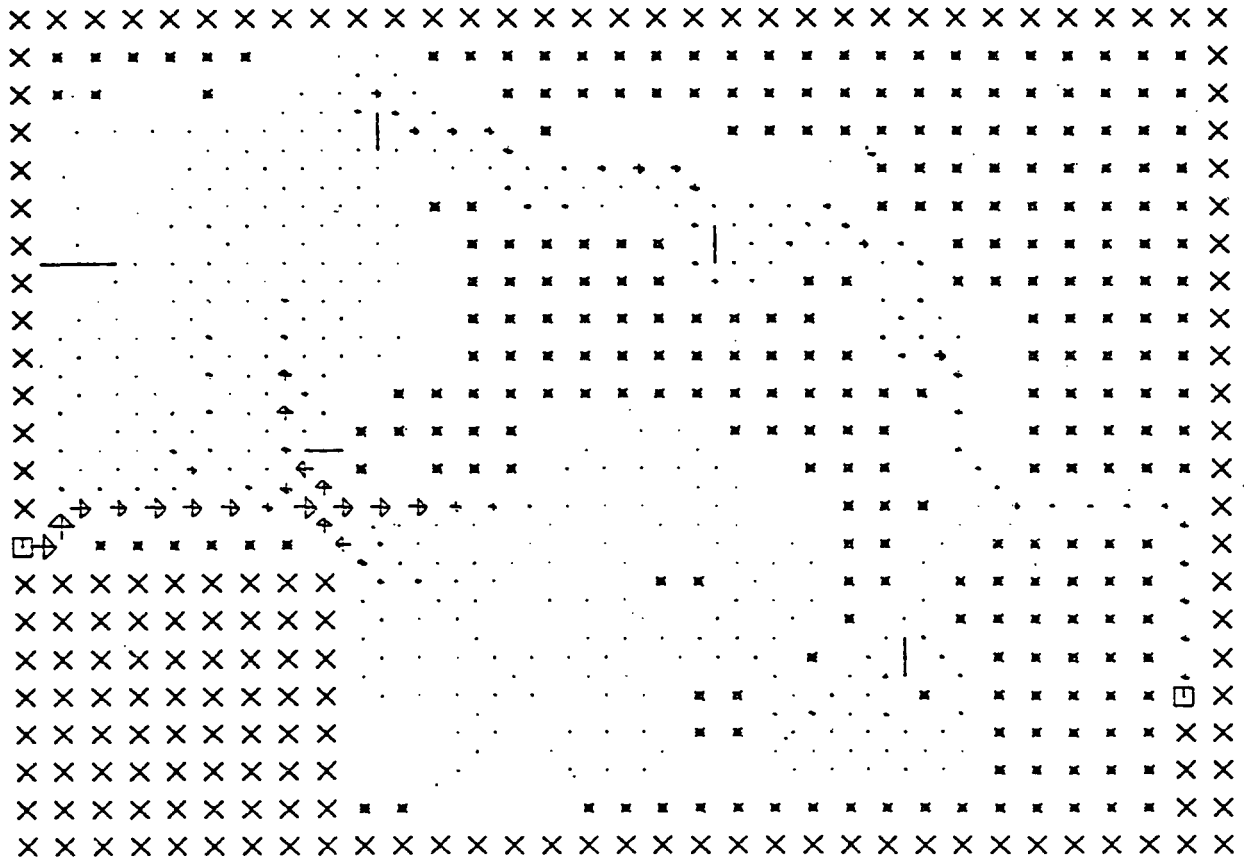
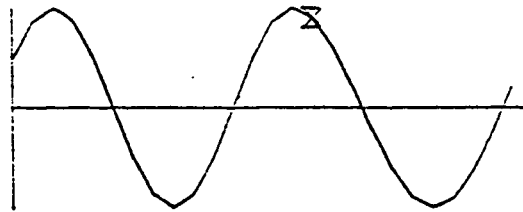
- - NO FLOW BOUNDARY

SCALE - 25000. CFS / INCH



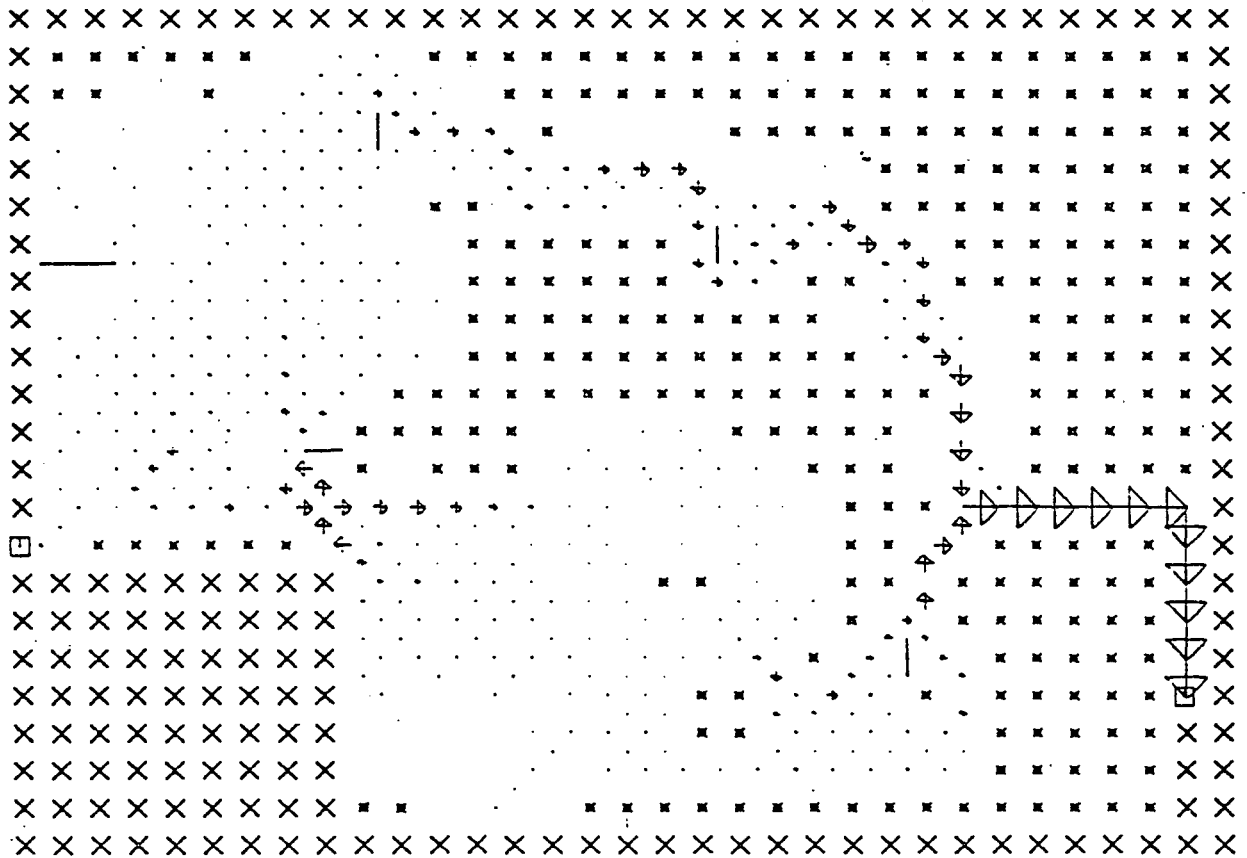
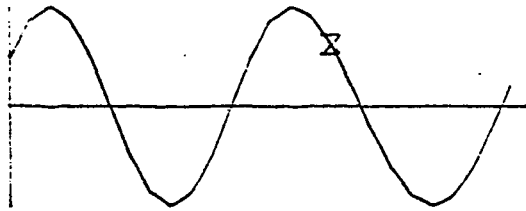
FLOW PATTERN FOR GRASSY  
AND RICHARDSON SOUNDS  
1500 HRS 26 AUG 1978

- X - LAND CELL
  - \* - INUNDATION CELL
  - - FORCING CELL
  - - NO FLOW BOUNDARY
- SCALE - 25000. CFS / INCH



FLOW PATTERN FOR GRASSY  
AND RICHARDSON SOUNDS  
1600 HRS 26 AUG 1978

- X - LAND CELL
  - \* - INUNDATION CELL
  - - FORCING CELL
  - - NO FLOW BOUNDARY
- SCALE - 25000. CFS / INCH





FLOW PATTERN FOR GRASSY

AND RICHARDSON SOUNDS

1700 HRS 26 AUG 1978

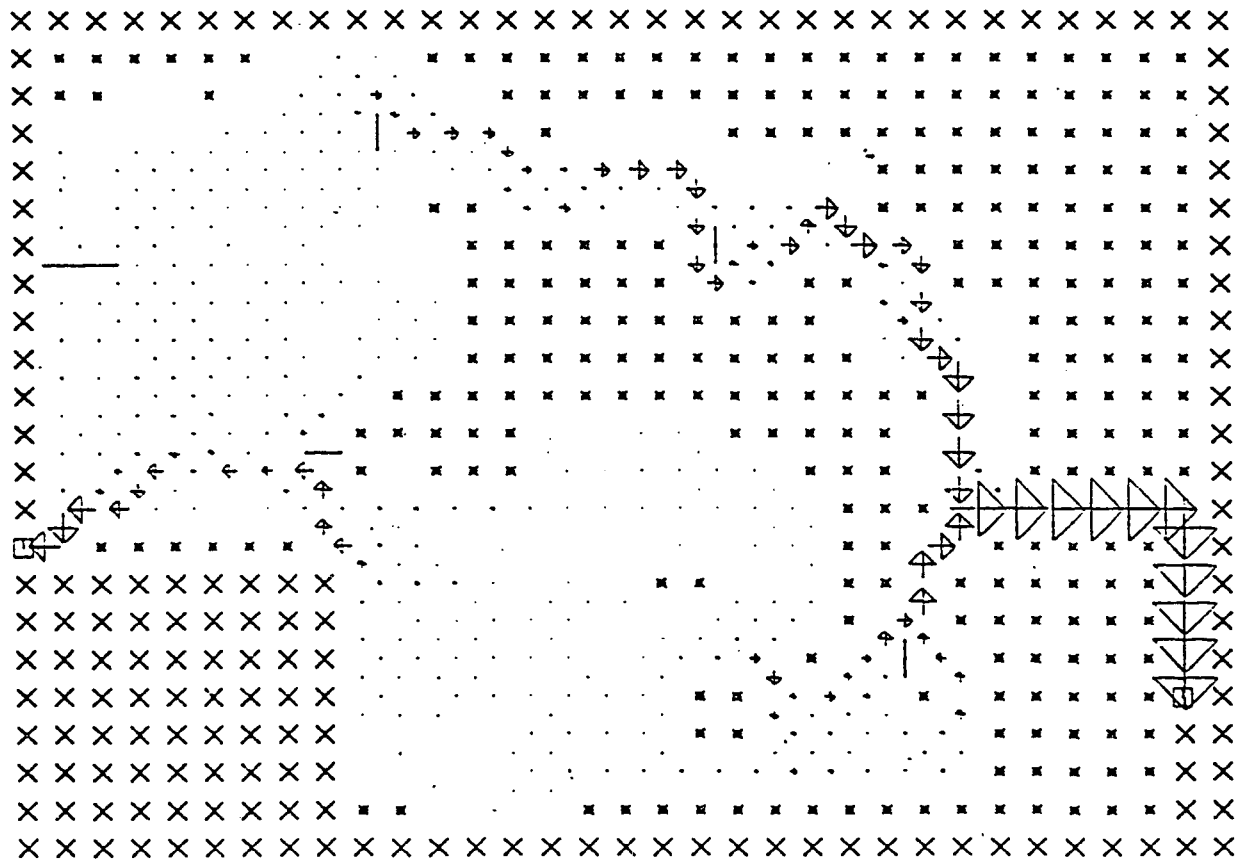
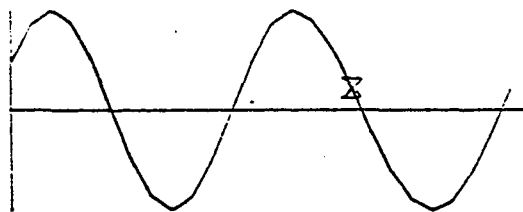
X - LAND CELL

\* - INUNDATION CELL

□ - FORCING CELL

- - NO FLOW BOUNDARY

SCALE - 25000. CFS / INCH



FLOW PATTERN FOR GRASSY  
AND RICHARDSON SOUNDS

1800 HRS 26 AUG 1978

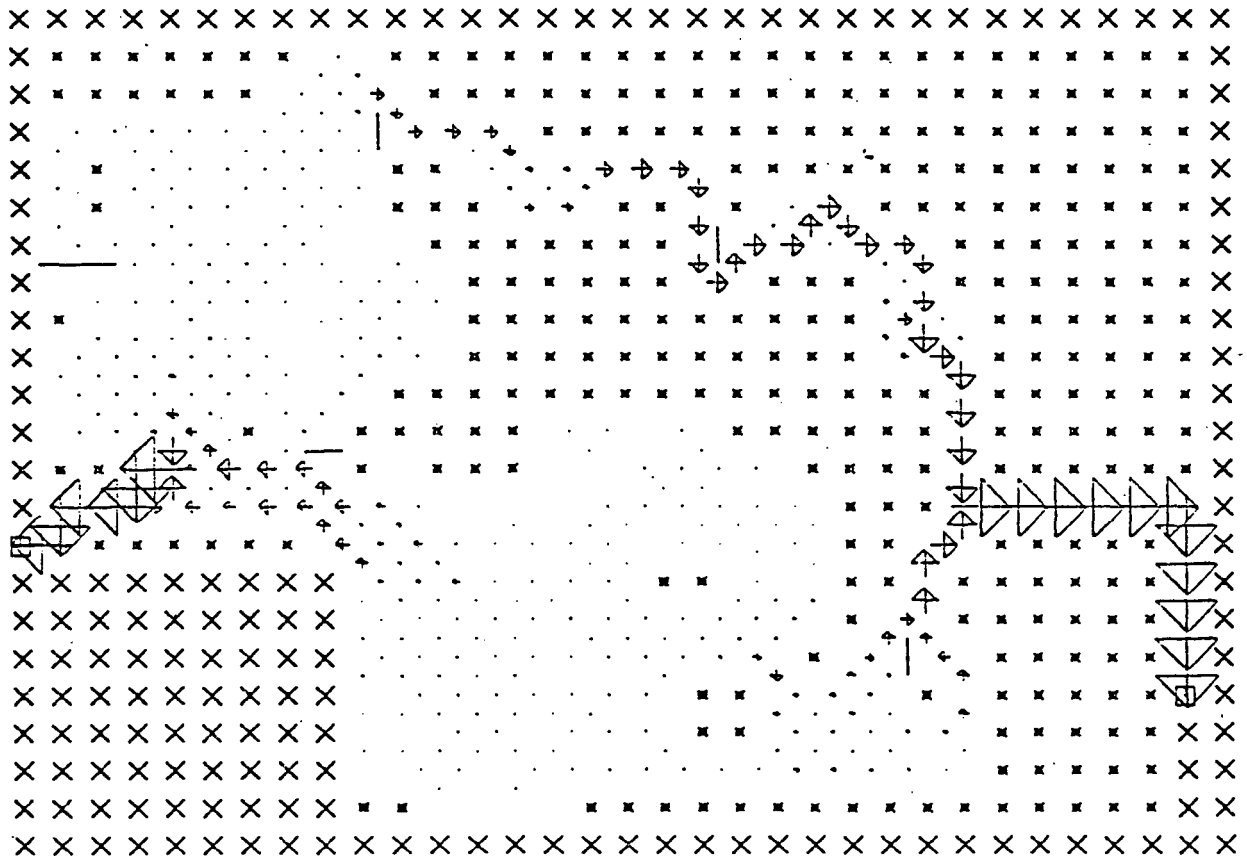
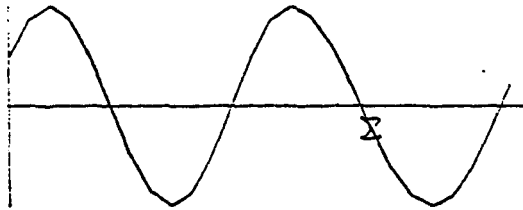
X - LAND CELL

\* - INUNDATION CELL

□ - FORCING CELL

- - NO FLOW BOUNDARY

SCALE - 25000. CFS / INCH



FLOW PATTERN FOR GRASSY

AND RICHARDSON SOUNDS

1900 HRS 26 AUG 1978

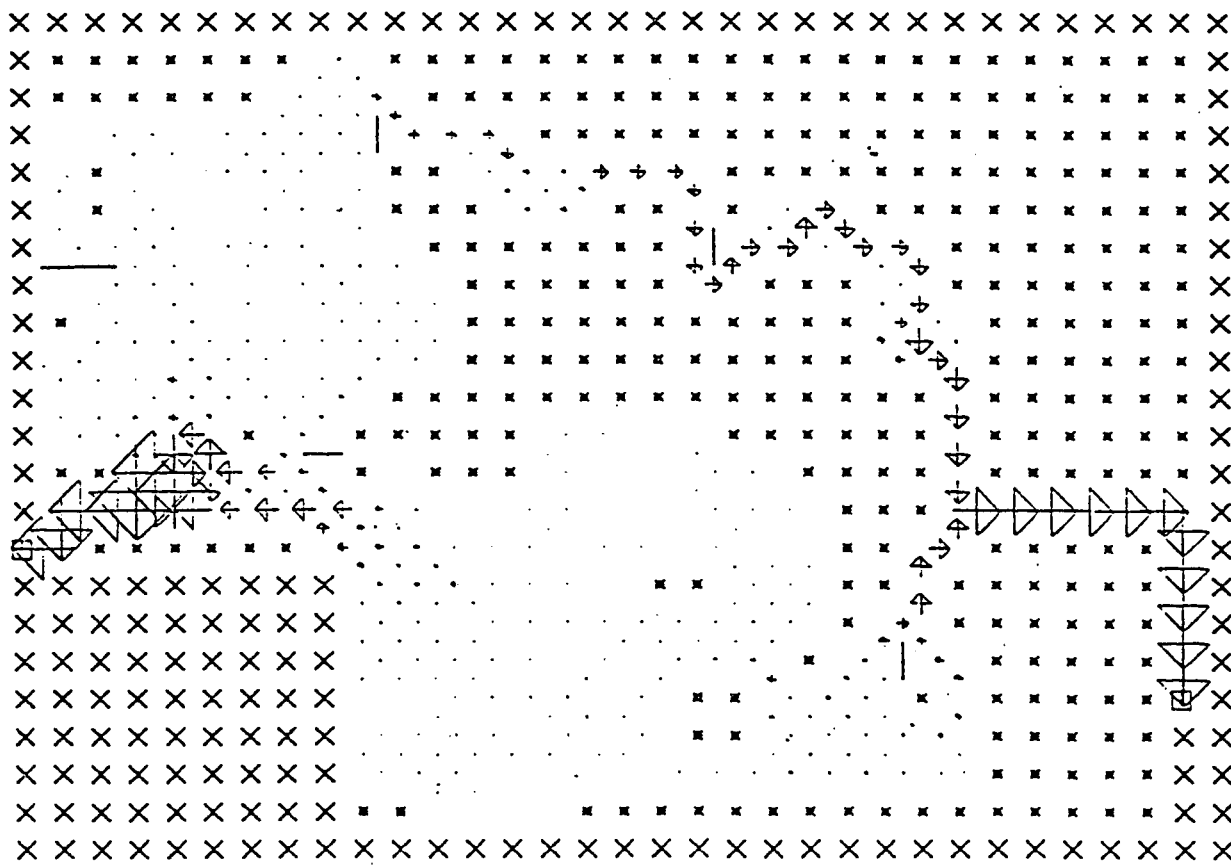
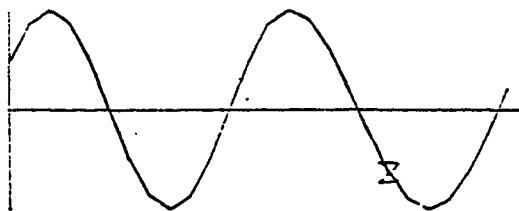
X - LAND CELL

\* - INUNDATION CELL

□ - FORCING CELL

- - NO FLOW BOUNDARY

SCALE - 25000. CFS / INCH



FLOW PATTERN FOR GRASSY  
AND RICHARDSON SOUNDS

2000 HRS 26 AUG 1978

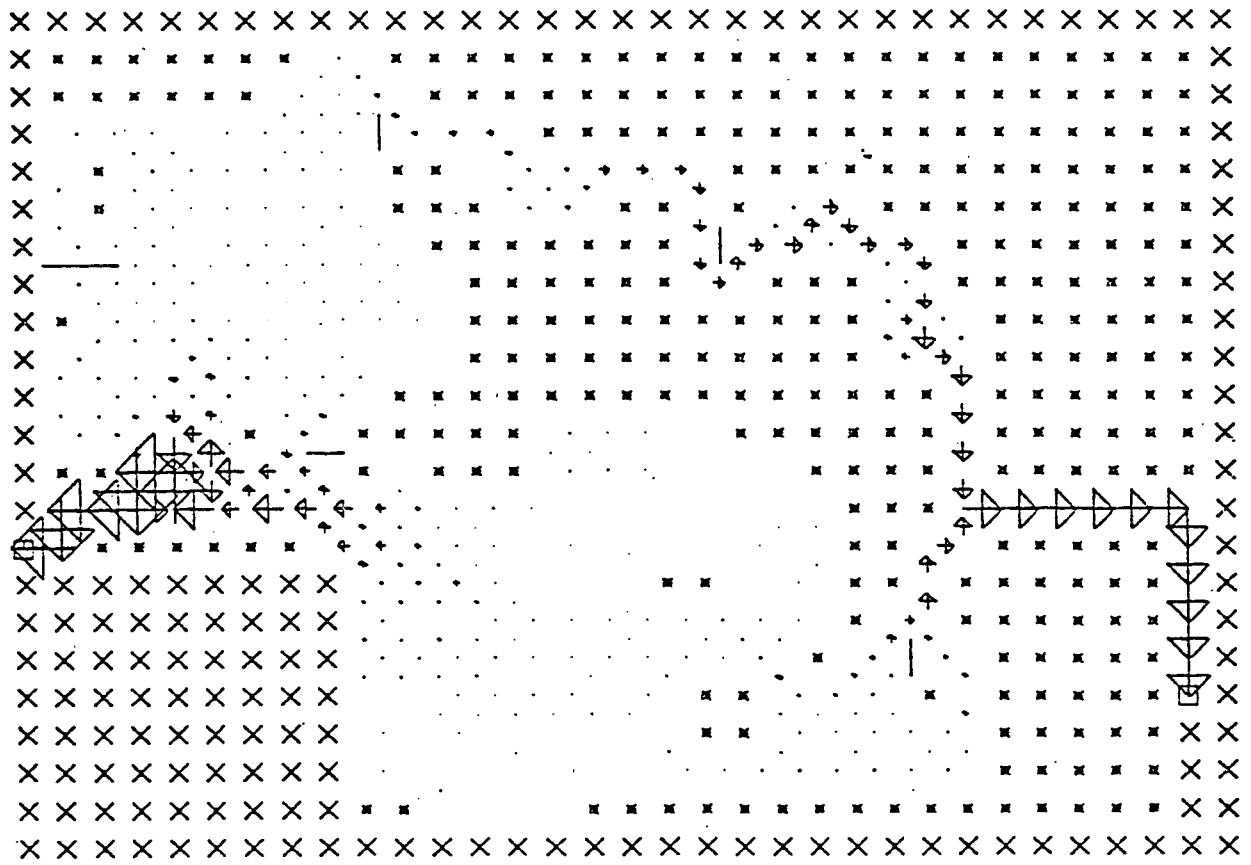
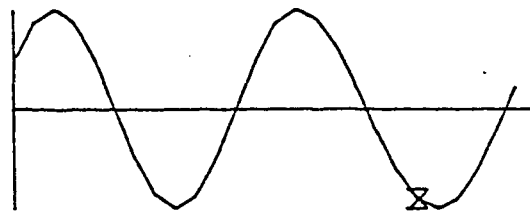
X - LAND CELL

\* - INUNDATION CELL

□ - FORCING CELL

- - NO FLOW BOUNDARY

SCALE - 25000. CFS / INCH



FLOW PATTERN FOR GRASSY

AND RICHARDSON SOUNDS

2100 HRS 26 AUG 1978

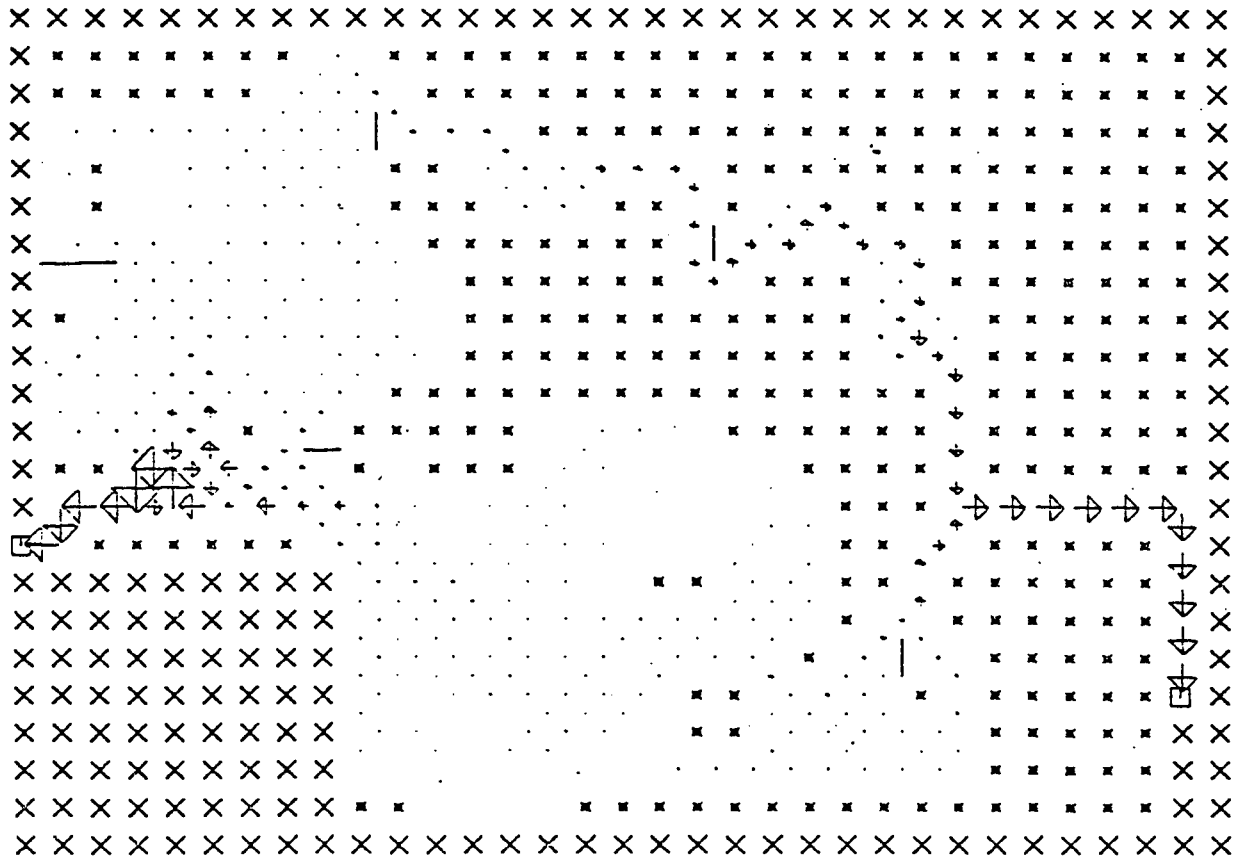
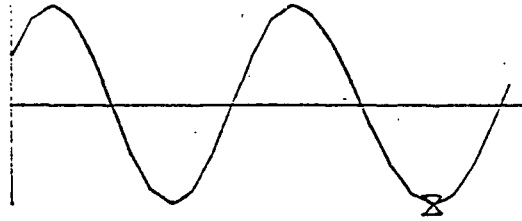
X - LAND CELL

\* - INUNDATION CELL

□ - FORCING CELL

- - NO FLOW BOUNDARY

SCALE - 25000. CFS / INCH



FLOW PATTERN FOR GRASSY  
AND RICHARDSON SOUNDS

2200 HRS 26 AUG 1978

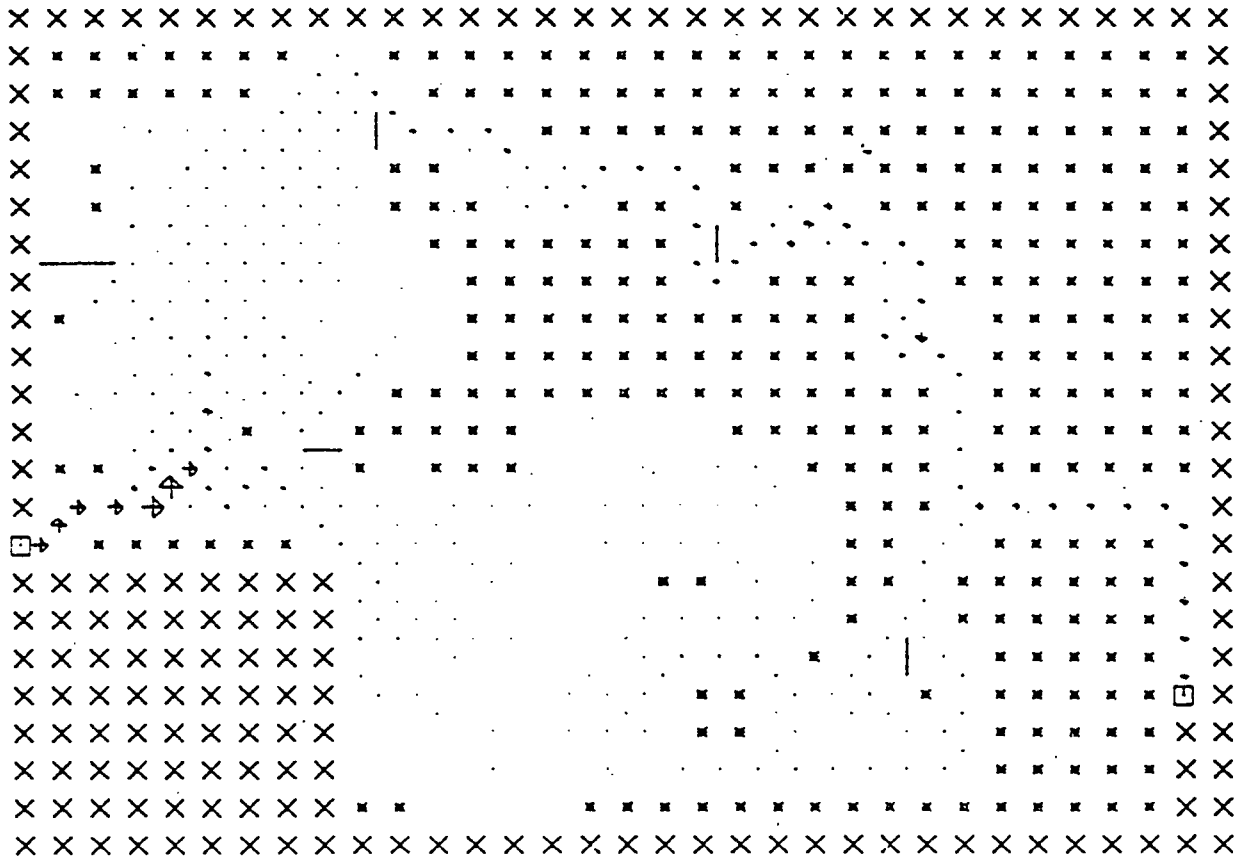
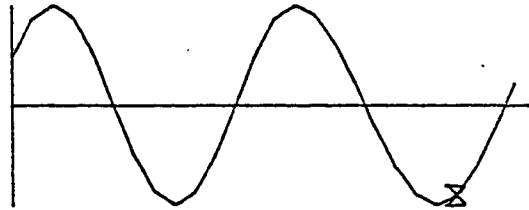
X - LAND CELL

\* - INUNDATION CELL

□ - FORCING CELL

- - NO FLOW BOUNDARY

SCALE - 25000. CFS / INCH



FLOW PATTERN FOR GRASSY  
AND RICHARDSON SOUNDS

2300 HRS 26 AUG 1978

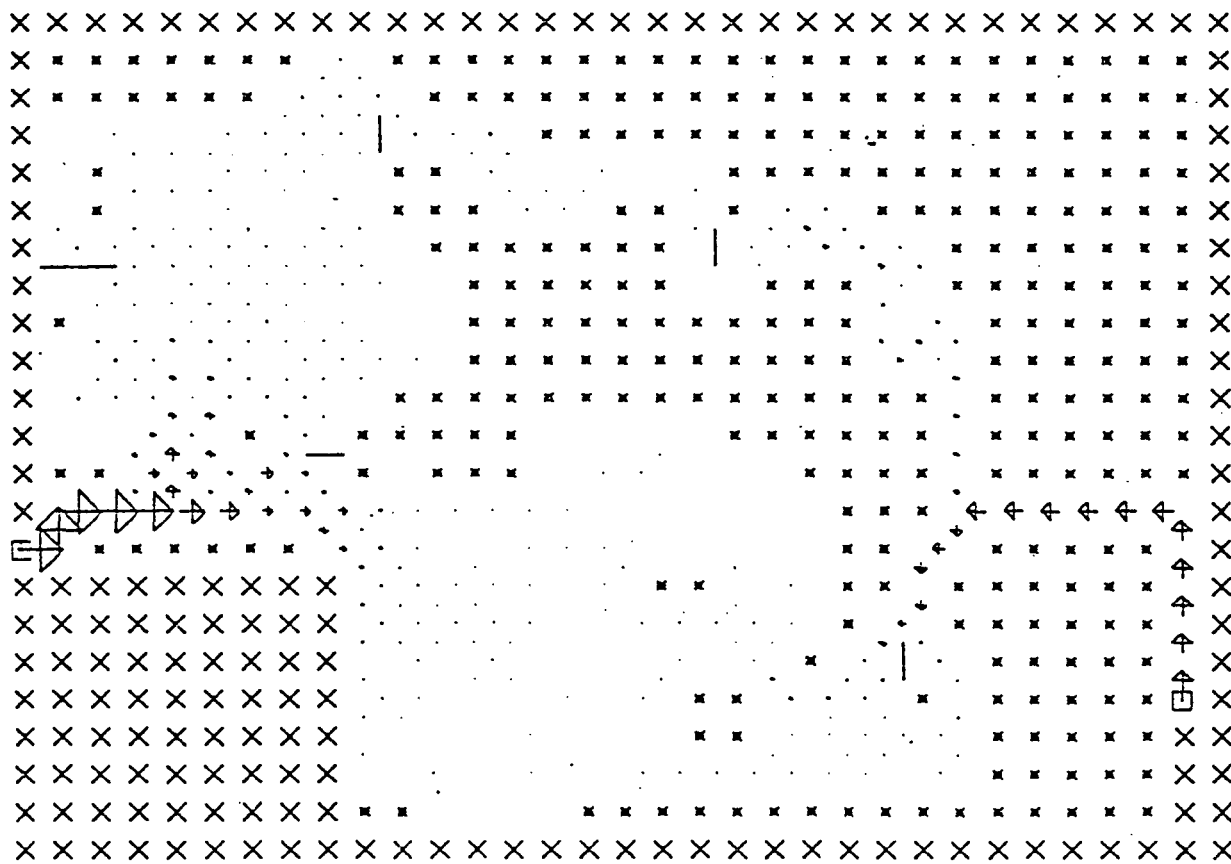
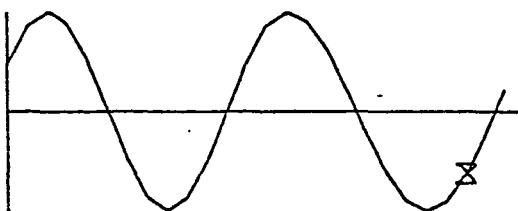
X - LAND CELL

\* - INUNDATION CELL

□ - FORCING CELL

- - NO FLOW BOUNDARY

SCALE - 25000. CFS / INCH

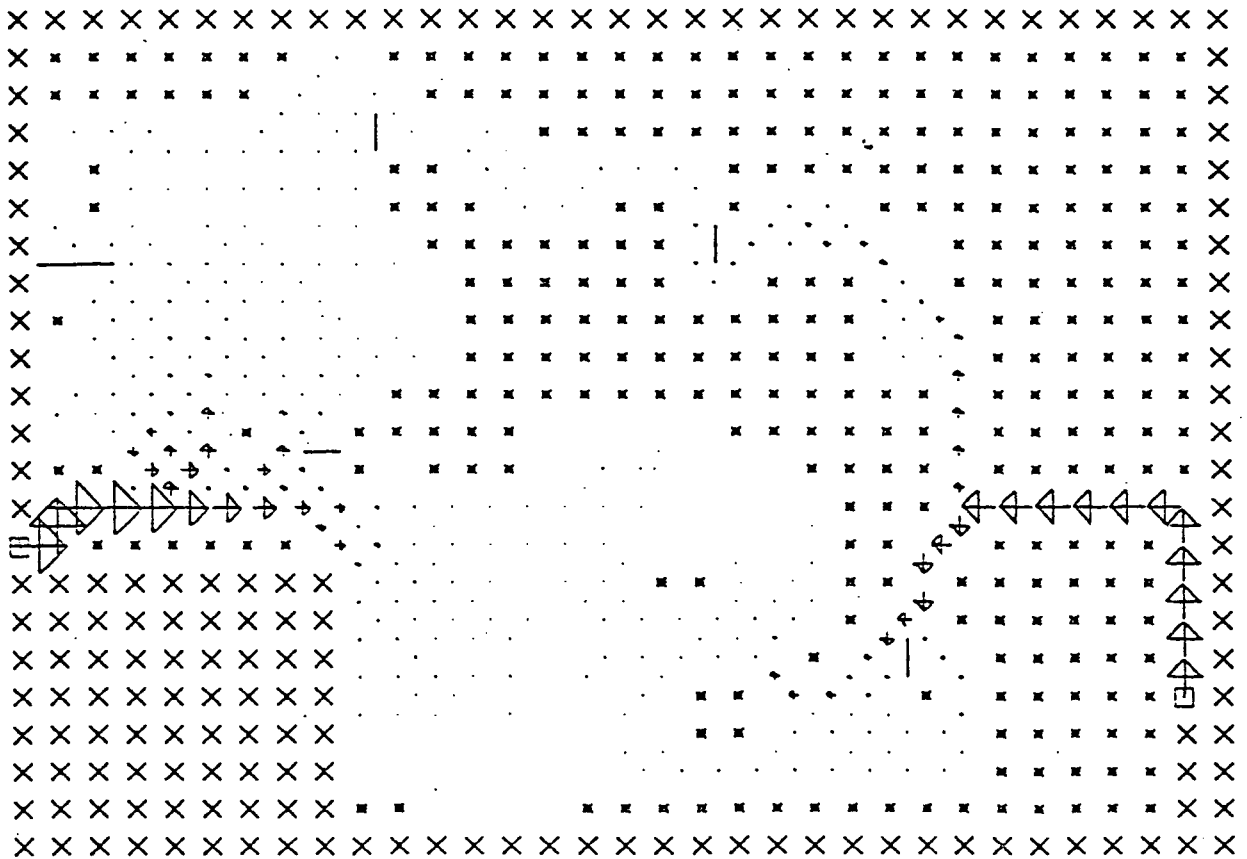
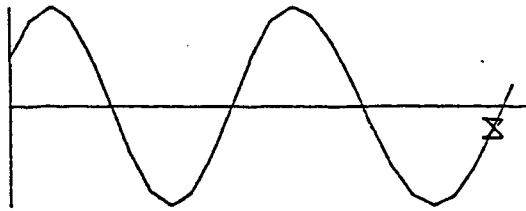


FLOW PATTERN FOR GRASSY  
AND RICHARDSON SOUNDS

2400 HRS 26 AUG 1978

- X - LAND CELL
- \* - INUNDATION CELL
- - FORCING CELL
- - NO FLOW BOUNDARY

SCALE - 25000. CFS / INCH





FLOW PATTERN FOR GRASSY

AND RICHARDSON SOUNDS

0100 HRS 27 AUG 1978

X - LAND CELL

\* - INUNDATION CELL

□ - FORCING CELL

- - NO FLOW BOUNDARY

SCALE - 25000. CFS / INCH

